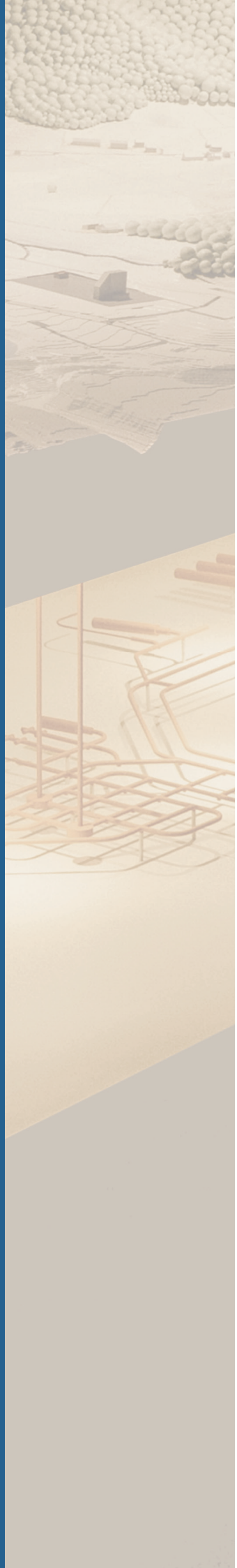

nagra.

TECHNICAL REPORT 22-04

Carbon-14 Sources, Speciation and Release from Radioactive Waste in the context of a Deep Geological Repository

December 2023

Nagra | National Cooperative for the Disposal of Radioactive Waste
Hardstrasse 73 | 5430 Wettingen | Switzerland
T. +41 56 437 11 11 | info@nagra.ch | nagra.ch

nagra.

TECHNICAL REPORT 22-04

Carbon-14 Sources, Speciation and Release from Radioactive Waste in the context of a Deep Geological Repository

December 2023

E. Wieland[1], E. Curti[1], G.D. Miron[1], J. Tits[1], L.R. Van Loon[1] & T. Guillemot[2]

[1]PSI - Paul Scherrer Institute, Switzerland

[2]Nagra

Nagra | National Cooperative for the Disposal of Radioactive Waste
Hardstrasse 73 | 5430 Wettingen | Switzerland
T. +41 56 437 11 11 | info@nagra.ch | nagra.ch

ISSN 1015-2636

Abstract

Carbon-14 (^{14}C) is a key radionuclide for safety assessment that is released from high- and low- and intermediate-level waste due to the degradation of ^{14}C-containing waste materials in deep geological repositories over time. ^{14}C is contained in waste generated during the operation and decommissioning of nuclear power plants, from reprocessing and in waste from medicine, industry and research. The ^{14}C released during the degradation of the various waste types is present in either inorganic or organic chemical form, in solution or gas phase. In the dissolved inorganic form, i.e., as $H^{14}CO_3^-$ or $^{14}CO_3^{2-}$, ^{14}C is strongly retained by the backfill materials (i.e., bentonite, cementitious materials) of the near-field and the host rock (Opalinus Clay) by isotopic exchange with carbonate of the calcite fractions and, therefore, decays within the repository. In the dissolved organic form, ^{14}C is mainly present as ^{14}C-bearing small molecules, such as ^{14}C-containing carboxylates, which are only weakly retained by the backfill materials of the near-field and the host rock and can, therefore, contribute to the dose release via the groundwater pathway. In the gaseous form, ^{14}C occurs mainly as ^{14}C-bearing small hydrocarbons, in particular ^{14}C-bearing methane, which migrate via the gas pathway. This report summarises the current state of knowledge on: (i) the sources of ^{14}C in the various waste types relevant to the Swiss waste inventory; (ii) the chemical forms of ^{14}C release through the degradation of ^{14}C-containing waste materials, and (iii) the retention of the ^{14}C-bearing species in the near -and far-fields of the deep geological repository. This report provides an overall appraisal of the behaviour of ^{14}C in the context of a Swiss deep geological repository for both high- and low- and intermediate-level waste. It is the scientific basis for defining post-closure safety assessments in the framework of the general licence application.

Zusammenfassung

Kohlenstoff-14 (^{14}C) ist ein wichtiges Radionuklid, das durch den langjährigen Abbau von ^{14}C-haltigen Abfallmaterialien aus geologischen Tiefenlagern für hochaktive sowie für schwach- und mittelaktive Abfälle freigesetzt wird und so zur Strahlendosis beiträgt. ^{14}C ist in Abfällen enthalten, die aus dem Betrieb von Kernkraftwerken, aus der Stilllegung und Wiederaufarbeitung von abgebrannten Brennelementen sowie aus Anwendungen in Medizin, Industrie und Forschung entstehen. ^{14}C, das während des Abbaus der verschiedenen Abfallarten freigesetzt wird, liegt entweder in gelöster oder gasförmiger, anorganisch- oder organisch-chemischer Form vor. In gelöster anorganischer Form, d.h. als $H^{14}CO_3^-$ oder $^{14}CO_3^{2-}$, wird ^{14}C von im Nahfeld vorkommenden Verfüllmaterialien (Bentonit, zementgebundene Werkstoffe) oder im Wirtgestein (dem Opalinuston) durch den Isotopenaustausch mit Karbonat aus Kalzitfraktionen stark zurückgehalten und zerfällt daher noch innerhalb des Tiefenlagers. In gelöster organischer Form liegt ^{14}C hauptsächlich in Form von ^{14}C-haltigen, kleinen Molekülen vor, wie z. B. ^{14}C-haltige Carboxylate. Diese werden von den Verfüllmaterialien im Nahfeld oder vom Wirtgestein nur schwach zurückgehalten und können daher zur Dosisfreisetzung über den Grundwasserpfad beitragen. Im gasförmigen Zustand kommt ^{14}C hauptsächlich in Form von ^{14}C-haltigen, kleinen Kohlenwasserstoffen vor, insbesondere ^{14}C-haltigem Methan, die über den Gasfreisetzungspfad migrieren. Dieser Bericht fasst den aktuellen Wissensstand über: (i) die Quellen von ^{14}C in den verschiedenen Abfallarten zusammen, die für das schweizerische Entsorgungsprogramm relevant sind, sowie (ii) die chemischen Formen von ^{14}C, die durch den Abbau von ^{14}C-haltigen Abfallstoffen freigesetzt werden und schliesslich auch (iii) die Rückhaltung ^{14}C-haltiger Kohlenstoffverbindungen im Nah- und Fernfeld eines geologischen Tiefenlagers. Dieser Bericht umfasst eine Gesamtbewertung des Verhaltens von ^{14}C im Zusammenhang mit einem Schweizer Tiefenlager für hoch- sowie schwach- und mittelaktive Abfälle. Er dient insbesondere als wissenschaftliche Grundlage für den Langzeitsicherheitsnachweis, der im Zusammenhang mit dem Rahmenbewilligungsgesuch erbracht wird.

Table of Contents

List of Tables

List of Figures

List of Acronyms

ACW	Artificial Cement Water
ATW	Alpha-Toxic Waste
AISI	American Iron and Steel Institute
ASTM	American Society for Testing and Materials
BWR	Boiling Water Reactor
CANDU	CANada Deuterium Uranium
CAST	CArbon Source Term (EU project)
CERN	Conseil Européen pour la Recherche Nucléaire (European Organisation for Nuclear Research)
COx	Callovian-Oxfordian claystone
^{14}C	Carbon-14
EBS	Engineered Barrier System
EGTS	Engineered Gas Transport System
EU	European Union
FGR	Fission Gas Release
GC	Gas Chromatography
HC	HydroCarbon
HCP	Hardened Cement Paste
HLW	High-Level Waste
HPIEC	High-Performance Ion-Exchange Chromatography
HPLC	High-Performance Liquid Chromatography
HWC	Hydrogen Water Chemistry
IER	Ion-Exchange Resin
IRF	Instant Release Fraction
KEG	KernEnergieGesetz (Swiss Nuclear Energy Act)
L/ILW	Low- and Intermediate-Level Waste
LMW	Low Molecular Weight
LSC	Liquid Scintillation Counting
LWR	Light Water Reactor
MIR	Medicine, Industry and/or Research
MIRAM	Modellhaftes Inventar für Radioaktive Materialien (Model Inventory of Radioactive Materials)

MOX	Mixed OXide (fuel)
MS	Mass Spectrometry
NPP	Nuclear Power Plant
NWC	Normal Water Chemistry
PSI	Paul Scherrer Institute
PWR	Pressurised Water Reactor
OM	Organic Matter
OPA	Opalinus Clay
RBG	RahmenBewilligungsGesuch (general licence application)
RH	Relative Humidity
SAE	Society of Automotive Engineers
SF	Spent Fuel
TOC	Total Organic Carbon

1 Introduction

1.1 Design concepts for the deep geological repository in Switzerland

The Swiss Nuclear Energy Act requires the disposal of all types of radioactive waste in deep geological repositories (KEG 2003). A deep geological repository encompasses an installation located deep underground with a system of passive safety barriers and comprises the main installation for the emplacement of the radioactive waste, a pilot repository and test areas, along with the underground access structures to the installations. Two types of repositories are planned for the disposal of radioactive waste in Switzerland: a repository for high-level waste (HLW) and a repository for low- and intermediate-level waste (L/ILW) (Nagra 2021a). The HLW repository contains spent fuel (SF) and vitrified HLW, while the L/ILW repository contains L/ILW and alpha-toxic waste (ATW). The current concept for a deep geological repository envisages the storage of both HLW and L/ILW at a shared site, i.e., in a so-called combined repository (Fig. 1-1). After an extensive exploration programme, Nagra selected the Nördlich Lägern siting region for hosting the combined repository which will be constructed in the Opalinus Clay (OPA) at a depth of around 900 m (Nagra 2024a, in prep.).

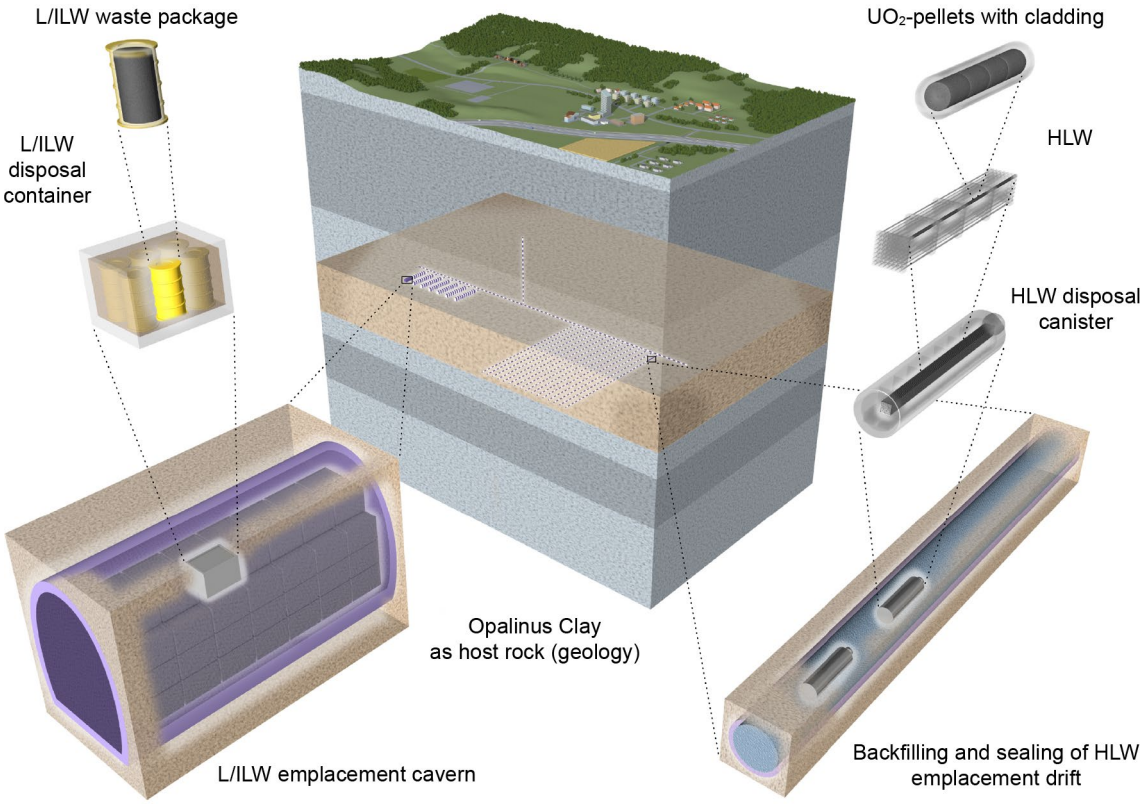

Fig. 1-1: Conceptual illustration of a combined repository for HLW and L/ILW

From Nagra (2021b)

Detailed descriptions of the design and safety concepts applied to the repositories are given elsewhere (Nagra 2021b; Nagra 2024b, in prep.). In brief, the design concept is based on the notion that the high level of safety requirements for the long-term disposal of radioactive waste are ensured by the various repository components (multi-barrier), in particular the engineered barriers and the geological formation. The engineered barrier system (EBS) comprises the waste

matrices, waste containers and disposal canister/containers, as well as backfilling/sealing materials. OPA is the host rock in all potential siting regions for a deep geological repository in Switzerland. It plays a key role as it isolates the waste from the human environment and ensures long-term stability through marked retardation of radionuclide transport. The planned HLW repository contains the SF assemblies and vitrified HLW from reprocessing encapsulated in disposal canisters, which are surrounded by a bentonite backfill (Fig. 1-1). In the L/ILW repository, the waste is emplaced in metal containers and usually conditioned in cementitious materials. The waste containers will be emplaced in disposal containers made of concrete. The voids between the drums in the disposal containers will be backfilled with a porous, free-flowing cementitious material. The void space between the waste containers and the cavern lining, the top heading, as well as transfer and unloading areas will also be backfilled with a porous, yet not free-flowing cementitious material composed of mono-grained aggregate material covered by hydrated cement. This backfill material ensures high mechanical stability through filling of voids between the waste containers and, due to its high porosity, simultaneously enables gas storage in the emplacement cavern.

1.2 ^{14}C in radioactive waste

Carbon-14 (^{14}C) is a key radionuclide in safety assessments for deep geological repositories worldwide, but also for near-surface facilities (Ahn 1994; Bracke & Müller 2008; Brady & Kozak 1995; Hesböl et al. 1990; Johnson & Schwyn 2008; Liepins & Thomas 1988; Moeller et al. 2006; Nagra 2002; NDA 2012; Van Konynenburg 1994; Yim & Caron 2006). ^{14}C is a radionuclide considered in safety analysis for several reasons: i) its rather long half-life (5,700 years); ii) ^{14}C can be present in the disposal facility and the host rock both as dissolved and gaseous species; iii) dissolved and gaseous ^{14}C-bearing organic compounds readily migrate in the near-field and the geosphere due to weak interaction with mineral surfaces in alkaline to near-neutral conditions; and iv) ^{14}C is taken up by the biosphere. The chemical form of the ^{14}C-bearing carbon species dictates the routes of ^{14}C migration in the EBS of a deep geological repository and the surrounding host rock and therefore determines the long-term contribution of ^{14}C to dose release from a repository for radioactive waste. If ^{14}C is released as dissolved (inorganic or organic) compounds, it can be retained within the multi-barrier system of the deep geological repository long enough for it to decay, while higher radiological consequences may occur if ^{14}C is released as volatile (inorganic or organic) compounds, for which weaker retention is anticipated.

In the Swiss waste inventory, the main sources of ^{14}C are activated metallic waste originating from the decommissioning of nuclear power plants (NPP), the operation of NPPs, reprocessing waste, reactor waste and waste from medicine, industry and research (MIR) (Nagra 2023). The ^{14}C-containing metallic (e.g., steel, Zircaloy), inorganic (e.g., vitrified HLW) and organic (e.g., spent ion-exchange resins) waste materials are prone to degradation processes in a deep geological repository. These processes start as soon as the waste materials are exposed to water and there is sufficient water for the degradation process to continue, which depends on the development of the saturation state of the deep geological repository. Corrosion of the activated metal components will occur upon disposal in the deep geological repository leading to the release of ^{14}C as aqueous and gaseous carbon compounds. The dissolution of fuel pellets and the glass matrix of vitrified waste from reprocessing also leads to the release of ^{14}C. Once exposed to porewater, ^{14}C is expected to be rapidly released from contaminated waste, where it is only present at the material surface. Over time, ^{14}C-bearing organic compounds released due to corrosion of activated metals and from contaminated waste will be subject to microbial, radiolytic and possibly chemical degradation processes, to an extent that is directly dependent on the local conditions in the deep geological repository. These compounds can be degraded by microbial processes in circum-neutral to weakly alkaline conditions and likely by non-biological processes in strongly alkaline conditions (pH > 11). All these processes may result in a slow but ongoing generation of ^{14}C in the near-field of a repository.

1.3 ^{14}C in the environment

^{14}C is naturally produced by interaction of cosmic rays with gases in the upper atmosphere (Broecker 2014; Larivière & Guérin 2010; UNSCEAR 2008). Cosmic radiation contains high-energy particles emanating from extraterrestrial sources, which produce a cascade of secondary particles and radiation upon interaction with the atmosphere, such as protons, spallation neutrons and gamma radiation. ^{14}C is generated by the interaction of thermal neutrons with nitrogen-14 (^{14}N) atoms present in the atmosphere and by subsequent decay of the nuclei into ^{14}C along with the release of a proton. The atmospheric production rate of ^{14}C was estimated at 2.5 atoms/cm^2/s ($\sim 1.4\times10^{15}$ Bq/a), which is the highest production rate among all other cosmogenic radionuclides (Larivière & Guérin 2010; UNSCEAR 2008). Once produced in the atmosphere, ^{14}C atoms become rapidly oxidised to ^{14}CO and subsequently to $^{14}CO_2$ gas, from which it enters Earth's carbon cycle. It decays by beta emission with a maximum energy of 0.155 MeV. The annual effective dose due to cosmogenic radionuclides, considered as a fixed value, is estimated at 0.01 mSv/a globally (UNSCEAR 2008). The rather long half-life of ^{14}C allows the radioisotope to be distributed through the Earth's various active carbon reservoirs. Isotopic dilution is the basic principle governing the transfer of ^{14}C between these reservoirs, which assumes that the isotopic ratio between radiocarbon and stable carbon is maintained in each compartment. This implies that the fate of ^{14}C is identical to that of stable carbon. The exchange with terrestrial carbon reservoirs occurs on various time scales (Broecker 2014). $^{14}CO_2$ exchange occurs with the inorganic carbon dissolved in surface waters (rivers, lakes, surface mixed layers of ocean). Photosynthesis leads to $^{14}CO_2$ uptake by both terrestrial and aquatic plants and subsequent incorporation in the human food chain. The ^{14}C specific activity of the human body is rapidly equilibrated with that of the atmosphere within a time period of only about 1.4 years (Nydal & Lovseth 1965). The steady-state fractional inventories of the various exchange reservoirs have been estimated as follows: 1.9% in the atmosphere, 4% on the surface of the earth, 94.2% in the mixed and deep layers of the ocean and 0.2% in ocean sediments (Larivière & Guérin 2010). ^{14}C is mainly diluted in the ocean water, while the amount of ^{14}C present in the atmosphere and on the surface of the Earth is significantly smaller. The resulting balance between production, exchange with reservoirs and decay has led to an almost steady atmospheric $^{14}CO_2$ concentration in the past.

Large-scale combustion of fossil fuels since about 1860 has resulted in the depletion of the natural atmospheric ^{14}C activity concentration (Suess effect). Fossil fuel contains only stable carbon (^{12}C and ^{13}C) and no ^{14}C, which is due to the extremely long residence time since their formation. Anthropogenic ^{14}C was produced during the late 1950s and early 1960s as a result of thermonuclear weapons tests carried out in the atmosphere (Broecker 2014; Nydal & Lovseth 1965; UNSCEAR 2008). The spallation neutrons captured by atmospheric ^{14}N were by-products of the fusion reactions. During this bomb-testing period, the number of anthropogenic ^{14}C atoms in the atmosphere was roughly equal to the number of naturally produced ^{14}C atoms. The production of anthropogenic ^{14}C (total $\sim 3.5\times10^{17}$ Bq) stopped with the implementation of the ban on atmospheric weapons tests on 1st January 1963 (Broecker 2014). Since then, the atmospheric excess of ^{14}C has strongly decreased due to exchange processes with oceanic CO_2 and the terrestrial biosphere. By 2000, bomb-produced ^{14}C constituted less than 10% of the atmospheric radiocarbon inventory (Broecker 2014).

In summary, Earth's atmosphere and biosphere are subjected to a constant flux of ^{14}C and exchange of natural and anthropogenic ^{14}C. ^{14}C is present in the chemical form of $^{14}CO_2$ and, through this species, is incorporated into Earth's carbon cycle. This implies that any dose impact of ^{14}C released from a deep geological repository has to be assessed with consideration of the natural ^{14}C background and the chemical form of the released ^{14}C (Neeft 2018).

1.4 Scope of the report

This report describes and evaluates the fate of ^{14}C in the context of a Swiss deep geological repository for both HLW and L/ILW. The main objective is to present a state-of-the-art overview of processes and phenomena associated with the ^{14}C release from a deep geological repository near-field into the host rock.

The following subjects will be specifically addressed and discussed:

- Chemical forms of ^{14}C in the waste forms to be disposed of in Switzerland.
- Chemical degradation of ^{14}C-containing waste materials leading to ^{14}C release.
- Speciation of ^{14}C in the repository near-field.
- Chemical stability of ^{14}C-bearing carbon compounds in the repository environment.
- Retention of the ^{14}C-bearing carbon species in the near-field and host rock.

This report provides an appraisal of the current understanding of ^{14}C sources, generation, reactions and interactions, and transport, summarising and reviewing the information available in the literature. In particular, it is the scientific basis for defining the ^{14}C-treatment in post-closure safety assessments in the framework of the general licence application.

Post-closure safety assessments and site-specific dose calculations for ^{14}C in both dissolved and gaseous phases are available in Nagra (2024f, in prep.) and Nagra (2024c, in prep.), respectively.

1.5 Outline

The report is structured as follows:

- Chapter 2 summarises sources and key processes, as well as the evolution of geochemical conditions in the L/ILW and HLW repositories.
- Chapter 3 gives an overview of the ^{14}C sources in specific waste materials and an assessment of the degradation of ^{14}C-containing metallic and organic waste materials.
- Chapter 4 reports an assessment of the ^{14}C speciation in the repository near-field based on thermodynamic calculations and kinetic considerations.
- Chapter 5 summarises current scientific understanding of the ^{14}C speciation during the degradation of activated metallic and organic waste materials.
- Chapter 6 summarises current scientific understanding of the retention of ^{14}C-bearing carbon compounds in the near-field and host rock.
- Chapter 7 provides an overall assessment of the chemical forms of ^{14}C generated under the conditions of the HLW and L/ILW repositories.
- Chapter 8 comprises a summary of this report and highlights the main conclusions.

2 Fate of ^{14}C in the context of a deep geological repository

2.1 Key processes

An overview of the key processes affecting the fate of ^{14}C in deep geological repositories is displayed in Fig. 2-1. This schematic layout of processes has been reported previously within the framework of the British waste management programme (NDA 2012; Hoch et al. 2016).

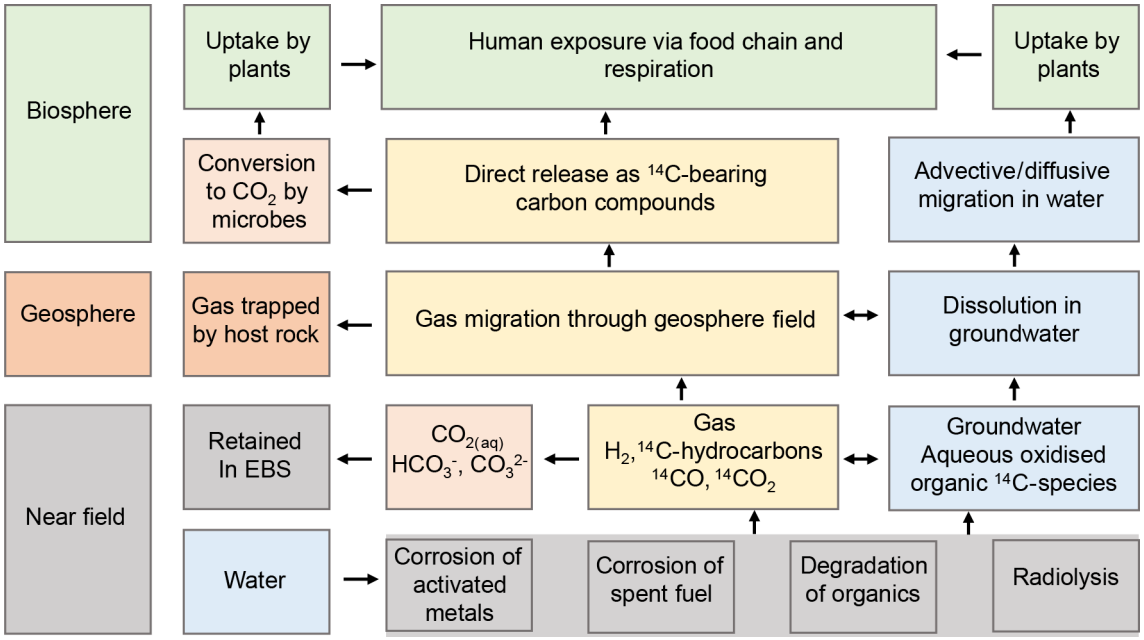

Fig. 2-1: Key generation and migration process of ^{14}C-bearing carbon compounds

Modified from Hoch et al. (2016)

^{14}C-containing waste materials, such as activated metals, SF and organic substances will be emplaced in deep geological repositories. The amounts (i.e., mass, volume) and the radionuclide inventories of the individual waste packages to be disposed of in the Swiss deep geological repository have been compiled specifically for the general licence application in the MIRAM-RBG database (Nagra 2023) (see Chapter 3).

Over time, these materials either corrode or degrade, thus giving rise to the release of ^{14}C in aqueous or gaseous chemical form (see Chapters 4 and 5). The corrosion of metals, radiolysis and the degradation of organic materials will generate gas in the near-field of a deep geological repository. At the same time, ^{14}C-bearing carbon compounds are produced as a result of the corrosion of activated metals, dissolution of SF and glass matrices and by the contact of contaminated waste with porewater. These are the main processes leading to the production of ^{14}C-bearing carbon compounds. Geochemical conditions in the near-field determine the kinetics and the products formed in the course of these processes, while the corresponding inventories of the waste materials determine the amount of products released over time.

Retention of the organic and gaseous ^{14}C-bearing carbon compounds in the near-field is weak (see Chapter 6). Organic ^{14}C will slowly diffuse into the host rock where a large portion of the released ^{14}C may decay over time due to the low permeability of the OPA host rock. Alternatively, $^{14}CO_2$ and $^{14}CH_4$ could be generated by the degradation of the ^{14}C-bearing organic molecules. Once

generated, CO_2(aq) (or its bases HCO_3^-, CO_3^{2-}) is strongly retarded both in the EBS and the host rock, likely due to an isotopic exchange process with calcite (see Chapter 6). By contrast, ^{14}C-bearing hydrocarbons (HCs), in particular $^{14}CH_4$, and possibly also ^{14}CO, can migrate through the host rock with time due to weak retention (see Chapter 6). Microbial activity in the OPA host rock and the overlying formations, however, may delay or even prevent gas migration (Fig. 2-1). If gas is able to reach the biosphere, it could be released directly as $^{14}CH_4$ or converted to $^{14}CO_2$ by microbes in the soil zone. $^{14}CO_2$ could then be taken up by plants and, hence, join the food chain. $^{14}CH_4$ could also be released to the atmosphere where it contributes to the atmospheric ^{14}C inventory in addition to other ^{14}C-bearing carbon compounds, such as naturally produced $^{14}CO_2$. More detailed descriptions of the migration of ^{14}C in the near-field and the host rock and its overlying formation to the biosphere have been reported elsewhere (Nagra 2024f, in prep.).

2.2 Source of ^{14}C in radioactive waste

2.2.1 Sources of ^{14}C from reactor operation

The main sources of ^{14}C are reactor waste and decommissioning waste. In LWRs, ^{14}C is present in fuel assemblies (SF, e.g., UO_2, cladding, and fuel assembly hardware), non-fuel assembly core-structural materials, and reactor cooling water (Van Konynenburg 1994; Yim & Caron 2006). The amount of ^{14}C produced during operation depends on the type of reactor used for electricity production, the properties of the structural materials used, the operation process, and the treatment applied to the coolant. The production rate of ^{14}C in activated materials further depends on the spectrum and flux of neutrons in the reactor, as well as on the cross-sections and concentration of activated isotopes (see Tab. 2-1). Due to the very high neutron flux in the core of an NPP, which is several orders of magnitude larger than the environmental neutron flux at the Earth's surface, ^{14}C is contained in some radioactive waste at high-activity concentrations (Neeft 2018). After decommissioning, activated reactor waste is subject to disposal. In the case of SF, ^{14}C is present in the SF, in Zircaloy cladding and stainless steel alloy assembly components.

Small quantities of the ^{14}C produced in NPPs can be released directly to the environment in gaseous discharges or in much smaller quantities in liquid effluents (Van Konynenburg 1994). The remaining ^{14}C inventory is associated with reactor waste produced during the operation of NPPs and ^{14}C produced by activation of the core structural materials and by fuel and fuel assembly parts. In the case of direct disposal of SF, the entire ^{14}C inventory remains in the fuel element components, while in the case of reprocessed SF, ^{14}C is redistributed among the different forms of reprocessing waste. Furthermore, a portion of ^{14}C in SF may be lost from the external surface during storage in SF pools (Van Konynenburg 1994). During reprocessing, some ^{14}C may be released during SF dissolution and released as gaseous ^{14}C-bearing CO_2. This inorganic ^{14}C is scrubbed out from the gas phase and discharged as a liquid effluent, or converted into a solid (NDA 2012), such as vitrified waste. Estimates of the annual normalised ^{14}C production rates by pressurised water reactors (PWR) and boiling water reactors (BWR) have been reported elsewhere (Yim & Caron 2006).

The principal source of ^{14}C production is the transmutation of ^{14}N by thermal neutrons (Tab. 2-1). Transmutation of carbon-13 (^{13}C) and oxygen-17 (^{17}O) are additional routes that can affect the ^{14}C inventory in some waste. The parent isotopes are present as major components or impurities in the source materials.

Tab. 2-1: ^{14}C generation mechanisms

Isotope	Nuclear reaction	Isotopic abundance (%)	Thermal neutron cross-section (barns)
^{14}N	$^{14}N(n,p)^{14}C$	99.632	1.82
^{17}O	$^{17}O(n,\alpha)^{14}C$	0.038	0.235
^{13}C	$^{13}C(n,\gamma)^{14}C$	1.07	0.0014

The main inventories of ^{14}C in waste from LWRs originate from the transmutation of ^{14}N impurities in fuel (UO_2 or mixed oxide (MOX)), Zircaloy cladding, stainless steel and nickel alloys used in fuel assemblies and support hardware (Johnson & Schwyn 2008; Yim & Caron 2006). For example, ^{14}N is introduced into UO_2 pellets during sintering (Ferrari 1963). UO_2 powder is manufactured by the reduction of UO_3 or U_3O_8 with H_2, while production routes exist that convert UO_3 into UF_6 (for enrichment) prior to reduction to UO_2 by the ammonium diuranate process (wet route) (Van Konynenburg et al. 1987). Sintering is performed in a commercial nitrogen, cracked ammonia or an H_2 atmosphere that contains some ^{14}N as an impurity (Ferrari 1963). For the sintering, binders made of polyethylene glycol with high molecular weights are employed, thus leading to the presence of carbon compounds (CO/CO_2) in the sintering atmosphere (Ferrari 1963). The cladding of the fuel rods of LWRs usually consists of zirconium alloys (trade name Zircaloy) with more than 90 weight (wt.) % Zr and minor additions of other metals such as Sn, Nb, Fe, Cr or Ni. Zirconium allows sustained fission reaction thanks to low absorption cross-sections for thermal neutrons, while the minor metals improve mechanical properties and corrosion resistance of the cladding (Adamson & Rudling 2013; Bragg-Sitton 2012; Garzarolli et al. 1996). Stainless steel and nickel alloys are used for specific parts of the fuel assemblies, such as bottom and top nozzle structures that provide mechanical support for the fuel assembly structure. Some ^{14}C contributions arise from the reaction $^{17}O(n,\alpha)^{14}C$ in case of the UO_2 fuel or MOX and from the reaction $^{13}C(n,\gamma)^{14}C$ in case of the stable carbon-containing metallic materials such as stainless steel (Yim & Caron 2006). The latter contributions, however, are expected to be small in comparison with the transmutation of ^{14}N in metals exposed to thermal neutrons (Johnson & Schwyn 2008; Yim & Caron 2006). Activation of ^{14}N is the dominant process due to the high isotopic abundance of ^{14}N and the large cross-section of ^{14}N for thermal neutron capture (Tab. 2-1). Nevertheless, despite its abundance and large cross-section, only a small fraction of ^{14}N is converted to ^{14}C (see Section 3.1). Abundance and thermal neutron cross-sections of ^{17}O and ^{13}C are much lower, thus limiting the contribution of these routes to ^{14}C production.

An additional source of ^{14}C is reactor coolant by transmutation of ^{17}O bound in H_2O and in oxidised aqueous carbon species (bicarbonate and organic compounds), as well as due to the presence of traces of dissolved N_2 in water. The main reaction in water is $^{17}O(n,\alpha)^{14}C$. Most of the ^{14}C produced in cooling water is exhausted to the atmosphere while only a small fraction is bound by ion-exchange resins (IER) integrated in the reactor coolant circuit (Kunz 1985; Van Konynenburg 1994). According to Yim & Caron (2006), about 30 - 45% of the ^{14}C inventory in BWRs originates from the transmutation of mainly ^{17}O in reactor coolant whereas 55 - 70% can be attributed to the transmutation of ^{14}N impurities in Zircaloy and fuel assemblies. The ^{14}C inventory originating from reactor coolant was reported to be slightly higher in PWRs, i.e., 50 - 60% (Yim & Caron 2006).

2.2.2 L/ILW

The ^{14}C inventory in L/ILW is fully reported in Nagra (2023) and detailed in Nagra (2024d, in prep.). The distribution of the ^{14}C-containing waste forms is shown in Fig. 2-2.

The largest proportion of the ^{14}C inventory is associated with activated metals (~ 67%), mainly originating from the decommissioning of NPPs. Decommissioning waste further includes activated and contaminated (metallic, organic, inorganic) materials, such as activated concrete from structural elements located close to the reactor core in NPPs. Some ^{14}C-containing L/ILW waste forms arise from reprocessing operations, however at much lower proportions, such as activated Zircaloy and vitrified waste. Operational waste mainly comprises ^{14}C-containing spent IERs and filters originating from the treatment of reactor coolant and poorly specified contaminated materials. Some ^{14}C is associated with contaminated MIR waste, i.e., metallic, organic and inorganic waste forms, presumably with ^{14}C present in various chemical forms. MIR wastes are mainly generated by the two research facilities, PSI and CERN. $Ba^{14}CO_3$ is present in MIR waste and reprocessing waste (vitrified $BaCO_3$ crud). The remaining ^{14}C inventory is associated with activated graphite from research reactors as well as incineration ashes and other poorly specified contaminated waste forms.

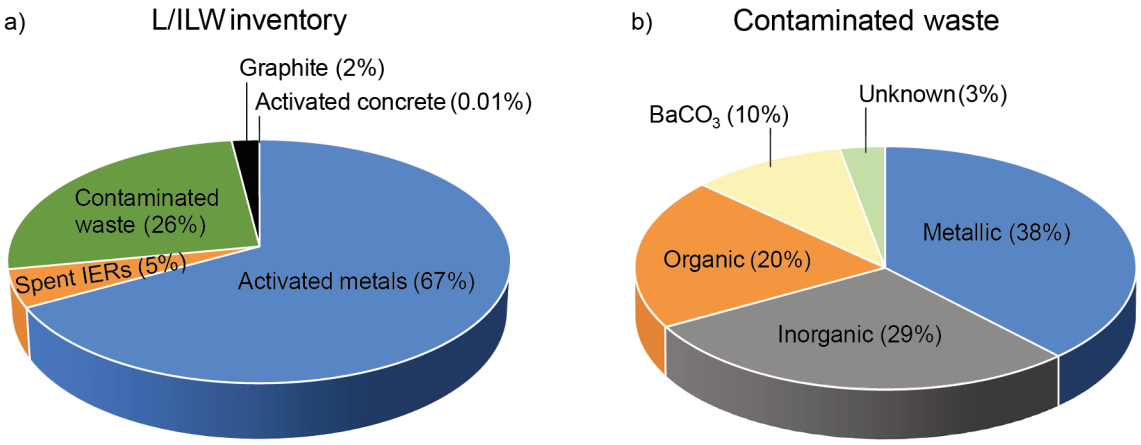

Fig. 2-2: ^{14}C inventories in L/ILW according to the MIRAM-RBG database. a) Important waste forms in L/ILW; b) Distribution of contaminated waste

From Nagra (2023)

2.2.3 HLW

The two HLW waste forms, i.e., SF components (activated fuel rods and fuel assembly parts) and vitrified HLW from reprocessing, will be loaded into disposal canisters (Nagra 2024d, in prep.). Activated fuel rods consist of stacks of cylindrical ceramic pellets of UO_2 (or a blend of UO_2 and PuO_2 for MOX) in tubes made of Zircaloy. SF contains a wide variety of radionuclides including fission products and activation products. ^{14}C is associated with both fuel pellets and structural materials (Zircaloy, and spacers and plates made from stainless steel and nickel alloys from fuel assemblies) generated by irradiation of the materials.

In the case of vitrified HLW, the highly radioactive liquid from reprocessing is evaporated, calcined and mixed at high temperatures with borosilicate glass-forming additives to produce a homogeneous glass matrix (Bradbury et al. 2014). The glassy mix is poured into stainless steel containers and allowed to solidify before being sealed by welding.

2.3 Evolution of repository and geochemical conditions

2.3.1 Near-field of the L/ILW repository

The long-term evolution and the geochemical conditions of a cement-based near-field have been addressed in detail elsewhere (Kosakowski et al. 2023; Nagra 2024i, in prep.). The main features of the EBS and the evolution of the geochemical conditions are briefly summarised as follows.

The current concept foresees that L/ILW is placed in waste packages and, in most cases, conditioned in cementitious materials and occasionally also in bitumen, polystyrene or borosilicate glass matrix. The waste packages will be packaged in prefabricated disposal containers made of reinforced concrete, which are filled with a porous hydraulic binder and emplaced in the cavern of the deep geological repository. Once filled with containers, L/ILW caverns are backfilled with cement. Overall, the large amount of cementitious material (concrete, backfill mortars) in the L/ILW repository imposes alkaline conditions on the near-field.

The evolution of the L/ILW near-field is mainly controlled by the very slow resaturation of the backfilled emplacement caverns by groundwater, gas production by metal corrosion, degradation of the organic waste materials and the physico-chemical interaction of the intruding porewater with the cementitious backfill and the waste materials (Nagra 2024e, in prep.). The gases will mix with the remaining air and accumulate in the porous mortar in the upper part of the cavern, while saturation with groundwater from the host rock is expected to preferentially intrude into the lower parts of the cavern. Hence, partially saturated conditions might persist in the near-field for a very long period of time (Nagra 2024e, in prep.). The geochemical conditions in the near-field critically determine the course of gas production with time, due to the pH dependence of the anoxic corrosion of carbon steel. In particular, pH alters with time due to the degradation of hydrated cement, which is caused by the degradation of organic waste materials (production of CO_2), the dissolution of aggregates (release of SiO_2) and the ingress of OPA porewater. However, the chemical reactions leading to the evolution of the system only proceed if a sufficient amount of water is present, either as an aqueous phase or as water vapour associated with the high humidity (Kosakowski et al. 2014, 2020). The average temperature in the L/ILW repository is expected to be below 50 °C, depending on the depth of the deep geological repository (Kosakowski et al. 2023; Nagra 2024i, in prep.). The temperature increase generated by exothermic cement hydration would occur within a few months, leading to a relatively short-term temperature increase within and around the repository. Heat-producing L/ILW is expected to be limited to around 5 – 10 °C (Leupin et al. 2016a).

The degradation of hydrated cement is usually described in terms of a series of consecutive stages of decreasing porewater pH, irrespective of the underlying degradation process (i.e., carbonation, dissolution of siliceous aggregates, ingress of formation water) (Kosakowski et al. 2014, 2020; Wieland & Kosakowski 2020). The duration of the different stages is controlled by the hydraulic permeability of the host rock (intruding groundwater), the degree of capillary suction and the kinetics of the degradation processes in the waste matrix (i.e., degradation of organic materials, ongoing pozzolanic reaction due to the dissolution of Si-containing aggregates). It is expected that the second stage of cement degradation, where the pH is controlled by portlandite solubility and fixed at ~ 12.5, will dominate over a long period of time (Kosakowski et al. 2014, 2023). Nevertheless, cement degradation by carbonation and the dissolution of aggregates may significantly shorten the duration of this stage (Kosakowski et al. 2020).

The evolution of the redox conditions in a cement-based ILW repository was reported in detail elsewhere (Wersin et al. 2003). It is assumed that residual oxygen is depleted within several hundreds of years after repository closure due to oxic corrosion of metals and microbial activity. Thus, the geochemical conditions are expected to remain reducing in the long term. The redox potential was found to be largely influenced by steel corrosion due to the large iron inventory in

L/ILW (Nagra 2023). Other processes that could influence redox conditions, such as radiolysis, the degradation of organic matter and other microbially mediated processes, were considered to be negligible with regard to the waste inventory and chemical conditions in the cementitious near-field. In the Swiss deep geological repository, the redox conditions were mainly controlled by Fe(III)/Fe(II) redox equilibria (Grauer 1988; Wersin et al. 2003). It was further assumed that magnetite is the only corrosion product that forms on the steel surface under anoxic conditions in the long term. Then, the assumption that the formed magnetite is in equilibrium with crystalline goethite, which should be the most thermodynamically stable Fe(III) mineral in hydrated cement, resulted in a very low E_h value of -742 mV at pH 12.55. However, the E_h value was estimated at -226 mV on the assumption that magnetite is in equilibrium with an unknown Fe(III)-containing cement material in cement paste. This assumption is supported by the relatively high Fe(III) concentration (10^{-7} M) that was experimentally determined in the porewater of hydrated cement. In general, the predicted E_h was found to be strongly dependent on the type of solid Fe(II,III) redox partners assumed to be present under the highly alkaline conditions of the cementitious near-field.

By way of illustration, a representative composition of a porewater in the second stage of cement degradation is listed in Tab. 2-2. The properties are consistent with those derived from models of the degradation of several cementitious materials that might be present in an emplacement cavern (Wieland & Kosakowski 2020).

Tab. 2-2: Representative compositions of porewaters in the L/ILW and HLW near-fields

	L/ILW – cement* Stage II porewater	HLW – bentonite** Reference water
pH	12.89	7.24
E_h (V)	- 0.38	- 0.173
I (m)	0.355	0.452
Element	Molality (mol/kg_w)	Molality (mol/kg_w)
Na (mol/kg_w)	0.156	0.375
K (mol/kg_w)	0.189	1.83×10^{-3}
Ca (mol/kg_w)	6.60×10^{-3}	1.77×10^{-2}
Mg (mol/kg_w)	$\leq 10^{-8}$	1.02×10^{-2}
Al (mol/kg_w)	1.69×10^{-5}	2.08×10^{-8}
CO_3 (mol/kg_w)	3.46×10^{-5}	2.94×10^{-3}
SO_4 (mol/kg_w)	5.07×10^{-4}	7.86×10^{-2}
Cl (mol/kg_w)	0.240	0.239
SiO_2 (mol/kg_w)	3.01×10^{-4}	1.70×10^{-4}
logpCO_2 (bar)	-	-2.20

* Kosakowski et al. (2023)
** Curti et al. (2023)

In some waste containers, conditions favourable for microbial activity may exist in isolated niches of the waste matrix due to less alkaline pH (heterogeneity of the waste matrix). Under these conditions, organic matter can be degraded by microorganisms to produce CO_2 and CH_4. Nevertheless, due to the large amounts of cementitious backfill surrounding the waste containers and allowing for high pH conditions, microbial activity in the cementitious backfill of the L/ILW repository is not expected to be significant (Guillemot et al. 2023).

2.3.2 Near-field of the HLW repository

The long-term evolution of temperature and geochemical conditions in an HLW repository has also been addressed in detail (Curti et al. 2023; Nagra 2024i, in prep.). The main features of the EBS and the evolution of geochemical conditions are briefly summarised below.

The current reference design envisages the disposal of SF assemblies and fabrication flasks with vitrified HLW in horizontal emplacement drifts excavated in the OPA formation. Both types of waste forms will be loaded into disposal canisters fabricated from carbon steel, possibly with a copper coating. The canisters will be emplaced coaxially, within a system of parallel tunnels, on a pedestal made of highly compacted bentonite blocks prior to backfilling of the remaining open spaces with granular, compacted bentonite. The bentonite blocks and granules together form a protective mechanical barrier and a chemical buffer in addition to the canisters containing the waste.

After emplacement of the canisters and sealing with bentonite, there will be a resaturation of the initially "dry" compacted bentonite with porewater intruding from the OPA host rock. Resaturation will start after closure of the repository and is expected to progress slowly over a period of about 200 years (Curti et al. 2023; Nagra 2024i, in prep.). The interplay of various thermal, hydraulic, mechanical and chemical (THMC) processes will control the evolution of the HLW near-field over time, i.e., saturation of the backfilled emplacement drifts, heat generation, gas production, swelling of the bentonite buffer and the reconsolidation of the surrounding host rock (i.e., the excavation-damaged zone, EDS).

The temporal evolution of the geochemical conditions in the near-field of the repository is determined by heat generation, saturation of the bentonite backfill with OPA porewater and gas production due to the corrosion of the carbon steel containers (Bradbury et al. 2014; Curti et al. 2023). Also, in the case of the HLW repository, the chemical reactions leading to the evolution of the system require the presence of a sufficient amount of water, either in the form of a (stagnant or mobile) aqueous phase or a humid atmosphere. In the presence of water, chemical processes start that lead to chemical interactions between the various near-field components and those at the tunnel-host rock interface. The oxygen content in the near-field will gradually decrease as oxygen is consumed by metal corrosion, microbial activity or oxidation of minerals (e.g., pyrite). The initially oxic conditions in the compacted bentonite backfill are expected to persist for only a few months after closure (Giroud et al. 2018), whilst reducing conditions will prevail in the long term despite the production of radiolytic oxidants at solid-water interfaces.

Temperature gradients will develop radially from the canister through the bentonite backfill into the OPA host rock as SF and HLW generate heat from the decay of radionuclides in the waste. The steep temperature gradient in the early stage of repository evolution is expected to prevent bentonite from being saturated in the short term and may lead to mineral transformations (Curti et al. 2023; Nagra 2024i, in prep.). In general, however, heat generation decreases over time, which will eventually lead to saturation of the bentonite.

Gas production in the near-field of the HLW repository is mainly the result of the anoxic corrosion of the carbon steel canisters over time, thus producing H_2 gas and corrosion products that interact with the bentonite backfill. The canisters are expected to remain intact for at least 10,000 years (Nagra 2024d, in prep.). During corrosion, the amount of gas produced from stable carbon

contained in the steel (e.g., the formation of CH_4, and other HCs) is much less than H_2 production. The evolution and extent of pressure build-up by H_2 in the near-field will depend mainly on the relative rates of gas production and consumption/dissipation (Nagra 2024e, in prep.). A slow but continuous pressure build-up in the near-field with time will impede the ingress of OPA porewater and thus, in addition to temperature gradients, slow down the saturation of the bentonite backfill.

The evolution of the geochemical conditions of the HLW repository will occur over a very long period, i.e., many hundreds of thousands of years. The time scale is determined by the time required for dissipation of gas from the near-field into the host rock and, conversely, for the diffusion-controlled ingress of groundwater from the host rock. The composition of a representative porewater for the HLW repository listed in Tab. 2-2 was reported by Curti et al. (2023). The geochemical conditions in the near-field of the HLW repository are very different from those of the cement-based L/ILW repository. In particular, the pH of ~ 7.2 is controlled by the carbonate system, in contrast to pH > 11 for a cementitious near-field controlled by portlandite solubility and the precipitation/dissolution of cement phases.

2.4 Summary of chapter

The most important sources of ^{14}C in the LWRs are nuclear fuel components, reactor core structural materials and reactor coolant. The ^{14}C inventories of the waste forms produced in Switzerland are fully described in the MIRAM-RBG database (Nagra 2023). In the cement-based L/ILW repository, ^{14}C-containing wastes will include wastes from reactor operation and decommissioning, such as activated Zircaloy and steel, spent IERs, filter cartridges and crud, but also reprocessing waste, such as $BaCO_3$. In an HLW repository, the ^{14}C inventory is associated with spent fuel components (SF, Zircaloy cladding, and fuel assembly hardware) as well as vitrified HLW from reprocessing.

The principal route of ^{14}C production is the transmutation of ^{14}N present as an impurity in the metallic parts exposed to thermal neutron flux in the reactor. Transmutation of ^{17}O is expected to contribute to the ^{14}C inventory in SF. Transmutation of ^{17}O bound in water molecules and in oxidised, aqueous carbon species (bicarbonate and organic compounds) as well as of ^{14}N present at trace levels in water are the source of ^{14}C in reactor coolant. In a deep geological repository, ^{14}C-bearing carbon compounds are released to the liquid and gas phases over time due to the degradation of ^{14}C-containing waste materials.

Evolution of the geochemical conditions in an L/ILW repository is controlled by the ingress of OPA porewater, the dissolution of aggregates (release of SiO_2 giving rise to ongoing pozzolanic reaction) and, in niches with lower pH, the degradation of organic waste materials (production of CO_2 leading to carbonation). Evolution of the HLW near-field is controlled by the initially steep temperature gradient and gas production from the corrosion of the carbon steel canisters. In both near-fields, resaturation of the backfilled emplacement caverns fundamentally determines the geochemical evolution over time, i.e., the chemical processes only take place if sufficient water is available. The presence of water in the near-field affects ^{14}C release from the ^{14}C-containing wastes in both repositories.

3 Carbon-14-containing waste materials

The following discussion focusses on the chemical forms of ^{14}C in the different waste materials and on the chemical forms in which ^{14}C is released, i.e., in the aqueous chemical form as inorganic or organic carbon compounds, or in the gaseous chemical form (Fig. 3-1). The three chemical forms exhibit very different physico-chemical properties, which gives rise to very different behaviours in the deep geological repositories. An understanding of the production of ^{14}C in the various waste forms allows a qualitative and quantitative assessment of the chemical form of ^{14}C in the waste streams.

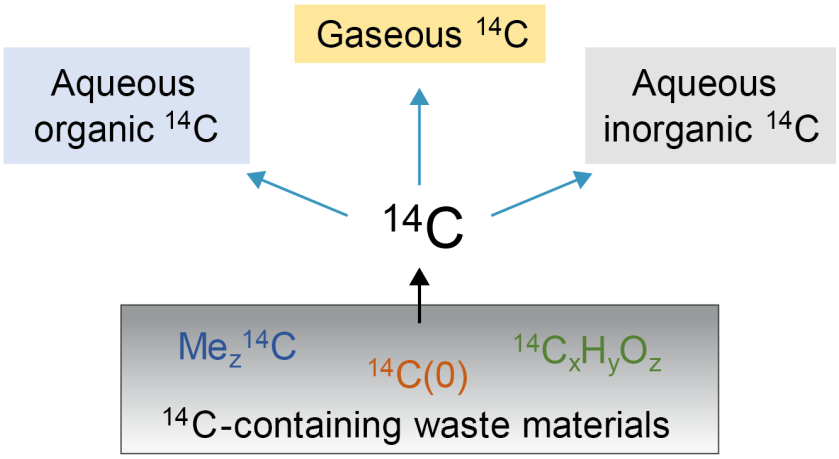

Fig. 3-1: Schematic illustration of potential chemical forms of ^{14}C in the waste materials and classification as one of the three main chemical forms after release (aqueous inorganic and organic species, and gaseous species[1])

Me_xC:carbides, C(0): elemental carbon, oxidised carbon compounds ($C_xH_yO_z$, $z \neq 0$)

3.1 Activated waste

3.1.1 Nitrogen and carbon content of steels

Carbon steel and stainless steel are, besides Zircaloy, the most important activated metallic waste forms. Cast irons are unlikely to be present in the activated waste and are therefore not considered further. All these metals contain stable carbon ($^{12/13}C$ isotopes) and nitrogen (^{14}N) of different contents, which are, in principle, subject to conversion into ^{14}C by activation (Tab. 2-1). Hence, the inventory of the elements subject to activation and duration of exposure to thermal neutron flux accounts for the ^{14}C inventory associated with the materials. In addition, stable carbon associated with metals is the source of stable carbon compounds released to the liquid and gas phases by metal corrosion along with H_2. Therefore, stable carbon compounds are also present in the porewater and in the gas phase of the HLW and L/ILW near-fields. While they do not

[1] The term gaseous species employed in this report only refers to organic compounds (i.e., CH_4) as inorganic ones (i.e., CO_2) are supposed to react with cementitious materials (for the L/ILW repository part) and carbonate content of the bentonite (for the HLW repository part).

contribute to dose release over time, they are simultaneously released with ^{14}C-bearing carbon compounds (and H_2).

The term “steel” identifies a large family of iron-based alloys containing manganese, carbon at typically less than 2.5 wt.%, and other alloying elements (e.g., Cr, Ni, Nb, etc.). The carbon content influences the strength and hardness of steels. Standard steels are alloys that consist mainly of iron and carbon and are divided broadly into two main groups with respect to their chemical composition: carbon steels and alloy steels, the latter including also stainless steels (Davis 1991; Oberg et al. 2012).

Carbon steel is an iron-carbon alloy with a carbon content of less than 2 wt.% containing small amounts of alloying elements, such as silicon, copper, phosphorous, sulphur, and oxygen. Various grades of carbon steel are available commercially, which differ in the production process and the exact concentrations of the minor elements, particularly carbon. A steel qualifies as carbon steel when the amounts of alloying elements are limited, i.e., manganese (1.65 wt.% max.), silicon (0.6 wt.% max) and copper (0.6 % wt.% max) (Davis 1991). Carbon steels are classified as low- (up to 0.3 % C), medium- (0.3 - 0.6 % C) and high-carbon steels (0.6 - 1 % C).

Alloy steel refers to a steel refined on the basis of carbon steel using alloying elements, such as chromium, nickel, molybdenum, tungsten, vanadium, titanium etc., in order to improve material performance, such as corrosion resistance. Stainless steel is an iron-carbon alloy with superior corrosion resistance to carbon steels and low-alloy steels due to the addition of at least 10 wt.% chromium with or without other elements, which induces passivity of the ferrous alloy (Oberg et al. 2012). Most stainless steels have nickel contents ranging between 1 wt.% and 30 wt.%. Stainless steels are used for service at elevated temperatures and in aqueous environments due to their corrosion resistance, which is provided by a very thin surface film of stable chromium oxyhydroxide. The so-called passive film is self-healing in a wide variety of environments.

Stainless steels are classified, according to the predominant crystal structure, as ferritic (body-centred cubic), austenitic (face-centred cubic), martensitic (body-centred tetragonal) or ferritic-austenitic, containing roughly equal proportions of the two structures (Davis 1991; Oberg et al. 2012). Addition of chromium, molybdenum and silicon promotes the formation of ferrite (magnetic), while addition of carbon, nickel, nitrogen and manganese promotes the formation of austenite (non-magnetic). Carbon and nitrogen promote the formation of austenitic steel. The carbon content ranges between ~ 0.05 wt.% and 0.3 wt.% in corrosion-resistant steels, while it is higher (0.2 - 0.8 wt.%) in heat-resistant alloys (Davis 1991). Refined processes in stainless steel melting practice have led to the introduction of nitrogen up to levels of ~ 0.06 wt.% - 0.09 wt.% on a routine basis. Nitrogen influences the phase equilibrium in Fe-Cr-Ni melts and the agglomeration of carbide, which determine the mechanical properties of austenitic steel. Up to 0.2 wt.% nitrogen can be accommodated in steel without difficulty.

A variety of stainless-steel grades are available commercially (App. A). The activated metallic materials expected to be disposed of in the deep geological repositories will comprise various types of steels. Stainless steel used in the nuclear industry seems to be primarily from the 300 series of austenitic, nickel-containing grades (18 wt.% chromium and 8 wt.% nickel) due to the specific requirements concerning durability, compressive strength and corrosion resistance (Feron 2012; Sedriks 1996). The two most widely used grades are Types 304 and 304L (L = low carbon) and Types 316 and 316L (classification according to the American Society for Testing and Materials (ASTM) and American Iron and Steel Institute (AISI), see App. A), being most likely alloy steels. Type 304 steels belong to the most common stainless steels used for industrial applications. Type 316 steel exhibits an increased ability to resist saltwater corrosion compared to Type 304 steel. NPPs have been designed for decades of operation, which has led to the use of corrosion-resistant steels for the various components of the primary water circuit and the water-steam cycle of LWRs. A compilation of the common stainless-steel grades used in nuclear applications was reported by Swanton et al. (2015) (see App. A).

Typical carbon concentrations can tentatively be assigned to the different groups of steels (Tab. 3-1). The carbon content of standard stainless steel is typically below 5,000 ppm (0.5 wt.%) (Davis 1991). High-strength low-alloy steels that are designed to provide greater resistance to corrosion have carbon contents ranging in value between 500 (0.05 wt.%) and 2,500 ppm (0.25 wt.%) (Davis 1991). The carbon concentration of low-carbon steel types 304L and 316L, which are expected to be present in L/ILW are even lower, i.e., 300 ppm (0.03 wt.%) (DIN EN10088-3 2005). It is further expected that the waste forms will contain mild (low carbon) steels with carbon concentrations ranging in value between 500 ppm (0.05 wt.%) and 3,000 ppm (0.3 wt.%) (Davis 1991). Furthermore, the carbon concentration of standard alloy steels was reported to typically range in value between 1,500 ppm (0.15 wt.%) and 6,000 ppm (0.6 wt.%) (Davis 1991).

Nitrogen is introduced during the course of refined processes in steel-making practice (Davis 1991). Various sources of this element exist during the melting, ladle processing and casting operations of steel. Nitrogen is always present as a trace element (impurity), but it may also be added to improve strength, such as in the case of nitrogen-strengthened 316LN steel (0.1-0.16 wt.%) (Davis 1991). Thus, nitrogen is embedded in the metal matrices of nuclear fuel and metal components of the core structural materials, either at trace levels in the case of nitrogen impurities, or up to several hundred ppm in the case that nitrogen has been introduced as an alloying element. Little variation among the different types of stainless steel is expected with respect to the nitrogen concentration of steels (Tab. 3-1). According to ASME standards, the normal nitrogen content for Type 304 is 400 ppm (0.04 wt.%), while 1,000 ppm (0.1 wt.%) is reported to be the maximum concentration for typical steels of the 304 and 316 series (Davis 1991; Swanton et al. 2015; Van Konynenburg 1994). Special grades may contain up to 2,000 ppm (0.2 wt.%). The nitrogen concentration of standard alloy steels has not been specified, but it may be assumed that the nitrogen concentration of the alloy steels used in NPPs is comparable to the value given above for stainless steel Types 304L and 316L.

Nitrogen solubility in liquid steel was found to inversely correlate with the sulphur content of liquid steel. On the assumption that the correlation between sulphur and nitrogen concentration holds for the different groups of steel, the nitrogen concentration in alloy steels should be similar to that in stainless steel. According to Davis (1991), the sulphur concentration in carbon steels is typically 500 ppm, which suggests that the nitrogen content could be about a factor of 2 higher in carbon steels than in stainless steel, i.e., a maximum of ~ 2,000 ppm (0.2 wt.%).

Tab. 3-1: Estimates of the carbon and nitrogen concentrations of various types of steels

Type	**Typical (maximum) carbon concentration (ppm)**	**Typical (maximum) nitrogen concentration (ppm)**
Carbon steel	1,500 (3,000)	600 (2,000)
Alloy steel	3,000 (6,000)	400 (1,000)
Stainless steel	300 (800)	400 (1,000)

3.1.2 ^{14}C inventory in activated steel

There are few studies reporting calculated and/or measured ^{14}C inventories in activated steel. Sakuragi et al. (2013) published ^{14}C inventories of stainless steel in hull-and-end-piece wastes obtained from modelling activation processes. The calculations account for the individual irradiation conditions in NPPs and the fuel characteristics. They were carried out for 6 and 12 types of fuel assemblies of BWRs and PWRs, respectively. The ^{14}C inventories were found to range from 0.25 to 0.50 μg ^{14}C/g material depending on the parameters applied in the activation calculations. Herm et al. (2017b) and Schumann et al. (2014) determined the ^{14}C inventory in activated steel and compared the measured values with theoretical predictions of the ^{14}C inventory (Tab. 3-2). The predictions require that the material properties (e.g., N content and irradiation parameters such as neutron flux, according to the position of the specimen in the reactor) and history are sufficiently well known (Mibus et al. 2018). The results from the two studies show that the measured ^{14}C contents of the activated steel specimens are about a factor of 3 to 4 higher than the predicted ones. This is likely due to uncertainties in the modelling parameters, such as the effective neutron flux. Furthermore, the data allow estimates of the efficiency of ^{14}N conversion into ^{14}C. The annual production of ^{14}C in activated steel was tentatively estimated based on the assumption that burnup in the Gösgen NPP (PWR) was similar over time (~ 50 GWd/t_{HM}) and that the two stainless steel samples were located at similar positions within the reactor pressure vessel (comparable neutron flux). The percentage of ^{14}N converted into ^{14}C per year of neutron exposure of stainless steel ranges in value between ~ 0.05 - ~ 0.25% of the total N content of the steels. This estimate is based on the following considerations: i) exposure of the materials investigated by Herm et al. (2017b) in the neutron field was ~ 1.5 times longer than that studied by Schumann et al. (2014); ii) the N content of the material (80 ppm) used by Herm et al. (2017b) was underestimated by a factor of ~3. The result indicates that only a small portion of ^{14}N accommodated by steel was converted into ^{14}C during exposure to thermal neutrons.

Tab. 3-2: Calculated and measured ^{14}C inventories in activated steel

	Herm et al. (2017b); Mibus et al. (2018)	**Schumann et al. (2014)**
Reactor	Gösgen PWR	Gösgen PWR
Material	stainless steel plenum spring	fuel assembly guide tube nut
Steel	X7CrNiAl17-7	X6CrNiTi18-10, X6CrNiNb18-10 or X6CrNiMoTi17-12-2
N content	0.008 wt.%*	0.0112 (± 0.0031) wt.%
C content	0.07 wt.%	≤ 0.08 wt.%
Irradiation duration	1,226 days	730 days
Burnup	50.4 GWd/t_{HM}	n.r.
Neutron flux	n.r.	~ 8×10^{12} n/cm^{2}s
Model/codes**	MCNP/SCALE/TRITON/ORIGEN-S	MCNP/GRS-AKTIV2
Pred. ^{14}C conc.***	0.57 ± 0.06 µg/g	0.03 µg/g
Meas. ^{14}C conc.***	1.68 ± 0.18 µg/g	0.11 ± 0.02 µg/g
% N activated	2.1 ± 0.2%****	0.1 ± 0.01%
Stable C/^{14}C ratio	417 ± 45%	7,500 ± 1,050%

* The effective N content was estimated at 200 – 300 ppm instead of 80 ppm.
** Irradiation models: MNCP: Monte Carlo N-particle reactor model (MNCP team 2003) of Gösgen PWR (Volmert & Pantelias 2013) and SCALE/TRITON model of fuel assembly (Rearden & Jessee, 2018); activation codes: GRS-Aktiv2 and SCALE/TRITON/ORIGEN-S (Gauld et al. 2009; Rearden & Jessee, 2018).
*** Converted from Bq/g (given in the references) into µg/g.
**** Based on an initial N content of 80 ppm.
n.r.: not reported.

The structural materials made of stainless steel are subjected to corrosion in NPPs. Thus, one may assume that a few nm-to-µm-thick oxide layer forms depending on the redox conditions and the water chemistry of the reactor coolant, i.e., reducing conditions in PWRs (O_2 < 1 ppb) due to the presence of H_2, and oxidising conditions (O_2 ~ 200 ppm) in BWRs (e.g., Tanabe et al. 2014). This assumption is further supported by observation of an external oxide layer on fuel cladding (see Section 3.1.4). Distinction between the ^{14}C inventory in base metal and in the external oxide layer of activated stainless steel parts is required, as they act as different sources of ^{14}C release (see Section 5.1.4).

3.1.3 Nitrogen and carbon content of Zircaloy and UO_2 matrix

As with steel, nitrogen and carbon are mainly introduced as impurities in the production of Zircaloy. Zircaloy is very resistant to aqueous corrosion (Adamson & Rudling 2013). However, the corrosion resistance of Zircaloy degrades when the nitrogen content exceeds 40 ppm N (Van Konynenburg 1994). ASTM standard specifications limit the C and N contents of Zircaloy for reactor service to 270 (0.027 wt.%) and 75 ppm (0.0075 wt.%), respectively (Van Konynenburg 1994; Johnson et al. 2023). Hesböl et al. (1990) adopted an upper limit of 40 ppm (0.004 wt.%)

for the N content in Zircaloy in the framework of the Swedish programme, while other tolerance limits are specified in other countries by Gras (2014), Kato et al. (2014), Necib et al. (2018b) and Sakuragi et al. (2013) (Tab. 3-3). Overall, the tolerances range from 20 to 200 ppm N as quantified in various Zircaloy samples, with typical concentrations between 20 and 40 ppm (Tab. 3-3). The nitrogen contents of Zircaloys are thus well controlled and very low, suggesting low ^{14}C inventories in this material.

Tab. 3-3: Estimates of the C and N concentrations of Zircaloy, Zircaloy cladding and SF

Type	Typical (maximum) C content (ppm)	Typical (maximum) N content (ppm)	Reference
Zircaloy	150 (270)	40 (80)	Van Konynenburg (1994)
Zircaloy	n.r.	22 – 45	Sakuragi et al. (2013)
Zircaloy-2	n.r.	200	Kato et al. (2014)
Zircaloy-4	n.r.	20	Necib et al. (2018b)
Zircaloy-2/4	80 – 270	30 – 40	Gras (2014)
Cladding	n.r.	40	Hesböl et al. (1990)
UO_2 matrix	n.r.	5 – 7	Hesböl et al. (1990)
UO_2 matrix	n.r.	25	Van Konynenburg (1994)
UO_2 matrix	n.r.	< 10	Neeb (1997)
UO_2 matrix	n.r.	8	Marimbeau & Estelin (2008)
UO_2 matrix	n.r.	5 – 10	Johnson et al. (2023)

n.r.: not reported.

The compilation of C and N concentrations to be expected in Zircaloy shows that the N content is generally lower than the C content by a factor of 5 to 10 (Tab. 3-3). Furthermore, the level of C and N contents in Zircaloy is about one order of magnitude lower than in steels. Therefore, the ^{14}C inventory resulting from the conversion of ^{14}N into ^{14}C is expected to be significantly lower than the stable carbon inventory in activated metallic wastes, especially because only a small fraction of ^{14}N is likely to be converted into ^{14}C by activation (Section 3.1.4).

SF largely consists of $UO_2(s)$ (or a blend of UO_2 and PuO_2 in MOX fuel) with only a small fraction of other actinides and fission products (Johnson et al. 2023). Nitrogen and carbon are both introduced during sintering of fuel pellets: nitrogen as an impurity and carbon due to the use and decomposition of binders (Ferrari 1963). Carbon influences the oxygen redistribution in specimens of hyperstoichiometric urania subjected to thermal gradients and allows nitrogen to be taken up into the matrix (Ferrari 1963; Adamson 1971). Nitrogen is introduced into UO_2 pellets through an intermediary reaction involving elemental carbon, which is present due to the decomposition of binders (Ferrari 1963). Elemental carbon formed by the decomposition of binders reacts with nitrogen and $UO_2(s)$ to form uranium nitrides (Ferrari 1963; Adamson 1971; Van Konynenburg 1994). Thus, nitrogen and carbon are an unavoidable impurity in oxide reactor fuels as a result of the production process of fuel (Ferrari 1963; Adamson 1971).

The reader is referred to Johnson et al. (2023) for a more extensive discussion of N contents in SF. In brief, the N concentration in $UO_2(s)$ was found to depend on the production process, ranging from less than 10 ppm to greater than 50 ppm based on a survey of actual fabrication

(Van Konynenburg 1994 and references therein). Van Konyenburg (1994) recommended 25 ppm as a best estimate. Hesböl et al. (1990) estimated the impurity level of N in fuel assemblies to be 10 ppm, assuming that they consist of 10 wt.% Zircaloy cladding (40 ppm N) and 90 wt.% UO_2 (5 - 7 ppm N). The limit for the N content in the UO_2 matrix was based on the detection limit for N. Marimbeau & Esbelin (2008) reported an N content of 8 ppm in UO_2 and MOX fuels. The ^{14}C activity determined in PWR and BWR fuels with different burnups allowed an estimate of the expected N level (Johnson et al. 2023). The activities were found to be consistent with N levels ranging between 5 and 10 ppm, while only a few outliers from samples at higher burnup suggested a higher N level (25 – 30 ppm). Recent information obtained from the EU project CAST suggests that the N content of UO_2 is in the range of ~ 35 ppm (Johnson et al. 2023 and references therein). For Nagra's safety assessment calculations, a reference value of 25 ppm N in the UO_2 matrix is used, with 75 ppm assumed as an upper limit (Johnson et al. 2023).

The presence of stable carbon in as-produced UO_2 pellets is expected due to the use and decomposition of the binders during sintering, although no information is available on C quantities.

3.1.4 ^{14}C inventory in Zircaloy cladding and UO_2 matrix

The production of ^{14}C in fuel assemblies of LWRs has been discussed in detail by Gras (2014). In the fuel assemblies, ^{14}C is mainly produced by ^{14}N rather than ^{17}O activation. In the cladding (considering only the base metal, without oxic layer), ^{14}C is produced solely by the activation of ^{14}N in zirconium alloys, while ^{14}C is produced by both ^{14}N and ^{17}O activation in the UO_2 pellets. For example, in a PWR fuel assembly activated to a burnup of 45 GWd/tHM, 63% of the ^{14}C inventory results from ^{17}O activation and 37% from ^{14}N activation (Gras 2014).

Data for the ^{14}C inventories of Zircaloy-2 and Zircaloy-4 have been published by Gras (2014), Necib et al. (2018b), Sakuragi (2017a) and Sakuragi et al. (2013) (Tab. 3-4). Comprehensive compilations of literature data are given in Gras (2014) and Necib et al. (2018b). The inventories were determined either experimentally or by modelling the activation process. The calculated inventories were often overestimated because the assumed N content of Zircaloy was usually too high compared to the effective N content. The ^{14}C inventories range from ~ 0.08 to ~ 0.50 µg ^{14}C/g (Tab. 3-4). The percentage of ^{14}N converted into ^{14}C is estimated to be ~ 0.3 - ~ 1% of the total N content in Zircaloy, suggesting that, as with activated stainless steel, activation affects only a small portion of the ^{14}N inventory.

Zirconium is electrochemically unstable in the conditions that prevail inside a nuclear reactor (Bragg-Sitton 2012). Therefore, Zr oxidises to ZrO_2, which forms passive oxide layers on the external and internal surfaces of the cladding due to contact with reactor coolant (external) or excess oxygen resulting from fission (internal). Attempts have been made to distinguish the ^{14}C inventory in the thicker, external oxide layer (ZrO_2) from that of the base metal (Zr) (e.g., Gras 2014; Sakuragi 2017a; Sakuragi et al. 2016a). The nuclear reaction $^{17}O(n,\alpha)^{14}C$ was found to increase specific ^{14}C activity in the oxide layer compared to the base metal (Sakuragi et al. 2016a). According to Yamaguchi et al. (1999) and Yamashita et al. (2014), ^{14}C activity in the oxide layer is about a factor of 2 higher than in the Zircaloy metal after irradiation in a reactor. The amount of ^{14}C in the oxide layer was found to increase with its thickness, which is likely to be determined primarily by the duration of irradiation and temperature of the coolant. The thickness may also be related to the burnup. The ^{14}C content in the external oxide layer was reported to be typically ≤ 20% of the total ^{14}C inventory of Zircaloy of PWR and BWR fuels with burnups ranging from ~ 40 to 50 GWd/tHM (Gras 2014; Sakuragi et al. 2016a and references therein). In a highly activated PWR fuel, the external oxide layer can contain up to 20% of the ^{14}C inventory of the cladding (Gras 2014). In general, the ^{14}C inventory of the thinner external oxide layer observed on BWR fuel was found to be about an order of magnitude lower than on PWR fuel.

In safety assessments, the instant release fraction (IRF) is used as a parameter that quantifies the short-term release of ^{14}C (and other fission and activation products) in the near-field of a deep geological repository (Johnson et al. 2023). Studies on the ^{14}C inventory associated with the IRF from the external oxide layer of Zircaloy and released from the bulk metal were reported by Sakuragi (2017a) and Sakuragi et al. (2016a). The authors estimated that < 10% of the total ^{14}C inventory can be attributed to the ^{14}C IRF by assuming that ^{14}C from the bulk metal was released in accordance with the uniform corrosion rate of Zircaloy. Furthermore, it was observed that the total amount of leached ^{14}C from the cladding (metal + oxide) was equivalent to only 0.0038% of the total ^{14}C inventory after 6.5 years of immersion (Sakuragi 2017a; Sakuragi et al. 2016a). This led to the conclusion that using ^{14}C release from the external oxide layer as an IRF would be too conservative due to the low amount of ^{14}C in the oxide layer and the low leaching rate from the oxide (Necib et al. 2018b). Thus, it appears that an IRF for ^{14}C of 20% of the total ^{14}C inventory, which is due to ^{14}C release from the external oxide layer, significantly overestimates the actual release in a repository.

In UO_2- and MOX-type SF, ^{14}C is produced by the two nuclear reactions $^{14}N(n,p)^{14}C$ and $^{17}O(n,\alpha)^{14}C$, as mentioned above (Tab. 2-1). Due to the low N content of UO_2 and MOX fuels and the higher oxygen content of oxide fuels, ^{14}C appears to be produced mainly by the activation of ^{17}O, despite the lower cross-section for neutron capture (Section 3.1.3) (Bush et al. 1984; Marimbeau & Esbelin 2008; Necib et al. 2018b, Gras 2014). For the whole fuel assemblies, activation calculations showed that ^{17}O activation in UO_2 contributes ~ 30% to the ^{14}C inventory (Gras 2014, and references therein). Hence, the remaining 70% results from the activation of ^{14}N in both Zircaloy cladding and in the UO_2 matrix. In general, the ^{14}C activity level in the UO_2 matrix increases with increasing burnup (Capouet et al. 2017). It should be noted that the main uncertainties in the concentrations of ^{14}C in the SF, the cladding and the structural materials of fuel assemblies result from uncertainties in the N contents of the non-activated materials and the neutron flux that are used in activation calculations of ^{14}C production (Heikola 2014; Johnson & Schwyn 2008).

Tab. 3-4: ^{14}C inventories of activated Zircaloy

Type	N content (ppm)	^{14}C inventory* (µg/g)	Burnup (GWd/tHM)	Oxide thickness (µm)	Reference
Zircaloy-2/4	20 - 40	0.25 – 0.50	27.5 - 51	20 - 50	Sakuragi et al. (2013)
Zircaloy-2	n.r.	0.09	41.6	25.3	Sakuragi et al. (2016a)
Zircaloy-2	(22 – 45)**	0.15	41.6	19.9	Sakuragi (2017a)
Zircaloy-2	(22 – 45)**	0.10	39.7	2.7	Sakuragi (2017a)
Zircaloy-2	(30 – 40)**	0.09 – 0.31	34 - 41	n.r	Necib et al. (2018b)
Zircaloy-4	17 - 50	0.08 – 0.23	7.5 - 60	n.r.	Necib et al. (2018b)
Zircaloy-4	34 ± 10	0.18 ± 0.06	~ 45	n.r.	Gras (2014)
Zircaloy-4	n.r.	0.23 ± 0.02	50.4	n.r.	Herm et al. (2018)
Zircaloy-4	17 - 25	0.08 – 0.12	60	n.r.	Caes et al. (2018)

* Converted from Bq/g (reported by the references) into µg/g (= ppm).
** Estimated from the references listed in Tab. 3-3.
n.r.: not reported.

3.1.5 Chemical forms of carbon and nitrogen in metallic waste materials

To assess the speciation and release of ^{14}C during the corrosion of steels, Zircaloy and SF requires more detailed considerations of the composition of the materials as well as structural bonding and speciation of carbon and nitrogen in the base matrices.

3.1.5.1 Steels

In steels, carbon is intermixed with the metal matrix in different chemical forms. While graphite is the predominant form in cast iron, carbon is present in the chemical forms of Fe_3C (cementite) and other carbides in steels (Davis 1991). Note that graphite may only be present in some steel materials, the so-called graphitic steels. The presence of carbon during steel manufacturing gives rise to the formation of Fe_3C and other carbides, such as pearlite (a metastable lamellar aggregate of ferrite and cementite), spheroidite (an aggregate of spherical carbides in a ferrite matrix), bainite (a metastable aggregate of ferrite and cementite), and iron-carbon martensite (a micro-structure formed by diffusionless phase transformation). Importantly, carbon is either bound as solid solution (solute) or in carbide form.

Ferrite (α-iron) and cementite (Fe_3C) are among the most important iron phases in steel (Bhadeshia & Honeycombe 2017). The chemical composition of ferrites can be given as

$MeO \cdot Fe_2O_3$ ($MeFe_2O_4$) with Me as bivalent alloying metal cations, such as Ni, Zn, Mn, Co, Cu, Mg, Cd, Ba, or Sr. Ferrite denotes a solid solution of one or more elements in a body-centred cubic crystal structure. It is essentially carbon-free or a solid solution with low carbon content, respectively. Carbon occupies interstitial positions in the crystal structure. During steel production, the crystals grow and produce grains of different sizes in the metal matrix. By contrast, Fe_3C is a hard, brittle compound of iron and carbon with an orthorhombic crystal structure. When it occurs in steel, the chemical composition can be altered by the inclusion of manganese and other carbide-forming alloying elements.

Two mechanisms exist by which a metal crystal can accommodate carbon and nitrogen atoms: a) as an interstitial solid solution whereby the solute atoms can fit into the spaces between the larger solvent atoms without appreciably distorting the metal structure, and b) as a substitutional solid solution whereby the impurity element replaces a solvent atom in a lattice position (Davis 1991). Note that, in addition to carbon and nitrogen, H_2 and boron are the only solute atoms which are small enough to fit into the interstices of metal crystals. Therefore, carbon and nitrogen are capable of dissolving in steel matrices up to element-specific levels due to the formation of an interstitial solid solution, such as in austenite in 300-series stainless steels and in ferrite in mild steel. About 0.02 wt.% carbon can be dissolved in ferrite (α-iron) as a solid solution. Increasing the carbon content above the latter level, however, gives rise to the formation of Fe_3C (Davis 1991). The presence of manganese and other carbide-forming elements changes the orthorhombic crystal structure of Fe_3C. Nitrogen can replace carbon in carbides, thus forming nitrides of iron and the alloying metals, though the extent of substitution has proven to be very low. In iron, the nitride phase is described as Fe_4N, which is analogous to cementite (Fe_3C). Al, Cr, Mo, Nb, Ti, Zr, and W are nitride-forming elements in steel. Carbonitrides may also form with iron and many alloying elements. Nevertheless, the largest fraction of nitrogen seems to be bound as interstitial solid solution.

The reactivity of carbides deserves further attention with a view to the carbon species generated during corrosion of activated steel in anoxic conditions (Section 4.2). Carbide denotes compounds in which carbon combines with elements of lower or about equal electronegativity. They are classified with respect to the type of chemical bonds, such as salt-like (ionic bonds), covalent compounds, interstitial compounds, or "intermediate" (transitional) metal carbides (Cotton & Wilkinson 1980). The chemical stability of carbides towards hydrolysis depends on the elements involved.

Salt-like carbides are formed with light and highly electropositive elements, such as alkali metals, alkaline earth metals, and some group III elements. These carbides contain isolated carbon atoms and readily decompose in water producing HCs, such as CH_4 (e.g., Al_4C_3, Mg_2C, Be_2C) or acetylene (e.g., Na_2C_2, CaC_2, ZnC_2, CdC_2, $La_2(C_2)_3$), according to the form of the carbide anion (i.e., C^{4-}, C_2^{2-}, C_3^{4-}). Note that in a similar way, ionic nitrides (e.g., Ca_3N_2, Li_3N) are readily hydrolysed by water to release ammonia.

Covalent carbides are formed with Si (SiC) and B (B_4C). Interstitial carbides are formed by most transition metals, especially those in groups IV, V, and VI, e.g., T, Zr, Nb, Mo, W etc. (Cotton & Wilkinson 1980; Toth 1971). Most of the carbides in these groups have metallic properties. They are hard and refractory with excellent high-temperature strength and very good chemical resistance and therefore react very slowly with water (Toth 1971). In interstitial carbides, carbon atoms occupy the octahedral holes in close-packed arrays of metal atoms. As carbon atoms are sufficiently small compared to the solvent ions, they occupy the interstices of the crystal lattice due to the presence of a large number of these vacancies without appreciably distorting the metal structure (Toth 1971).

"Intermediate" (or transitional) metal carbides are transitional between typical ionic and interstitial carbides and comprise those carbides formed with Mn, Fe, Co, Ni, and Cr. They show multiple stoichiometries, such as the chromium carbides $Cr_{23}C_6$, Cr_7C_3 and Cr_3C_2 in the case of Cr, and

Fe_3C, Fe_7C_3, and Fe_2C in the case of Fe. The radii of these metals are smaller than those of the fourth to sixth series elements and therefore, they do not form typical interstitial carbides (Cotton & Wilkinson 1980). Rather, the structures are made by carbon chains running through distorted metal lattices. In steels, iron, nickel, manganese, and chromium carbides are possible (e.g., Fe_3C, Mn_3C, Ni_3C). Carbides of these transition metals (e.g., Cr_3C_2 and M_3C, where M = Mn, Fe, Ni, Co) are comparatively easily hydrolysed by water and dilute acids forming HCs and H_2 upon dissolution (Cotton & Wilkinson 1980). In the case of Fe_3C, even free carbon may be produced (Cotton & Wilkinson 1980). Similarly to carbides, the ratio of the atomic radii of nitrogen to the transition metal determines the form and reactivity of nitrides (Cotton & Wilkinson 1980; Swanton et al. 2015). For example, the constitution and the properties of nitrides formed with transition metals (e.g., Mn, Fe, Ni, Co) are analogous to those of the carbides (Cotton & Wilkinson 1980).

The nature of the metal carbides formed in the steel will affect not only the rate of release of carbon but also the type of carbon compounds released (Swanton et al. 2015). Swanton and co-workers suggested that the types of carbides and nitrides present will depend on the steel composition, such as the presence of carbide-forming elements (e.g., titanium, niobium) or nitride-forming elements (e.g., aluminium, titanium), the nature of the iron phase (e.g., ferrite, austenite) and the solubility of the carbon and nitrogen therein. For example, austenitic steel with its face-centred cubic lattice exhibits higher solubility of both carbon and nitrogen as compared to ferritic steel with its body-centred cubic lattice due to the larger interstices available in the former structure. Above the solubility limit of the carbon and nitrogen in these structures, separate carbide and nitride phases are produced, which can be seen as precipitates or separate phases within the microstructure of the metal, such as Fe_3C in the case of steel. Thus, one may speculate that the chemical form of carbon in steels, e.g., either accommodated in the interstices or as a carbide phase, has an impact on the reactivity of carbon and hence the type of the carbon compounds released.

The chemical form of ^{14}C in activated steel can be assessed on the basis of the above information regarding the chemical forms of carbon and nitrogen in steel and with a view to previous assessments reported by Swanton et al. (2015) and Mibus et al. (2018). In stainless steel, nitrogen is expected to be accommodated mainly as solvent molecules in the interstices of solid solutions of solvent metals, while only a small fraction might be bound as metal nitride. This may also be true in the case of austenitic steel with a higher solubility of nitrogen. If the nitrogen is originally present as nitride or carbonitride in steel, then ^{14}C may eventually be accommodated by carbides and/or carbonitride upon nuclear reaction of ^{14}N (Swanton et al. 2015). Below the solubility of nitrogen in steels, however, transmutation of ^{14}N into ^{14}C upon capture of thermal neutrons may predominantly generate elemental ^{14}C atoms accommodated in the interstices of the crystal structure, while the amount of ^{14}C-bearing carbide produced by the conversion of nitrides might be negligibly small. Elemental ^{14}C bound in the interstices presumably has a high chemical potential for further reaction with metal matrices to form carbides. A possible reaction is tentatively given by $^{14}C + nMe \rightarrow Me_n{}^{14}C$ (where Me denotes other metal atoms). These Me–C compounds are dispersed in the metal matrix and cannot form carbide crystals. Furthermore, it is assumed that the formation of Me–C compounds consisting of several C atoms is unlikely. Partial uptake into carbides could also occur by isotopic exchange with stable carbon of Fe_3C, which increases the fraction of ^{14}C-bearing metal carbides in steel. Nevertheless, the reactivity of the different carbide species in steel on contact with water may vary considerably. In summary, there is evidence to suggest that the chemical form of ^{14}C in activated steel might predominantly be elemental ^{14}C, still retained in the interstices of the crystal structure, and/or, to some degree, ^{14}C accommodated by carbides. It is conceivable that ^{14}C produced by activation in steel will not be in the same chemical form as stable carbon at the time of production, while the nature of stable carbon compounds released from activated steel during corrosion might still be identical to that of the ^{14}C-bearing carbon compounds released in the same process (Swanton et al. 2015).

3.1.5.2 Zircaloy cladding and spent fuel

There is limited knowledge from experimental studies on the chemical nature of ^{14}C species in the UO_2 (or MOX) matrix and Zircaloy cladding with its oxide layers (Necib et al. 2018b). Bush et al. (1984) and Van Konynenburg (1994) previously presented a series of considerations based on properties and application of the materials activated in NPPs with the aim of evaluating the chemical form of ^{14}C. To this end, the authors discussed possible sources of ^{14}C in three separate systems: 1) inside the fuel rods, including UO_2, the fill gas (helium) and the inner surfaces of the cladding with its oxide layer; 2) the bulk of the cladding wall thickness and the interior of other fuel assembly structural components; and 3) the reactor primary coolant and the external surfaces of the cladding and other fuel assembly components (Necib et al. 2018b; Van Konynenburg 1994).

Zircaloy cladding (bulk metal) contains a small amount of ^{14}N as an impurity (Section 3.1.3). The ^{14}C associated with the inside surface of the cladding may be present as zirconium carbide or zirconium cyanonitride, such as $Zr(C,N,O)_x$ with $x < 1$ (Blumenthal 1958; Van Konynenburg 1994). They are expected to remain near the surface. In addition, ^{14}C is probably enriched in the zirconium oxide layers on the internal and external sides of the cladding. Note that the measured ^{14}C specific concentration in the outside layer of zirconium oxide was found to be about twice that of Zircaloy metal after irradiation in a reactor (Yamaguchi et al. 1999; Yamashita et al. 2014). Furthermore, it is possible that residual air remains in the rods during filling with inert gas (helium), which is an additional source of ^{14}C and ^{14}N (Van Konynenburg 1994). The chemical form of ^{14}C from the fill gas has been proposed as CO or CH_4 due to the low oxygen potential arising from the reaction of fission-generated O_2 with Zircaloy (Van Konynenburg 1994). Thermodynamic modelling calculations recently reported by Curti & Kulik (2020), however, suggest that oxygen potentials of UO_2 in LWRs increase with burnup and operating temperature, reaching a “steady state” at about 40 GWd/tHM. These conditions favour the formation of oxygenated carbon species (e.g., CO(g) and CO_2(g)), while reduced carbon species, such as CH_4(g) and C(s), are not stable.

^{14}C produced by transmutation of interstitial ^{14}N impurities in the bulk of the cladding and the interior of other fuel structural components is expected to be stationary bound in the metal matrices. Since (i) the ^{14}N impurities are uniformly distributed, (ii) the temperature gradient in the cladding during in-reactor irradiation is relatively low and (iii) the associated solid-state diffusion is slow, correspondingly, the activation products are also expected to be uniformly distributed on a microscopic scale (Johnson & McGinnes 2002). Due to the very low nitrogen content of Zircaloy, it is assumed that nitrogen is accommodated as an interstitial solid solution in the Zr lattice, thus fitting into the spaces between the larger metal atoms without distorting the structure. Therefore, it can be assumed that, after activation of ^{14}N, ^{14}C is present as elemental carbon. ^{14}C can be present as isolated atoms that may diffuse to a certain extent and form zirconium carbides (Van Konynenburg 1994).

The chemical form of ^{14}C in the primary coolant circuit of the reactor and on the external surfaces of the cladding and other fuel structural components may depend on the type of reactor. It is expected to differ between BWRs and PWRs because of the different modes of operation. Bush et al. (1984) concluded that ^{14}C in the coolant is released from the reactor in gaseous or dissolved form. Analyses of off-gas from the primary system showed that most of the ^{14}C released from BWRs is in the chemical form of $^{14}CO_2$, thus indicating prevailing oxidising conditions in the reactor coolant. In contrast, the off-gas analysis at PWRs showed mostly $^{14}CH_4$ and other HCs, suggesting prevailing reducing conditions in the reactor coolant. There is some evidence to suggest that ^{14}C retained by the oxide layer on the external surface of cladding is presumably in the oxidised chemical form (Yamaguchi et al. 1999; Yamashita et al. 2014). ^{14}N present as interstitial impurity in the external Zircaloy layers and subject to activation and oxidation may be converted to ^{14}C-containing oxygenated carbon compounds and remain trapped in the oxide layer.

The ^{14}C inventory might be different in the oxide layers of Zircaloy exposed in BWRs and PWRs due to differences in the chemical conditions in the reactor primary coolants of the two types of NPPs. In the bulk material, however, which is not subject to corrosion and/or exposure to chemical conditions of the reactor coolants, the interstitial ^{14}N can be converted to elemental ^{14}C by activation and remain in interstitial sites within the Zr metal lattice, or else it can be accommodated as zirconium carbide or zirconium cyanonitride (Van Konynenburg 1994).

UO_2- and MOX-type fuels contain a small amount of nitrogen as uranium nitrides, mainly UN formed by sintering under H_2 (Ferrari 1963), or uranium carbo-nitrides introduced during fuel fabrication (N content < 10 ppm) in addition to uranium carbides (UC, UC_2, U_2C_3) (Section 3.1.3). The chemical form of ^{14}C in UO_2 is not known, while there is evidence to suggest that ^{14}C could be present as carbide, oxycarbide, elemental carbon or as entrapped CO_2 or CH_4 (Ferrari 1963; Hesböl et al. 1990; Van Konynenburg 1994). Activation of ^{17}O in both types of fuel is also likely to be an important process that generates ^{14}C (Marimbeau & Esbelin 2008; Necib et al. 2018b). The chemical form of ^{14}C generated from ^{17}O activation in UO_2 and MOX is unclear.

In summary, the above discussion allows only a preliminary assessment of the chemical forms of ^{14}C in Zircaloy cladding and the SF. In the bulk matrix of Zircaloy, ^{14}C may be present as carbide or elemental C, while it can be assumed that ^{14}C-bearing oxygenated carbon compounds (e.g., CO_2) are present in the oxide layer of Zircaloy cladding. There is some evidence to suggest that carbide, oxycarbide, or elemental C are the likely chemical forms of ^{14}C in UO_2 and MOX fuel. Nevertheless, the formation of oxygenated carbon species (e.g., CO, CO_2) is anticipated due to the presence of fission-generated O_2.

3.1.6 Vitrified HLW

Vitrified high-level waste contains fission products and actinides chemically separated from used nuclear fuel during reprocessing. About one third of the fuel used by Swiss NPPs was reprocessed in the Orano (formerly AREVA, COGEMA, France) and Sellafield Ltd. (formerly BNFL, United Kingdom) reprocessing plants (Bradbury et al. 2014). The highly radioactive acidic liquid is evaporated, the residues then calcined at ~ 400 °C and mixed at very high temperatures (> 1000°C) with borosilicate glass-forming additives to produce a homogeneous molten glass-matrix. The homogenous mix is then poured into stainless steel flasks and allowed to solidify before sealing by welding. The release of radionuclides from vitrified HLW into aqueous solutions occurs according to a specific corrosion kinetics, which depends on a number of chemico-physical factors (pH, temperature, porewater composition) and is further influenced by the interaction with the surrounding engineered barrier materials (canister and bentonite buffer) (Bradbury et al. 2014). During vitrification, most of the ^{14}C is likely to be released into the atmosphere at elevated temperatures, while the remaining, presumably small portion of organic ^{14}C in the acidic liquid from reprocessing is converted into inorganic ^{14}C ($^{14}CO_2$) and accommodated by the glass matrix (Nagra 2008b).

The waste form denoted as $BaCO_3$ crud was produced during reprocessing operations carried out by BNFL (British Nuclear Fuel Limited) and disposed of as L/ILW (Alder & McGinnes 1993). The $BaCO_3$ crud consists of two components: 1) crud arising from the use of multiple element bottles for transport to, and the storage of the fuel assemblies in the ponds, as well as the pond filter crud; and 2) the $BaCO_3$ arising from the scrubbing of the vitrification process off-gas. The waste was mixed and conditioned in cement by BNFL. This waste form contains mainly ^{14}C and iodine isotopes conditioned in cement (NDA 2016). ^{14}C is expected to be in the inorganic chemical form.

3.1.7 Activated concrete and graphite

Activated materials include activated concrete used in NPPs and research facilities for shielding ionising radiation and graphite from research reactors. Small amounts of activated graphite were produced during operation of research reactors. While the chemical speciation of ^{14}C and its release rate from activated graphite has been studied in detail (e.g., RWM 2016; Toulhoat et al. 2018), there is no information available for activated concrete (see Sections 5.7 and 5.8).

3.2 Non-activated waste

Non-metallic, ^{14}C-containing or ^{14}C-contaminated waste forms arise during operation of NPPs and reprocessing, and they are also an important component of MIR waste.

3.2.1 Reactor coolant systems of NPPs

During operation of NPPs, ^{14}C is produced in the reactor coolant in accordance with the nuclear reactions listed in Tab. 2-1 from: a) oxygen atoms in the water molecules; b) nitrogen dissolved in the water; and c) dissolved carbon-containing species in water (carbonate and organic compounds). Oxygen is abundant in the reactor coolant system contrary to nitrogen, which is present at low concentration. It should be noted that generation of ^{14}C from ^{13}C is orders of magnitudes lower than from ^{14}N and ^{17}O activation. Yim & Caron (2006) estimated that ^{14}C generation by interaction of thermal neutrons with ^{17}O is the dominant source of ^{14}C in reactor coolant.

Transport pathways of ^{14}C in BWRs and PWRs have been detailed elsewhere (Hesböl et al. 1990; Rizzato et al. 2015; Vance et al. 1995). In brief, BWRs are operated with neutral high-purity water containing various amounts of dissolved O_2, H_2O_2, and H_2 from water radiolysis in the reactor core and with O_2 and H_2 additions to the feed water in some cases (Seifert & Ritter 2005). In contrast to H_2, which is volatile and escapes to the steam phase, H_2O_2 remains in the recirculated water of BWRs, which becomes rich in oxidants (Was 2012). Seifert & Ritter (2005) reported concentrations of the products from radiolysis and H_2 as follows: 100 - 500 ppb O_2, 50 – 1,000 ppb H_2O_2 and 5 – 40 ppb H_2 in normal water conditions, and < 5 ppb O_2, < 10 ppb H_2O_2, and 50 – 300 ppb H_2 in conditions where excess H_2 was added to the reactor coolant. Thus, conditions are predominantly oxidising in the reactor coolant. ^{14}C is generated in the coolant inside the reactor vessel. Steam produced in the reactor continuously removes gaseous compounds from the coolant. These are carried to the turbines and eventually to the steam condenser. Thus, only a small portion of ^{14}C (~ 2%) is contained in the reactor coolant and carried to the reactor coolant purification system where ^{14}C is partly retained by the IERs. The largest portion of ^{14}C (~ 98%), however, is carried by the steam flow to the turbines. These are gaseous ^{14}C-bearing carbon species. Only a small portion of the volatiles condense in the steam condenser and follow the condensate to the condensate purification system. The majority of the volatiles are released from the condenser into the off-gas system. A fraction of ^{14}C dissolved in the condensate is retained by the IERs of the demineraliser. The condensate is then returned to the reactor vessel as feed water. In BWRs, ^{14}C-bearing IERs are produced during reactor coolant purification, condensate purification and, additionally, the treatment of the SF pool water. The major contribution of ^{14}C is likely in the inorganic form as a result of the oxidising conditions in the coolant circuit and associated with IERs from condensate cleaning.

In PWRs, the reactor coolant including ^{14}C is circulated from the reactor vessel to the steam generator and back in several circuits. The circuits involve various systems: chemical and volume control, primary effluent treatment, reactor pool and SF cooling and treatment, steam generator blow down, water purification, and liquid waste treatment. Water purification in the various circuits, i.e., primary circuit, secondary circuit and effluent treatment, employs a chain of filters and demineralisers using IERs. One circuit connects to the water purification and water control

system. This circuit is composed of the water clean-up system containing mixed-bed IERs, a fibre filter for particulates, dumping tank and a chemical volume control tank. The water chemistry of the primary coolant differs considerably between BWRs and PWRs (Van Konynenburg 1994). Addition of H_2 and N_2 to the primary coolant is common practice in PWRs to control the redox conditions and pressure in the volume control tank (Vance et al. 1995; Van Konynenburg 1994), along with the addition of LiOH to control pH and $B(OH)_3$ as a neutron absorber for reactivity control (Van Konynenburg 1994). ^{14}C produced in the reactor coolant seems to be mainly present in the organic chemical form due to the specific water chemistry, while inorganic ^{14}C is a minor form in these conditions. Thus, dissolved ^{14}C-bearing carbon compounds in the inorganic and organic chemical forms are expected to be retained by filters and IERs. Volatile ^{14}C-bearing carbon compounds are vented from the gas space of the dumping tanks and chemical volume control tanks into the decay tanks or gas treatment system from which they are discharged.

3.2.2 Spent IERs

The fraction of ^{14}C retained in the reactor coolant of BWRs and PWRs is removed by IERs of the various water clean-up systems (reactor coolant, condensate, SF pool, effluent) and therefore, spent IERs are a source of organic and inorganic ^{14}C-bearing carbon compounds. IERs used for water clean-up and liquid waste treatment in NPPs are anion exchangers with ammonium or amine functional groups, cation exchangers with carboxylate or sulfonate functional groups or mixed-bed exchangers including both types of exchangers. Overviews on the sources and the chemical form of ^{14}C retained by IERs have been reported elsewhere (Hesböl et al. 1990; Kunz 1985; Magnusson & Stenström 2005; Martin 1986; Stenström & Magnusson 2008; Vance et al. 1995; Yim & Caron 2006). Brief surveys of earlier work have been reported by Stenström & Magnusson (2008) and more recently by Rizzato et al. (2015). Reports by Rizzo et al. (2017), Bucur et al. (2017) and Reiller (2018) summarise the results from studies on the chemical form of ^{14}C in spent IERs that have been carried out in the framework of the European Union (EU)-financed project "CAST" (Carbon Source Term). In addition, several studies report on ^{14}C quantification in the waste streams of BWRs and PWRs (Hesböl et al. 1990; Kunz 1985; Martin 1986; Vance et al. 1995; Yim & Caron 2006).

Information on ^{14}C production and the chemical form of ^{14}C in reactor coolant allows a first appraisal of the ^{14}C storage by IERs as well as other waste materials resulting from the purification of reactor coolant. Yim & Caron (2006) estimated that ^{14}C production in reactor coolant contributes ~ 20% to the total ^{14}C inventory produced in PWRs and ~ 40% to the total ^{14}C inventory produced in BWRs. Hence, ^{14}C production in the coolant was estimated to be ~ 2 - 3 times lower in PWRs compared to BWRs (Yim & Caron 2006). Kunz (1985) determined discharge rates and the chemical form of ^{14}C in the primary coolant. The author reports that $^{14}CO_2$ is the predominant form of ^{14}C (> 95%) released from BWRs whereas those released from PWRs are $^{14}CH_4$ and other ^{14}C-bearing HCs. Martin (1986) determined the largest amounts of ^{14}C in the resins and filters used for reactor water clean-up. The chemical form of ^{14}C is controlled by the redox conditions in the reactor coolant. As outlined above, oxidising conditions (100 – 500 ppb O_2) are indicated for the reactor primary circuit of BWR-NWC (normal water chemistry, NWC), while reducing conditions (< 5 ppm O_2) prevail in the reactor coolant of PWRs and presumably BWR-HWC (H_2 water chemistry, HWC), where H_2 is added to the feed water (Seifert & Ritter 2005; Tanabe et al. 2014). This assessment of redox conditions is further supported by the analysis of off-gas from the primary system showing that most of the ^{14}C released from BWRs with NWC is in the chemical form of $^{14}CO_2$ (Kunz 1985). By contrast, off-gas analysis showed mostly $^{14}CH_4$, other HCs and ^{14}CO in the case of PWRs (Bush et al. 1984; Hesböl et al. 1990; Kunz 1985; Vance et al. 1995; Van Konynenburg 1994). Magnusson & Stenström (2005) quantified ^{14}C in reactor coolant and in ejector off-gas in Swedish NPPs. In reactor coolant of BWRs operated with NWC, almost 100% of ^{14}C was found in its inorganic chemical form ($^{14}CO_2$) of which ~ 70% was in the

gas phase. By contrast, almost 100% of ^{14}C was found in the organic chemical form in reactor coolant of PWRs (0.3% in inorganic form) and > 80% in BWRs operated with HWC. Generally, the ^{14}C activity in the water was divided equally between the gas and water phases. These results agree with the earlier work of Kunz (1985). Interestingly, the organic ^{14}C detected in the water samples were not CH_4, volatile HCs or CO. Instead, the presence of HCOOH and CH_3COOH in reactor coolant was observed. The various measurements of ^{14}C in the primary and secondary circuits of BWRs and PWRs indicated that a large fraction of ^{14}C escapes through the off-gas system while the other portion is retained by the IERs of the water clean-up system. They further suggested that the proportions of inorganic and organic ^{14}C might be different in the coolant and in the various components of the water clean-up systems.

Measurements of ^{14}C in reactor coolant and on spent IERs by Vance et al. (1995) show that ~ 52 - 87% of ^{14}C in primary coolant of BWRs is in the inorganic chemical form (i.e., $H^{14}CO_3^-$) while ~ 58 - 95% of ^{14}C in the PWR reactor coolant exists as organic species. Magnusson & Stenström (2005) quantified organic and inorganic ^{14}C in spent IERs from a PWR and found ~ 30% of ^{14}C in the organic form with the remaining ~ 70% as inorganic ^{14}C. In BWR-HWC, the fraction of organics was < 10% and typically < 5%. The authors report that in the PWRs, only a small fraction of the ^{14}C in the reactor coolant was attached to the IERs whereas the ^{14}C uptake by IERs in BWRs was significantly higher, suggesting that organic ^{14}C is only weakly retained by IERs in contrast to inorganic ^{14}C. This finding supports the idea that different chemical forms of ^{14}C exist in the reactor coolant of BWRs and PWRs. Magnusson & Stenström (2005) observed only ~ 19% of the ^{14}C inventory of spent IERs in the organic form, thus leaving ~ 81% as inorganic ^{14}C. However, spent IERs were found to carry different ^{14}C inventories depending on the chemical nature of the exchanger resins. A higher fraction of ^{14}C was observed on IERs with carboxylate groups than on IERs with sulfonate groups. Magnusson & Stenström (2005) concluded that a larger fraction of the acidic species ($H^{14}CO_3^-$, $HCOO^-$, CH_3COO^-) is captured by the weakly acidic carboxylate IERs compared to the strong acidic sulfonate IERs.

A great number of experimental studies have used methods to distinguish the organic from the inorganic ^{14}C fractions in reactor coolant and those bound on IERs, while there are few studies to directly identify the ^{14}C-bearing species bound on IERs. The final reports published in the framework of the EU project “CAST” summarise the current state of knowledge as follows (Bucur et al. 2017; Rizzo et al. 2017; Reiller 2018):

- The major chemical form of ^{14}C taken up by spent IERs is inorganic (i.e., $H^{14}CO_3^-$) both in IERs from BWRs (> 90%) and PWRs (> 70%);
- The organic fraction mainly contains small organic molecules, such as formate ($H^{14}COO^-$) and acetate ($^{14}CH_3COO^-$);
- Leaching of ^{14}C from spent IERs was only observed under alkaline conditions;
- Leaching of ^{14}C from cemented, spent IER-containing waste forms was not observed;
- The amount of ^{14}C released to the gas phase during dry storage of spent IERs is small and occurs under alkaline conditions, and mainly in the inorganic chemical form.

The current state of knowledge indicates that inorganic and organic forms of ^{14}C might be associated with spent IERs. ^{14}C is taken up by an anion exchange process on IERs used in water clean-up and liquid waste treatments systems of BWRs and PWRs (Magnusson & Stenström 2005; Vance et al. 1995; Yim & Caron 2006). There is a general consensus that the major chemical form of ^{14}C taken up by IERs under oxidising conditions, typically in BWRs, is inorganic C, i.e., bicarbonate ($H^{14}CO_3^-$). Under the reducing conditions of reactor coolant in PWRs, however, the concentration of the radiolytically generated oxidising agents, such as H_2O_2, is strongly diminished due to significant amounts of H_2 added to the reactor coolant. Reducing

conditions are expected to favour the formation of dissolved organic species rather than inorganic C species. In particular small molecules of organic oxygenated carbon compounds, such as alcohols and aldehydes (e.g., CH_2O, CH_3OH, CH_3CHO, CH_3CH_2OH, CH_3COCH) and mono-carboxylic acids (e.g., HCOOH, CH_3COOH), may form, along with volatile carbon compounds, such as CH_4, other HCs and CO (Magnusson & Stenström 2005; Matsumoto & Banba 1999; Matsumoto et al. 1995; Vance et al. 1995). There is evidence to suggest that the organic form of ^{14}C are small molecules, like formate ($H^{14}COO^-$) and acetate ($^{14}CH_3COO^-$). These are negatively charged species in the given water chemistry of reactor coolant and may, therefore, be retained by an anion exchanger. In the Swedish study of Magnusson & Stenström (2005), about 20% of the ^{14}C inventory of spent IERs was in the organic chemical form, which is expected to be small, oxygenated carbon compounds, such as $H^{14}COO^-$ and $^{14}CH_3COO^-$, and about 80% was inorganic ($H^{14}CO_3^-$). Hence, there is evidence to suggest that also in spent IERs from PWRs, the major chemical form is inorganic ($H^{14}CO_3^-$), indicating that $H^{14}CO_3^-$ is much more strongly retained by IERs than the carboxylates. The presence of other classes of oxygenated carbon compounds, e.g., alcohols and aldehydes, which are neutral species in water, as well as volatile carbon compounds present in the reactor coolant, such as $^{14}CH_4$, ^{14}CO and ^{14}C-bearing HCs, is considered unlikely.

3.2.3 ^{14}C-contaminated waste

Filter cartridges are ^{14}C-carrying waste forms produced during water clean-up in Swiss BWRs and PWRs. Experimental studies on the chemical speciation of ^{14}C on filters are lacking. Nevertheless, it may be assumed that the chemical form of ^{14}C in the filter cartridges is similar to that in spent IERs, i.e., ^{14}C is predominantly present as inorganic carbon, while the presence of small amounts of ^{14}C in the organic form cannot be excluded in waste from PWRs.

Contaminated materials may include operational wastes from NPPs that are likely to be generated during monitoring and cleaning activities. Contaminated materials further include poorly characterised waste forms, such as incineration ashes. In these wastes, ^{14}C is likely to be present mainly in inorganic chemical form.

In addition to the waste arising from NPP-related activities (operation, reprocessing, decommissioning), there is also radioactive waste arising from applications of radioactive materials in MIR (Nagra 2021a).

Quite a significant amount of ^{14}C-containing waste is present as $Ba^{14}CO_3$ arising from industrial and military waste producers. For example, it is used as fluorescent pigments on military items, such as assault rifle sights, compasses, etc., and is applied as a powder (Nagra 2023). $BaCO_3$ is practically insoluble under the strongly alkaline conditions of the L/ILW near-field.

3.3 Summary of chapter

Knowledge of the ^{14}C inventories and chemical forms of ^{14}C in the different types of waste is of fundamental importance to assessments of the potential for release of ^{14}C in the deep geological repository. In the case of Zircaloy and steels, the content of ^{14}N impurities in the materials is the most important factor determining the ^{14}C inventory. Nitrogen is embedded in the metal matrices of nuclear fuel and metal components of the core structural materials, either as an impurity or at levels up to several hundred ppm when introduced as an alloying element in steels. The nitrogen content of Zircaloy is significantly lower (range ~ 20 - 40 ppm), whereas the nitrogen content of the SF is typically < 10 ppm. A comparison of the experimentally determined ^{14}C inventory of activated steels and Zircaloy with the estimated ^{14}N contents of these materials shows that, at most, 1% of ^{14}N embedded in the base metal has been converted into ^{14}C during irradiation in an NPP.

Carbon and nitrogen are capable of dissolving in steel matrices up to element-specific levels through the formation of interstitial or substitutional solid solution. For example, up to ~ 0.02 wt.% carbon can be dissolved in ferrite, while higher contents lead to the formation of Fe_3C. In stainless steel, nitrogen is expected to be accommodated mainly in the interstices, while only a small fraction is bound as metal nitride. Therefore, it can be assumed that the conversion of ^{14}N into ^{14}C by neutron capture generates predominantly elemental ^{14}C atoms rather than ^{14}C-bearing carbides produced by the conversion of nitrides. Nevertheless, the elemental ^{14}C bound in the interstices could have a high chemical potential for further reaction with metal matrices to form carbides. Similarly, ^{14}C is expected to be uniformly distributed in Zircaloy. In the bulk matrix of Zircaloy, ^{14}C may be present as carbides or elemental carbon, whereas ^{14}C-bearing oxygenated carbon compounds may be accommodated by the oxide layer of Zircaloy cladding. In case of the SF, it has been suggested that ^{14}C is present as carbide, oxycarbide and elemental carbon, while the presence of some entrapped CO and CO_2 was also suspected.

Vitrified HLW and $Ba^{14}CO_3$ crud are reprocessing wastes containing ^{14}C, presumably in the inorganic chemical form, if at all. Non-metallic activated waste forms include activated graphite, where ^{14}C is mainly released in the inorganic chemical form, and concrete, for which no information about the ^{14}C source term is available. Non-metallic and non-activated waste forms from the operation of NPPs, such as spent IERs and filter cartridges, are likely to contain ^{14}C mainly in the form of inorganic carbon with only a small amount of ^{14}C in the organic chemical form, which is present in reactor coolant. MIR wastes are expected to contain a negligible portion of ^{14}C in activated metals and some $Ba^{14}CO_3$ originating from military applications. However, the largest amount of ^{14}C is associated with contaminated materials (either as metals, organic or inorganic materials), with ^{14}C likely present in the organic and inorganic chemical form.

4 Thermodynamic and kinetic control of carbon speciation

Predictions of the expected species distribution in the C-H-O system allow a first assessment of the chemical nature of potentially existing carbon compounds under conditions relevant to a deep geological repository. A consistent thermodynamic database for carbon species was established by Helgeson, Shock and co-workers because organic compounds play an important role in a variety of geochemical processes (Amend & Helgeson 1997; Helgeson et al. 1998; Plyasunov & Shock 2000 a,b; Plyasunova et al. 2004; Schulte & Shock 1993; Shock 1988, 1995; Shock & Helgeson 1990). In this study, predictions of the thermodynamic stability of small organic molecules are of particular interest in conjunction with the release of carbon compounds during metal corrosion and the degradation of organic waste materials. The first comprehensive paper on the equilibrium distribution of small organic molecules in the environment was published by Thorstenson (1970) based on the thermodynamic data available five decades ago, while an analysis of the distribution of organic compounds under the conditions of an L/ILW repository was recently published by Wieland & Hummel (2015) based on updated thermodynamic data.

There is evidence from the literature to suggest that complete thermodynamic equilibrium is seldom achieved in the C-H-O system, at least at moderate temperatures, and consequently kinetic aspects are essential in assessing the species distribution in the C-H-O system. The concept of partial thermodynamic equilibrium was introduced to assess the type and concentration of organic compounds found in sedimentary basins (Shock 1988). The persistence of thermodynamically metastable states in environmental systems at ambient temperature and pressure states has been attributed to kinetic constraints and thus exceeds the predicted distribution of organic compounds as functions of temperature, pressure and redox conditions using the well-established tool of chemical thermodynamics. Consequently, kinetic processes leading to the formation of small organic molecules at the metallic iron-water interface and to the abiotic and biotic degradation of organic matter are discussed in the following sections along with thermodynamic predictions of the species distribution.

4.1 Thermodynamic modelling of carbon speciation

The thermodynamic data used for the speciation calculations in the C-H-O system carried out in this study are compiled in App. B. The database was developed on the basis of consistent appraisals of the previously reported thermodynamic data for aqueous organic species containing up to five carbon atoms (Cox et al. 1989; Hummel et al. 2005; Schulte & Shock 1993; Shock & Helgeson 1990). The thermodynamic data are further in line with those previously reported by Wieland & Hummel (2015). The equilibrium concentrations of 39 dissolved species in the C-H-O system were computed as a function of pe and pH at 25 °C for a concentration of total dissolved carbon of $C_t = 10^{-3}$ mol/kg_{H2O} (Figs. 4-1 to 4-3). In addition, the species distributions were calculated for various geochemical conditions relevant to HLW and L/ILW deep geological repositories (Figs. 4-4 and 4-5). Organic compounds in the solid or gaseous state were not considered in the modelling, while the solubility of the predominantly gaseous HCs was considered, i.e., their presence as dissolved species.

In the case of complete thermodynamic equilibrium, the predominant dissolved species are carbonic acid (CO_2(aq)), bicarbonate (HCO_3^-(aq)), carbonate (CO_3^{2-}(aq)) and CH_4(aq) (Fig. 4-1). All other carbon compounds are present solely at trace concentrations or they were found to be thermodynamically unstable. The results reported by Wieland & Hummel (2015) in the case of complete thermodynamic equilibrium were found to be consistent with those reported earlier by Thorstenson (1970). The modelling of Thorstenson (1970) showed predominance of CH_4 and carbonate species in the C-H-O system under conditions similar to those selected by Wieland & Hummel (2015), even on the basis of a less comprehensive thermodynamic database.

Wieland & Hummel (2015) further calculated the species distribution for partial thermodynamic equilibrium on the assumption that the formation of dissolved HCs, in particular CH_4 and the higher alkanes, is kinetically hindered (Fig. 4-1). This assumption considers that the C-H-O system is rarely in a completely stable redox equilibrium and shows an extreme case in which the formation of HCs does not occur. In this scenario of metastability, the predominant dissolved species were found to be carboxylic acids and, at a low pH and very reducing conditions, a higher alcohol. Note, however, that the stability field of these organic species is smaller than the stability field of CH_4 in the case of complete thermodynamic equilibrium, in line with an increasing predominance of carbonate (CO_2(aq), HCO_3^- and CO_3^{2-}) (Fig. 4-1). Especially at a high pH, metastable carboxylic acids were found to be in partial thermodynamic equilibrium with carbonate only under the most reducing conditions, at the verge of the stability of water.

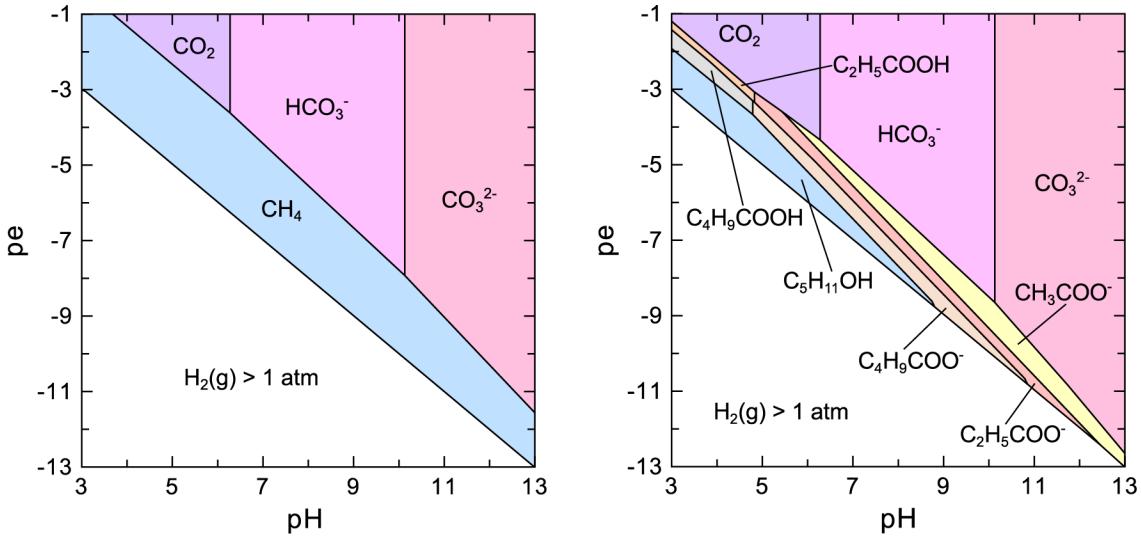

Fig. 4-1: Predominance diagram of aqueous species (left) for complete thermodynamic equilibrium and (right) partial thermodynamic equilibrium in the C-H-O system at 25 °C

Total dissolved carbon, $C_t = 10^{-3}$ mol/kg_{H2O} (adapted from Wieland & Hummel 2015)

4.1.1 Carbon speciation in the conditions of an L/ILW repository

The species distribution was modelled for the base case of an L/ILW repository, i.e., a simplified solution with pH 12, for the two scenarios accounting for complete and partial thermodynamic equilibrium, respectively (Fig. 4-2).

In the case of complete thermodynamic equilibrium, the modelling shows that the concentrations of CO_2(aq), HCO_3^-, CO_3^{2-} and CH_4(aq) are at least five orders of magnitude higher than the maximum equilibrium concentrations of the organic species, which do not exceed 10^{-8} mol/kg_{H2O} (Wieland & Hummel 2015). At pH 12, $HCOO^-$, CH_3COO^- and ethane (C_2H_6(aq)) are the only aqueous carbon compounds predicted at trace concentrations below 10^{-9} mol/kg_{H2O} besides the predominant carbonate/CH_4 species (Fig. 4-2a). Furthermore, the organic carbon compounds were found to be stable only in a very small pe range (~ -11.5 < pe < ~ - 9.5; ~ -0.68 eV < E_h < ~ -0.56 eV) at the boundary of CH_4/carbonate species; outside this small pe range, the organic species rapidly become thermodynamically unstable (Fig. 4-2a).

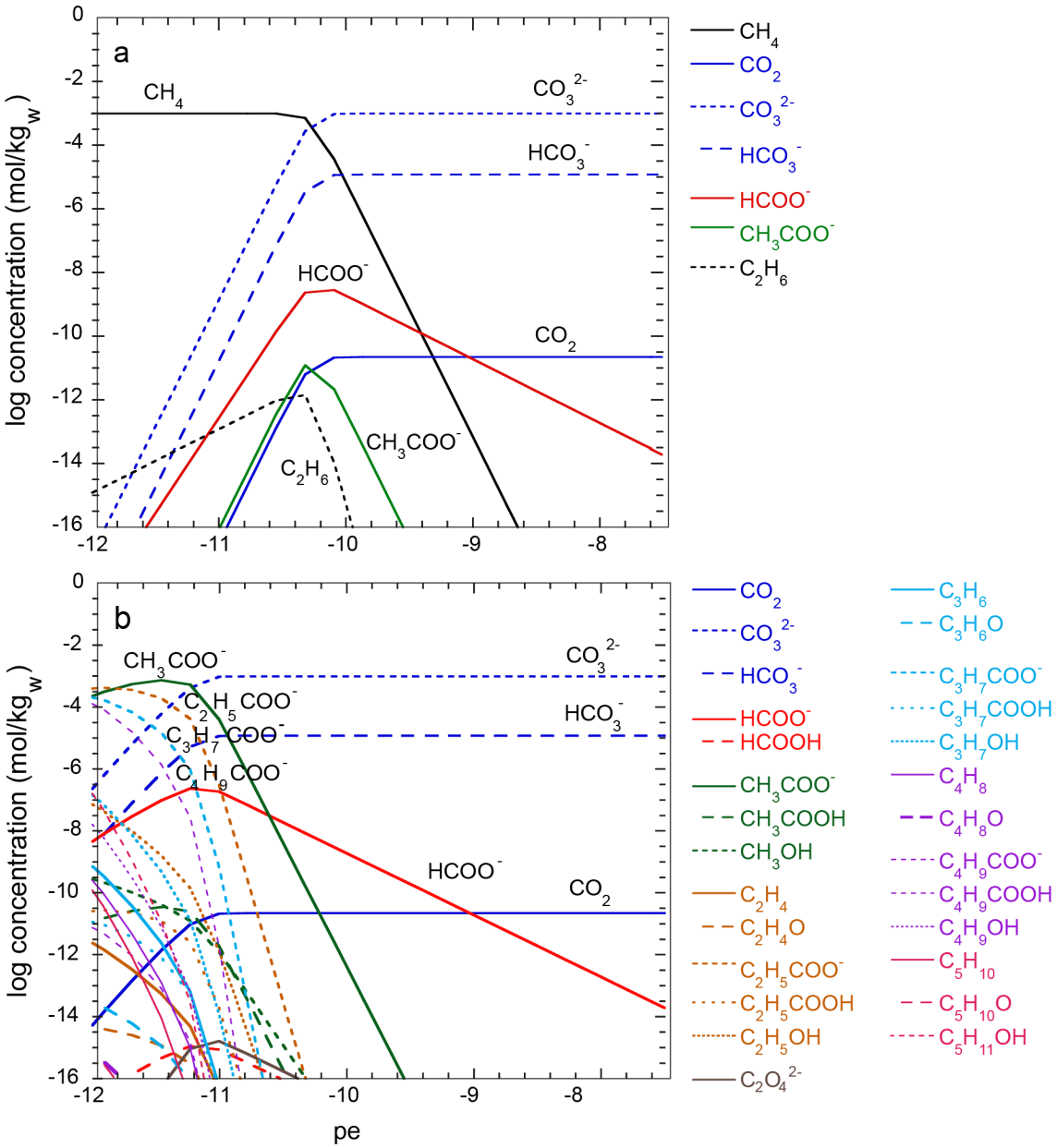

Fig. 4-2: Aqueous species distribution for (a) complete thermodynamic equilibrium and (b) partial thermodynamic equilibrium in the C-H-O system at pH 12 and 25 °C

Total dissolved carbon, $C_t = 10^{-3}$ mol/kg$_{H2O}$. In the case of partial thermodynamic equilibrium, it was assumed that the formation of alkanes is kinetically hindered (adapted from Wieland & Hummel 2015).

In the case of partial thermodynamic equilibrium, it was assumed that the formation of alkanes is kinetically hindered. In these conditions, HCO_3^- and CO_3^{2-} are the predominant species at pH 12 over a large pe range (pe > -10.5; E_h > -0.62 eV) (Fig. 4-2b). However, below this pe range, i.e., pe < - 10.5 (E_h < - 0.62 eV), carboxylates, such as $HCOO^-$ and CH_3COO^-, are the most important oxygenated carbon compounds. Therefore, in this pe range, the importance of kinetic hindrance of the formation of HCs on the predicted species distribution is evident. Similar thermodynamic calculations were performed on the assumption that only the formation of CH_4(aq) is kinetically hindered while the formation of C_2H_6(aq) and C_3H_8(aq) was allowed. The calculations revealed, as expected, that these HCs become thermodynamically stable in this pe range at the expense of oxygenated carbon compounds (data not shown). This finding indicates that the predominance of oxygenated carbon compounds in the entire stability field of the HCs, i.e., under strongly reducing conditions (Fig. 4-2), increases proportionally to the increase in the reactive barrier for the formation of HCs.

4.1.2 Carbon speciation in the conditions of an HLW repository

Thermodynamic modelling of the species distribution under HLW conditions shows that the distributions of carbon species are similar at pH 7.5 and 12 (Fig. 4-3). Also at pH 7.5, the predominant dissolved species in the case of complete thermodynamic equilibrium are CO_2(aq), HCO_3^-, CO_3^{2-} and CH_4(aq) (Fig. 4-3a). All other organic species are present in concentrations that are at least three orders of magnitude lower than those of the dominant carbon species, or they are thermodynamically unstable. Also at pH 7.5, the organic carbon compounds are only stable over a very small pe range, i.e., between -5.5 < pe < -3.5 (-0.33 eV < E_h < -0.21 eV) at the boundary of CH_4/carbonate species. Note that the organic species are thermodynamically unstable outside this small pe range.

In the case of complete thermodynamic equilibrium, the order of organic compounds present in the ppm to ppb range is as follows: $HCOO^- > CH_3COO^- > C_2H_6$(aq). Note that acetate and formate are present at very low concentrations, i.e., in the ppb to ppt range. In the ultra-trace concentration range below the ppt level, i.e., at the verge of insignificance, methanol (CH_3OH(aq)), propane (C_3H_8(aq)), propionate ($C_2H_5COO^-$), as well as oxalate ($C_2O_4^{2-}$) are visible (Fig. 4-3a). At pH 7.5 and pe < -5.5 (E_h < -0.33 eV), CH_4(aq) dominates the speciation in equilibrium with the carbonates and C_2H_6(aq). Other HCs (e.g., C_3H_8(aq) and butane (C_4H_{10}(aq)) are present at much lower concentrations. At the boundary of CH_4/carbonate (pe = -4.5; E_h = -0.27 eV), the concentrations of the main carboxylates are at least three orders of magnitude lower than those of the dominant carbonate species and CH_4(aq). It should be noted that at pH 7.5, the maximum equilibrium activities of trace organic species calculated by Thorstenson (1970) were 10^{-9} mol/kg_{H2O} for CH_3COO^- and 10^{-11} mol/kg_{H2O} for $HCOO^-$ and C_2H_6(aq). Thus, given the less reliable thermodynamic database used by Thorstenson (1970), the results of previous and current studies are consistent.

In the case of partial thermodynamic equilibrium where no alkanes are formed, the predominant dissolved species are carboxylates and alcohols (Fig. 4-3b). At pH 7.5 and -6.5 < pe < -5 (-0.38 eV < E_h < -0.30 eV) the predominant species are CH_3COO^-, $C_2H_5COO^-$, $C_3H_7COO^-$ and $C_4H_9COO^-$, while $HCOO^-$ remains only a minor species. Under the most reducing conditions (pe < -6.5; E_h < -0.38 eV) at the border of water stability, equilibria between different alcohols are predicted, while the concentrations of the alcohols decrease with an increase in the number of carbon atoms in the compounds.

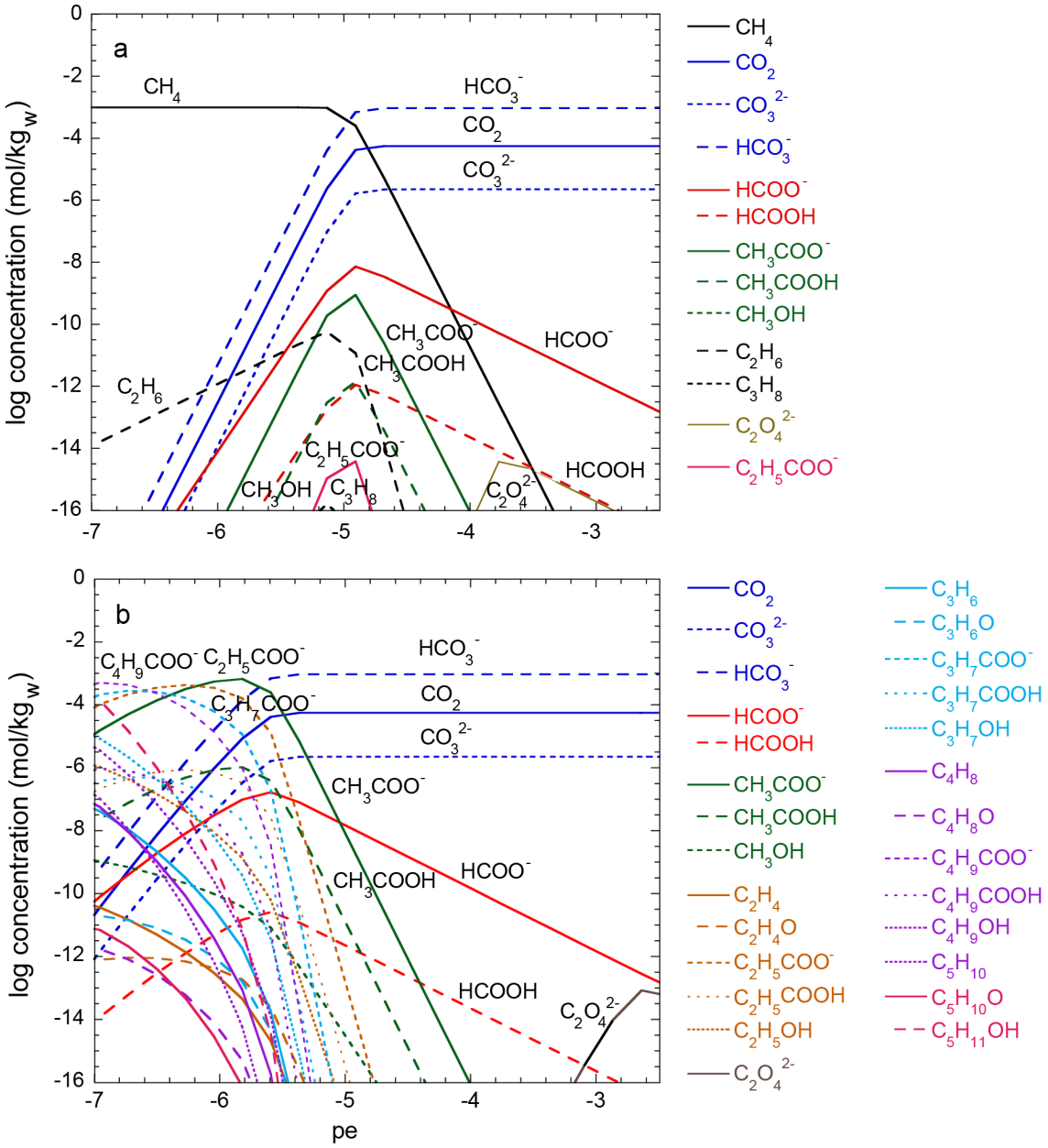

Fig. 4-3: Aqueous species distribution for (a) complete thermodynamic equilibrium and (b) partial thermodynamic equilibrium in the C-H-O system at pH 7.5 and 25 °C

Total dissolved carbon, $C_t = 10^{-3}$ mol/kg$_{H2O}$. In the case of partial thermodynamic equilibrium, it was assumed that the formation of alkanes is kinetically hindered.

4.1.3 Carbon speciation for various repository systems

Species distributions were calculated for a range of specific porewater compositions anticipated in a deep geological repository, such as cement-type porewaters in the three stages of cement degradation (CEM-St.1-St.2-St.3) and OPA and bentonite (MX80) porewater, with the assumption of partial thermodynamic equilibrium (Figs. 4-4 and 4-5) (see App. B for porewater compositions and thermodynamic data). The porewater carbon speciation was calculated using the GEM-Selektor code (Kulik et al. 2013), and the PSI thermodynamic data base 2020 (Hummel & Thoenen 2021) was complemented with the relevant carbon species (Wieland & Hummel 2015).

Three calculation scenarios were considered for each porewater: A – assuming that the formation of alkanes is kinetically hindered and no carbon complexes form with cations; B – full carbon speciation; C – assuming that no CH_4(aq) or alkanes form, but conditions are reducing due to equilibrium with reactive H_2(g).

In the case of scenario A, all carbon is present as inorganic species in all porewaters considered: i) mainly as HCO_3^- in low-pH (OPA, bentonite MX80) porewaters (Fig. 4-4); ii) mainly as CO_3^{2-} in high-pH porewaters of the two early degradation stages; and iii) evenly distributed between HCO_3^- and CO_3^{2-} for stage 3 of the cement degradation (Fig. 4-5). The results for scenario B show the same distribution between organic and inorganic carbon speciation as for scenario A. In this scenario, carbon is allowed to form inorganic species with the dissolved cations Na^+, K^+, Ca^{2+}, and Sr^{2+}. The proportion of these species is around 11 mol% in the OPA and MX80 porewaters (mainly $NaHCO_3$(aq) followed by $CaHCO_3^+$) (Fig. 4-4) and increases up to 40, 50 and 80 mol% in the CEM-St.1, CEM-St.2, and CEM-St.3 porewaters, respectively (Fig. 4-5). Within the inorganic species, carbon is present mainly as KCO_3^- in CEM-St.1; evenly distributed between $NaCO_3^-$, KCO_3^-, and $CaCO_3$(aq) in CEM-St.2 and mainly as $CaCO_3$(aq) in CEM-St.3. Scenario C is the only scenario in which a large proportion of carbon is stable in the form of organic species (carboxylates). In this scenario, the systems are equilibrated with reactive H_2 gas (partial pressure of 1 bar). Only the cement porewaters contain between 5 and 22 mol% inorganic carbon species, and the organic carbon is mainly in the form of acetate (61 - 70 mol%), followed by propionate (15 - 23 mol%), in all stages of the cement degradation (Fig. 4-5). Acetate (Ace-), propionate (Prop-), butanoate (But-) and pentanoate (Pent-) are the dominant carboxylates at low pH (OPA, MX80), while inorganic carbon species are completely absent. For example, propionate accounts for more than 40 mol% of the carbon in the MX80 porewater and more than 38 mol% of the carbon in the OPA porewater (Fig. 4-4).

The thermodynamic calculations show that inorganic carbon (HCO_3^- CO_3^{2-}) rather than organic carbon is the predominant chemical form of carbon under mildly reducing to oxidising conditions of the porewaters. However, organic carbon is the predominant chemical form of carbon under reducing conditions in the presence of reactive H_2 and with kinetic inhibition of HC formation.

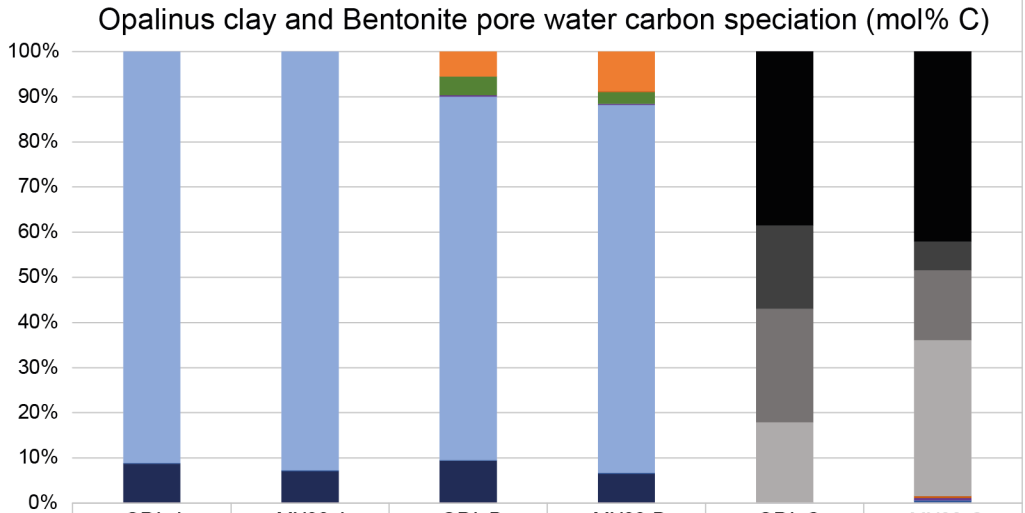

	OPA-A	MX80-A	OPA-B	MX80-B	OPA-C	MX80-C
Prop-	0.00	0.00	0.00	0.00	38.46	42.03
Pent-	0.00	0.00	0.00	0.00	18.50	6.42
But-	0.00	0.00	0.00	0.00	25.11	15.46
Ace-	0.00	0.00	0.00	0.00	17.78	34.49
SrCO3(aq)			0.00	0.00	0.00	0.00
NaHCO3(aq)			5.33	8.59	0.00	0.00
NaCO3-			0.08	0.19	0.01	0.49
KCO3-			0.00	0.00	0.00	0.00
CaHCO3+			3.96	2.57	0.00	0.00
CaCO3(aq)			0.26	0.23	0.05	0.46
HCO3-	91.10	92.66	77.85	80.10	0.00	0.00
CO3-2	0.22	0.31	0.15	0.25	0.03	0.64
CO2(aq)	8.68	7.03	9.11	6.34	0.00	0.00

Fig. 4-4: Modelling of carbon speciation in clay systems

In the case of partial thermodynamic equilibrium, it was assumed that the formation of alkanes is kinetically hindered. See text for details of the scenarios A, B, and C. Input data are given in App. B.

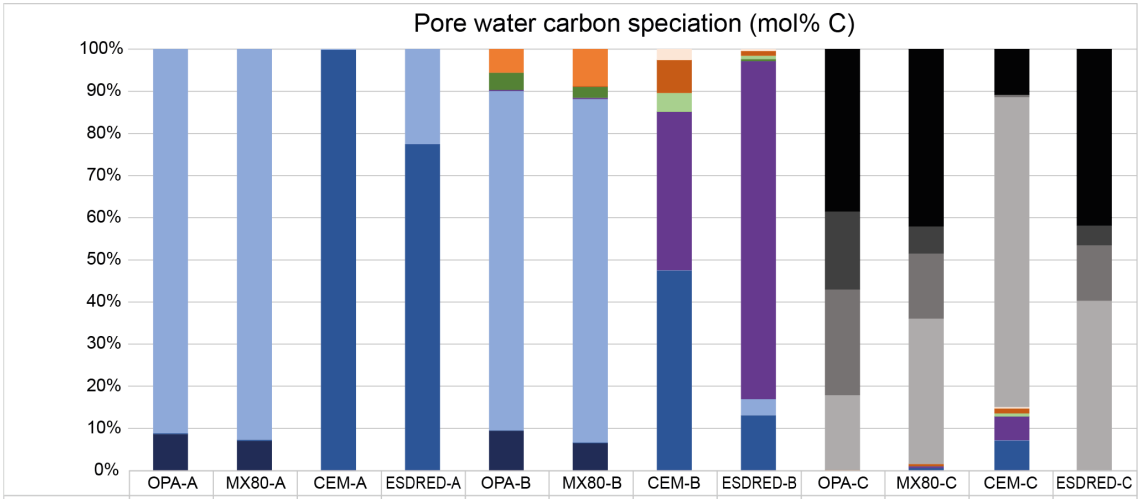

	OPA-A	MX80-A	CEM-A	ESDRED-A	OPA-B	MX80-B	CEM-B	ESDRED-B	OPA-C	MX80-C	CEM-C	ESDRED-C
Prop-	0.00	0.00	0.00	0.00	0.00	0.00	0.00	0.00	38.46	42.03	10.84	41.49
Pent-	0.00	0.00	0.00	0.00	0.00	0.00	0.00	0.00	18.50	6.42	0.02	4.61
But-	0.00	0.00	0.00	0.00	0.00	0.00	0.00	0.00	25.11	15.46	0.48	13.01
Ace-	0.00	0.00	0.00	0.00	0.00	0.00	0.00	0.00	17.78	34.49	73.52	39.92
SrCO3(aq)					0.00	0.00	2.59	0.42	0.00	0.00	0.39	0.00
NaHCO3(aq)					5.33	8.59	0.00	0.04	0.00	0.00	0.00	0.00
NaCO3-					0.08	0.19	7.81	1.09	0.01	0.49	1.18	0.00
KCO3-					0.00	0.00	4.43	0.80	0.00	0.00	0.67	0.00
CaHCO3+					3.96	2.57	0.00	0.53	0.00	0.00	0.00	0.00
CaCO3(aq)					0.26	0.23	37.60	80.10	0.05	0.46	5.69	0.02
HCO3-	91.10	92.66	0.16	22.53	77.85	80.10	0.07	3.83	0.00	0.00	0.01	0.00
CO3-2	0.22	0.31	99.84	77.47	0.15	0.25	47.48	13.14	0.03	0.64	7.16	0.00
CO2(aq)	8.68	7.03	0.00	0.00	9.11	6.34	0.00	0.00	0.00	0.00	0.00	0.00

Fig. 4-5: Modelling of carbon speciation in cementitious systems

In the case of partial thermodynamic equilibrium, it was assumed that the formation of alkanes is kinetically hindered. See text for details of the scenarios A, B, and C. Input data are given in App. B.

4.1.4 Complete versus partial thermodynamic equilibrium

Field observations and results from experimental studies have been successfully interpreted in terms of metastable thermodynamic equilibria in the C-H-O system, for example, the high concentrations of acetic acid observed in some sedimentary basins (see e.g., Wieland & Hummel 2015 for further discussion and references therein). Nevertheless, a number of field observations and experimental results could not be interpreted in terms of metastable equilibria, for example, the relative abundances of acetic and propionic acids observed in the sedimentary basins. Thus, it is believed that the predictive capability of thermodynamic modelling is limited due to uncertainties associated with the concept of metastability in the C-H-O system even though this concept is often very useful to rationalise field observations and experimental findings (Wieland & Hummel 2015).

In this study, the concept of metastability was applied to assess the effect on the predominance of carbon species in conditions relevant to L/ILW and HLW repositories. Species distributions predicted on the basis of complete thermodynamic equilibria suggest that the predominant carbon species over the entire pe ranges at pH 7.5 and 12 are CO_2(aq), HCO_3^-, CO_3^{2-} and CH_4(aq). The concentrations of C_2H_6(aq) and especially those of the carboxylates and alcohols are orders of magnitude lower. On the basis of partial thermodynamic equilibrium, the importance of these compounds increases under strongly reducing conditions, while the carbonates (CO_2(aq), $HCO_3^-$and CO_3^{2-}) still dominate under mildly reducing to oxidising conditions

(pe > -2.5 eV; E_h > -0.15 eV). On the assumption that the formation of HCs (CH_4 and higher alkanes and alkenes) is inhibited, the stability field of the carbonates increases slightly at the expense of the stability field of HCs (in particular CH_4(aq)) and the long-chained alcohols at pH 7.5, while at pH 12, carboxylates become the most thermodynamically stable carbon compounds. Nevertheless, C_2H_6(aq) and other higher alkanes become the dominant species on the assumption that only the formation of CH_4(aq) is inhibited. Hence, appearance of oxygenated carbon compounds, i.e., carboxylates in L/ILW and alcohols in HLW, is expected if the formation of all HCs is inhibited. This finding implies that the key to assessing the speciation of carbon under the reducing conditions of a repository environment is a more detailed understanding of the kinetic processes leading to the formation of the carbon compounds, in particular, the availability of abiotic and biotic catalysts. In the following sections, the kinetics of those processes controlling the carbon speciation at the metallic iron/steel-water interface and in connection with the degradation of organic matter is discussed.

4.2 Kinetic-related processes determining carbon speciation

4.2.1 Carbon species formed during anoxic corrosion of iron and steel

The type of carbon species generated during the corrosion of iron and steel is likely to be determined both by the chemical form of the carbon in the base metal and the corrosion conditions (Mibus et al. 2018). For example, the availability of oxygen may be an important parameter determining the ratio between oxygenated and reduced carbon compounds. As discussed in Sections 3.1.1 and 3.1.5.1, carbon may be present in the form of interstitial carbides and/or carbonitrides dissolved in the principal iron phase of iron or steel (e.g., ferrite in carbon steel or austenite in the 300-series of stainless steel). It is expected that the abundance of the different carbon species in the metal matrix is determined by the steel composition and the production process of the steel (Mibus et al. 2018). For example, the presence of alloying components (e.g., Cr, Mn, Nb, Ti etc.) may have an influence on the reactivity of carbides (Section 3.1.5.1). In the following sections, the processes controlling the formation of carbon species at the metallic iron/steel-water interface are discussed with respect to the influence of corrosion conditions.

4.2.1.1 Fischer-Tropsch process

To date, only a limited number of studies have investigated the mechanistic aspects of the formation of carbon species at the metallic iron/steel-water interface during corrosion in circum-neutral to alkaline solutions (see Wieland & Hummel 2015 and references therein; Cvetković et al. 2018a; Deng et al. 1997; Guillemot et al. 2020a; Hardy & Gillham 1996; Swanton et al. 2015). Hardy & Gillham (1996) observed the formation of HCs in metallic iron-water systems using commercial iron filings immersed in CO_2-containing, simulated groundwater for their experimental studies. They further noted that the relative ratios of the HC products were consistent with those reported in Fischer-Tropsch (F-T) processes. Deng et al. (1997) showed that carbon initially present in zero-valent iron (ZVI) powders is the source of HCs produced during iron corrosion. The authors further postulated that HCs are produced by an F-T-type process. Deng and co-workers proposed that iron carbide present in the iron fillings used for the experiments react through processes similar to those that occur in F-T synthesis. The results from the experimental studies of Cvetković et al. (2018a) and Guillemot et al. (2020a) further support the idea that the formation of volatile HCs at the surface of corroding iron can be attributed to an F-T-type process.

In the F-T synthesis, CO and H_2 in the gas phase are passed over a catalyst at elevated temperatures to produce HCs. The polymerisation reactions occur on the surface of the metal catalysts leading to the formation of long-chain HC products, such as n-paraffins and α-olefins, but also smaller HCs, as initially proposed by Fischer & Tropsch (1923). Process conditions of

the F-T synthesis typically involve pressures between 10 and 60 bar and temperatures ranging from 200 to 350 °C with cobalt, ruthenium or iron catalysts (Anderson 1984). The reaction includes several steps including reactant adsorption, chain initiation, chain growth, chain termination, product desorption and re-adsorption (Ordomsky et al. 2015; Van der Laan & Beenackers 1999). Polymerisation occurs by the addition of the monomeric units -CH_2- to a growing HC chain. The probability for either chain propagation or termination is essentially constant irrespective of the length of the HC chain, while it can be influenced by the catalyst properties and reaction conditions (Anderson 1984; Van der Laan & Beenackers 1999).

The molecular size distribution in the linear condensation of polymers was originally developed by Flory (1936) and later applied to describe the product distribution in F-T synthesis, also known as Anderson-Schulz-Flory (ASF) product distribution (Anderson 1984; Friedel & Anderson 1950; Henrici-Olivé & Olivé 1976; Van der Laan & Beenackers 1999). The molar distribution of HCs with n carbon atoms produced by F-T synthesis is given by:

$$m_n = (1-\alpha)\alpha^{n-1} \quad (1)$$

where m_n is the mole fraction of the molecule having a chain length n. The product distribution can also be expressed in terms of a weight distribution:

$$w_n = n(1-\alpha)^2\alpha^{n-1} \quad (2)$$

The product distribution is determined by the chain growth probability α, which is given by the ratio between the rate of propagation and the sum of the rates of propagation and termination:

$$\alpha = R_p/(R_p+R_t) \quad (3)$$

where R_p and R_t are the rates of propagation and termination, respectively. The growth probability factor α is independent of the chain length n.

Several mechanisms have been proposed for the F-T synthesis, but a proof of the true mechanism is challenging (Anderson 1984; Dry 1981; Van der Laan & Beenackers 1999). Nevertheless, there is a general consensus that the carbide mechanism is the dominant one (Fig. 4-6) (Anderson 1984). This mechanism is based on the dissociative adsorption of both CO and H_2. The surface carbide is hydrogenated to form a reactive CH_2 radical ($CH_2^{\bullet}$) as a building entity. Polymerisation of these building blocks gives rise to the formation of longer HC chains attached to the catalyst surface. The products are formed by termination reactions such as hydrogenation or hydrogen abstraction. Other products like alcohols and aldehydes can be formed via termination reactions with oxygen-containing surface species (Anderson 1984).

The E_h-pH diagram for the Fe(0)-H_2O system indicates a negative redox potential at the iron-water interface and the production of H_2 during corrosion in anoxic conditions (Jelinek & Neufeld 1982; Ning et al. 2014). It has been shown that H_2 is a reductant on catalysts in the synthesis of long-chain HCs by the F-T process (Anderson 1984; Dry 1981). Therefore, there is evidence to suggest that the carbide mechanism invoked for F-T synthesis can adequately describe the formation of HCs during anoxic corrosion of iron/steel.

4.2.1.2 Formation of hydrocarbons

An F-T-type process based on the carbide mechanism was considered to account for the product distribution during iron/steel corrosion (Cvetković et al. 2018a; Deng et al. 1997; Guillemot et al. 2020a). The notion of an F-T-type process is further supported by the material properties of iron and steel. Iron carbide Fe_3C (cementite) is the predominant chemical form of carbon in mild and stainless steels with low carbon contents (Section 3.1.5.1) (Davis 1991; Mitchell 2004). Thus, it is conceivable that the formation of HC during corrosion occurs by the formation of reactive carbide atom ($C^{\bullet}$) with H radicals ($H^{\bullet}$) at the iron/steel surface. Polymerisation of the $CH_2^{\bullet}$ units then generates longer chain HCs (Fig. 4-6). It should be noted that methylidyne ($^{\bullet}CH$), methylene ($:CH_2$), and methyl fragments ($^{\bullet}CH_3$) were shown to be key intermediates in the reaction between CO with H_2 in the F-T process (Kaminsky et al. 1986).

Guillemot et al. (2020a) interpreted the product distribution during corrosion of non-activated ZVI powders in terms of an ASF product distribution (Fig. 4-6). This finding implies that the relative proportion of HC decreases with increasing chain length. Hence, CH_4 is the predominant HC formed during corrosion, while the proportions of the HCs containing between 2 and 4 C atoms decreases although the total of C2-C4 carbon compounds is larger (C2-C4 in Fig. 4-6). Measurements of HC concentrations in metallic iron-water systems corroborated the order of abundance: $CH_4 > C_2H_6 \sim C_2H_4 > C_3H_8 \sim C_3H_6 > C_4H_{10}$ etc. (Cvetković et al. 2018a; Guillemot et al. 2020a). The experimental and modelled data shown in Fig. 4-6 further agree for α ranging between 0.5 and 0.7, which is considered as the growth probability factor on catalytic iron surfaces (Van der Laan & Beenackers 1999).

Heikola & Ollila (2018) identified the carbon compounds in leaching experiments with Fe_3C under anoxic, near-neutral and alkaline conditions (simulated groundwaters with pH 8.5 and 12.5). The authors identified the following HCs: C_2H_6, C_3H_8, 2-methylpropane, pentane at pH 8.5, and C_2H_6, C_3H_8, propylene, butane, 2-butene, 2-methylbutane, pentane, pentene and hexane at pH 12.5. The presence of alcohols was indicated, while their concentration was found to be below the limit of quantification. The study also supports the idea that only small gaseous molecules (here < C6) are formed during iron/steel corrosion.

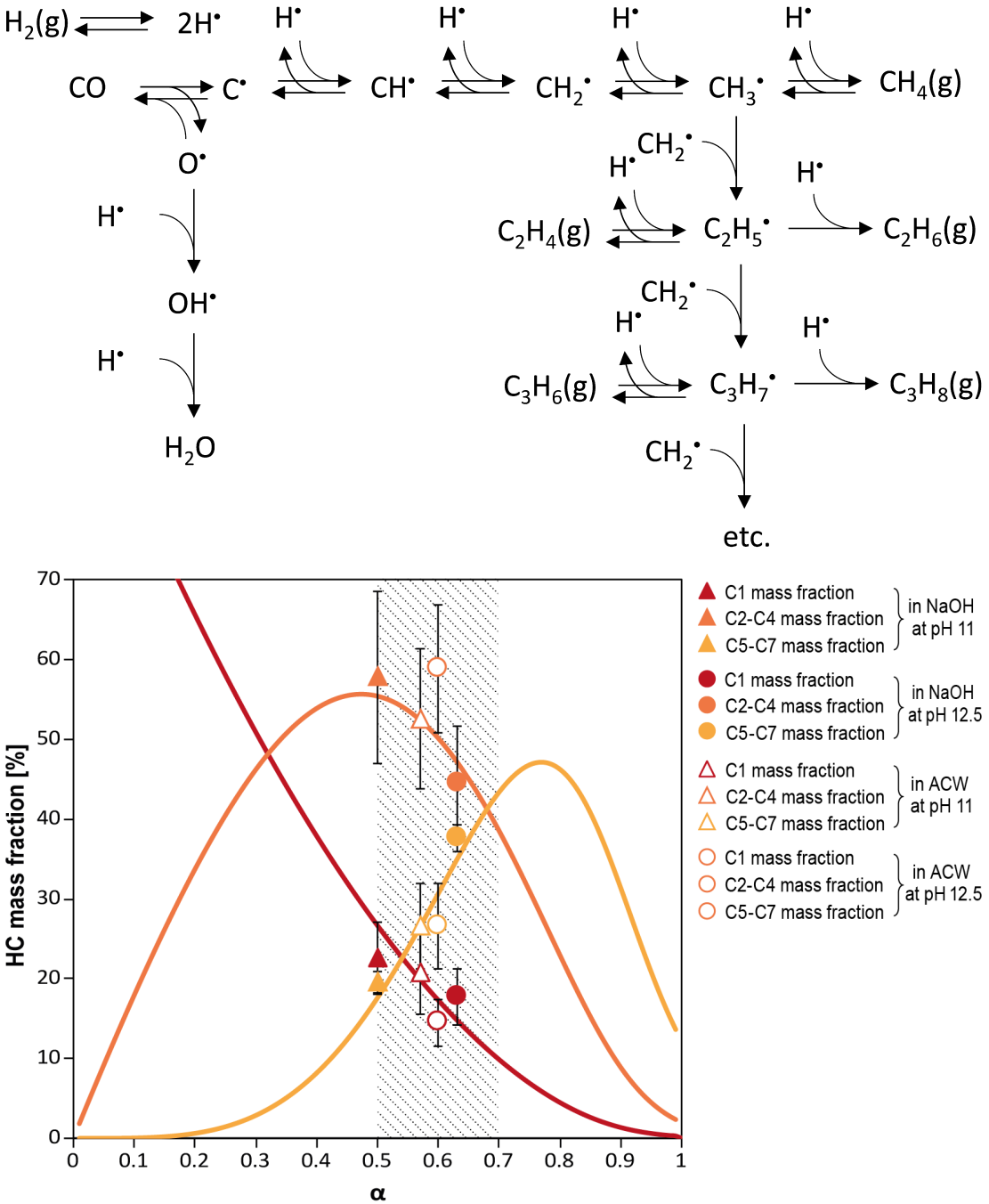

Fig. 4-6: a) Schematic of the carbide mechanism (from De Deugd 2004). b) HCs selectivity as a function of the chain growth probability factor α (from Guillemot et al. 2020a)

The lines (bottom) represent the modelled data: HC with one carbon (CH_4; in red), HCs with between two and four carbons (in orange) and HCs with between five and eleven carbons (in yellow). Experimental data are illustrated by points with error bars: C1 (red), C2-C4 (orange), C5-C7 (yellow). The mass fractions were calculated from HC concentrations measured during the corrosion of BASF-pre powder in NaOH (full symbols) and artificial cement water (ACW) (empty symbols) at pH 11 (triangle symbols) and at pH 12.5 (round symbols) as reported by Cvetković et al. (2018a) and Guillemot et al. (2020a). The shaded area highlights the expected range of α on catalytic iron/steel surfaces (Van Der Laan & Beenackers 1999).

The HCs expected to be formed during the course of iron/steel corrosion are listed in Tab. 4-1. This compilation is based on an earlier literature review by Wieland & Hummel (2015) and more recent studies on the carbon speciation during iron corrosion.

Tab. 4-1: Carbon species expected to be formed as a result of iron/steel corrosion and Fe_3C leaching in alkaline conditions

Modified from Wieland & Hummel 2015

Gaseous compounds[*]	**Alcohols/aldehydes**[**]	**Carboxylates**[***]	**Carbonate**[****]
Methane (CH_4)	Methanol (CH_3OH)	Formate ($HCOO^-$)	HCO_3^-
Ethane (C_2H_6)	Ethanol (C_2H_5OH)	Acetate (CH_3COO^-)	CO_3^{2-}
Ethene (C_2H_4)	Propanol (C_3H_7OH)	Propionate ($C_2H_5COO^-$)	
Propane (C_3H_8)	Formaldehyde (CH_2O)	Butanoate ($C_3H_7COO^-$)	
Propene (C_3H_6)	Acetaldehyde (C_2H_4O)	Lactate ($CH_3CHOHCOO^-$)	
Butane (C_4H_{10})	Propionaldehyde (C_3H_6O)	Malonate ($CH_2(COO^-)_2$)	
Butylene (C_4H_8)[*****]		Oxalate ($C_2O_4^{2-}$)	
Pentane (C_5H_{12})[******]			
Pentene (C_5H_{10})[******]			
Hexane (C_6H_{14})			
Carbon monoxide (CO)			
Carbon dioxide (CO_2)			

* Hardy & Gillham (1996), Deng et al. (1997), Kaneko et al. (2003), Noshita (2008), Cvetković et al. (2018a), Guillemot et al. (2020a), de Visser-Týnová et al. (2018b), Heikola & Ollila (2018).

** Kaneko et al. (2003), Sasoh (2008a,b), Takahashi et al. (2014), Cvetković et al. (2018a), Heikola & Ollila (2018), Tanabe et al. (2007).

*** Kaneko et al. (2003), Sasoh (2008a,b), Takahashi et al. (2014), Cvetković et al. (2018a), Guillemot et al. (2020a), Tanabe et al. (2007).

**** Kaneko et al. (2003), Noshita (2008), de Visser-Týnová et al. (2018b).

***** Including isomers (e.g., trans-2-butene, cis-2-butene, 1-butene, iso-butene) (Heikola & Ollila 2018).

****** Including isomers (e.g., 2-methylbutane, cis-2-pentene, trans-2-pentene) (Hardy & Gillham 1996; Deng et al. 1997; Heikola & Ollila 2018).

4.2.1.3 Presence of oxygenated carbon compounds

Cvetković et al. (2018a) and Guillemot et al. (2020a) demonstrated that oxygenated carbon compounds are also present in metallic iron-water systems during anoxic corrosion of ZVI powders. The presence of oxidised carbon species during iron/steel corrosion and Fe_3C leaching, such as carboxylic acids, alcohols and aldehydes, was previously reported (Kaneko et al. 2003; Noshita 2008; Sasoh 2008a; Takahashi et al. 2014; Tanabe et al. 2007). Cvetković et al. (2018a) and Guillemot et al. (2020a) show, however, that both HCs (i.e., reduced carbon species) and oxygenated carbon species are simultaneously present in metallic iron-water-systems and further that their formation can presumably be attributed to different processes occurring at the metallic iron-water interface in systems with non-activated iron powders. In line with the study of Deng et al. (1997), the authors concluded that HCs are generated under the reducing conditions prevailing at the metallic iron-water interface during the course of the corrosion process under anoxic alkaline conditions, while oxygenated carbon species were identified in line with the Japanese studies, and their formation was attributed to exposure of the iron surface to oxic conditions.

Small carboxylic acids were found to be the predominant oxygenated carbon compounds during the anoxic corrosion of ZVI powders while the concentration of aldehydes (acetaldehyde, formaldehyde) and alcohols (methanol, ethanol) was much lower (Cvetković et al. 2018a). Acetate (CH_3COO^-), formate ($HCOO^-$), oxalate ($C_2O_4^{2-}$), lactate ($CH_3CHOHCOO^-$), and malonate ($CH_2(COO^-)_2$) were identified as the main carboxylates present in alkaline metallic iron-water systems (Cvetković et al. 2018a; Guillemot et al. 2020a). The tentative order of abundance was given as follows: $CH_3COO^- \geq HCOO^- > C_2O_4^{2-} > CH_3CHOHCOO^- > CH_2(COO^-)_2$. The concentrations of other carboxylates, such as propionate and butanoate, were found to be below the detection limit. The studies of Cvetković et al. (2018a) and Guillemot et al. (2020a) further show that the carboxylates are released to solution by a fast process of detachment accomplished within less than three days upon contacting ZVI with alkaline solution. Fast release occurred irrespective of the type of oxidative pre-treatments of ZVI, the exposure time of the ZVI powder to oxic conditions or the chemical composition of the solution in which the ZVI powder was immersed for the corrosion studies. Furthermore, the concentrations of the carboxylates did not increase during the course of the anoxic corrosion of ZVI. The latter process was indicated by an increase in H_2 concentration with time. Note that the production of H_2 occurs during anoxic corrosion according to the reaction $3Fe + 4H_2O \rightarrow Fe_3O_4 + 4H_2$ (e.g., Jelinek & Neufeld 1982). This finding implies that the presence of carboxylates in the alkaline metallic iron-water system was not related to the ongoing corrosion process. Cvetković et al. (2018a) postulated that oxygenated carbon compounds are formed during exposure of ZVI to oxic conditions (Fig. 4-7). These compounds are accommodated by the oxide layer of the iron/steel surface and instantaneously released upon contact of the metal with water. It is assumed that the release of organic and inorganic ^{14}C occurs by diffusion through the oxide layer and/or as a result of the conversion of iron oxyhydroxides into magnetite (Ishikawa et al., 1998; Tamaura et al., 1983). Oxidation of carbon accommodated by the iron/steel oxide layer may occur at different stages of the service life of the material (handling, storage and treatment in oxic conditions). As a result, carbon compounds with very different redox properties (i.e., HCs, carboxylates) are released in corroding, metallic iron-water systems. The carboxylates identified during iron/steel corrosion are listed in Tab. 4-1.

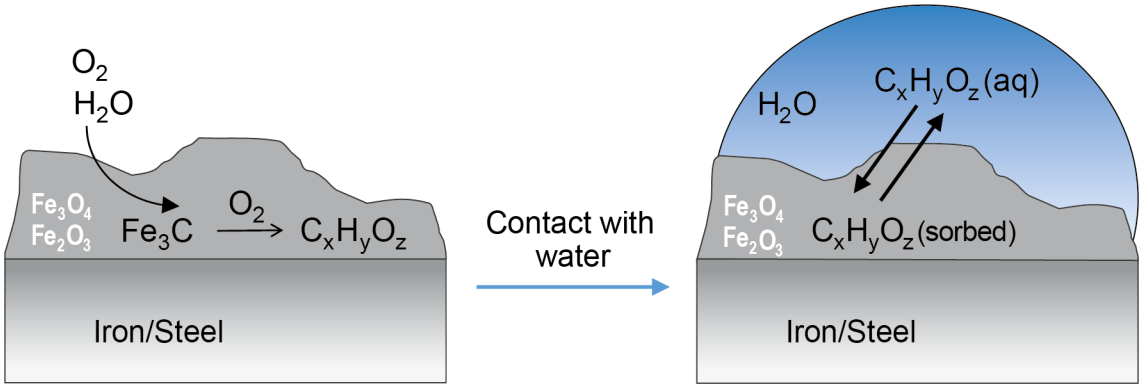

Fig. 4-7: Schematic presentation of the oxidation of carbon in iron/steel during exposure to oxic conditions and subsequent release from the oxide layer to solution

4.2.1.4 Effect of radiation on carbon speciation

The waste materials will be a source of α-, β- and γ-radiation resulting from the decay of radionuclides, thus leading to an activated near-field environment. Nevertheless, the intensity of radiation will decrease with time. Ionising radiation emitted from the activated waste materials (e.g., activated steel, SF) gives rise to the decomposition of water (water radiolysis), which results in the production of both radicals (e^-_{aq}, $H^\bullet$, $HO^\bullet$, $HO_2^\bullet$) and molecules (O_2, H_2, H_2O_2, CO, CO_2, CH_4). The radicals and molecules can act either as oxidants (e.g., $HO^\bullet$, $HO_2^\bullet$, H_2O_2, O_2) or reductants (e.g., e^-_{aq}, $H^\bullet$, H_2) (Le Caer 2011; Mincher & Mezyk 2009; Spinks & Woods 1990). The production rate and species distribution depend on the dose rate and the nature of radiation (α, β, γ), over the period of concern for a deep geological repository. Furthermore, water radiolysis may be affected by processes at solid/liquid interfaces (Le Caer 2011). For example, enhanced concentrations of H_2 produced by radiolysis of water and the anoxic corrosion of steel has an impact on steel corrosion (Daub et al. 2010) and the oxidative dissolution of SF (Jonsson et al. 2007; Spahiu et al. 2004). In particular, oxidative dissolution of the UO_2 matrix of SF was found to be strongly inhibited at concentrations of dissolved H_2 above 4 mM (Spahiu et al. 2004).

Examples of the effect of radiation on the decomposition of low molecular weight (LMW) organic compounds have been reported by Kani et al. (2008) and Toste et al. (1994). Toste et al. (1994) investigated the effect of radiolysis on the stability of citrate ($C_6H_8O_7$) (initial concentration 43.5 mM) in a simulant of a mixed waste (pH 13.5) using a ^{60}Co source with a high dose rate of 750 Gy/h (total absorbed dose ranging between ~ 3.8 and 75 kGy). The authors observed rapid decomposition of citrate with time. The only product identified at significant concentrations was propanedioic (malonic) acid ($C_3H_4O_4$), while the largest portion of the decreasing organic C content (i.e., decreasing concentration of citrate) could not be characterised. There is evidence to suggest that CO_3^{2-} was an important product in this experiment, which might have precipitated as carbonate in the given conditions (high pH, high initial concentration). Kani et al. (2008) studied the decomposition of organic carbon compounds (acetic acid, ethanol, formaldehyde) by γ-radiation at dose rates ranging between 10 and 1,000 Gy/h (total absorbed dose ~ 2 kGy) under conditions relevant to a cement-based repository (pH 12.5). The decomposition of the organics was explained in terms of a reaction with OH radicals while there was no assessment reported regarding the presence of other oxidising species (e.g., H_2O_2). The authors observed that the LMW organic acids, alcohols and aldehydes reacted with OH radicals to generate carbonic acid (H_2CO_3). Interestingly, the decomposition efficiency of acetic acid was independent of the dose rate, thus implying that a dose rate of 10 Gy/h (at a total absorbed dose of ~ 2 kGy) was already sufficient to produce enough oxidants to decompose ~ 90 % of the initially present molecules (10^{-6} mol/L). This finding shows that radiolysis could promote the conversion of LMW organic carbon compounds present in metallic iron-water systems into the inorganic form (i.e., carbonates).

The type of radiation largely determines the nature of the radiolytic products. α- and β-radiations allow a high radical yield, while γ-radiation mainly produces molecular radiolysis products, such as H_2, O_2 and H_2O_2 (Spahiu et al. 2004). For these two oxidants, H_2O_2 is considered to be the more important one under the conditions of a deep geological repository (Ekeroth & Jonsson 2003). High concentrations of H_2 were found to influence the radiolytic production rate and yield of H_2O_2, partially due to the conversion of hydroxyl radicals into H atoms. For example, radiolysis products, such as H_2O_2, were not detected in γ-irradiated water with H_2 concentrations above the aforementioned threshold. By contrast, almost no effect of dissolved H_2 was observed on the production of H_2O_2 by high-energy α-particles (Pastina et al. 1999; Pastina & LaVerne 2001). The reaction between H_2 and H_2O_2 in water at low temperature, however, seems to be very slow although the reaction is thermodynamically favourable (Nilsson & Jonsson 2008). Under such conditions, H_2O_2 produced further away from the steel surface may significantly contribute to corrosion (Ekeroth et al. 2006; Toijer & Jonsson 2019). The latter authors further concluded

that the relative impact of H_2O_2 on the corrosion of steel and SF could very well exceed that of the $HO^{\bullet}$ by orders of magnitude at room temperature. The current assessment suggests that H_2O_2 is a potential oxidant in the near-field of a deep geological repository that could influence carbon speciation.

Regarding the long-term assessment of carbon speciation, however, ^{60}Co should be taken into account as this is the main radioisotope in activated steel (Schumann et al. 2014) and largely determines the dose rate over time in the L/ILW repository. Although an initial high dose rate associated with ^{60}Co decay may occur, this will rapidly decrease with time (^{60}Co half-life of 1,925 days) such that low dose rates in the near-field of the L/ILW repository are anticipated in the long term. Hence, the importance of radiolysis will diminish with time and lead to negligible concentrations of oxidants in the long term. In an HLW repository, α-radiation will be dominant in "old" SF (> 1,000 years) (Spahiu et al. 2004) and the presence of dissolved H_2 may have limited impact on the H_2O_2 concentration. The presence of significant concentrations of oxidising agents could lead to the preferential formation of oxygenated carbon compounds. Nevertheless, the inventory of carbon is negligibly small in the HLW repository compared to the L/ILW repository and, therefore, the formation of oxygenated carbon compounds is likely negligible.

4.2.2 Degradation of organic carbon compounds

According to the MIRAM-RBG database (Nagra 2023), when ^{14}C is associated with organic materials (i.e., cellulose, plastics), they are considered *contaminated* (i.e., ^{14}C is present on their surface only), rather than *activated* (i.e., when ^{14}C is bound in the structure). Hence, ^{14}C-contaminated organic materials (i.e., cellulose, plastics) are not considered to release ^{14}C congruently with degradation. Instead, ^{14}C is expected to be instantaneously released from these wastes once their surface is in contact with solution (cf. Section 5.8). ^{14}C-organic compounds released from contaminated materials are subjected to further degradation and release ^{14}C congruently in smaller chemical forms. The degradation processes of LMW organics in the context of a deep geological repository is, therefore, briefly described in this section. More detailed information can be found in Guillemot et al. (2023).

Organic carbon compounds will decompose with time under the conditions of a deep geological repository (Hallbeck 2010). However, the rate of degradation may vary considerably among the organic compounds depending on their chemical nature (e.g., monomeric, polymeric) and conditioning. Furthermore, the degradation process may be influenced by the geochemical conditions of the near-field. For example, microbial degradation of organic carbon compounds is expected to take place under circum-neutral to weakly alkaline conditions (typically pH < 11), while abiotic degradation, if possible, may be the only pathway that leads to chemical instability of the organic compounds under strongly alkaline conditions.

Abiotic degradation of specific polymeric organic carbon compounds under alkaline conditions has been observed and, in the context of the safe disposal of radioactive waste, this process has been explored in detail in numerous studies in the case of cellulose (e.g., Glaus et al. 1998; Glaus & Van Loon 2008; Glaus et al. 1999; Knill & Kennedy 2003; Pavasars et al. 2003; Van Loon & Glaus 1998). The degradation studies focussed on the formation of complexing ligands during cellulose degradation, in particular the formation of isosaccharinic acid and its complexation properties. The abiotic degradation of cellulose is not further discussed in the framework of the present study.

Abiotic degradation of organic carbon compounds takes place via redox processes and results in the formation of small carbon compounds such as CO_2 and CH_4. Most of these redox reactions are expected to be extremely slow at the moderate temperatures in the L/ILW repository (T ~ 40 °C) (Kosakowski et al. 2014, 2023) and at the elevated temperatures (T < 100 °C) in the

HLW repository (Bradbury et al. 2014; Curti et al. 2023). Nevertheless, some reactions may be accelerated in the presence of catalytic surfaces, such as Fe(II,III) oxides on steel surfaces. The corrosion of activated metals and the degradation of organic carbon compounds are expected to mainly produce ^{14}C-carrying LMW molecules (see e.g., Tab. 4-1). These small molecules are either water-soluble or volatile and may be retarded by interaction with near-field materials and/or the host rock. Carboxylic acids are among those water-soluble carbon compounds that could carry ^{14}C and could be subject to further degradation processes, both of abiotic and biotic nature. In this context, the results of an investigation of the carbon speciation during the abiotic degradation of $HCOO^-$ and CH_3COO^- in alkaline media are summarised in the following section. The two carbon compounds are representatives of LMW carboxylic acids present in a deep geological repository (Tab. 4-1). The consequences for carbon speciation due to biotic degradation of organic carbon compounds will be briefly discussed in Section 4.2.2.2.

4.2.2.1 Abiotic degradation of organic carbon compounds under alkaline conditions

There is little information in the scientific literature on the abiotic degradation of LMW organic molecules at temperatures below 100 °C. Several studies have focussed on degradation processes under hydrothermal conditions (high temperature and pressure) in connection with geochemical research exploring the formation of petroleum and natural gas reserves or the chemistry of hydrothermal fluids in deep-sea environments (Amend et al. 2013; McCollom 2016; McCollom & Seewald 2003a,b; McCollom & Seewald 2007; Seewald et al. 2006). Further research into the degradation processes of LMW organic carbon compounds has been conducted in the context of research for industrial applications, such as the conversion of biomass into HC fuels (Bennett et al. 2017; Wang & Iglesia 2017) or the storage of hydrogen in the chemical form of formic acid (HCOOH) (Grasemann & Laurenczy 2012; Loges et al. 2010). The results from these studies can be considered with a view to assessing the kinetic parameters that might be important during abiotic degradation, although they cannot be used directly to predict the long-term fate of LMW organic compounds in the near-field of a deep geological repository, where temperature and pressure are significantly lower.

CH_3COO^- and $HCOO^-$ are the main oxygenated carbon compounds present during the corrosion of iron/steel in alkaline media (Section 4.2.1.3) and are, therefore, potentially ^{14}C-carrying compounds. Tits et al. (2019) recently published an investigation on the abiotic degradation of CH_3COO^- and $HCOO^-$ under alkaline conditions at enhanced partial pressure of H_2 and in the presence of a potential catalyst. The aim was to explore the abiotic degradation of the two molecules under conditions that simulate *in situ* long-term conditions in the near-field of a cement-based repository. This is the only reported study of degradation of LMW organic compounds carried out in conditions relevant to a repository environment (alkaline media, presence of H_2 and catalyst). The degradation of CH_3COO^- and $HCOO^-$ in gas-tight pressurised reactors and autoclaves was followed as a function of time using ^{13}C- and ^{14}C-labelled molecules of the two compounds. The experiments were carried out in high-purity, deionised water and in 0.01 M NaOH (pH 12) as well as in solutions containing different $Ca(OH)_2$ concentrations between 10^{-3} M (pH ~ 11) and 2×10^{-2} M (pH ~ 12.5) in an oxygen-free atmosphere (either N_2 or 5/95% H_2/N_2 (forming gas)) at elevated pressures (2 bar $\leq p \leq$ 16 bar) and at elevated temperatures (50 °C $\leq T \leq$ 200 °C) to accelerate the decomposition. Such temperatures are significantly higher than the maximum temperatures expected in a deep geological repository. Therefore, the results of this study should be interpreted as a worst-case scenario for degradation. The potential catalytic effect of iron or steel on the decomposition of $HCOO^-$ and CH_3COO^- was investigated by adding ZVI or exposing the solutions to the inner steel surface of the reactor vessel. Selected experimental data from Tits et al. (2019) are displayed in Fig. 4-8. The technical aspects and the complete set of experimental data are detailed elsewhere (Tits et al. 2019).

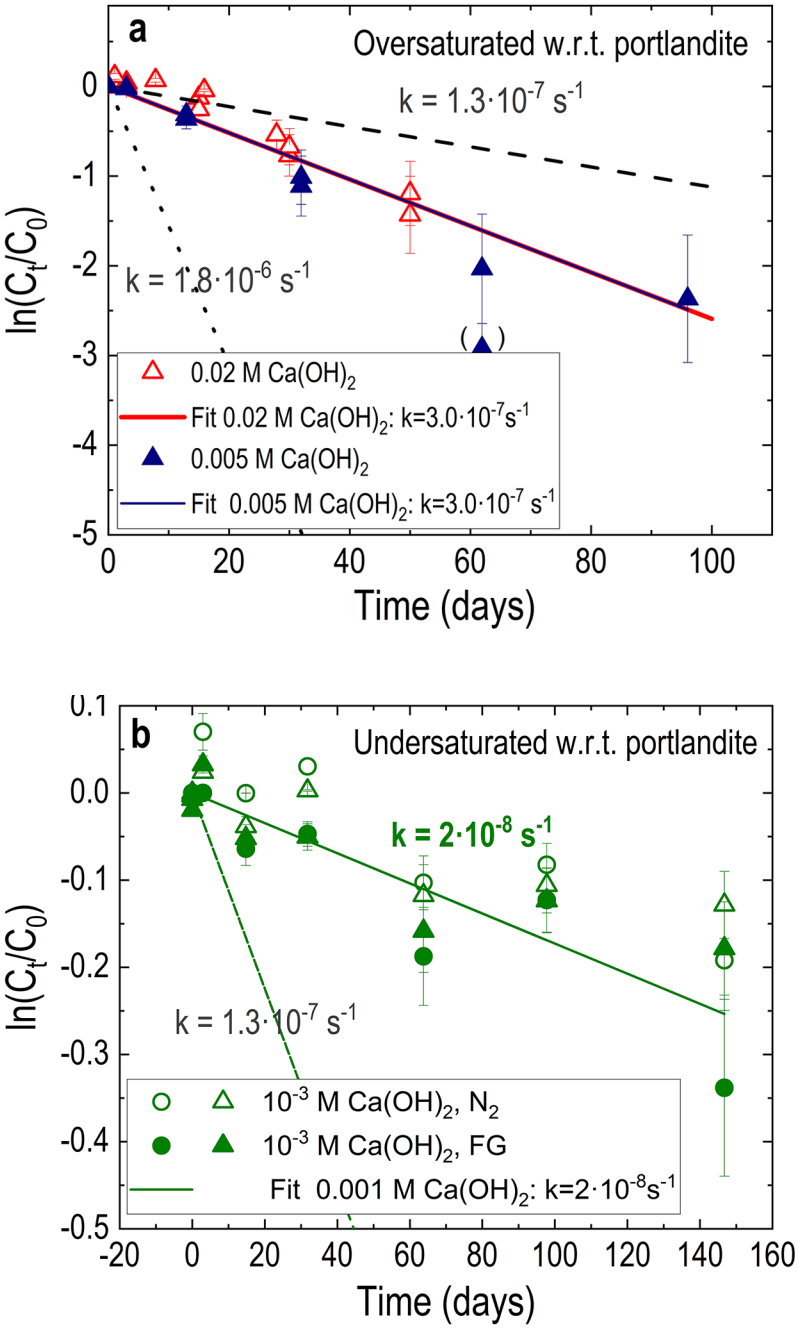

Fig. 4-8: Decomposition kinetics of $HCOO^-$ measured at 150 °C under saturated vapour pressure in contact with the stainless steel reactor wall in the systems a) oversaturated w.r.t. portlandite and b) undersaturated w.r.t. portlandite

From Tits et al. (2019)

Data are plotted as the natural logarithm of the ratio of the $HCOO^-$ concentration at time (t), to the initial $HCOO^-$ concentration (C_t/C_0) as a function of reaction time. Dashed and dotted lines represent first-order kinetic behaviour with decomposition rate constants determined by McCollom & Seewald (2003) in the presence of an NiFe alloy ($k = 1.3\times10^{-7}$ s^{-1}) and in presence of a hematite and magnetite mixture (1.8×10^{-6} s^{-1}).

Complementary to the experiments, thermodynamic calculations were conducted to simulate the carbon speciation at equilibrium (Tits et al. 2019). From a thermodynamic point of view, $HCOO^-$ and CH_3COO^- proved to be unstable under the experimental conditions used by Tits and co-workers. On the assumption of complete thermodynamic equilibrium, $HCOO^-$ should decompose into CO_2 or CH_4 until equilibrium $HCOO^-$ concentrations are reached (Wieland & Hummel 2015). The ratio of $HCOO^-$ to degradation products depends on the redox potential. However, it is known that most of the reactions leading to the formation of CH_4 are very slow. For example, Seewald et al. (2006) showed that, under hydrothermal conditions, $HCOO^-$ oxidation to CO_2 and reduction to formaldehyde (CH_2O) and CH_3OH proceed quite rapidly, while further reduction to CH_4 is a very slow process. The influence of the very different kinetics of the various reaction steps was simulated in the thermodynamic calculations by switching off the reactions with slow kinetics responsible for the further reduction to CH_4.

The study of Tits et al. (2019) shows that $HCOO^-$ is thermodynamically unstable in alkaline media at moderately elevated temperatures under anoxic conditions. $HCOO^-$ was found to decompose into CO_2 and H_2 by a decarboxylation reaction (McCollom & Seewald 2003a):

$$HCOO^- + H^+ \rightarrow CO_2 + H_2 \quad (4)$$

Here, the electrons released during the oxidation of $HCOO^-$ reduce H^+ to H_2, such that the amount of H_2 produced equals the amount of $HCOO^-$ decomposed. This reaction has a high activation energy, though there is evidence in the literature that the presence of mineral phases such as magnetite and hematite may act as catalysts and reduce this energy barrier, thus accelerating the decomposition process (Maiella & Brill 1998; McCollom & Seewald 2003a).

The results reported by Tits et al. (2019) indicate that the decomposition of $HCOO^-$ occurs both in the presence and absence of Fe(0). Note, however, that in the absence of added Fe(0) powder, the stainless steel surface of the reactor could have acted as a catalyst. Furthermore, the addition of metallic Fe(0) to the experimental system established more strongly reducing conditions, which, from a thermodynamic point of view, stabilises $HCOO^-$. For this reason, it appears that at an E_h value of -0.74 V, only 80% of the $HCOO^-$ was decomposed.

McCollom & Seewald (2003a) determined the decomposition rate constants of HCOOH and $HCOO^-$ in weakly acidic and circum-neutral solutions under hydrothermal conditions (constant pressure of 350 bar, absence of a vapour phase, temperatures ranging from 175 to 260 °C). The authors also examined the effect of potential catalysts on the decomposition rate, such as NiFe alloy powder, hematite and magnetite powder mixtures, and olivine. NiFe alloy could act as a catalyst similarly to the inner stainless steel surface of the reactors in the study of Tits et al. (2019). Meanwhile, hematite and magnetite are produced during iron/steel corrosion. The study of McCollom & Seewald (2003a) shows that HCOOH and $HCOO^-$ decomposition follows a first-order-rate law. In addition, the decomposition rate of $HCOO^-$ was found to be about one order of magnitude lower than that of HCOOH. Tits et al. (2019) report decomposition rates of $HCOO^-$ similar in value to those observed in the literature under hydrothermal conditions. This result suggests that the same processes are responsible for the degradation of $HCOO^-$ under hydrothermal conditions and in a deep geological repository, although it should be noted that processes in a deep geological repository are much slower due to the much lower temperature compared to hydrothermal systems.

The decomposition of $HCOO^-$ was found to be temperature-dependent (Tits et al. 2019). At ambient temperature, the reaction is kinetically inhibited, thus making the quantification of $HCOO^-$ decomposition impossible under these conditions as the experimental period was limited to a few months. Thus, it was necessary to experimentally determine the kinetics of decomposition at elevated temperature.

The presence of Ca influences the decomposition rate (Tits et al. 2019). In NaOH at elevated temperature, the decarboxylation of $HCOO^-$ was found to proceed more slowly than in the Ca-containing solutions. This is not due to the increased thermodynamic stability of $HCOO^-$ in Na-containing solutions, but rather the result of accelerated decomposition in the presence of Ca. Experimental evidence suggests that the $HCOO^-$ decomposition reaction is accompanied by the production of CO_2 and thus proceeds via the decarboxylation process (Eq. 4). The CO_2 formed subsequently reacts with Ca to form $CaCO_3$. Tits et al. (2019) postulated that an increase in the Ca concentration promotes $HCOO^-$ degradation due to stabilisation of the carbonate formed as $CaCO_3$(aq) and $CaCO_3$(s). Therefore, the thermodynamically favoured formation of $CaCO_3$, either as aqueous species or precipitates, was considered to be the driving force that accelerates $HCOO^-$ decomposition.

Previous experimental studies carried out under hydrothermal conditions suggested that the decomposition of CH_3COOH occurs primarily by decarboxylation according to the reaction:

$$CH_3COOH \rightarrow CH_4 + CO_2 \quad (5)$$

Or, *via* oxidation of carbon according to the reaction:

$$CH_3COOH + 2\,H_2O \rightarrow 2\,CO_2 + 4\,H_2 \quad (6)$$

(Bell et al. 1994; Drummond & Palmer 1986; Kharaka et al. 1983; McCollom & Seewald 2003b; Palmer & Drummond 1986).

There is evidence that both decomposition pathways can be catalysed in the presence of some minerals, in particular by Fe-bearing minerals (Bell et al. 1994; Palmer & Drummond 1986). McCollom & Seewald (2003b) showed that CH_3COOH and CH_3COO^- decompose by a combination of the two reaction pathways. The authors further observed that both reactions are promoted by minerals. The oxidation reaction was catalysed by hematite, while magnetite catalysed decarboxylation. The oxidation reaction was found to be much faster. Thus, in the presence of hematite, oxidation was suggested to be the prevailing pathway of the decomposition of CH_3COOH and CH_3COO^-. In the absence of hematite or other suitable oxidants, however, mineral-catalysed decarboxylation is likely to dominate the decomposition reaction, resulting in a mixed CH_4/CO_2 gas. McCollom & Seewald (2003b) further observed that CH_3COO^- decomposes at slightly faster rates than CH_3COOH in the presence of minerals. The authors concluded that the reactivity of dissolved organic acids and acid anions in geologic environments are strongly dependent on mineralogy and temperature.

Preliminary tests showed that the decomposition of CH_3COO^- is significantly slower compared to that of $HCOO^-$ under conditions expected in a cement-based deep geological repository (Tits et al. 2019). No decomposition of CH_3COO^- was observed up to a reaction time of eight months even under conditions that favoured $HCOO^-$ decomposition in alkaline solutions at elevated temperature (Tits et al. 2019). It appears that the cleavage of C-C bonds required for decarboxylation or carbon oxidation is associated with a very high activation energy. Furthermore, it appears that the presence of iron and stainless steel does not reduce this energetic barrier sufficiently to accelerate the degradation kinetics (Tits et al. 2019). Therefore, the abiotic degradation of CH_3COO^- and presumably also the degradation of the long-chain monocarboxylates larger than CH_3COO^- appear to be extremely slow under conditions relevant to a repository environment (ambient temperature, high H_2 partial pressure, presence of Fe(0)). This consideration also implies that the abiotic degradation of carboxylates, as they occur in corroding metallic iron-water systems, is not likely to be a relevant process in the context of the long-term assessment of the fate of water-soluble carboxylates.

In summary, abiotic degradation reactions of organic carbon compounds are expected to be generally very slow. Activation energies of the decomposition reactions are lower in the presence of catalytic surfaces such as stainless steel. $HCOO^-$ was found to decompose predominantly to CO_2 and H_2 by a decarboxylation reaction under the conditions relevant to a cement-based deep geological repository (Eq. 4). This means that ^{14}C-bearing $HCOO^-$ could be converted to $^{14}CO_2$. The latter carbon species (as well as its bases HCO_3^- and CO_3^{2-}) is, however, strongly retarded or even retained by the cementitious near-field where ^{14}C decays. Decarboxylation of $HCOO^-$ is therefore considered to be a relevant process leading to $^{14}CO_2$ production over the period of concern for a deep geological repository. The decomposition of CH_3COO^- could occur by magnetite-catalysed decarboxylation into CH_4 and CO_2 (Eq. 5). However, preliminary studies by Tits et al. (2019) indicate that the decomposition of CH_3COO^- is an extremely slow process under repository-relevant conditions and is, therefore, hardly relevant over the period of concern for a deep geological repository. Very likely, the latter conclusion also applies to other organic carbon compounds that require C-C bond cleavage during abiotic degradation.

4.2.2.2 Biotic degradation of organic carbon compounds

Microbial activity does not seem to be relevant under the geochemical conditions of the near-field of the HLW repository due to the low carbon content and high temperature, whereas microbial activity in the near-field of the L/ILW repository could be significantly limited by the high pH of the cement-type near-field porewater (typically pH > 11) (Stroes-Gascoyne 2011; Leupin et al. 2016a). Nevertheless, as the L/ILW repository could contain significant amounts of organic carbon compounds, microbial activity might be relevant in niches with moderately alkaline pH conditions. Within a few months after closure of a deep geological repository, all residual O_2 will have been consumed by metal corrosion, by the reaction with reducing minerals and by aerobic microbial degradation of organic matter. Thus, based on the current repository concept, conditions in the near-field will remain O_2-free (reducing) in the long term and, if microbial degradation takes place despite the unfavourable conditions, will allow anaerobic microbial degradation of organic carbon compounds through fermentation or anaerobic respiration (Hallbeck 2010; Madigan et al. 2015).

Microorganisms are expected to utilise common electron acceptors, i.e., O_2, NO_3^-, Fe^{3+}, and SO_4^{2-} and carbon in case of methanogenesis (Leupin et al. 2016a) (Fig. 4-9). Anaerobic respiration is activated in the presence of NO_3^-, Fe^{3+}, and SO_4^{2-}. The products formed are, typically, CO_2 and reduced species of the electron acceptors, i.e., N_2, Fe^{2+}, and HS^-. However, in the long term, after exhaustion of oxidants with a higher energy yield, mineralisation of organic matter will occur through a fermentative process coupled with methanogenesis, where CO_2 is the oxidant and CH_4 is formed. From a microbiological perspective, CO_2 and CH_4 are expected to be the end products of the oxidation and fermentation (as well as subsequent methanogenesis) of organic carbon compounds under conditions relevant to a deep geological repository (Leupin et al. 2016a). Therefore, the degradation of ^{14}C-containing organic carbon compounds by microbial process is expected to produce either $^{14}CO_2$ or $^{14}CH_4$ (Fig. 4-9).

Methanogenic microorganisms are able to oxidise H_2 by using carbon dioxide as an electron acceptor according to the following reaction:

$$CO_2(aq) + 4\ H_2 \rightarrow CH_4 + 2\ H_2O \quad (7)$$

This allows the generation of $^{14}CH_4$ by microbial utilisation of inorganic ^{14}C in the form of $^{14}CO_2(aq)$ and, by extension, through carbonate equilibria: $H^{14}CO_3^-$ and $^{14}CO_3^{2-}$. Thus, it is conceivable that a hydrogen-fuelled, closed carbon cycle in the EBS and deep subsurface exists,

comprising autotrophic hydrogen oxidisers, fermenting bacteria producing acetate from the dead biomass of the autotrophs and the utilisation of CH_3COO^- by heterotrophic sulphate reducers (Leupin et al. 2016a).

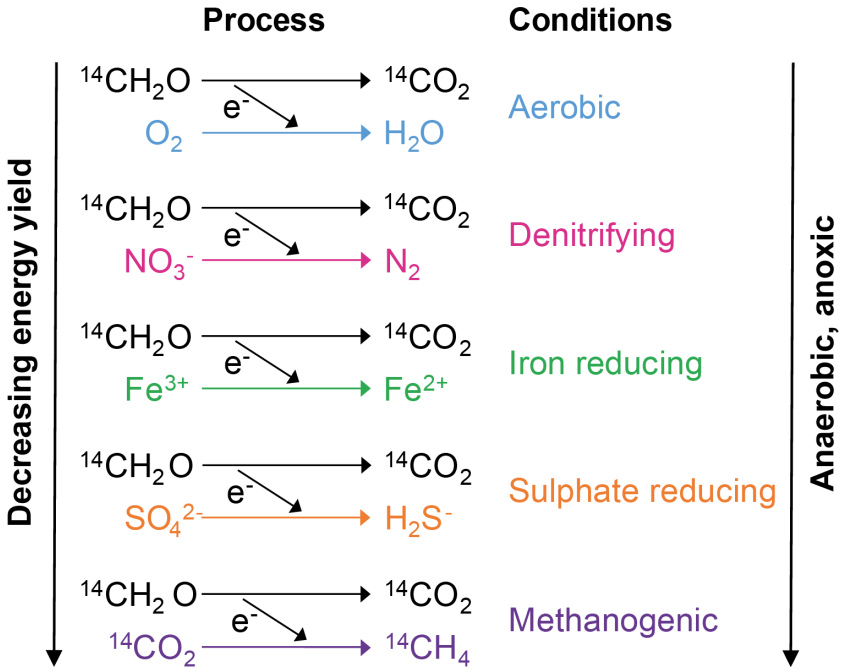

Fig. 4-9: Redox scale for microbial reactions

Adapted from Leupin et al. 2016a. CH_2O is used as a surrogate representing the average oxidation state of carbon in organic matter.

4.3 Summary of chapter

The thermodynamic modelling of the C-H-O system shows that small carbon compounds (< C5) are expected to be the dominant carbon species under the reducing conditions of L/ILW and HLW repositories. The most important limitation of the predictive capability of thermodynamic modelling, however, is the fact that complete thermodynamic equilibrium is rarely attained in the C-H-O system, at least at moderate temperatures, and the system can be in metastable thermodynamic equilibrium. This implies that the kinetics of the processes leading to the formation of carbon compounds, such as corrosion of metals, may have an effect on the species distribution in the C-H-O system.

In corroding metallic iron/steel-water systems, carbon compounds with very different redox properties (i.e., HCs, carboxylates) have been identified. The corrosion of metals generates volatile HCs, in particular CH_4. The process of HC formation can be described in terms of an F-T-type process. However, due to the action of oxic conditions during the service life of the materials, also oxygen-containing carbon compounds, such as monocarboxylic acids, are formed. Thus, it is expected that both ^{14}C-bearing oxygenated and reduced carbon species are present during the corrosion of activated metals.

The abiotic degradation of organic carbon compounds released from ^{14}C-contaminated waste can take place in the gaseous as well as the aqueous phases. The activation energies of the decomposition reactions are lower in the presence of water and catalytic surfaces such as stainless steel. Abiotic degradation tests with $HCOO^-$ suggest that the decomposition of the molecule into CO_2 and H_2 can occur by a decarboxylation reaction under conditions that are relevant for a cement-based deep geological repository. The decomposition of CH_3COO^- by magnetite-catalysed decarboxylation into CH_4 and CO_2, i.e., a C-C bond cleavage, was not observed over the time period of a few months. Under repository-relevant conditions, the decarboxylation of ^{14}C-bearing $HCOO^-$ is thus considered to be a relevant process that leads to the formation of $^{14}CO_2$, while the decomposition of CH_3COO^- is an extremely slow process and therefore, hardly relevant over the period of concern for a deep geological repository. This might also apply to other organic carbon compounds that require C-C bond cleavage during abiotic degradation.

The microbially-induced degradation of organic carbon compounds released from ^{14}C-contaminated waste takes place under circum-neutral to weakly alkaline conditions (typically pH < 11) in a deep geological repository. In the HLW repository, however, the availability of substrates and the pore space is limited and hence, microbial degradation of organic molecules does not seem to be a relevant process. In the L/ILW repository, the microbial activity might only be relevant in moderately alkaline niches of the near-field. In the long term, degradation of organic molecules will take place anaerobically by a methanogenic process. Hence, it is expected that the biotic degradation of ^{14}C-bearing organic carbon compounds released from ^{14}C-contaminated materials, if it occurs at all, will produce roughly equal amounts of $^{14}CO_2$ and $^{14}CH_4$.

5 ^{14}C release processes

Corrosion of activated metals, dissolution of fuel pellets, glass and graphite and instantaneous release from the surface of contaminated waste are the main processes leading to the release of ^{14}C. It should be noted that the main source of ^{14}C is activated metals (Nagra 2023) (Section 2.3). The release of ^{14}C also occurs due to the degradation of graphite and vitrified waste, though this is a smaller contributor. The ^{14}C inventory associated with other waste forms, such as spent IERs, filter cartridges, activated concrete and $Ba^{14}CO_3$, as well as contaminated materials can be expected to be released by the rapid detachment of the ^{14}C-bearing carbon compounds bound to these materials. Therefore, ^{14}C release will not involve the degradation of the main waste matrices. For example, in the case of spent IERs, the ^{14}C release will not require the degradation of the polystyrene-based backbone. The release of ^{14}C by degradation of ^{14}C-containing waste materials will be discussed with a view to: i) the corrosion of activated metals (steels, Zircaloy) and SF dissolution, and ii) the degradation of ^{14}C-bearing organic compounds. The corrosion of metals and the dissolution of SF account for the disintegration of the lattice structure of the waste materials by chemical surface reactions with aggressive components of the environment, while the degradation of organics is the consequence of abiotic or, in most cases, microbially mediated decomposition processes. The degradation processes of metals, SF and organic materials have already been taken into consideration in the framework of the previous safety assessment for the planned Swiss repositories for HLW and L/ILW (Nagra 2002).

5.1 ^{14}C release during corrosion of activated steel

A large body of literature exists on the corrosion of iron and steels in oxic and anoxic conditions. Reviews of earlier studies have been reported elsewhere in connection with the appraisal of the process of steel corrosion and corrosion rates in safety assessment (e.g., Diomidis 2014; King 2008; Kursten 2019; Smart et al. 2004). The following sections provide a brief introduction of corrosion processes and their rates, with an emphasis on discussing the chemical forms of ^{14}C released during the corrosion of activated steel. It should be noted that activated iron/steel will be disposed of both in the L/ILW and HLW repositories.

5.1.1 Corrosion process

Corrosion of iron and steels in aqueous media are described in terms of an electrochemical process involving two separate but coupled anodic and cathodic processes proceeding simultaneously (Broomfield 2003). The anodic process involves the oxidation of the metal, which produces metal ions and releases electrons. The electrons are subsequently consumed by the cathodic process, which involves the reduction of an oxidising agent that acts as electron acceptor. Overall, electrical neutrality is preserved.

The redox conditions in the repository environment will evolve from oxidising to very reducing conditions due to consumption of oxygen (Kosakowski et al. 2023; Curti et al. 2023). During the operational period and during the early stage after repository closure until all available oxygen is consumed, the corrosion of metals will proceed by the reduction of oxygen (electron acceptor). The two half-reactions accounting for the corrosion of iron and steel in the presence of O_2 can be written as (Broomfield 2003):

$$Fe(0) \rightarrow Fe^{3+} + 3\ e^- \quad (8a)$$

$$½\ O_2 + 2\ e^- + H_2O \rightarrow 2\ OH^- \quad (8b)$$

Ferric (Fe^{3+}) iron and hydroxyl (OH^-) ions react in solution to produce iron(III) oxide, such as Fe_2O_3, which may contain a variable amount of water. In a simplified manner, the overall reaction can be written as:

$$2\ Fe(0) + 1.5\ O_2 \rightarrow Fe_2O_3 \quad (8c)$$

Thus, the common corrosion products identified under oxic conditions are Fe(III) (oxy)hydroxides and oxides.

In the long-term, O_2-free conditions will prevail and, if no other oxidising agent is present, metal corrosion will involve the reduction of water, which results in the production of H_2 and the formation of Fe(II,III) corrosion products. The two half-reactions accounting for the corrosion of iron and steel in the absence of O_2 can be written as:

$$Fe(0) \rightarrow Fe^{2+} + 2\ e^- \quad (9a)$$

$$2\ H_2O + 2\ e^- \rightarrow 2\ OH^- + H_2 \quad (9b)$$

Ferrous (Fe^{2+}) iron and hydroxyl (OH^-) ions react in solution to produce ferrous hydroxide ($Fe(OH)_2$) which precipitates on the metal surface. The overall reaction for the anoxic corrosion of Fe(0) can be written as:

$$Fe(0) + 2\ H_2O \rightarrow Fe(OH)_2 + H_2 \quad (9c)$$

Ferrous hydroxide may convert into magnetite as given by the Schikorr reaction (Jelinek & Neufeld 1982; Schikorr 1933; Smart et al. 2002):

$$3\ Fe(OH)_2 \rightarrow Fe_3O_4 + H_2 + 2\ H_2O \quad (9d)$$

This results in an overall reaction for the anoxic corrosion of iron and steel as follows:

$$3\ Fe(0) + 4\ H_2O \rightarrow Fe_3O_4 + 4\ H_2 \quad (9e)$$

Magnetite (Fe_3O_4) is the most important corrosion product at the metallic iron/steel interface during the anoxic corrosion of iron and steel. Magnetite has a low solubility and is expected to be in equilibrium with aqueous Fe^{2+} and Fe^{3+} species.

The corrosion of both carbon and stainless steels can be expressed in terms of the aforementioned reaction sequence. In addition, however, the corrosion of stainless steel involves the alloying metals. The presence of such alloying elements, and their respective corrosion products, changes the chemical composition, structure and properties of the surface layer of stainless steel considerably; it gives rise to the formation of a few nm-thick passive layer on stainless steel, which results in significantly lower corrosion rates compared to carbon steel.

The speciation of carbon released during corrosion might be affected by reactants present at the metallic iron/steel-water interface, for example the presence or absence of O_2, H_2 or radicals (from radiolysis), and the overall physico-chemical conditions (redox, pH etc.).

5.1.2 Corrosion rates

In the context of the present study, the corrosion of steel is only discussed with regard to the release rate of ^{14}C in a repository environment. For this reason, some parameters that can influence corrosion rates and processes, such as temperature, the presence of chloride, and the effect of the interaction of steel with waste materials (e.g., glass), backfill (e.g., bentonite) and host rock (e.g., clays), are not discussed in detail. These aspects have been discussed in detail elsewhere, such as temperature effects (e.g., Kursten et al. 2021; Necib et al. 2019; Schlegel et al. 2018; Smart et al. 2021; Swanton et al. 2015; Uyama et al. 2020) and the effects in compacted systems (e.g., Engelhardt et al. 2020; Guo et al. 2020; Ishidera et al. 2008; King 2008; Leupin et al. 2021; Macdonald et al. 2013; Necib et al. 2016; Ngo et al. 2015; Schlegel et al. 2008), and therefore, they are not discussed further in the framework of this study.

A large number of studies have published measurements of the corrosion rate of carbon and stainless steel under anoxic conditions using different experimental techniques. Critical reviews and comprehensive compilations of corrosion rates for steels under conditions relevant to the long-term evolution of a repository (anoxic, near-neutral and alkaline pH) have been reported elsewhere (Diomidis et al. 2023; King 2008; Kursten 2019; Smart 2002; Smart 2009; Smart et al. 2004; Smart et al. 2001; Swanton et al. 2015). Long-term uniform corrosion rates for carbon steel in anoxic circum-neutral conditions (pH range 7 – 8) and ambient temperature, selected according to the Swiss deep geological repository concept, range between 0.0003 and 7.5 µm/a (Diomidis et al. 2023). In highly alkaline conditions, the selected rates are significantly lower and range between 0.03 and 20 nm/a (Diomidis et al. 2023).

Long-term uniform corrosion rates of stainless steel are generally lower than those reported for carbon steel. To date, however, only few studies have reported corrosion rates for stainless steel under the conditions relevant to a deep geological repository. The presence of alloying elements in stainless steel (e.g., Cr, Mo, etc.) and the formation of the respective corrosion products, considerably affect the corrosion rate. On stainless steel, the passivating layer is only a few nm thick, and it is enriched in the corrosion products formed from the alloying elements (e.g., Cr, Mo etc.).

Most recent measurements of corrosion rates for steels have been reported by He et al. (2017), Kursten et al. (2017), Kursten et al. (2021), Sakuragi et al. (2016b,c), Senior et al. (2023 a,b) and Smart et al. (2016, 2017, 2021). The development of very sensitive methodologies for measuring uniform corrosion rates as low as 0.01 nm/a allows more precise measurements of the slow corrosion of steels under anoxic alkaline conditions (Sakuragi et al. 2016b,c, Senior et al. 2020). Significantly lower corrosion rates were observed in anoxic alkaline media. Senior et al. (2017, 2023b) published rates for the anoxic corrosion of carbon steel in a cementitious environment at 50 °C (steel specimens cast in grout with solution pH ~ 13). The carbon steel specimens were found to passivate within 100 days, leading to corrosion rates of less than 10 nm/a. Sakuragi et al. (2016b,c) monitored the corrosion of stainless steel under anoxic conditions at ambient temperature in an NaOH solution with pH = 12.5 over a time period of 6.5 years. The corrosion rate was found to gradually decrease with time over the first year and was constant thereafter at about 0.4 nm/a. Smart et al. (2017) determined the corrosion rates of activated and non-activated carbon steel wires under anoxic conditions at 25 °C and 80 °C by measuring the generation of H_2 in gas cells. The solution had the composition of porewater in equilibrium with fresh cement (pH ~ 13.4). The rates for the long-term corrosion of non-activated steel specimens at 25 °C were determined to be < 0.1 µm/a. They still showed a trend to lower values after about three years of corrosion. Parallel experiments with a different experimental set-up resulted in rates in the order of < 0.03 µm/a. Also in this set-up, the rates were still decreasing after nearly four years of corrosion (Kursten et al. 2017; Smart et al. 2017).

Ionising radiation, in particular γ-radiation, may impact ^{14}C release during corrosion of activated steel. According to Swanton et al. (2015) there are two ways that corrosion is affected by radiation: i) radiation-induced radiolysis can generate reactive species (see Section 4.2.1.4) that can have an influence on the chemical and electrochemical processes involved in the corrosion reactions, and ii) the properties of the materials themselves can be changed, for example by promoting the segregation of trace elements in the steel matrix that leads to changes in the microstructure and thus corrosion susceptibility (Was 2012). The currently published studies indicate that the presence of γ-radiation can influence the anoxic alkaline corrosion of carbon steel, likely in the initial phase of the corrosion process (Smart et al. 2008, 2021). Steady state corrosion rates were attained faster at moderate dose rates (25 ± 7 Gy/hr) as compared to non-activated specimens. By contrast, high dose rates were found to slightly accelerate the corrosion of activated carbon steel exposed to bentonite (Liu et al. 2017). Smart et al. (2021) suggested that the faster kinetics of the formation of the passivating layer and/or a different morphology of the corrosion product layer improves passivation. Radiation-induced changes in the morphology of the corrosion product layer have been reported previously by Daub et al. (2011). Hence, there is evidence to suggest that the corrosion rates of activated steel are higher only during early exposure to alkaline solution at moderate dose rates, while the long-term rates of activated and non-activated materials are comparable. This implies a similar morphology of the passivating layer. Nevertheless, at higher dose rates, radiolysis-induced generation of reactive oxidants can enhance the corrosion rate.

The thickness of the passive oxide layer was reported to be typically less than 10 nm on non-activated stainless steel during anoxic alkaline corrosion (pH = 12.5) (Sakuragi 2017b), while it can reach values up to ~ 2 µm after 1,640 day-exposure of carbon steel under anoxic conditions and in alkaline solution (pH ~ 13.4) containing sulphur species (Smart et al. 2014). In the latter case, it was considered that the layer consists of a very thin (a few nm thick) barrier film and a thicker, but less protective, outer film. Johnson & King (2008) report a maximum oxide thickness, possibly comprising inner and outer corrosion layers, between 0.2 and 0.3 µm on carbon steel canisters for HLW at an elevated temperature of ~ 100 °C and a conservative "thermal-conduction" temperature profile at the canister-bentonite backfill interface. These findings suggest that the thickness of the passivating corrosion product layer typically ranges between ten and a few hundred nanometres.

Diomidis et al. (2023) published a comprehensive review of corrosion rates reported for stainless steel and carbon steel under the near-neutral pH conditions of the HLW repository and the alkaline pH conditions of the L/ILW repository and defined the rates for use in Nagra's safety and performance assessment calculations.

5.1.3 Experimental investigations on the chemical forms of ^{14}C

Earlier studies on the corrosion of activated steel and the chemical forms of ^{14}C were conducted in the framework of the Japanese waste management programme (Kaneko et al. 2003; Sasoh 2008a). Kaneko and co-workers carried out leaching experiments with activated steel and iron carbide (Fe_3C) in a glove box with a reducing atmosphere. The authors identified both organic and inorganic carbon compounds as ^{14}C carriers in leach solutions (pH 8 and 12.5). The concentration of total carbon (organic plus inorganic) in these solutions was found to increase over a time period of 15 months. Furthermore, the amount of carbon leached from activated steel was higher at pH 12.5 than 8. The latter finding contrasts with the general trend of the corrosion rate of steels, which is about 2 orders of magnitude higher at pH 8 than pH 12.5 (Diomidis et al. 2023; Kursten 2019; Smart 2009). Kaneko et al. (2003) used high performance liquid chromatography (HPLC) to identify the carbon compounds released during leaching of activated steel and Fe_3C. The organic carbon species identified were LMW monocarboxylic acids, aldehydes and alcohols, such as HCOOH, CH_3COOH, CH_2O, methanol (CH_3OH) and ethanol (C_2H_5OH). Furthermore, LMW

carbon compounds were observed in both leach solutions, i.e., solutions obtained during the leaching of activated steel and Fe_3C, which prompted the authors to conclude that the main chemical form of carbon (and presumably also ^{14}C) in both metallic materials was carbide. The study of Sasoh (2008a) further supported the conclusions by Kaneko and co-workers. It is noteworthy that Sasoh (2008a) mentions the existence of gaseous carbon compounds in his study, such as CH_4, C_2H_6 etc., but does not provide any experimental data.

Several studies on the chemical form of ^{14}C were performed in the framework of the EU project "CAST". They focussed on the speciation of ^{14}C released from activated steel under various chemical conditions (Cvetković et al. 2018c; de Visser-Týnová et al. 2018a,b; Druyts et al. 2018; Herm et al. 2017a,b; Rodriguez et al. 2018). The formation of 14C species was investigated during release from activated steel in acidic oxic conditions by Herm et al. (2017a,b) and Rodriguez et al. (2018) and in alkaline anoxic conditions by Cvetković et al. (2018c), de Visser-Týnová et al. (2018a,b) and Druyts et al. (2018). The digestion of activated steel in strongly acidic conditions (24 % H_2SO_4 + 3 % HF) generated dissolved organic ^{14}C-bearing compounds (~ 70 ± 10% of the initial ^{14}C inventory) and gaseous organic ^{14}C-bearing compounds (~ 29 ± 10%) (Herm et al. 2017b). Furthermore, Herm and co-workers report only a very low content of inorganic ^{14}C-bearing carbon compounds (i.e., $^{14}CO_2$ < 1%) in the gaseous and the aqueous phases. Digestion in acidic media allowed the ^{14}C inventory of activated steel to be quantified (Herm et al. 2017a). Exposing activated steel to oxic conditions in alkaline (NaOH at pH ~ 12) and acidic media (1M H_3PO_4) revealed the presence of CO(g), while the concentration of carboxylates was found to be below the detection limit of the applied analytical technique, i.e., high-performance ion-exchange chromatography with mass spectrometry detection (HPIEC-MS) (Rodriguez et al. 2018). The above findings suggest that oxygenated carbon compounds are preferentially formed under oxic conditions in acidic media.

Druyts et al. (2018) performed immersion and potentiostatic corrosion tests to explore the chemical form of ^{14}C released during the corrosion of activated carbon steel in a saturated portlandite ($Ca(OH)_2$) solution of pH 12.5. The authors identified gaseous stable carbon compounds CH_4, CO_2, C_2H_4 and C_2H_6 by gas chromatography (GC) with MS detection as the main products after a reaction time of 231 days. It is unclear whether these compounds carried ^{14}C or not, as no ^{14}C-specific analytics were used. The corrosion rate was estimated at 68 to 117 nm/a on the assumption that carbon was uniformly distributed throughout the steel and all the carbon released from the steel was transformed into gaseous compounds.

Investigations into the chemical form of ^{14}C under alkaline conditions were reported by de Visser-Týnová et al. (2018a,b). De Visser-Týnová and co-workers determined the rate and speciation of ^{14}C released from activated 316L(N) stainless steel through leaching under anoxic high-pH conditions (de Visser-Týnová et al. 2018a,b). The stainless steel samples had been activated in a reactor with a very high neutron flux. The gamma contact dose rate of the material was estimated at ~ 10 to 20 Gy/hr at the front face. The leaching experiments were performed in duplicate by immersing the steel samples (three per experiment, each weighing 74 g, total surface area of 114 cm^2) in 0.1 M NaOH (pH 13) in an inert zirconia crucible emplaced as an inner container within glass containers. The leaching tests were performed in a shielded 'hot' cell under an inert, nitrogen atmosphere. Regular sampling of the liquid and gas phases was conducted over 59 weeks. Note that Swanton et al. (2022) report the results from further samplings up to 105 weeks. Gas phase sampling and analysis involved the periodic purging of the head-space of the experimental container with nitrogen, the selective oxidation and capture of carbon species from the gas phase as CO_2 in a series of three separate soda lime columns and ^{14}C determination by liquid scintillation counting (LSC), as detailed in de Visser-Týnová et al. (2018a). The method allowed the following ^{14}C fractions to be separated from each other and quantified: i) the ^{14}C fraction released as CO_2 (CO_2 column), ii) the ^{14}C fraction released as CO ("CO" column), including, also, volatile oxygen-containing organic species (alcohols, aldehydes and ketones), and iii) the ^{14}C fraction released as volatile HCs, principally CH_4, ("CH_4" column) and any other

volatile HCs. Each column was pre-loaded with fossil CO_2 as bulk carrier. The total inorganic ^{14}C in solution was determined in an aliquot of sample solution by acidifying and purging with N_2 to capture CO_2 on an analytical Carbosorb material for direct LSC measurements. The total dissolved ^{14}C in solution was determined on a few solution samples by combustion in a two-stage catalytic pyrolyser. The $^{14}CO_2$ produced was captured in a bubbler containing a carbon-trap and measured by LSC (de Visser-Týnová et al. 2018a). The fraction of organic ^{14}C ($TO^{14}C$) was determined from the difference between the total carbon activity and the total inorganic carbon activity in solution. The results reported by de Visser-Týnová et al. (2018b) are summarised in Figs. 5-1 and 5-2.

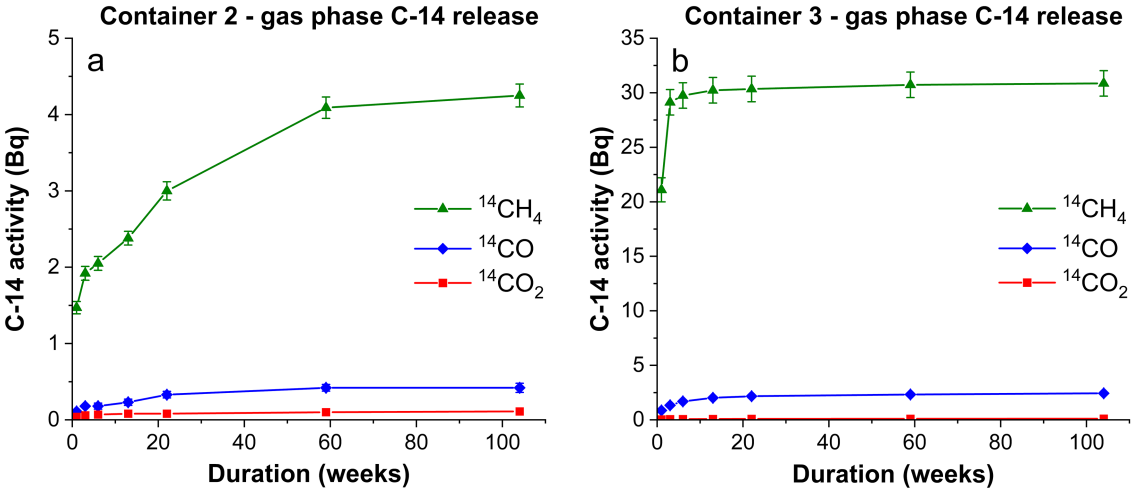

Fig. 5-1: Cumulative gas phase ^{14}C release in the two separate containers. a) Container 2; b) Container 3

From de Visser-Týnová et al. (2018b) and Swanton et al. (2022)

The error bars on these figures represent the uncertainties in the cumulative releases and not in the individual measurements.

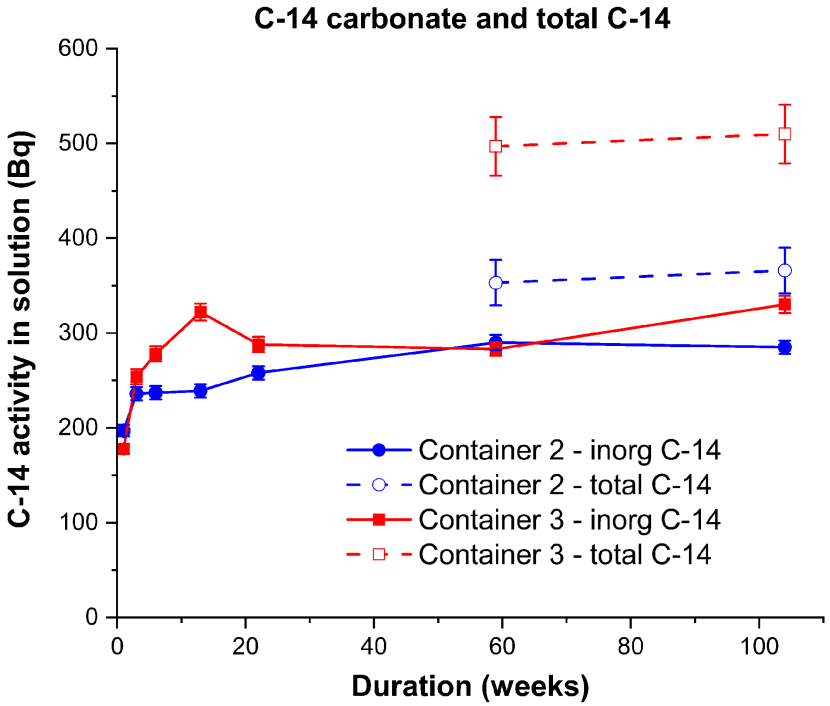

Fig. 5-2: Cumulative ^{14}C release (inorganic and total ^{14}C) to solution in the two separate containers

From de Visser-Týnová et al. (2018b) and Swanton et al. (2022)

Inorganic ^{14}C (filled symbols) and total ^{14}C (open symbols) are displayed, respectively.

An initial fast release of ^{14}C from the surface of the activated steel was observed during the first week of leaching, followed by a drop in the release rate over the longer term. This drop in the rate was different in the duplicate experiments for presently unknown reasons. The main ^{14}C activity (> 94 %) was detected in solution (compare activities shown in Figs. 5-1 and 5-2) indicating that only a small portion of ^{14}C was released to the gas phase. In solution, ~ 20% of the ^{14}C in experiment 2 and ~ 50% in experiment 3 was present in the organic form. Thus, there is a non-negligible ^{14}C activity in solution that is related to the presence of ^{14}C-carrying organic compounds (e.g., carboxylates). ^{14}C-carrying CH_4 was found to be the main species released to the gas phase. The ^{14}C activity associated with ^{14}CO (including alcohols, aldehydes and ketones) and $^{14}CO_2$ was significantly less.

In addition to the work of de Visser-Týnová and co-workers, Cvetković et al. (2018c) investigated the chemical form of ^{14}C during corrosion of activated steel in alkaline media. The latter corrosion study with activated steel was carried out over a time period of 412 days and continued after the EU project "CAST" finished. The results obtained up to 1,637 days of reaction are reported by Guillemot et al. (2021b, 2022) and displayed in Fig. 5-3. In this study, two activated steel nut specimens (total weight of 1.718 g) were immersed in a saturated $Ca(OH)_2$ solution of pH 12.5 (200 mL) in a gas-tight reactor (500 mL) under an inert, N_2 atmosphere (300 mL) (Wieland et al. 2017, 2018). The specimens were prepared from a guide-tube nut that had been mounted at the top and bottom ends of fuel rods and exposed to thermal neutron flux for about two years (activation terminated in June 2011) in the Gösgen NPP (Schumann et al. 2014). In this corrosion experiment, the liquid and gas phases were regularly sampled over the time period of 1,637 days. The ^{14}C concentrations were determined by accelerator mass spectrometry (AMS), including also compound-specific radiocarbon analysis (CSRA).

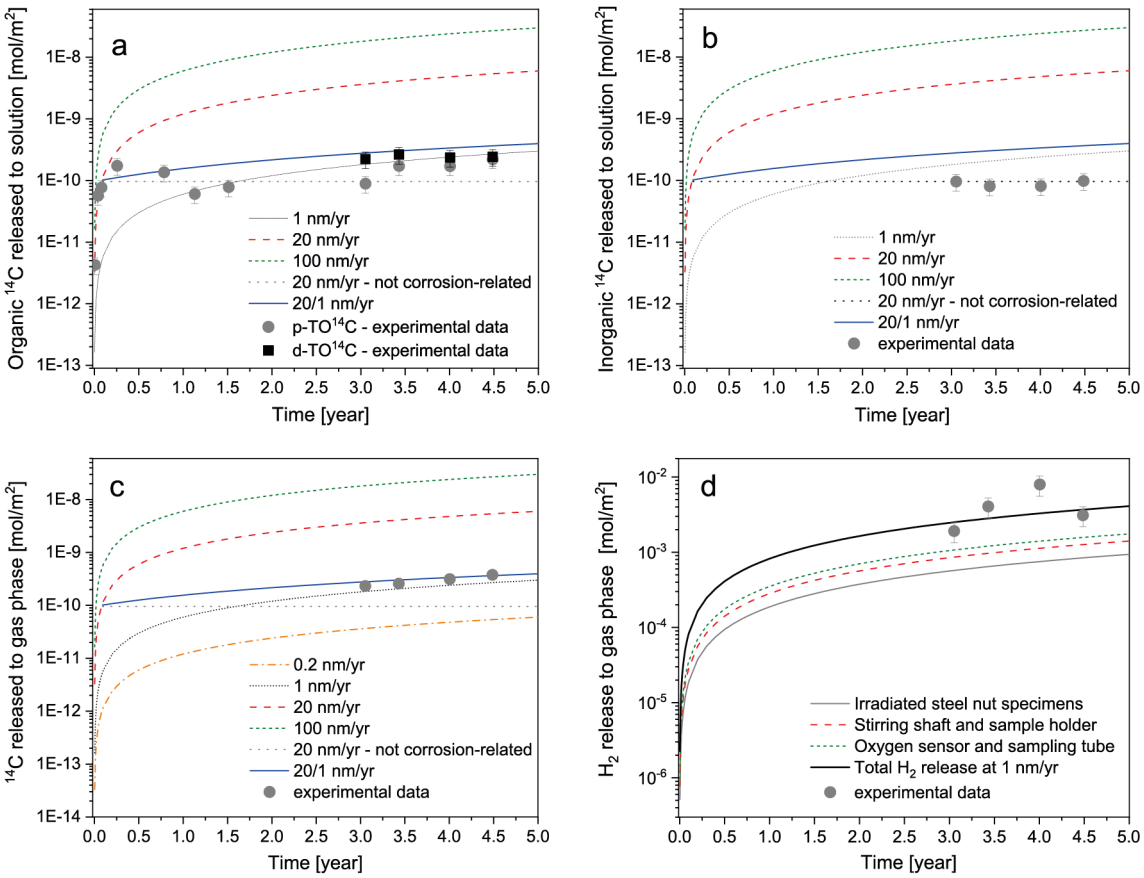

Fig. 5-3: Temporal evolution of a) p- and d-TO^{14}C; b) TI^{14}C; c) TG^{14}C and d) H_2 generation as a function of corrosion rates (lines) calculated for the experimental set-up and comparison with experimental data (symbols)

From Guillemot et al. (2021b)

Modelling assumption for TO^{14}C, TI^{14}C and TG^{14}C: the total amount of ^{14}C released from activated steel is either entirely present in the aqueous or in the gaseous phase (release expressed in terms of moles per surface area of activated steel).

Modelling assumption for H_2: The contribution of the corrosion of the assembly parts to gas generation is considered. All stainless steel parts, i.e., assembly parts and stainless steel nuts, corrode at a rate of 1 nm/a. The surface areas used are as follows: stirring shaft with sample holder = 16.75 cm^2, O_2 sensor and sampling tube = 20.84 cm^2, steel nut specimens = 11.15 cm^2. H_2 generation is expressed in terms of moles per surface area of activated steel. Note that the activated steel samples only contribute about 23% of the total H_2 production at a corrosion rate of 1 nm/a.

The AMS-based methods allowed the quantification of the following ^{14}C concentrations in the gas phase: i) total gaseous ^{14}C (TG^{14}C), and ii) single ^{14}C-carrying carbon compounds, such as $^{14}CH_4$ and other ^{14}C-bearing HCs, as well as ^{14}CO. The methods are described in detail by Guillemot et al. (2021a) and Guillemot et al. (2020b). The following parameters were determined in solution: i) total inorganic ^{14}C (TI^{14}C); ii) total organic ^{14}C (TO^{14}C) before (d-TO^{14}C) and after filtration through an ion-exchanger cartridge (p-TO^{14}C); and iii) single ^{14}C-carrying carboxylates by CSRA. Note that pre-treatment with the cartridge removed interfering anions (e.g., Cl^-) from solution and reduced the pH to ~ 6, which improved peak resolution of the single compounds

during HPIEC analysis. The methods are described in detail by Cvetković et al. (2018b) and Guillemot et al. (2021a). CSRA involved the separation of single compounds by chromatographic separation, i.e., GC in the case of gas phase analysis and HPIEC in the case of liquid phase analysis, in combination with ^{14}C quantification by AMS. The development of the very sensitive AMS-based analytical methods for ^{14}C quantification was required due to the low amount of activated material used, the low ^{14}C inventory of the activated steel (Schumann et al. 2014), the very slow corrosion of stainless steel at pH 12.5 (see Section 5.1.2), and the limited volumes of the sampled liquid and gas phases that were available for analysis. Overall, these constraints required ^{14}C quantification in the pico- to femto-molar range (Guillemot et al. 2021b).

In solution, the concentration of the ^{14}C-bearing organic compounds after cartridge treatment of the sampled solution (p-TO^{14}C) was quantified from the beginning of the corrosion experiment in 2016 (Guillemot et al. 2021b). Direct measurements of TO^{14}C (d-TO^{14}C) and TI^{14}C were, for the first time, possible on day 1,114 (Figs. 5-3a, b and 5-4). The two indicators of ^{14}C carried by organic compounds are consistent, although the p-TO^{14}C only amounts to 67 ± 27% of the d-TO^{14}C (Guillemot et al. 2021b). The difference between d- and p-TO^{14}C suggests that a non-negligible portion of the TO^{14}C was retained in the Ag/Ba/H cartridge during filtration of the sample solution, presumably as particulate matter. Both indicators of TO^{14}C seem to be constant with time within the given uncertainty (Fig. 5-3a). Inorganic ^{14}C (i.e., $^{14}CO_2$(aq) and its bases) quantified as TI^{14}C was also found to be constant over the period from 1,114 to 1,637 days (Fig. 5-3b). Furthermore, TI^{14}C only contributed ~ 26 ± 2% to the ^{14}C inventory in solution (Guillemot et al. 2021b). The temporal evolution of TO^{14}C (i.e., p-TO^{14}C and d-TO^{14}C) and TI^{14}C with time was modelled on the assumption that a fast release occurred during the first ~ 30 days of corrosion of activated steel at a corrosion rate of 20 nm/a (Fig. 5-3a). In the long term, however, no time-dependent increase was observed.

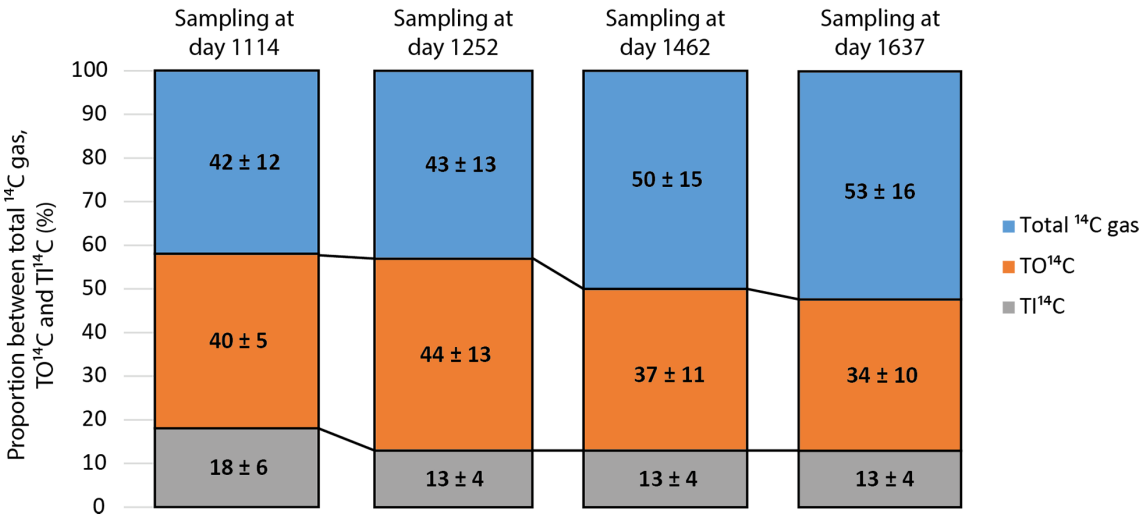

Fig. 5-4: Distribution of the ^{14}C-bearing compounds in the liquid and gas phases of the reactor between samplings days 1,114 and 1,637

From Guillemot et al. (2021b)

Proportions are based on the ^{14}C concentrations corrected for dilution during sampling and analysis.

In the gas phase, the total ^{14}C content ($TG^{14}C$) content was found to increase with time (Fig. 5-3c). Temporal evolution of the $TG^{14}C$ was modelled by assuming a fast release in the early phase of the experiment (corrosion rate of 20 nm/a). This assumption is supported by de Visser-Týnová et al. (2018b) (Fig. 5-1). The long-term increase in $TG^{14}C$ could be modelled by assuming a corrosion rate of 1 nm/a for activated steel. Hence, it was concluded that ^{14}C release to the gas phase occurred at a corrosion rate of ~ 1 nm/a (Guillemot et al. 2021b). The continuous increase of ^{14}C in the gas phase during the course of the corrosion of activated steel is also visible by plotting percentages of $TG^{14}C$, $TI^{14}C$ and $TO^{14}C$ in relation to the total ^{14}C released (Fig. 5-4). The relative proportion of $TG^{14}C$ increases with time while the corresponding proportions of $TI^{14}C$ and $TO^{14}C$ decrease.

Mass-balance calculations further revealed that since the beginning of the experiment, ~ 0.006% of the ^{14}C inventory of the two activated steel nut specimens had been released to solution and gas phases during 1,637 days of corrosion (Guillemot et al. 2021b). H_2 generation in the gas phase was modelled based on a corrosion rate of 1 nm/a by assuming that the corrosion of the stainless steel assembly parts also contributed to H_2 release to the gas phase (Fig. 5-3d). Both H_2 release and ^{14}C release can be consistently modelled with a corrosion rate of 1 nm/a within the given uncertainties on the experimental data, indicating that ^{14}C release is congruent with the anoxic corrosion of the activated steel.

5.1.4 ^{14}C chemical form in anoxic alkaline conditions

New information on the ^{14}C species formed during the anoxic alkaline corrosion of steel was obtained in the framework of the EU project "CAST" by Cvetković et al. (2018c) and de Visser-Týnová et al. (2018b) and by Guillemot et al. (2021b, 2022) in the framework of the Swiss waste management programme. The results substantiate earlier findings previously reviewed by Wieland & Hummel (2015). Tab. 5-1 shows the ^{14}C-bearing carbon compounds identified in metallic iron-water systems during the anoxic alkaline corrosion of activated steel. In addition, Tab. 5-2 provides a compilation of the totals of gaseous ($TG^{14}C$) and dissolved inorganic ($TI^{14}C$) and organic ($TO^{14}C$) species reported in the literature.

Tab. 5-1: ^{14}C-bearing compounds identified during anoxic alkaline corrosion of activated stainless steel

See Tab. 4-1 for comparison.

Corrosion of activated steel	
Gaseous ^{14}C-bearing carbon compounds	**Aqueous ^{14}C-bearing carbon compounds**
Methane	Formic acid
Ethane	Acetic acid
Propane	Malonic acid
Carbon monoxide	Oxalic acid
Carbon dioxide	Lactic acid
	Carbonates ($^{14}CO_2(aq)$, $H^{14}CO_3^-$, $^{14}CO_3^{2-}$)

Tab. 5-2: Distribution of released ^{14}C between the liquid and gas phases determined in corrosion experiments and leaching tests with steels under near-neutral and alkaline conditions

Given in percentage of total ^{14}C (%), as reported in the literature.

Reference	System*	Gas-phase ^{14}C	Inorganic ^{14}C	Organic ^{14}C
Sasoh (2008a)	Carbon steel pH 8 and 12.5	~ 0.01	15 – 30	70 – 85
Takahashi et al. (2014)	Stainless steel 42 months	25	37	38
de Visser-Týnová et al. (2018b)	Stainless steel pH 13 59 weeks	< 6	66 – 75	25 – 34
Guillemot et al. (2021b, 2022)	Stainless steel pH 12.5 1,637 days	53 ± 16	13 ± 4	34 ± 10

* System description (if reported in reference): type of material, pH of leaching test or corrosion experiment, respectively, and duration of leaching and corrosion experiments.

Guillemot et al. (2021b, 2022) identified $^{14}CH_4$, $^{14}C_2H_6$, $^{14}C_3H_8$ and ^{14}CO. $^{14}CH_4$ was found to be the main gaseous ^{14}C-carrying HC representing more than 80% of the TG^{14}C (Fig. 5-5b). These results are in agreement with the earlier corrosion studies carried out in anoxic alkaline metallic iron-water systems with non-activated iron powders (Cvetković et al. 2018a; Guillemot et al. 2020a). In these studies, it was observed that CH_4 was the main gas-phase species produced, and the increase in the concentrations of HCs was caused by the corrosion process. The additional HCs identified (i.e., $^{14}C_2H_6$ and $^{14}C_3H_8$) were only minor species in the corrosion experiment with activated steel, each contributing between 1% and 2% to the TG^{14}C (Guillemot et al. 2021b). Likewise, ^{14}CO was found to contribute only 2% to the TG^{14}C. Guillemot et al. (2021b) suggested the presence of one or more, still unknown, ^{14}C-bearing gas-phase species, which contribute a maximum of ~ 20% to the TG^{14}C.

In solution, ^{14}C-carrying carboxylates were identified as major contributors to TO^{14}C, i.e., ^{14}C-formic acid, ^{14}C-acetic acid, ^{14}C-oxalic acid, ^{14}C-malonic acid and ^{14}C-lactic acid (Fig. 5-5a). The concentrations of the ^{14}C-carrying carboxylates were assumed to be constant within the given uncertainty (Guillemot et al. 2021b). The contribution of the ^{14}C-bearing carboxylates to the TO^{14}C was estimated by assuming that each carboxylate carries only one ^{14}C atom. The total concentration of the ^{14}C-bearing carboxylates represented on average 42 ± 19% of the d-TO^{14}C (Guillemot et al. 2021b). The remaining ~ 50% of the TO^{14}C are still unknown ^{14}C carriers. The results imply that carboxylic acids are important ^{14}C-bearing organic carbon compounds present in solution during anoxic alkaline corrosion of activated steel (~ 50% of the ^{14}C content in solution), even though a non-negligible part of the ^{14}C-bearing organics remains unidentified (~ 50%). The ^{14}C-bearing species contributing to the remaining 50% of the TO^{14}C fraction are presently unknown and may include alcohols or aldehydes (Cvetković et al. 2018a; Guillemot et al. 2020a) as well as nitrogen-containing carbon compounds (e.g., Brinkman 1987).

The remaining ~ 25% of total ^{14}C in solution was associated with TI^{14}C, which is a measure of the ^{14}C-carrying carbonates ($^{14}CO_2$(aq) and its bases). In summary, ~ 25% of the total ^{14}C in solution were present as carbonates and ~ 75% bound by organics of which ~ 50% were ^{14}C-bearing carboxylates.

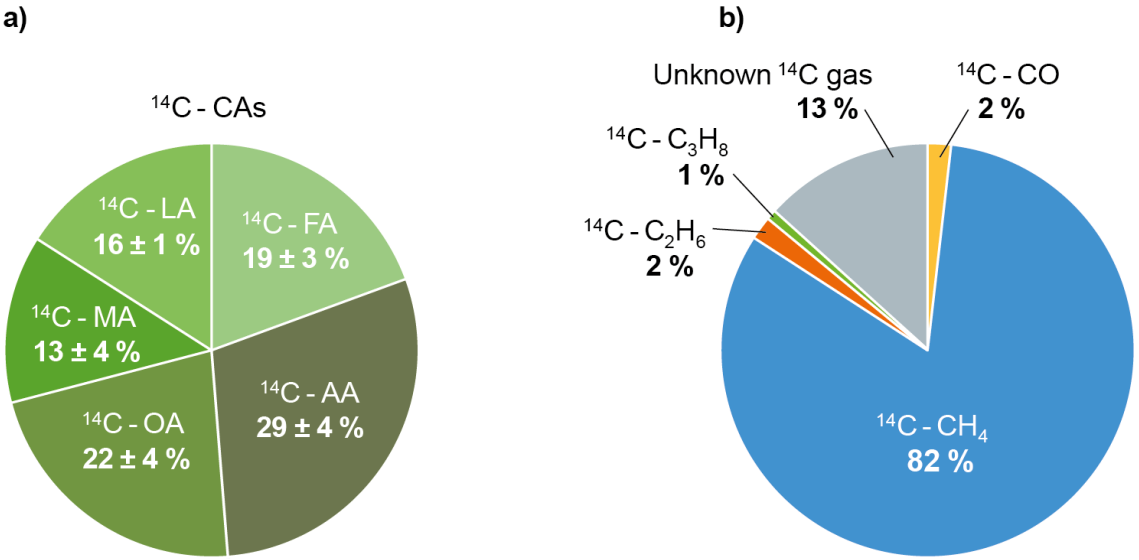

Fig. 5-5: Distribution of ^{14}C-bearing species released from activated steel under anoxic high-pH conditions, quantified by AMS. a) ^{14}C-bearing carboxylates in solution (averaged data over the period 1,114 to 1,637 days); b) ^{14}C-carrying gas compounds at sampling day 1,637

From Guillemot et al. (2021b)

Abbreviations: FA: formic acid, AA: acetic acid, OA: oxalic acid, MA: malonic acid, LA: lactic acid.

De Visser-Týnová et al. (2018b) identified $^{14}CH_4$ as the gaseous species contributing ~ 90% to the cumulative ^{14}C release to the gas phase (Fig. 5-1). ^{14}CO only added ~ 10% to the gaseous ^{14}C inventory, while the contribution of $^{14}CO_2$ was negligibly small. No information is available on the aqueous ^{14}C-carrying carbon compounds. Nevertheless, the determination of the total ^{14}C and the total inorganic ^{14}C in solution suggests that dissolved organic and inorganic ^{14}C-bearing carbon species contribute ~ 30 and ~ 70%, respectively, to the total ^{14}C in solution.

The results reported by de Visser-Týnová et al. (2018b) and Guillemot et al. (2021b, 2022) are surprisingly consistent regardless of the very different designs of the corrosion experiments with activated steel. $^{14}CH_4$ was found to be the predominant gaseous ^{14}C-carrying compound. The amount of $^{14}CH_4$ increases with time in one experiment reported by de Visser-Týnová et al. (2018b) (Fig. 5-1), which agrees with the results reported by Guillemot et al. (2021b) (Fig. 5-3c). The different proportions of the total ^{14}C released to gas phase (mainly as HCs) to the total ^{14}C released to solution (as carboxylates and carbonate) observed in the two studies is likely the result of the differences in the surface areas of the specimens in contact with solution and the different conditions to which the material was exposed prior to use in the corrosion experiment (i.e., the material's preparation, storage and processing history). Cvetković et al. (2018a) and Guillemot et al. (2020a) postulated that the formation of carboxylates, and presumably also carbonate, occurs due to the action of oxic conditions during the service life of the materials, such as during storage in air, pre-treatment in oxidising conditions, etc. Carboxylates and carbonate are formed by the oxidation of carbon in the base metal, adsorbed by the oxidised surface layer of the material and de-sorbed on contact with solution. In fact, instantaneous release of ^{14}C-carrying carboxylates and carbonate was observed in the corrosion experiments with activated steel (Cvetković et al. 2018c; de Visser-Týnová et al. 2018b; Guillemot et al. 2021b, 2022). De Visser-Týnová et al. (2018b) report a low proportion of ^{14}C in the gas phase (~ 6% of total ^{14}C) as compared to the total ^{14}C in

solution ($TO^{14}C + TI^{14}C \sim 94\%$ of total ^{14}C) after the 59 weeks of corrosion. The relatively high concentration of oxygenated carbon compounds observed by de Visser-Týnová et al. (2018b) as compared to the concentration of the gaseous species can be attributed to either the action of oxic conditions on the material prior to use in the corrosion experiment (Section 5.1.5) or to the orders of magnitude difference in the contact dose rate of the materials (radiolysis) used by de Visser-Týnová and co-workers and Guillemot and co-workers (see discussion in Section 5.1.6). Both processes are expected to increase the amount of oxidised carbon species accommodated by steel.

5.1.5 ^{14}C release rates in anoxic alkaline conditions

The release of ^{14}C during corrosion of activated steel appears to occur in two steps (Cvetković et al. 2018a; de Visser-Týnová et al. 2018b; Guillemot et al. 2020a, 2021b, 2022):

i) A fast release of ^{14}C over a time period of a few days to few weeks as a result of the detachment of ^{14}C from the oxide layer of activated steel;

ii) A slow release of ^{14}C in accordance with the corrosion rate of activated steel under the given conditions.

Fast release

This process was revealed by the measurements of $TO^{14}C$ and the concentrations of single carboxylates by Cvetković et al. (2018a), de Visser-Týnová et al. (2018b), Guillemot et al. (2021b) and Guillemot et al. (2020a) as well as HCs by Cvetković et al. (2018a), de Visser-Týnová et al. (2018b) and Guillemot et al. (2020a). It accounts for the detachment of oxygenated carbon compounds from the oxide layer of the base metal, while the amount of gaseous carbon compounds released in this phase is expected to be low. In the context of the safe disposal of radioactive waste, this implies that the period of action of the oxic conditions on the material before final disposal (e.g., storage in air, radiolysis-induced oxidation in nuclear power plants, etc.) determines the amount of ^{14}C released in organic and inorganic form into the porewater of the repository near-field. The fast release of HCs is likely due to the presence of highly reactive sites on the metal surface. In safety assessments, this process of fast ^{14}C release has been defined as the instant release fraction (IRF) (Nagra 2024f, in prep.). Tab. 5-3 is a compilation of the IRF of ^{14}C and carbon to solution, which were quantified based on the data reported by Cvetković et al. (2018a), de Visser-Týnová et al. (2018b), Guillemot et al. (2020a, 2021b, 2022). It should be noted that these values depend on the surface area to volume ratio of the materials used.

Slow release

According to Guillemot et al. (2021b, 2022), the increase in total ^{14}C in the gas phase ($TG^{14}C$) (Fig. 5-3c) and H_2 generation (Fig. 5-3d) can be modelled within the given uncertainty of the experimental data in accordance with a corrosion rate of 1 nm/a (Fig. 5-3c). This finding implies that both the ^{14}C release and corrosion rates are identical, thus indicating congruency of the two processes. Time-dependent release of ^{14}C to the gas phase was also observed in the two experiments reported by de Visser-Týnová et al. (2018b) (Fig. 5-1). Note that the initial release of $^{14}CH_4$ was very high in experiment 3 reported by de Visser-Týnová and co-workers (10 times higher IRF compared to experiment 2), which might cover the slow and continuous release of $^{14}CH_4$ by the corrosion of stainless steel in experiment 3. Thus, the measurements of $^{14}CH_4$ release reported by de Visser-Týnová et al. (2018b) are also consistent with the continuous generation of gaseous ^{14}C species by the anoxic corrosion of stainless steel in alkaline solution. In safety assessments, this process of slow release congruent with corrosion has been defined as the congruent release fraction (CRF) (Nagra 2024f, in prep.).

The above considerations suggest that after disposal of activated metals in a deep geological repository, a small fraction of ^{14}C will be instantaneously released upon contact with the porewater of the near-field. The IRF is expected to be in the range of 10^{-3}% of the total ^{14}C inventory of the activated metals. The main fraction of the ^{14}C inventory (> 99.99%), however, is likely to be released in accordance with the corrosion of the metals over the period of concern for a deep geological repository.

Tab. 5-3: Instant release fraction of ^{14}C

System	IRF to solution		IRF to gas phase		Reference
	(mol/m^2)	% of total ^{14}C or C	(mol/m^2)	% of total ^{14}C or C	
$^{14}C^{*}$ (pH 12.5)	2×10^{-10}	1.7×10^{-3}	-	-	Guillemot et al. (2021b)
$^{14}C^{**}$(pH 13)	5.7×10^{-8}	1.0×10^{-3}	2.3×10^{-10}/ 4.8×10^{-8}	4.1×10^{-6}/ 8.6×10^{-4}	de Visser-Týnová et al. (2018b)

* Based on total ^{14}C in solution ($TO^{14}C$ +$TI^{14}C$).
** Based on total ^{14}C in solution or gas phase, respectively. Release to the gas phase accounts for the difference observed in the two experiments (Fig. 5-2).

5.1.6 Effect of chemical conditions on ^{14}C speciation

Oxic versus anoxic corrosion

Several studies have been carried out in recent years focusing on the formation of ^{14}C-carrying carbon compounds during the anoxic corrosion of iron and steels in alkaline solution (see Section 5.1.4), while the corresponding information during the oxic corrosion of iron/steel is still limited (see Section 5.1.3). There is evidence to suggest that oxygenated carbon compounds, such as CO_2(aq) and its bases as well as carboxylates, are preferentially generated during oxic corrosion of steel (Rodriguez et al. 2018). However, there is still a lack of reliable data. During anoxic corrosion, however, HCs, i.e., reduced carbon species, are expected to dominate as outlined in Section 5.1.4. The presence of oxygenated carbon compounds in metallic iron/steel-water systems is considered to be the consequence of a memory effect by the material as a result of the action of oxic conditions during its service life (e.g., exposure to air, oxidants produced by radiolysis, etc.). Thus, the presently available data do not indicate a continuous production of oxygenated carbon compounds by the corrosion of steel in anoxic conditions. Note that thermodynamic modelling also predicts preferential formation of HCs under the reducing conditions anticipated on the steel surface (Ning et al. 2014) (see Section 4.1).

pH dependence of ^{14}C speciation

Several corrosion studies with activated steel have been performed under alkaline conditions since most of the activated metallic waste materials will be disposed of in a cement-based deep geological repository. In contrast, corresponding studies with activated steel in circum-neutral pH conditions are lacking, to the best of the authors' knowledge. Information on the pH dependence of the stable carbon speciation was obtained from leaching experiments performed at pH 8 or 8.5

(simulated groundwater) and 12.5 (simulated cement porewater) with non-activated carbon steel (Kaneko et al. 2003; Sasoh 2008a) and stainless steel (Heikola & Ollila 2018). The limited data from these studies show no significant effect of pH on speciation of stable carbon. Herm and co-workers report on studies on the speciation of ^{14}C release under acid conditions (Herm et al. 2017a, b). To this end, the authors completely dissolved a stainless steel plenum spring in a mixture of dilute H_2SO_4/HF. About 70% of the total ^{14}C inventory of the steel spring was released as dissolved organic compounds into the aqueous phase and about 30% as organic compounds into the gas phase. Note that the individual ^{14}C-bearing species were not identified by Herm and co-workers. Thus, the portion of ^{14}C released in the inorganic form to the liquid and gas phases was much less than 1%. This finding implies that the same chemical forms of carbon compounds are present during the anoxic corrosion of steel in acid and alkaline solutions, though the proportions of these different chemical forms can vary. Therefore, there is evidence to suggest that the chemical forms of carbon (i.e., organic and inorganic), and likely the species distribution of carbon, released during the anoxic corrosion of steel are not influenced by kinetic effects, such as faster corrosion of steel under acid and neutral conditions compared to alkaline conditions. Despite the lack of robust experimental evidence, it can be postulated that the ^{14}C speciation generated by the anoxic corrosion of steel is not significantly different in alkaline and circum-neutral conditions.

Effect of radiation

Gamma radiation emitted from activated metals as a result of ^{60}Co decay may give rise to the decomposition of water (water radiolysis), which produces oxidants, reductants and gaseous compounds (Section 4.2.1.4). The corrosion studies of de Visser-Týnová et al. (2018b) were conducted with activated steel that had a gamma contact dose rate in the range of 10 - 20 Gy/hr. By contrast, the specimens used by Guillemot et al. (2021b, 2022) had a significantly lower gamma contact dose rate of ~ 0.12 Gy/hr. Note that ~ 25 Gy/hr is considered as a representative dose rate at the surface of carbon steel overpacks used for SF and HLW at the time of disposal (Smart et al. 2021). The initially high dose rate will rapidly decrease with time due to the relatively short half-life of the main gamma emitter ^{60}Co ($t_{1/2}$ = 1,925 days). Hence, the dose rates used in the studies of Guillemot and co-workers and de Visser-Týnová and co-workers likely cover the range of relevant dose rates in a deep geological repository. The formation of oxidants and radicals, such as $HO^{\bullet}$, $HO_2^{\bullet}$, H_2O_2, as a result of water radiolysis, may affect ^{14}C speciation during corrosion. The oxidising effect of the radicals and H_2O_2, which is the most important oxidant, would be expected to lead to a continuous increase in the concentrations of oxygenated carbon compounds with time, such as carboxylates and carbonate. Therefore, the increase in the concentrations of the latter carbon compounds should be reflected by an increase in $TO^{14}C$ or $TI^{14}C$ with time. Neither study shows a significant increase in either parameter with time beyond the stated uncertainties on the experimental data (Figs. 5-2 and 5-3a/b), suggesting that radiolysis very likely has little or even no effect on ^{14}C speciation during the anoxic alkaline corrosion of activated steel. However, it should be noted that Visser-Týnová and co-workers observed a continuous slow release of ^{14}CO to the gas phase (total gas of ~ 4% of release), indicating that radiolysis could promote the formation of oxidised species.

5.2 ^{14}C release during corrosion of Zircaloy

The literature on the corrosion behaviour of Zircaloy under conditions in an NPP and a deep geological repository is extensive. Less extensive, however, are experimental studies on the release and speciation of ^{14}C during the corrosion of Zircaloy under conditions relevant to a deep geological repository, where it will be present in both L/ILW and HLW inventories.

5.2.1 Corrosion process

The corrosion resistance of Zircaloy resembles that of zirconium. A protective ZrO_2 layer forms on the surface of both zirconium and Zircaloy due to the electrochemical instability of Zr. The overall electrochemical reaction of zirconium is given as follows (Bart & Bertsch 2005; Wada et al. 1999):

$$Zr + 2\,H_2O \rightarrow ZrO_2 + 2\,H_2 \quad (10a)$$

This overall reaction can be split into anodic and cathodic half-cell reactions:

Anodic half cell:

$$Zr(0) + 2\,O^{2-} \rightarrow ZrO_2 + 2\,\Upsilon^{\theta} + 4\,e^{-} \quad (10b)$$

Cathodic half cell:

i) water dissociation

$$2\,\Upsilon^{\theta} + 2\,H_2O \rightarrow 2\,O^{2-} + 4\,H^{+} \quad (10c)$$

ii) proton discharge step

$$4\,H^{+} + 4\,e^{-} \rightarrow 2H_2 \quad (10d)$$

The anodic half-cell reaction implies that two oxygen anions of the ZrO_2 lattice react with a new Zr metal atom at the metal–oxide interface. As a result, two oxygen lattice vacancies (Υ^{0}) are created and diffuse outwards through the oxide layer that formed along the ZrO_2 crystallite grain boundaries. The vacancies emerging at the oxide-water interface induce detachment of oxygen anions from the water molecules leaving protons behind, which are readily reduced to molecular H_2.

Similar to steels, a passivating ZrO_2 layer forms and improves the corrosion resistance of Zircaloy under the aggressive conditions inside a commercial nuclear reactor (Adamson & Rudling 2013; Bragg-Sitton 2012; Garzarolli et al. 1996) or under extreme chemical conditions (e.g., strong acids, alkaline media, organic acids) (Fraker 1989). The rate of oxidation of Zircaloy is temperature-dependent, i.e., it increases with increasing temperature, and is diffusion-controlled, i.e., it decreases with increasing thickness of the passive layer. Under reactor conditions, a layer thickness of 2 -3 µm was observed after about 100 days of operation. A maximum thickness of about 60 to 100 µm was observed for Zircaloy-4 exposed to the H_2-rich reducing conditions of PWRs (Bart & Bertsch 2005). The corrosion resistance of the material was reported to degrade significantly in the presence of impurities in the matrix, e.g., > 270 ppm carbon or > 80 ppm nitrogen (Section 3.1.3). Hence, the typical carbon and nitrogen contents of Zircaloys are kept very low to avoid such a detrimental effect on their corrosion resistance in NPP applications (Section 3.1.3).

The limited thickness of the oxide layer means that, as with steels, the amount of Zircaloy that needs to be disposed of in deep geological repositories in oxide form will be much less than the amount that needs to be disposed of in metallic form. This further implies that the inventories of carbon and nitrogen in Zircaloy are predominantly associated with the base metal rather than the

oxide layer. The mass of metal converted to the oxide form can be quantified using the known surface areas of the Zircaloy components to be disposed of and based on assumptions about the thickness of the oxide layer.

Lefebvre & Lemaignan (1997) published a comprehensive overview of the effect of irradiation on the corrosion of Zr alloy claddings, focusing on Zircaloy applications in NPPs in particular. Irradiation leads to microstructural changes that affect the corrosion rate, such as elemental redistribution within the metal matrix. In addition, the oxide layer of activated materials has coarser oxide crystallites and fewer areas with a distinct common orientation than in non-activated material, where the oxide layer grew with a strong preferential orientation. Thus, the study of Lefebvre & Lemaignan (1997) suggests that the corrosion behaviour of Zircaloy disposed of in a deep geological repository may be influenced by the irradiation history of the material.

Shoesmith & Zagidulin (2011) summarised the current knowledge on the corrosion behaviour of zirconium under the conditions of a deep geological repository. These authors concluded that passive corrosion is the only long-term corrosion mechanism, rather than pitting, because reducing conditions prevail in a deep geological repository due to the presence of the reducing agents Fe^{2+} and H_2 produced by steel corrosion. Passive corrosion is based on a balance between the chemical dissolution of the oxide at the oxide/solution interface and the corrosion process that regenerates the oxide layer at the metal/oxide interface. The authors further emphasised that knowledge of the properties of the materials on discharge from the reactor are essential to evaluate the performance of Zircaloy under the conditions of a deep geological repository.

5.2.2 Corrosion rates

The studies of Kurashige et al. (1999) and Wada et al. (1999) report rates of the anoxic alkaline corrosion of Zircaloy-4. The rates were determined in artificial seawater-based groundwaters with pH adjusted to values between 10 and 13.5 at 30 and 50 °C (controlled temperature in a water bath). In both studies, a high corrosion rate was observed initially (e.g., 6 - 12 nm/a for about 100 days by Kurashige and co-workers), which decreased with time due to the formation of the passive oxide layer. Wada et al. (1999) report a long-term corrosion rate (after 180 days reaction) ranging from 0.1 to 1 nm/a irrespective of pH (10, 12.5 and 13.5). Kurashige et al. (1999) determined long-term corrosion rates (> 400 days reaction) of 1 to 2 nm/a under similar conditions (pH = 10.5 and 12.5; T = 30 and 45 °C). Wada et al. (1999) found no pH-induced changes in the rate, while the rate was found to slightly increase with temperature. Also, Kurashige and co-workers observed no pH-dependence of the corrosion rate of Zircaloy-4 in the reported pH range. However, in both studies, H_2 uptake by Zircaloy during corrosion was not taken into account, which may have led to an underestimation of the corrosion rate (Gras 2014). Furthermore, it should be noted that Wada and co-workers also investigated the corrosion of stainless steel using the same experimental set-up and found comparable corrosion rates for both stainless steel and Zircaloy (range 0.1 - 1 nm/a).

Further measurements of the corrosion rates of Zircaloy-2 and Zircaloy-4 have been reported more recently by Sakuragi et al. (2012, 2013) and Kato et al. (2014). These authors used a similar experimental approach as Wada et al. (1999), i.e., metal specimens were immersed in glass ampoules, and the amount of H_2 produced during corrosion was measured by GC. In addition, the amount of H_2 adsorbed on Zircaloy was determined by using an inert gas melting system coupled to a GC. The corrosion rate was further determined by measuring the weight of the samples before and after the corrosion tests and compared with the equivalent corrosion rate from H_2 measurements. Sakuragi et al. (2012) showed that the H_2 adsorption by Zircaloy-4 is considerable, thus requiring a distinction between H_2 adsorbed/desorbed versus H_2 generation during the course of corrosion. Sakuragi and co-workers determined corrosion rates for Zircaloy-4 ranging between ~ 2.5 and ~ 7 nm/a, with corrected H_2 generation.

Based on the approach previously reported by Sakuragi and co-workers, Kato et al. (2014) determined the corrosion rates of Zircaloy-2 and Zircaloy-4 for different environmental conditions (pH, water composition, temperature). Over longer periods (180 days of corrosion or longer) and at 30 °C, Kato et al. (2014) measured rates ranging from ~ 4 to 12 nm/a. There was no significant difference between the corrosion rates of Zircaloy-2 and Zircaloy-4. The rates were found to increase with temperature, i.e., by a factor of ~ 2.8 at most, as the temperature increased from 30 to 80 °C over 180 days of corrosion or longer for all water compositions. The effect of temperature was found to be greater than the effects of changes in pH and the chemical compositions of the alkaline solutions and the seawater-derived, cement-equilibrated groundwater. For example, only a small increase in the rates, by a factor of ~ 1.5 at most, was observed between corrosion in pure water (pH not reported) and pH 12.5 (NaOH or $Ca(OH)_2$ solutions) at 30 °C after 180 days of corrosion. Thus, the addition of Na or Ca as the predominant cation to the alkaline solutions had no measurable effect on the rates. Likewise, the composition of the seawater-derived, cement-equilibrated groundwater with pH 12.5 had only a minor influence on the corrosion rate compared to the rates measured in pure water (pH not reported) (a factor of < 1.4). In summary, uniform, very low corrosion rates were observed for the two different types of Zircaloys in anoxic neutral or alkaline media at ambient temperature, with an upper limit of 20 nm/a (Kato et al. 2014).

The range of corrosion rates given above is consistent with those recommended by Shoesmith & Zagidulin (2011), based on a detailed review of the electrochemically determined Zircaloy corrosion rates. The authors recommended a uniform rate of passive corrosion of Zircaloy at 20 nm/a (upper limit) and a base case value of ~ 5 nm/a, suggesting a more likely rate of less than 1 nm/a.

Within the framework of the EU project "CAST", several studies were carried out with the aim of quantifying the release of ^{14}C during the corrosion of Zircaloy in alkaline solution and at ambient temperature and identifying the ^{14}C species released into the liquid and gas phases (see overview by Necib et al. 2018a,b). In addition, the ^{14}C inventory of activated Zircaloy was determined by Bucur et al. (2018), Herm et al. (2017c, 2018) (Section 3.1.4), while the corrosion rates reported by Sakuragi (2017a) and Caes et al. (2018) are compiled in Necib et al. (2018b). The corrosion rates were determined by electrochemical methods, but also by measuring the time-dependent release of H_2 and ^{14}C. Necib et al. (2018b) summarise the corrosion rates for Zircaloy determined in the framework of the "CAST" project. They were found to range from ~ 0.5 to ~ 100 nm/a for non-activated and activated as-received or pre-oxidised Zircaloy under alkaline conditions (NaOH or $Ca(OH)_2$ solutions at pH 12.5) and with a corrosion duration from ~ 0.5 to ~ 6.5 years. The rates were found to depend on the material properties (e.g., the absence or presence of an oxide layer, i.e. whether as-received or pre-oxidised, respectively) and the experimental approach used, e.g., determination by applying a potentiodynamic polarisation technique or measurement of H_2 release. It should be noted that some recent measurements appear to yield significantly higher corrosion rates than previously reported (e.g., Shoesmith & Zagidulin 2011, Sakuragi et al. 2012, Kato et al. 2014). For example, Caes et al. (2018) determined a rate of ~ 54 nm/a (upper limit) from potentiodynamic polarisation measurements over 7 days of corrosion under anaerobic highly alkaline conditions, while rates between 57 and 84 nm/a were determined from measurements of gas generation under the same conditions. Corrosion rates were also reported by Sakuragi (2017a). Zircaloy samples were immersed in either NaOH (pH 12.5), saturated $Ca(OH)_2$ (pH ~ 12.5) or a solution with the composition of a cement-type porewater at ambient temperature (25 and 30 °C). After 2 or 5.5 years of corrosion, rates between 0.5 and 10 nm/a were determined, respectively, and are within the range recommended by Shoesmith & Zagidulin (2011).

Diomidis et al. (2023) published a comprehensive review of corrosion rates reported for Zircaloy under L/ILW and HLW conditions and defined the rates for use in Nagra's safety assessment calculations.

5.2.3 Chemical form of ^{14}C

Studies on the chemical form of ^{14}C released during the leaching or corrosion of Zircaloy have been carried out in the framework of the Japanese disposal programme by Yamaguchi et al. (1999), Kaneko et al. (2003), Tanabe et al. (2007), Sasoh (2008a), and Takahashi et al. (2014). Additional studies have been conducted as part of the EU project "CAST", as reported by Sakuragi (2017a), Bucur et al. (2018), Caes et al. (2018), and Necib et al. (2018a, b). Tab. 5-4 summarises the potential ^{14}C-bearing carbon compounds identified during the anoxic alkaline corrosion of Zircaloy, though it should be noted that the employed analytical techniques for the identification of these carbon compounds were not ^{14}C-specific but for stable carbon compounds.

The compilation in Tab. 5-4 shows that many of the compounds observed during Zircaloy corrosion were also identified in the corrosion of activated steel (Tab. 5-1), namely the gaseous compounds CH_4, C_2H_6, CO, and CO_2 as well the aqueous species HCOOH and CH_3COOH.

Tab. 5-4: Potential ^{14}C-bearing compounds identified during anoxic alkaline corrosion of Zircaloy

Corrosion of Zircaloy*	
Gaseous carbon compounds	**Aqueous carbon compounds**
Methane	Methanol
Ethane	Ethanol
Ethene	Formaldehyde
Carbon monoxide	Formate
Carbon dioxide	Acetate
	Oxalate
	Propionate
	Glycolate
	Carbonate

* Compounds reported by Yamaguchi et al. (1999), Kaneko et al. (2003), Tanabe et al. (2007), Sasoh (2008a), Caes et al. (2018), Necib et al. (2018a, b). See Tab. 4-1 for comparison.

The totals of released ^{14}C determined as gaseous ($TG^{14}C$), dissolved inorganic ($TI^{14}C$) and organic ($TO^{14}C$) species, as reported in the literature, are listed in Tab. 5-5.

Tab. 5-5: Distribution of released ^{14}C between the liquid and gas phases determined in corrosion experiments and leaching tests with Zircaloy under near-neutral and alkaline conditions

Given in percentage of total ^{14}C (%), as reported in the literature.

Reference	System*	Gas-phase ^{14}C	Inorganic ^{14}C	Organic ^{14}C
Yamaguchi et al. (1999) Tanabe et al. (2007)	Hull specimen cement-type solution 5.5 months	< 0.3	21.1	78.9
Kaneko et al. (2003)	ZrC 16 months pH 8 pH 12.5	 n.m. n.m.	 ~ 30 ~ 60	 ~ 70 ~ 40
Sasoh (2008a)	Zr, ZrC pH 8 & 12.5	≤ 0.1	10 - 45	55 - 90
Takahashi et al. (2014)	Zry base metal 30 months	71	17	12
Takahashi et al. (2014)	Zry ox. layer 30 months	8	30	62
Necib et al. (2018a)	M5™ pH 12 14 days and 6 months	n.m.	55	45
Necib et al. (2018a)	Zircaloy-4 pH 12 14 days and 6 months	n.m.	80	20
Necib et al. (2018a) Bucur et al. (2018)	CANDU-Zry4 pH 12 18 days to 18 months	n.m.	40	60
Necib et al. (2018) Sakuragi (2017a) Sakuragi et al. (2016a)	Zircaloy-2 pH 12.5 6.5 years	16	21	63

* System description (if reported in reference): type of material, pH of leaching test or corrosion experiment, respectively, and duration of leaching and corrosion experiments.

n.m. not measured.

Large variations were observed in the proportions of gaseous, inorganic, and organic ^{14}C (Tab. 5-5). It is difficult to assess the differences in the speciation between the different studies with Zircaloy and steel due to the variety of analytical techniques used in these studies. In general, however, it can be stated that only small molecules are present in the liquid and gas phases. Furthermore, both oxygenated carbon compounds and HCs have been identified. The coexistence of reduced and oxidised carbon species with low molecular weights thus appears to be a common feature observed in aqueous metal corrosion (Tabs. 4-1, 5-1, 5-4). In general, the fraction of gaseous ^{14}C is lower compared to inorganic and organic ^{14}C. This can be explained by the

relatively short duration of most corrosion studies and the slow corrosion of Zircaloy, which limits the amount of corrosion of the bulk metal and thus, the amount of gaseous species released. It should be noted that the amount of gaseous ^{14}C seems to increase with longer experimental duration (e.g., the values reported by Sakuragi 2017a and Necib et al. 2018a), suggesting that the release of gaseous ^{14}C is related to the corrosion process of the base metal and not due to the IRF.

The ^{14}C taken up by the external oxide layer of Zircaloy cladding is assumed to be the largest contributor to the IRF of ^{14}C (Necib et al. 2018b). The IRF of ^{14}C from cladding of PWRs was previously estimated to be, at most, 20% of the total ^{14}C inventory, corresponding to an oxide layer thickness of 80 µm. On the other hand, 80% of the ^{14}C inventory was assumed to be congruently released by the slow corrosion of non-oxidised Zircaloy metal (Sakuragi 2017a; Yamaguchi et al. 1999). Note that the ^{14}C inventory in the external oxide layer of Zircaloy claddings was reported to be about one order of magnitude lower for BWR fuel cladding than PWR fuel cladding (Section 3.1.4).

The uniform corrosion of Zircaloy at low to moderate temperatures, the diffusion of ^{14}C from the zirconia oxide layer, and/or the dissolution of the zirconia oxide layer have been proposed as mechanisms that control the rate of ^{14}C release from the cladding at the time of its contact with the near-field porewater of a deep geological repository (Necib et al. 2018b). However, there is currently limited evidence to allow differentiation between mechanisms, nor to explicitly link them to the ^{14}C IRF or to corrosive release. Despite this, there is improved information on the ^{14}C inventories in the bulk metal and oxide layer (see Section 3.1.4), though questions regarding the chemical forms of ^{14}C released from the two components of the cladding remain.

Recent studies on the ^{14}C distribution in activated fuel cladding show that the fractions of the total ^{14}C inventory in the oxide layer and the base metal are 7.5% and 92.5%, respectively, and that the specific ^{14}C activity of the external oxide layer is higher than that of the base metal by a factor of 2.8 (Sakuragi 2017a; Sakuragi et al. 2016a). This finding suggests that the ^{14}C IRF could be less than 10% of the total ^{14}C inventory. The same authors found that, after 6.5 years of immersion of activated material in pH 12.5 NaOH solution, the proportions of the ^{14}C released as gaseous, inorganic, and organic ^{14}C species were 16%, 21% and 63%, respectively (Tab. 5-5). Mass balance calculations further suggested that the largest portion of ^{14}C was released from the external oxide layer, while corrosion-induced congruent release from the Zircaloy base metal contributed only a small fraction of the released ^{14}C over this period (Sakuragi et al. 2016a). In addition, the ^{14}C inventory leached from the cladding (metal + oxide) over the 6.5 years of corrosion accounted for only 0.0038% of the total ^{14}C inventory of the material. This result implies that, as with steels, two different mechanisms with different rates could account for the observed release of ^{14}C from activated Zircaloy: i) a relatively rapid release of ^{14}C from the oxide layer (relative in relation to the period of concern for a repository), contributing to the IRF, and ii) a slow, corrosion-induced congruent release of ^{14}C from the Zircaloy base metal. The rapid release involves less than 0.01% of the total ^{14}C inventory, while the majority (> 99.99%) is expected to be released congruently in accordance with Zircaloy corrosion in the deep geological repository. In leaching experiments with activated cladding or non-activated Zr-based materials (Zr and ZrC powders), gaseous, organic and inorganic carbon species were detected, though mainly small organic molecules.

5.2.4 Effect of chemical conditions on ^{14}C speciation

Oxic versus anoxic corrosion

No systematic studies on the effect of redox conditions on the ^{14}C release during corrosion of Zircaloy have been performed to date. It can be assumed that, as with steel, oxygenated ^{14}C species, such as carboxylates, are preferentially formed under oxic conditions. Note, however, that conditions are expected to be reducing at the Zircaloy/water interface during corrosion of Zircaloy in a deep geological repository (see below).

pH dependence of ^{14}C speciation

The study of Sasoh (2008a) is the only available source allowing a tentative appraisal of the pH dependence of the speciation of stable carbon during Zircaloy corrosion in a deep geological repository (Tab. 5-6). The studies were carried out with non-activated materials. The author reports differences in the proportions of the individual stable carbon compounds to be within a factor of 2 at pH 8 and 12.5. This finding suggests that the type of ^{14}C-bearing species may not be significantly different during Zircaloy corrosion under these conditions. Kaneko et al. (2003) determined a higher organic carbon fraction at pH 8 than at pH 12.5 while, vice versa, the fraction of inorganic carbon at pH 12.5 is higher as compared to pH 8. Note, however, that measurements of inorganic stable carbon at high pH are prone to artefacts caused by CO_2 ingress. On the basis of the currently available experimental data with stable carbon compounds, there is evidence to suggest that the ^{14}C speciation generated during Zircaloy corrosion could be similar under circum-neutral and alkaline conditions.

Effect of radiation

^{60}Co is the main activation product in Zircaloy and therefore the predominant gamma emitter (Dey et al. 2020). As with activated steel, an initially high dose rate of gamma radiation could produce oxidants, reductants and gaseous compounds (radiolysis) (Section 4.2.1.4). However, the radiation intensity decreases rapidly over time due to the short half-life of ^{60}Co. It can be assumed that the assessment made in Section 5.1.6 about the effect of radiation on the ^{14}C species released during the corrosion of activated steel also applies to activated Zircaloy. In brief, it can be postulated that gamma radiation will have no or only a limited effect on the chemical nature of the ^{14}C-bearing compounds generated during Zircaloy corrosion under the dose rates relevant to a deep geological repository. It should be noted, however, that valid experimental evidence for this assumption is lacking.

Tab. 5-6: Proportions of single, potentially ^{14}C-bearing compounds quantified as stable carbon compounds in leaching tests with Zircaloy at pH 8 and 12.5.

Values given as percentages. From Sasoh 2008a.

pH	Formic acid	Acetic acid	Formaldehyde	Methanol	Ethanol
8	17	33	20	n.d.	30
12.5	9	56	16	3	15

n.d. not determined.

5.2.5 Comparison of activated Zircaloy and stainless steel corrosion

From the experimental investigations, it appears that there are similarities between Zircaloy and steel during the corrosion process in terms of ^{14}C release and speciation. These can be summarised as follows:

i) Corrosion rate: High initial corrosion rates have been observed for both materials over a period of days to months, while the long-term corrosion rates in alkaline media are comparatively low, ranging from a tenth of a nanometre to a few nanometres per year. However, the corrosion of stainless steel could be faster under circum-neutral conditions compared to Zircaloy.

ii) IRF: As with activated steel, a rapid release of ^{14}C-bearing species is expected in the early phase of the corrosion process. The IRF of ^{14}C mainly comprises ^{14}C in inorganic and organic forms, while the proportion of ^{14}C in gaseous form is smaller. The IRF of ^{14}C could be higher for activated Zircaloy than for activated steel, as a thicker oxide layer is formed on the former.

iii) Long-term release: Most of the ^{14}C inventory of activated Zircaloy is likely to be released in the chemical form of ^{14}C-bearing gaseous carbon species, mainly $^{14}CH_4$, as previously suggested for activated stainless steel.

iv) ^{14}C speciation: Similar stable carbon compounds (potentially ^{14}C-bearing) were detected in metallic iron/steel-water systems and metallic Zircaloy-water systems both in solution and in the gas phase.

There is evidence that essentially the same release models for ^{14}C can be applied to activated stainless steel and activated Zircaloy. In safety assessments, the conservative assumption was made that the oxide layer does not retard the release of radionuclides (Necib et al. 2018b). As already shown for steel, it can be assumed that, in the long term, ^{14}C release from corroding activated Zircaloy occurs congruently in accordance with the low corrosion rate of the base metal.

5.3 ^{14}C release during dissolution of the spent fuel

Fuel pellets are the third source of ^{14}C in SF, in addition to activated Zircaloy and activated stainless steel parts of the SF cladding, due to the presence of N impurities and abundant oxygen in UO_2/MOX fuels and subsequent activation of ^{14}N and ^{17}O in NPPs (Sections 3.1.3 and 3.1.4). Uncertainties arise regarding the N content of non-activated fuel and the proportions of ^{14}C produced by either ^{14}N or ^{17}O activation. For example, it has been estimated that ^{17}O activation in UO_2 fuel pellets contributes ~ 30% to the ^{14}C inventory of SF (Section 3.1.4). Notwithstanding the inherent uncertainties, there are reasons to assume that the SF will be a source of ^{14}C in a deep geological repository, even if the inventory is limited.

5.3.1 Radionuclide mobilisation during aqueous dissolution of the spent fuel

Radionuclide release from SF starts after containment failure and water ingress, and proceeds in two steps with distinctly different time scales: i) rapid release of soluble, easily accessible radionuclides, leading to the definition of nuclide-specific IRFs, ii) sustained long-term release of radionuclides as a result of the dissolution of the UO_2 crystalline lattice (UO_2/PuO_2 in MOX fuel), commonly referred to as "matrix dissolution" (Bradbury et al. 2014; Curti 2021b; Ekeroth et al. 2012; Ferry et al. 2008; Johnson et al. 2005, 2012; Nagra 2005; Poinssot et al. 2005; Johnson et al. 2023). The rapid release includes a range of fission products, including ^{14}C (Johnson et al. 2023). Dissolution of the UO_2 matrix is expected to proceed at a very low rate under the strongly reducing conditions at the interface between UO_2 and the solution due to the presence of H_2 produced by the anoxic corrosion of steel in the deep geological repository (Johnson et al. 2023). The release of radionuclides, i.e., fission and activation products, occurs in accordance with the dissolution of the UO_2 matrix (Johnson et al. 2023).

5.3.2 Dissolution rate of spent fuel

Johnson et al. (2023) published a comprehensive review of the dissolution of the SF. Dissolution rates of SF for the Swiss safety assessment were derived on the basis of the so-called "dissolution rate" model, which is partly based on actual measurements of UO_2 and spent fuel dissolution rates under repository-like conditions. This led to the selection of a dissolution rate constant of 10^{-7} a^{-1} for the SF for use in safety assessments (Johnson 2014). The largest fraction of the radionuclide inventory of SF, comprising fission and activation products as well as the actinides, is released at the same rate as the SF dissolves (Johnson et al. 2023).

This value is much lower than radiolysis-induced oxidative UO_2/SF dissolution rates and is based on the assumption that the presence of H_2 evolving during corrosion of the carbon steel canister protects the UO_2 fuel from oxidation. The existence of an H_2-protection mechanism has been experimentally demonstrated and is now well understood (Broczkowski et al. 2005, 2007; Röllin et al. 2001; Shoesmith 2008; Trummer et al. 2008, 2009; Trummer & Johnson 2010). The main operating mechanism is the catalytic dissociation of H_2 to $H^{\bullet}$ radicals at the surface of noble metal inclusions (ε-particles). The lone electrons of the $H^{\bullet}$ radicals formed at the surface of the ε-particles are galvanically coupled to UO_2 and protect it against oxidation by radiolytic species such as H_2O_2. This mechanism is further favoured by the increase in conductivity, which is induced by trivalent rare earth elements and actinides at high fuel burnup.

After completion of steel corrosion and complete evacuation of H_2, the residual alpha activity would be insufficient to induce oxidative fuel oxidation via water radiolysis (Bradbury et al. 2014), so that reductive UO_2 dissolution can be assumed even in the absence of H_2 at late stages of the evolution of the deep geological repository. This justifies the assumption of a continuous dissolution rate constant of 10^{-7} a^{-1} for the SF (and correspondingly, the release of the radionuclide inventory), which is maintained until 10^6 years after repository closure.

The dissolution rate for SF used in current Nagra's safety assessment is given in Johnson et al. (2023).

5.3.3 Chemical form of ^{14}C during dissolution of the spent fuel

No information is available on the chemical form of ^{14}C released in the IRF or during dissolution of the SF. Regarding the IRF, Johnson (2014) stated that "there is no basis for clearly identifying the chemical form (organic vs. inorganic) of the released ^{14}C". An appraisal of the chemical form of ^{14}C during fuel dissolution is therefore speculative and essentially based on considerations previously made for activated steel and Zircaloy (Sections 5.1.5 and 5.2.4).

There is experimental evidence that a thin oxidised layer exists on the UO_2 matrix due to the high sensitivity of U(IV) to oxidants (Johnson et al. 2023). However, it was found that the presence of H_2 at the interface of the UO_2 matrix, in addition to the complete neutralisation of radiolytic oxidants, also leads to a reduction of redox-sensitive radionuclides accommodated by the pre-oxidised layer (Johnson et al. 2023; Spahiu 2021). Oxidised carbon species, such as carbonates and carboxylic acids, are expected to be the dominant species in the pre-oxidised layer, comparable to steel (Section 5.1.4). These compounds are released on contact with the solution if reduction to gaseous species (e.g., CH_4) at the interface of the UO_2 matrix is inhibited, i.e., if complete thermodynamic equilibrium is not reached (Section 4.1). However, under conditions of complete thermodynamic equilibrium, gaseous species could be released from the oxide layer of the UO_2 matrix. There is experimental evidence that ^{14}C-bearing gaseous species (CO_2, CO and CH_4) are either not present during rod puncture tests for fission gas or only at very low levels and that, furthermore, the vast majority of ^{14}C is retained in the matrix of the fuel (Johnson et al. 2023). The results suggest that ^{14}C-bearing compounds released instantaneously from the oxide layer are water-soluble rather than gaseous carbon compounds, as observed in the case of activated steel.

The chemical forms of carbon in the UO_2 matrix are elemental carbon or carbide. Like other transition-metal carbides, uranium carbide undergoes hydrolysis producing CH_4 as the main gaseous hydrolysis product. The hydrolysis of uranium carbide has been studied extensively in acidic media in connection with efforts to develop nuclear fuel reprocessing (Charyulu et al. 1991, Maslennikov et al. 2009, Legand et al. 2014). A literature review of the reaction of uranium carbides with water is found in Griess (1974).

The reaction of uranium monocarbide with water at neutral pH and 25 - 99 ˚C generated hydrous uranium oxide, H_2 gas and a mixture of gaseous HCs dominated by CH_4 with small amounts of C_2H_6 and saturated C3-C6 HCs (Bradley et al. 1962). An investigation of neutron-activated uranium monocarbide reaction with water (Bradley et al. 1964, Bradley et al. 1965) showed a decrease of the hydrolysis rate with increased burnup. Additionally, a change in the composition of the gaseous reaction products was observed, with much more H_2 (28 vol.%) and less CH_4 (67 vol.%) produced compared to the non-activated material (9 vol.% H_2 and 88 vol.% CH_4). The content of non-volatile HCs also increased to ~ 20% of the total carbon from almost zero for non-activated uranium carbide.

The reaction of uranium carbides with alkaline solutions resulted in the oxidation of part of the uranium to the hexavalent state with the accompanying evolution of H_2 (Bradley Sears et al. 1968). The HCs produced in reactions with uranium monocarbide and sesquicarbide (U_2C_3) were the same as those produced with water. With the dicarbide, some of the H_2 resulting from the oxidation of the uranium reacted with the carbide carbon, forming more gaseous HCs (and presumably less wax) than were obtained in water. The relative concentrations of the various C2- to C8-HCs were found to be independent of the NaOH concentration.

The above findings indicate that the reaction of uranium carbides and the anoxic corrosion of steel might produce similar ^{14}C-bearing carbon compounds. The corrosion experiments with activated steels (Section 5.1.3) show that ^{14}C-bearing CH_4 is the main gaseous carbon compound produced as a result of the anoxic corrosion of the steel matrix. This compound dominates the ^{14}C inventory in the gas phase irrespective of the surface dose rate of the activated material. Besides $^{14}CH_4$, HCs and ^{14}CO were identified as possible gaseous compounds. As with the SF, carbon is present in the steel matrix either in elemental or carbide form, and the carbon speciation at the interface between activated steel and solution is strongly determined by the availability and reactivity of H_2. In a surface-mediated reduction process, H_2 or its radicals react with the carbon of the metal matrix (either as elemental C or in carbide form) to produce CH_4 and other HCs (see Fig. 4-5a). The available evidence suggests that similar conditions exist for UO_2 fuel. The presence of reactive H_2 at the interface between the UO_2 matrix and the solution ensures strongly reducing conditions, which promotes the reduction of carbon species released during the dissolution of the UO_2 matrix. Thus, it can be assumed that ^{14}C is likely to be released predominantly as $^{14}CH_4$ and in much smaller amounts than other HCs, also during dissolution of the SF.

5.4 ^{14}C release during dissolution of vitrified HLW

There is very little information on the release and speciation of ^{14}C from vitrified HLW (Curti 2023). In contrast to SF and activated metals, a preferential sudden release of ^{14}C from vitrified HLW is not expected, as borosilicate glass is a very homogeneous material. It is assumed that ^{14}C accommodated by the glass matrix and released congruently with dissolution (rates defined in Curti 2023) is present in the inorganic form.

$BaCO_3$ crud is a ^{14}C-containing vitrified waste form produced during reprocessing. This waste form is expected to contain ^{14}C mainly in the inorganic form ($^{14}CO_3^{2-}$). The solubility of $BaCO_3$ in alkaline media is very low, which strongly limits the free $^{14}CO_3^{2-}$ concentration in solution. Consequently, it can be safely assumed that ^{14}C bound to $BaCO_3$ is retained in this waste form

and therefore decays in the repository. The same assessment applies to $Ba^{14}CO_3$, which originates from industrial and military applications and belongs to the MIR waste.

5.5 ^{14}C release from spent IERs

Investigations into the ^{14}C source term and leaching from spent IERs have been conducted in the framework of the EU project "CAST" (Bucur et al. 2017; Reiller 2018; Rizzato et al. 2015; Rizzo et al. 2017). The main findings have been summarised in Section 3.2.1.

5.5.1 Release process

There is currently no evidence that the release of ^{14}C from spent IERs is related to the degradation of the polystyrene-based exchanger matrix, while there is evidence that the functional ion-exchanger groups carrying ^{14}C can be detached from the polymeric exchanger matrix. Release of ^{14}C from spent IERs was observed under alkaline conditions, whereas leaching of ^{14}C from cemented, spent IER-containing waste forms was not observed (Section 3.2.1) (Večernik et al. 2018). This finding suggests that ^{14}C in spent IERs was predominantly bound in the inorganic chemical form (as $H^{14}CO_3^-$) to the functional ion-exchanger groups, which are strongly retarded by cement paste (see Chapter 6). The ^{14}C fraction associated with the organic chemical forms must be much lower, as the retention of small organic molecules (e.g., $HCOO^-$ and CH_3COO^-) is much weaker than that of inorganic ^{14}C. Consequently, these compounds would have been detected in the leaching solution.

5.5.2 Release rate

The desorption of the ^{14}C-bearing carbon compounds from spent IERs will occur as soon as the waste material comes in to contact with the porewater of a deep geological repository. Therefore, rapid release of ^{14}C is assumed, which is a conservative assumption in view of the fact that IERs are chemically stable under alkaline conditions (e.g., Guillemot et al. 2023).

5.5.3 Chemical form of ^{14}C

^{14}C associated with spent IERs is expected to be mainly present in the inorganic form as $H^{14}CO_3^-$. The remaining fraction is considered to be organically bound ^{14}C due to the presence of small, oxygenated carbon compounds such as formate ($H^{14}COO^-$) and acetate ($^{14}CH_3COO^-$). It should be noted that, based on the study of Magnusson & Strenström 2005, Cloet et al. 2014 assumed a ratio of 70% inorganic ^{14}C and 30% organic ^{14}C for spent IERs and contaminated materials originating from PWRs, and a ratio of 90% inorganic ^{14}C and 10% organic ^{14}C for spent IERs and contaminated materials originating from BWRs. The formation of mainly inorganic ^{14}C in IERs from BWRs and the formation of a large fraction of organic ^{14}C in IERs from PWRs was supported by recent CAST studies (Rizzo et al. 2017; Večernik et al. 2018). In these studies, leaching experiments indicated that the amount of monocarboxylates is small. The presence of other oxygenated carbon species, e.g., alcohols and aldehydes, is considered unlikely as these uncharged species are not expected to be retained by the IERs. Furthermore, the amount of ^{14}C released in a deep geological repository to the gas phase (e.g., ^{14}CO) by leaching of spent IERs is considered negligible.

5.6 ^{14}C release from graphite

Graphite is a non-homogenous composite material usually made from petroleum coke or coal-tar derived coke using a pitch binder. The material is highly porous but manufactured in a manner to be isotropic or near-isotropic (Wareing et al. 2013). The properties and radionuclide inventory of

activated (i-)graphite depend on several factors, such as the type of raw material and the manufacturing process leading to different impurity levels and radionuclide precursors, alteration of its physical, mechanical and thermal properties during irradiation, the type of exposure environment and the position in a nuclear reactor (Wareing et al. 2013). Therefore, the radionuclide inventory, and the ^{14}C inventory in particular, is essentially influenced by the source of graphite and environment in the reactor during irradiation. The activation of ^{14}N and ^{17}O, which are trapped in the pores or adsorbed on the surface of graphite, and the activation of ^{13}C, which is a structural isotope and therefore uniformly distributed in the graphite lattice, are the two principal routes of ^{14}C production in i-graphite. The former activation process leads to ^{14}C hot spots on graphite, while the latter process results in a uniformly distributed background ^{14}C activity (Toulhoat et al. 2018). Therefore, the degree of heterogeneity of the ^{14}C distribution in i-graphite is significantly influenced by the distribution of these precursors. The location of ^{14}C in i-graphite determines its mobility; and its distribution may provide potential for segregation (Wareing et al. 2013). Investigations into the treatment of i-graphite and the ^{14}C source term from i-graphite have been performed in the framework of the EU projects "CARBOWASTE" (Wareing et al. 2013) and "CAST" (Toulhoat et al. 2018). In addition, further investigations on the behaviour of graphite under repository conditions have been carried out within the framework of the disposal programme in the United Kingdom (e.g., RWM 2016).

5.6.1 Release process

In i-graphite, the largest fraction of the radioactive inventory is only accessible for aqueous leaching and release if water penetrates the porous matrix. While the penetration of water into the porosity of non-activated graphite was found to be relatively slow and controlled by a diffusion process, irradiation significantly increased the kinetics and the permeation rate (Wareing et al. 2013). Therefore, water ingress into i-graphite is rapid with a view to the time period under consideration for a repository and does not limit radionuclide release.

The majority of ^{14}C was found to remain in i-graphite on immersion in alkaline solution under oxic and anoxic conditions at ambient temperature (Baston et al. 2012; RWM 2016; Toulhoat et al. 2018). After long-term leaching over a several-month period of i-graphite from the UK under oxic conditions, the cumulative fraction of ^{14}C released was only ~ 0.1% of the total ^{14}C inventory (Baston et al. 2012; Toulhoat et al. 2018). Furthermore, ^{14}C was found to be mainly released to the solution (~ 0.1%), while only a small fraction was released to the gas phase (~ 0.004% as CO/CO_2 and ~ 0.001% as gaseous organic species). For the same type of i-graphite, the cumulative release of ^{14}C was similar under both oxic and anoxic conditions at ambient temperature in alkaline solution (Toulhoat et al. 2018). It should be noted, however, that the cumulative release of ^{14}C was found to depend on the type of graphite, which is likely due to differences in the source and the exposure conditions in the reactor. In general, the amount of ^{14}C released from i-graphite to solution was found to be low compared to other radionuclides associated with the matrix of i-graphite (e.g., ^{36}Cl) (Wareing et al. 2013).

5.6.2 Release rate

^{14}C release was found to occur in two stages: a rapid initial release followed by the subsequent slow release beyond about 28 days (Baston et al. 2012, Toulhoat et al. 2018). The two stages were tentatively assigned to two different mechanisms of ^{14}C production in the reactor, i.e., ^{14}N and ^{17}O activation of surface-adsorbed air leading to rapid release, and ^{13}C in the graphite structure leading to slow release (Wareing et al. 2013; Toulhoat et al. 2018). It was, however, noted that ^{14}C release was comparable for air-cooled piles and CO_2-cooled reactors indicating that the activation of all three isotopes, i.e., ^{14}N, ^{17}O and ^{13}C, can contribute to rapid ^{14}C release due to sorbed air or CO_2. The long-term, steady-state leaching rate of ^{14}C from different types of French i-graphite under

near-neutral and alkaline conditions was achieved within less than one year (Toulhoat et al. 2018). This finding shows that an instant release of ^{14}C occurs in contact with solution, while the long-term release of ^{14}C is a very slow process. It should be noted that a similar two-stage release process of ^{14}C was observed for activated steel. Rate constants for the rapid and slow release of ^{14}C from i-graphite were reported to be 30 a^{-1} (with a range of 10 – 100 a^{-1}) and 0.01 a^{-1} (with a range of 0.001 – 0.1 a^{-1}), respectively (RWM 2016; Toulhoat et al. 2018).

5.6.3 Chemical form of ^{14}C

Leaching experiments on various types of i-graphite from the German, French and UK disposal programmes carried out in strongly alkaline solutions (0.1M and 1M NaOH) under inert atmospheres showed that ~ 99% of the released ^{14}C was present as dissolved, inorganic species (carbonates), while the amount of ^{14}C released to the gas phase (gaseous organic C or CO) was ~ 1% (Toulhoat et al. 2018). This indicates that under both conditions, the dominant fraction of released ^{14}C remains in solution as dissolved carbonate species. The gaseous ^{14}C was predominantly in the form of organic species (HCs and other volatile organic carbon compounds) and CO (Toulhoat et al. 2018). The fraction of gaseous species was found to be similar under both near-neutral and alkaline conditions, while the amount of gaseous $^{14}CO_2$ was significantly reduced in the presence of alkaline leach solutions due to improved CO_2 solubility. It should be noted that inorganic forms of carbon (CO_2(aq), HCO_3^-, CO_3^{2-}) are strongly retained by cementitious materials due to adsorption on, and/or incorporation into, cement phases and calcite (isotopic exchange; see Chapter 6). Thus, under anoxic alkaline conditions, almost the entire inventory of released ^{14}C (~ 0.1% of total ^{14}C inventory of i-graphite) is present as ^{14}C-bearing carbonate species, while the gaseous species only represented ~ 1% of the inventory of released ^{14}C (~ 0.001% of the total ^{14}C inventory of i-graphite). The gaseous species are considered to be mainly in the organic form (HCs and other volatiles), while the proportion of CO is small. Therefore, only a small fraction of the ^{14}C inventory of i-graphite will be released via the gas pathway, but the largest fraction of ^{14}C released from i-graphite will be retained in the cementitious near-field of the deep geological repository.

5.7 ^{14}C release from activated concrete

In activated concrete, ^{14}C is expected to be mainly generated by the activation of ^{13}C and ^{17}O as C and O are important structural elements. By contrast, ^{14}N activation is expected to be negligible as the amount of air entrapped in saturated cement paste is small, as pores are mainly filled with water. Carbon is present mainly as calcium carbonate in hardened cement paste (HCP), while small amounts of carbonate could be bound to some cement phases. Wieland & Kosakowski (2020) and Kosakowski et al. (2023) estimated the amount of carbon to be 0.227 mol/kg HCP in a hydrated CEM I cement and the amount of oxygen to be 22.9 mol/kg HCP. Thus, the amount of oxygen is about a factor of 100 higher than the amount of carbon in HCP. In view of the isotopic abundance of ^{13}C and ^{17}O and their cross-sections for activation by thermal neutrons (Tab. 2-1), it is expected that ^{17}O activation mainly contributes to ^{14}C formation in concrete. The chemical form of ^{14}C is subject to speculation. As oxidising conditions prevail in fresh cement paste (Wieland & Kosakowski 2020; Kosakowski et al. 2023), it is expected that ^{14}C is present in the inorganic form ($^{14}CO_3^{2-}$). Release occurs in terms of a solubility-controlled process as the overall concentration of CO_3^{2-} in near-field porewater is controlled by $CaCO_3$(s) solubility.

5.8 ^{14}C release from contaminated materials

Contaminated materials comprise all metals, organic and inorganic materials with ^{14}C present as surface contaminations. They will be, almost exclusively, stored in the L/ILW repository. There is no experimental information on the release processes, release rates and chemical forms of ^{14}C

for these waste forms. Therefore, the following assessment was made on the basis of expert judgement.

Filter cartridges are ^{14}C-containing waste forms produced from the clean-up systems of reactor coolant in Swiss NPPs. Therefore, the chemical form of ^{14}C taken up by the filter cartridges is expected to be similar to that of spent IERs, i.e., ^{14}C predominantly present as $H^{14}CO_3^-$, whilst a smaller proportion of ^{14}C may be associated with $H^{14}COO^-$ and $^{14}CH_3COO^-$. Consequently, comparable release processes (and rates) are assumed for spent IERs and filter cartridges.

Contaminated metals, inorganic and organic materials are largely contained in operational and decommissioning waste from NPPs and research facilities (MIR waste). The release of ^{14}C-carrying surface contaminations is expected to be instantaneous after contact with a solution as ^{14}C is not bound in the structure of the materials but only adsorbed to their surface. Due to the different origins, conditioning processes and storage conditions of the contaminated materials, assessment of the chemical form of ^{14}C has to be based on simplified assumptions. It is expected that organic ^{14}C dominates, while the presence of inorganic ^{14}C in some waste forms cannot be excluded, such as in residues from incineration facilities (Nagra 2024e, in prep.).

Low molecular weight ^{14}C-bearing organic compounds expected to be released from contaminated waste are assumed to be further degraded to $^{14}CO_2$ and $^{14}CH_4$ in the near-field of a cementitious L/ILW repository by abiotic and/or biotic degradation processes as described in Guillemot et al. (2023).

5.9 Summary of chapter

The release of ^{14}C during corrosion of activated metals (i.e., steel, Zircaloy) and the SF occurs in two steps, i.e., a fast release of ^{14}C upon contact of the materials with water, corresponding to the IRF, and a slow release of ^{14}C in accordance with the corrosion rate of the activated base metals and the dissolution rate of the SF, respectively. The IRF process accounts for the release of predominantly ^{14}C-bearing oxygenated carbon compounds in the organic (e.g., carboxylates) and inorganic chemical forms ($^{14}CO_2(aq)$ and its bases) from the oxide layer produced during corrosion, while the amount of ^{14}C-bearing gas phase species released in this phase is assumed to be low. Overall, the portion of rapidly released ^{14}C is expected to be less than 0.01% of the total ^{14}C inventory of the materials based on experimental studies with activated steel. The high fractions of rapidly released ^{14}C from Zircaloy (20%) and SF (10%) that were previously assumed for safety assessments being considered as over-conservative. The slow release of ^{14}C is associated with the continuous corrosion of the activated metallic waste materials or to the dissolution of the SF over the period of concern for a deep geological repository. ^{14}C will be released in the gaseous form, mainly as $^{14}CH_4$. It can be speculated that similar ^{14}C-carrying carbon species are also produced during the dissolution of the SF.

The ^{14}C-compounds in MIR waste, if present at all, are expected to be rapidly desorbed from contaminated materials. These molecules are expected to be rapidly degradable carbon compounds whose degradation with time produces equal amounts of $^{14}CH_4$ and $^{14}CO_2$ on the basis of a simplified degradation model. Furthermore, a fast release of ^{14}C sorbed onto spent IERs and contaminated materials (e.g., filter cartridges) is expected to occur in a deep geological repository, producing mainly ^{14}C in the inorganic form and a smaller portion in the organic form. Vitrified reprocessing wastes, MIR wastes in the form of ^{14}C-bearing $BaCO_3$, and activated concrete are expected to contain ^{14}C mainly in the inorganic form, congruently released with the glass dissolution rate and the solubilities of $BaCO_3$ and $CaCO_3(s)$, respectively. As ^{14}C-inorganic compounds are strongly retained in the cementitious near-field, ^{14}C is assumed to decay within the deep geological repository. The amount of ^{14}C released from i-graphite is expected to be very small and occurs mainly as inorganic ^{14}C (~ 99%), while the fraction of gaseous species (mainly in the organic form) is small (~ 1%).

6 Sorption processes of ^{14}C in the near-field and host rock

Retention of ^{14}C-bearing carbon compounds is a key process for predicting ^{14}C release from the repository environment (Nagra 2021a). Retention can occur through the interaction of ^{14}C-carrying carbon compounds with minerals during migration from the near-field to the far-field and further into the biosphere and/or through their conversion into other organic molecules or carbonate during the migration process. The interaction of ^{14}C-carrying molecules with minerals of the EBS (cement and clay minerals, calcite, etc.) is particularly important as it determines the mobile portion of ^{14}C. In the case of a reversible and weak interaction of ^{14}C-bearing carbon compounds with minerals, sorption only leads to a retardation in migration, but ^{14}C can eventually reach the biosphere where it enters the carbon cycle (see Section 7.3). In contrast, if sorption is sufficiently strong, retardation can be so great that decay of ^{14}C occurs along the transport pathways from the near-field to the biosphere, thus strongly reducing its contribution to dose release. Finally, irreversible sorption of ^{14}C on solids is an effective sink for ^{14}C leading to ^{14}C decay in the repository environment.

The repository concept for L/ILW envisages the presence of large amounts of cementitious materials, which will be emplaced to function as the major physical and chemical barrier to the release of radionuclides from the near-field into the host rock. HCP is the most important sorbent for radionuclides. It is composed of a complex mixture of different cement phases, such as calcium silicate hydrate (C-S-H), portlandite, ettringite, AFm phases, Fe/Al silica hydrogarnet, hydrotalcite, and a few percent by weight of calcium carbonate, which is added as a filler material (Wieland 2014). In the case of the HLW repository, the bentonite backfill is the main sorbent in the near-field. Similar to HCP, bentonite is a mixture of different clay minerals with montmorillonite as the main component and smaller proportions of other accompanying minerals such as quartz, mica, feldspar, pyrite or calcite.

According to the current concepts for the L/ILW and HLW repositories, the OPA host rock may form an additional barrier against the transfer of ^{14}C into the biosphere as a result of ^{14}C sorption onto its minerals. In the literature, sorption values quantifying retention of radionuclides are expressed in terms of distribution ratios (R_d) or distribution coefficients (K_d) in the case of linear, reversible sorption. Fig. 6-1 shows a conceptual representation of adsorption (surface-bound) and absorption (uptake in micropores or structure) by minerals.

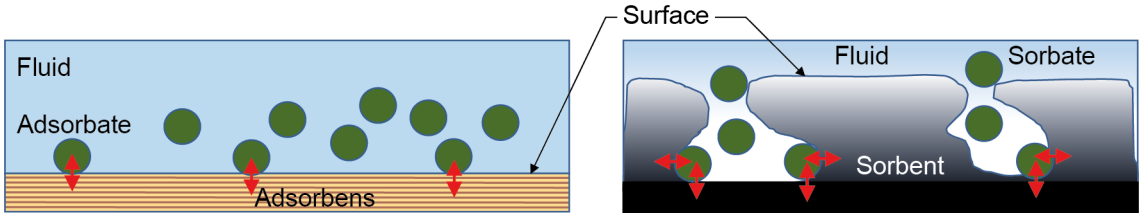

Fig. 6-1: Schematic representation of sorption processes. a) Adsorption on the surfaces of minerals and cement phases; b) Absorption by organic matter

Previous safety assessment calculations for the L/ILW repository have shown that ^{14}C in the organic form contributes to the released doses under the assumption that no sorption occurs, while migration of ^{14}C in the inorganic form is significantly retarded both in the cementitious near-field and in the OPA host rock due to isotopic dilution of ^{14}C-bearing carbonate with the calcite (Nagra 2002, 2008a). In the SF emplacement drifts of the HLW repository, ^{14}C is transported by diffusion

through the bentonite buffer surrounding the SF canisters and ultimately through the OPA host

rock. As the porosity in clay rocks is associated mainly with the clay phase, sorption of organics on clays has been identified as an important process to be considered (Van Loon 2019).

6.1 Sorption of dissolved inorganic ^{14}C

The retention of inorganic ^{14}C ($H^{14}CO_3^-$,$^{14}CO_3^{2-}$) takes place via isotopic exchange processes with CO_3^{2-} (stable carbon) of the calcium carbonate fractions of the cementitious near-field, bentonite and OPA host rock. This process has already been taken into account to derive sorption values for $^{14}CO_3^{2-}$ as part of the development of sorption databases for the Swiss disposal programme (Baeyens et al. 2014; Wieland 2014; Tits & Wieland 2023). In addition, experimental data have substantiated the concept of isotopic exchange (e.g., Boylan et al. 2017; Cowan et al. 1990; Curti 1997; Davis et al. 1987; Pointeau et al. 2003). Isotopic exchange between $^{14}CO_3^{2-}$ and CO_3^{2-} in calcium carbonate can be expressed in terms of the respective fractionation factors, i.e., the ratios of their concentrations in solid and in solution. Dynamic processes at the solid-liquid interface (e.g., recrystallisation) are the main driving force of isotopic exchange processes (Fig. 6-2).

Calcium carbonate is present in varying proportions in near-field materials and the host rock. Carbonate is predominantly associated with calcium carbonate (typically ~ 5 wt.%) and calcium monocarboaluminate (AFm-CO_3) in the cementitious materials (total carbonate content 10 – 15 wt.%) (Lothenbach & Wieland 2006), with calcite in bentonite backfill (median value ~ 0.7 wt.%; range 0.1 – 1.4 wt.%) (Bradbury & Baeyens 2009; Section 6.4.1.1) and with calcite, dolomite and siderite (median value ~ 11 wt.%; range ~ 3 and ~ 40 wt.%) in the OPA (Nagra 2002; Van Loon & Mibus 2015; Section 6.4.1.1). Furthermore, $CaCO_3$ is expected to precipitate in the cementitious near-field due to the reaction of CO_2, generated by the degradation of organic waste, with dissolved Ca; along with precipitation in the pore space of the interface between the near-field and the host rock, due to the mixing of CO_3^{2-}-rich groundwater from the geological formation with Ca-rich cement porewater. The retention of $^{14}CO_3^{2-}$ is thus expected to increase with time as the amount of $CaCO_3$ formed at the interface increases. In the cementitious near-field, the pH decreases with time as the cement degradation proceeds (i.e., from stages I to III; Section 2.3.1). Hence, the decreasing solubility of $CaCO_3$ with decreasing pH leads to decreasing aqueous $^{14}CO_3^{2-}$ concentrations, which improves the retention of inorganic ^{14}C with time. The above considerations show that the uptake of inorganic ^{14}C in the near- and far-fields can be well predicted.

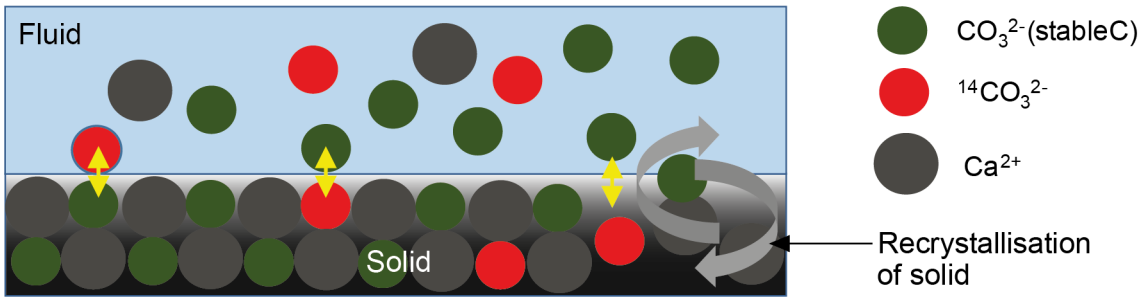

Fig. 6-2: Schematic representation of the isotopic exchange processes of $^{14}CO_3^{2-}$ and $^{12/13}CO_3^{2-}$ (stable C) at the solid-liquid interface

6.2 Sorption of dissolved ^{14}C-carrying small organic molecules

6.2.1 Sorption onto cementitious materials

There are only a limited number of experimental studies on the interaction of ^{14}C-bearing small organic molecules (alcohols, aldehydes, carboxylates) with cementitious materials (Kaneko et al. 2003; Matsumoto & Banba 1999; Matsumoto et al. 1995; Sasoh 2008b; Wieland et al. 2016). Sorption values for the ^{14}C-bearing small organic molecules have already been assigned in the context of previous safety assessments (Wieland 2014). In general, the interaction of alcohols (e.g., methanol, ethanol), aldehydes (e.g., formaldehyde, acetaldehyde) and carboxylates (e.g., formate and acetate) formed in the course of the corrosion of non-activated and activated metals (Tabs. 4-1 and 5-1) with cementitious materials was found to be very weak (Matsumoto & Banba 1999; Matsumoto et al. 1995; Wieland et al. 2016). Reliable measurements of sorption values can only be achieved in experimental systems with a high solid content, i.e., a high solid-to-liquid ratio. R_d (or K_d) values were reported to range between ~ 2×10^{-5} and ~ 5×10^{-3} m^3/kg (Sasoh 2008b; Wieland et al. 2016) (Fig. 6-3).

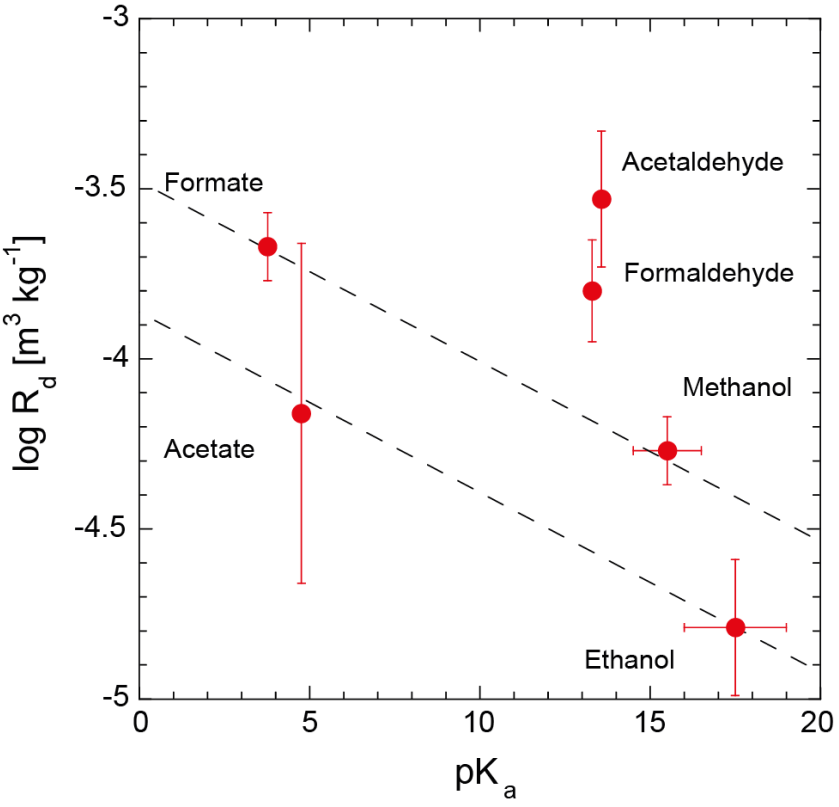

Fig. 6-3: Sorption values of alcohols, aldehydes and monocarboxylates on HCP as a function of the pK_a values of the carbon compounds

From Wieland et al. (2016)

The R_d values were determined in diffusion experiments through HCP carried out at pH 13.3 in cement-type porewater.

The weak interaction of the small molecules occurs by electrostatic attraction between the negatively charged anions and the positively charged surface sites of some cement phases, such as in the case of HCOOH and CH_3COOH. In the case of non-ionised, polar organic compounds, such as alcohols and aldehydes, non-specific interaction with oxidic surface sites may occur through hydrogen bonding or van der Waals forces. It is assumed that the organic compounds are predominantly bound to the surface of cement phases (Fig. 6-1a). Intercalation resulting from the uptake by the structure or into the interlayer of some cement phases is probably less important, as the sorption values of selected organic carbon compounds during hydration of cement were found to agree with those measured in batch-type sorption experiments on HCP, within the uncertainties (Wieland et al. 2016). The extent of interaction was assigned as follows: formate > acetate ~ acetaldehyde > formaldehyde ~ methanol ~ ethanol, indicating decreasing uptake with decreasing average oxidation state of carbon in small organic molecules (Fig. 6-3). It should be noted that the interaction of these small organic molecules with cementitious materials is much weaker than that of multidentate polycarboxylates, e.g., isosaccharinate, gluconate or citrate (Dario et al. 2004; Garcia et al. 2020; Pointeau et al. 2006; Van Loon et al. 1997) or aminopolycarboxylates (e.g., ethylenediaminetetraacetate/EDTA, nitrilotriacetate/NTA) (Pointeau et al. 2006, 2008). It is also expected that the interaction of dicarboxylates (e.g., oxalate or malonate) with cementitious materials is stronger than that of monocarboxylates.

6.2.2 Sorption onto clay minerals

The sorption of organic molecules on clay minerals retards migration in clay-rich rocks (Van Loon 2019). Bentonite and OPA are the clay-type materials that limit the migration of organic molecules in the near-field and far-field of a deep geological repository for HLW/SF, respectively. In the HLW repository near-field, the ^{14}C released from the waste is transported by diffusion through the bentonite buffer to the OPA host rock.

There are several studies that have investigated the interaction of organic compounds, mainly polycarboxylates, with montmorillonite, the main clay mineral of bentonite (Ramos et al. 2011; Ramos & Huertas 2014; Soma & Soma 1989; Wang & Lee 1993). Ramos et al. (2011) and Ramos & Huertas (2014) investigated the sorption of lactate, glycine and citrate on montmorillonite in the pH range from 2 to 10. Lactate, an α-hydroxy monocarboxylic acid, showed the strongest interaction with the clay surface, which is likely due to surface complexation at the aluminol surface sites by a ligand exchange reaction (Ramos & Huertas 2014; Soma & Soma 1989). This result is consistent with observations reported recently by Chen et al. (2018a,b). These authors investigated the interaction of small organic molecules with the clay minerals illite and kaolinite (Fig. 6-4). Alcohols and aliphatic carboxylates were found to interact only very weakly with the surfaces of the clay minerals. Only α-hydroxy carboxylates showed significant interaction with the clay surface (R_d values ranging from 0.6 to 6×10^{-4} m^3/kg depending on ionic strength) (Chen et al. 2018b). It was postulated that the relative position of the hydroxo group leads to the formation of surface complexes of the ligands with the aluminol surface sites (Chen et al. 2018b). In contrast, the interaction of alcohols and aliphatic carboxylates, such as propanoate and butanoate, was found to be very weak due to non-specific interaction with the surface sites ($R_d \sim 10^{-5}$ m^3/kg).

Wang & Lee (1993) studied the adsorption-desorption processes of aliphatic amines, amino acids and also acetate on the organic-free clay minerals kaolinite and montmorillonite. It was observed that sorption of acetate was only partially reversible, while no sorption values were reported. In the case of acetate, the electrostatic attraction between the functional carboxyl group of the compound and the clay particle surfaces was considered to be the effective adsorption mechanism (Fig. 6-1a).

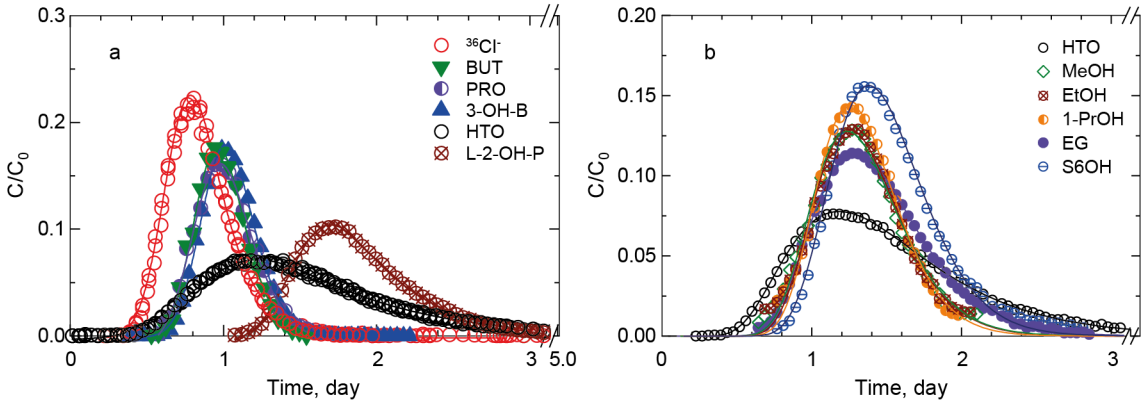

Fig. 6-4: Breakthrough curves of (a) carboxylates and (b) LMW alcohols in percolation experiments with compacted illite at an NaCl concentration of 0.2 M in comparison to HTO (tritiated water) and ^{36}Cl[2]

Adapted from Chen et al. (2018b).

Abbreviations of compounds: Na-butanoate (BUT), Na-propanoate (PRO), Na-DL-3-hydroxybutanoate (3-OH-B), Na-L-2-hydroxypropanoate (L-2-OH-P), methanol (MeOH), ethanol (EtOH), 1-propanol (1-PrOH), ethane-1,2-diol (EG), d-sorbitol (S_6OH).

Several studies on the interaction of organic compounds with Callovian-Oxfordian claystone (COx) and a soft clay-rich sedimentary rock have been carried out in the framework of the French disposal programme (Dagnelie et al. 2014, 2018; Guo et al. 2021; Rasamimanana et al. 2017). Dagnelie et al. (2014) conducted diffusion experiments with EDTA, isosaccharinate, phthalate and oxalate on COx. It should be noted that due to the possibility of bidentate coordination (e.g., OH substitution in α-position in polycarboxylates), these compounds are expected to interact strongly with mineral surfaces. Sorption values determined from batch experiments ranged from 1.4 to 30×10^{-3} m^3/kg, while K_d values determined from diffusion experiments were lower by a factor of ~ 15 to ~ 80 (ranging from 0.08 to 1.03×10^{-3} m^3/kg). Dagnelie et al. (2018) proposed an empirical correction factor to account for the deviation between sorption values in dilute and compacted clay systems based on the idea that retardation depends on the accessible porosity of the diffusing solute in compacted clay systems. The latter authors also gave upper limits for the sorption value of acetate: $R_d < 0.1\times10^{-3}$ m^3/kg from batch sorption and $R_d < 0.01\times10^{-3}$ m^3/kg from diffusion experiments. This finding supports previous observations on cementitious systems that the interaction of monocarboxylates with oxidic surface sites on cement phases is significantly weaker than that of multidentate polycarboxylates (e.g., isosaccharinate, oxalate) or amino-polycarboxylates (e.g., EDTA) (Section 6.1).

Rasamimanana et al. (2017) followed up on previous work on the interaction of multidentate polycarboxylates and aminopolycarboxylates with COx. Very weak sorption of acetate on COx was reported for those experiments, where bacterial activity was suppressed by the addition of NaN_3. The authors confirmed significant adsorption of multi-dentate polycarboxylates and aminopolycarboxylates by COx (R_d ranging between ~ 1.5 and 55×10^{-3} m^3/kg) and correlated the extent of sorption with the dipole moment (μ(D)) of the organic compounds (non-polar versus polar molecules). The correlation shows that increased sorption of the polycarboxylates can be interpreted in terms of an increasing molecular dipole moment. This finding indirectly supports

[2] The solid lines are best-fit curves obtained from STANMOD (STudio ANalytical MODels), a public domain Windows-based computer software package for evaluating solute transport in porous media using analytical solutions of the convection-dispersion solute transport equation (/www.pc-progress.com).

the experimentally observed very weak sorption of monocarboxylates, as their dipole moment is small. Guo et al. (2021) determined the uptake of hydrophobic (toluene, benzene, naphthalene) and hydrophilic (adipate, oxalate, ortho-phthalate, benzoate) organic compounds by a soft, clay-rich sedimentary rock in batch sorption and diffusion experiments. Note that no experimental studies were carried out with aliphatic monocarboxylates. Sorption values ranged from 0.14 to 8.80×10^{-3} m^3/kg (batch sorption) and from 2.33 to 4.65×10^{-3} m^3/kg (diffusion). The adsorption of hydrophobic compounds was found to correlate with their lipophilicity (octanol-water partition coefficient K_{OW}), despite the low content of natural organic matter in the sedimentary rock (< 0.5%). This result suggests an absorption (Fig. 6-1b) rather than adsorption process (Fig. 6-1a). Interestingly, the extent of sorption of ionisable (hydrophilic) and non-ionisable (hydrophobic) organic compounds on the clay rock was found to be similar.

The above studies show that the interaction of aliphatic monocarboxylates (e.g., formate, acetate, propionate, etc.) with clay minerals is very weak. In particular, it is much weaker than that of multidentate polycarboxylates (e.g., isosaccharinic, gluconate, oxalate, citrate, glutarate, succinic, adipic acids, etc.) or aminopolycarboxylates (e.g., EDTA, NTA). This observation can be interpreted in relation to the respective molecular properties (dipole moment, K_{OW}) and supports observations made on cementitious materials. It can be assumed that the surface binding of aliphatic monocarboxylates to clay minerals is the main retention mechanism. This also applies to non-ionisable small organic molecules, such as alcohols and aldehydes.

6.2.3 Sorption onto calcite

The interaction of small organic molecules (alcohols, aldehydes, carboxylates) with calcite has been investigated with regard to possible effects on the dissolution and growth kinetics of this mineral in soils, sediments and aerosols, as well as in connection with industrial applications (e.g., Bovet et al. 2015; Chen et al. 2021; Compton & Brown 1995; Dobberschütz et al. 2018; Fredd & Fogler 1998; Suess 1973). Wet chemical and spectroscopic studies were carried out to investigate the extent of sorption of small organic molecules to calcium carbonate under different conditions, such as sorption from gas phase (Bovet et al. 2015), sorption from pure organic liquids (Hakim et al. 2017), and sorption of organic molecules dispersed in water (Plank & Bassioni 2007). Further information has been obtained from computational studies (Ataman et al. 2016; Budi et al. 2018; Hakim et al. 2017). Currently, there is no quantitative information on the sorption of small C1 to C5 carbon compounds from aqueous solution on calcite. The computational studies conducted by Ataman et al. (2016) show that the extent of adsorption of functional groups on calcite is in the following order: carboxylate (R-COO) > water ~ alcohol (R-OH) > aldehyde (R-CHO). Side groups I were found to have an influence on the electronic structure of some functional groups and thus affect surface binding through electrostatic interaction and hydrogen bonding. For example, the nature of the side groups alters the adsorption behaviour of -OH and -CHO functional groups, while it has no significant effect on bonding through -COO functional groups. Weak sorption of small organic molecules emerges from the study of Budi et al. (2018). These authors performed density functional theory calculations to decipher the effect of solvation on the adsorption of small organic molecules on calcite. The results show that only a few molecules tend to interact with the surface of calcite in solution, such as formic and acetic acid as well as methanol. The molecules were found to bind to the calcite surface via their functional groups (Bovet et al. 2015; Hakim et al. 2017). Nevertheless, none of the molecules showed a free energy of adsorption significantly < 0, which would indicate strong sorption. It should be noted that the transferability of the information obtained from the above studies to the conditions relevant to a deep geological repository is uncertain, especially for a quantitative estimation of the sorption of small organic molecules on calcite.

The above literature review indicates that small C1 – C5 organic molecules seem to interact only weakly with calcite. Furthermore, the weak interaction indicates an adsorption rather than an absorption process. The statements are supported by previous conclusions by Van Loon (2019): "In general, sorption of organic molecules on calcite is possible, but the interaction is rather weak than strong so that sorption of organic molecules on calcite results in a weak retardation rather than in a sink for ^{14}C-molecules".

6.3 Sorption of gaseous ^{14}C-carrying carbon compounds

Gas sorption (especially of CH_4, CO_2) on clay minerals has been studied with regard to shale gas extraction and in the context of CO_2 sequestration (e.g., review by Klewiah et al. 2020). In shale rocks, gas sorption includes various processes, such as adsorption onto the surfaces of organic matter (OM), mainly kerogen, and minerals (Fig. 6-1a), absorption into molecular openings of kerogen (Fig. 6-1b), and capillary condensation in micropores (< 2 nm) (Gasparik et al. 2014; Klewiah et al. 2020). It has been observed that gas sorption is a combination of these sorption processes, which are inherently difficult to distinguish. In general, gas sorption accounts for the storage of gas molecules in a denser phase in relation to the bulk (free gas) phase in open pores (Ross & Bustin 2009).

The content of OM is one of several parameters that can influence gas storage, such as that of CH_4 in shale rock (e.g., Chalmers & Bustin 2007, 2008; Klewiah et al. 2020; Lu et al. 1995; Ross & Bustin 2008, 2009; Zhang et al. 2012). A positive correlation has been observed between CH_4 storage capacity and total organic carbon (TOC) content (e.g., Lu et al. 1995; Zhang et al. 2012), indicating that the microporosity associated with OM is mainly responsible for CH_4 storage in shales (Chalmers & Bustin 2007, 2008; Gasparik et al. 2014; Ross & Bustin 2008, 2009). Previous work suggests that pore-filling in micropores of OM controls gas sorption rather than adsorption on OM (Dubinin 1975). This also implies that the volume of micropores determines the gas sorption capacity of shale. CH_4 sorption capacities of dry shales were found to correlate positively with the TOC, but significant deviations from this trend have been observed for individual samples (Gasparik et al. 2014). In addition, maturation of OM was considered to also have an effect on gas sorption capacity, although it is currently unclear whether this effect only occurs at low gas pressures (Zhang et al. 2012).

In addition to OM, clay minerals are also thought to influence the gas sorption capacity, especially in clay-rich shales. For this reason, several studies have addressed the influence of mineral surfaces on gas sorption (Gasparik et al. 2012; Ji et al. 2012; Lu et al. 1995; Ross & Bustin 2009; and additional references given by Klewiah et al. 2020). For example, gas partitioning between bulk water and clay interlayer micropores (e.g., in the case of smectites) was reported to be an important process, which may be responsible for retarding gas migration (Gadikota et al. 2017). Gaseous molecules were found to have a higher affinity for interlayer water than for bulk water, which was attributed to a higher hydrophobic solvation of HCs (e.g., CH_4) and other gases (e.g., CO_2, H_2, noble gases) in the clay interlayer. In swelling clays, small HC molecules can be incorporated into the clay interlayer in addition to water molecules (Rao & Leng 2014). In this study, molecular dynamic simulations were carried out showing that CH_4 intercalation is strongly influenced by the relative humidity (RH) and the total gas pressure of the clay system. Atomic density profiles of water, ions, and gases indicate that different gases have different relative affinities for interlayer water compared to bulk water, supporting the idea that dissolved gases do not behave as inert tracers in water-saturated porous media (Gadikota et al. 2017). Thus, there is evidence from several studies that the high internal surface (or micropore volume) of clays may provide additional gas sorption capacity, particularly also for CH_4 sorption. CH_4 adsorption on mineral surfaces in the absence of water has been attributed to physisorption due to weak van der Waals and electrostatic interaction forces between adsorbate and adsorbent (Klewiah et al. 2020). The extent of CH_4 adsorption has been reported to follow the order: montmorillonite >

illite/smectite mixed layers > kaolinite > chlorite > illite (Ji et al. 2012). Note that this order was determined from sorption measurements on dry materials. The results show that the type of clay mineral has a major influence on the gas sorption capacity of shales.

Fan et al. (2018) investigated the effect of water on CH_4 sorption by clays. The authors report a three-stage sorption process with increasing moisture content: i) a linear decrease in sorption at a water content < 1%, ii) an almost constant sorption in the water content range from ~ 1 to ~ 4%, and iii) a convex decreasing sorption curve above a water content of ~ 4% (max. 10%). Two threshold moisture contents were observed at ~ 1% and ~ 4%, respectively. At ~ 1% it corresponds to the coverage of the entire hydrophilic surface of clay by a monolayer of water, while at ~ 4%, another process controls the reduction of the adsorption capacity with increasing moisture content. At a water content < 1%, a steady reduction in CH_4 sorption was observed due to competition between water and CH_4 for adsorption sites on the surface of the clay pores. The third stage with the convex sorption behaviour indicates water condensation in the pores of OM, which further reduces CH_4 adsorption by water blocking.

Li et al. (2016) developed a unified model to describe gas (i.e., CH_4)-water-clay interaction by considering separate gas-solid and gas-liquid sorption processes. The retention of CH_4 by clays in the presence of a water film was modelled by the following processes: a) CH_4 adsorption on dry clay was described in terms of a gas–solid interface Langmuir-adsorption equation; b) CH_4 adsorption on the water film was described in terms of a gas-liquid interface Gibbs-adsorption equation; c) gas-liquid-solid interaction was described by an equation integrating "gas-solid" and "gas-liquid" interactions. The study by Li and co-workers shows that the water film thickness in shale clay pores mainly depends on RH and pore size. The water present under the given humidity conditions was found to be distributed in pores of different sizes, mainly as capillary water in pores < 6 nm. A water film formed in larger pores. Thus, the authors concluded that moisture affects the CH_4 adsorption capacity due to the water distribution characteristics: i) pores < 6 nm are blocked by water and are, therefore, not accessible for CH_4 adsorption; ii) in large pores with a water film, CH_4 adsorption corresponds to a gas-liquid interaction rather than a gas-solid interaction.

The above studies suggest that moisture content plays an important role in CH_4 sorption by the clay and OM constituents of shale, as moisture was found to greatly reduce the gas sorption capacity of coals and shales (see Klewiah et al. 2020; Gasparik et al. 2014; Merkel et al. 2015 and references therein). For example, Gasparik et al. (2014) report that the sorption capacity in moisture-equilibrated samples (at 97% RH) was reduced by 40 to 60% compared to dry samples, However, no difference was observed between 97% and 75% RH, indicating that the effect of moisture on gas sorption is only effective up to a certain critical moisture content. The latter threshold value represents the maximum moisture saturation of the shale surfaces and thus the threshold for condensation in the pores. Similar observations were reported by Merkel et al. (2015).

The mechanism leading to a reduction of the gas sorption capacity in shales due to moisture is not yet fully understood, particularly regarding the assumption that OM is the main absorbent of gas. It appears that the reduction in the connectivity of the micropores by the formation of water layers on the sorbents (blocking of micropore space by water) accounts for the observed effect of moisture on gas adsorption. It is generally assumed that the pores in OM (or kerogen pores) are water-free due to their hydrophobic nature (Klewiah et al. 2020). However, it should be noted that in the case of OM, water was reported to strongly interact with organic functional groups via hydrogen bonding (Dubinin 1980). Recent molecular dynamic simulations further show that water clusters can adsorb on functional groups in organic pores (Hu et al. 2015). The hydrophilic nature of the oxidic surface sites favours the adsorption of water molecules on mineral surfaces and thus competes with gaseous molecules for sorption sites. Therefore, the influence of moisture on the gas sorption capacity on mineral surfaces may be stronger than with OM.

The importance of clays for gas sorption in shales has been investigated in several studies. For example, the contribution of clays to gas sorption was found to increase with decreasing TOC of the shale formations (Klewiah et al. 2020 and references therein). It should be noted that the corresponding weight contents (wt.%) of the two constituents in shales range from ~ 1 to 15 wt.% for OM and from ~ 1 to 60 wt.% for clay (Gasparik et al. 2014). Furthermore, the sorption energies (isosteric heats) of CH_4 were reported to be greater for OM (kerogen) than clay minerals, indicating a significantly stronger affinity of CH_4 for OM than clays (Ji et al. 2012; Lu et al. 1995; Zhang et al. 2012). In organic-rich shales, Gasparik et al. (2014) observed that the TOC-normalised sorption capacity for CH_4 does not correlate with the clay content, indicating a negligible influence of clay minerals on CH_4 sorption. Merkel et al. (2015) observed a reduction in CH_4 sorption in shale by moisture, which was attributed to a loss of the sorption capacity on illite. The authors concluded that the contribution of clay minerals to CH_4 sorption is negligible at high water saturation. Thus, there is evidence to suggest that the retardation of gases in shales is primarily determined by the interaction with OM. This would allow gas-solid interaction, especially in the case of HCs, to be quantified in terms of an n-octanol/water partition coefficient (K_{ow}), i.e., OM-water interaction. The K_{ow} is defined as the ratio of the concentration of a substance in n-octanol and water at equilibrium at a specified temperature and thus is a measure of the relationship between the lipophilic and hydrophilic nature of a substance. The K_{ow} has been used to model diffusion-retention of natural gas (CH_4, C_2H_6, C_3H_8) in OPA (Vinsot et al. 2017).

To the authors' knowledge, there is no information on the sorption of CH_4 and other HCs on concrete and cement under unsaturated and saturated conditions.

6.4 Assignment of sorption values for ^{14}C (organic, inorganic, gaseous) to the near and far-fields of the deep geological repository

6.4.1 Dissolved inorganic and organic ^{14}C

Aliphatic carboxylates are considered to be the main carriers of organic ^{14}C. These carbon compounds are released in the IRF from activated metals and SF and are thus likely to be released from spent IERs, filter cartridges and contaminated materials. Inorganic ^{14}C, as $H^{14}CO_3^{2-}$ or $^{14}CO_3^{2-}$, is instantaneously released from contaminated wastes. It is also likely to be released from activated metals (IRF), activated concrete and vitrified reprocessing waste.

6.4.1.1 Sorption onto clay minerals

In the case of organic ^{14}C, the R_d value is assumed to be zero for both bentonite and OPA as a best estimate and lower limit (Tab. 6.1). The upper limit is set based on the study of Chen et al. (2018b).

Tab. 6-1: Sorption values (Rd in m^3/kg) for the various chemical forms of ^{14}C in the repository environment under fully saturated conditions

Best estimate with upper and lower bounds given in brackets (lower/upper).

	Organic ^{14}C	**inorganic ^{14}C**	**gaseous ^{14}C***
L/ILW near-field**	0 (0/10^{-3})	1.60 (1.00 – 2.24)	0
HLW near-field***	0 (0/10^{-3})	7.35×10^{-5} $(0.54/27.6)\times10^{-5}$	0
OPA host rock****	0 (0/10^{-3})		2×10^{-5} $(0 – 2\times10^{-5})$
NL/ZNO siting regions*****		1.41×10^{-3} $(0.19/10.7)\times10^{-3}$	
JO siting region*****		9.17×10^{-4} $(1.58/67.8)\times10^{-4}$	

* Saturated conditions: Van Loon & Chen (2021), Vinsot et al. (2017). Zero sorption is anticipated under fully saturated conditions on bentonite and cementitious materials (see text).
** Sorption of organic and inorganic ^{14}C on HCP from Tits & Wieland (2023).
*** Sorption of organic and inorganic ^{14}C on bentonite from Baeyens et al. (2014).
**** Sorption of organic and inorganic ^{14}C on OPA from Chen et al. (2018b).
***** NL: Nördlich Lägern siting region, ZNO: Zürich Nordost siting region, JO: Jura Ost siting region.

Inorganic ^{14}C, however, is retained in the bentonite and OPA. The retardation is assumed to be due to isotopic dilution with the surface layers of the calcite present in the bentonite and OPA (Baeyens et al. 2014). Thus, isotope exchange on the calcite surface is considered to be the main sorption mechanism for inorganic carbon ($H^{14}CO_3^-/^{14}CO_3^{2-}$). The sorption values for inorganic carbon on bentonite and OPA were calculated according to Baeyens et al. (2014). Baeyens et al. (2014) assumed that ~ 0.3% of the total amount of calcite is subject to isotopic exchange. The sorption values for $H^{14}CO_3^-/^{14}CO_3^{2-}$ in the different groundwaters were obtained based on the respective aqueous concentrations of the porewaters and the calcite contents in the argillaceous rocks (Nagra 2024g, in prep.). The relevant parameters are reported for bentonite (Tab. 6-2) and OPA from the three potential siting regions (Tabs. 6-3 and 6-4). Reference values and upper and lower limits of the sorption values for inorganic ^{14}C sorbed to bentonite and OPA were selected from the data matrices listed in Tab. 6-1 and presented in Tab. 6-2 through Tab. 6-4.

The very weak retention in the bentonite does not significantly retard the transport of inorganic ^{14}C through the bentonite. However, the stronger retardation in the OPA due to the higher calcite content of the formation, ensures its almost complete decay during transport through the host rock.

Tab. 6-2: Bentonite: calcite contents, aqueous carbonate concentrations and calculated inorganic ^{14}C sorption values for bentonite in-situ porewaters

	Bentonite in-situ porewater types		
	Reference	High pCO_2	Low pCO_2
Isotopic exchangeable carbonate	2.7×10^{-2} mol/kg		
$H^{14}CO_3^-/^{14}CO_3^{2-}$ [mol/kg_{H2O}]	2.94×10^{-3}	4.99×10^{-3}	1.37×10^{-3}
R_d for 100% calcite [m^3/kg]	9.18×10^{-3}	5.41×10^{-3}	1.97×10^{-2}
Calcite content [wt.%]	R_d value [m^3/kg]		
0.1	9.18×10^{-6}	5.41×10^{-6}	1.97×10^{-5}
0.8	7.35×10^{-5}	4.33×10^{-5}	1.58×10^{-4}
1.4	1.29×10^{-4}	7.58×10^{-5}	2.76×10^{-4}

Tab. 6-3: OPA: calcite contents, aqueous carbonate concentrations and calculated inorganic ^{14}C sorption values for porewater types from the Nördlich Lägern (NL) and Zürich Nordost (ZNO) siting regions

	OPA porewater types NL/ZNO			
	Reference	High pCO_2	Low pCO_2	High salinity
Isotopic exchangeable carbonate	2.7×10^{-2} mol/kg			
$H^{14}CO_3^-/^{14}CO_3^{2-}$ [mol/kg_{H2O}]	2.11×10^{-3}	3.52×10^{-3}	1.01×10^{-3}	4.46×10^{-3}
R_d for 100 % calcite [m^3/kg]	1.28×10^{-2}	7.67×10^{-3}	2.67×10^{-2}	6.05×10^{-3}
Calcite content [wt.%]	R_d value [m^3/kg]			
11	1.41×10^{-3}	8.44×10^{-4}	2.93×10^{-3}	6.66×10^{-4}
3.1	3.97×10^{-4}	2.38×10^{-4}	8.29×10^{-4}	1.88×10^{-4}
40.2	5.14×10^{-3}	3.08×10^{-3}	1.07×10^{-2}	2.43×10^{-3}

Tab. 6-4: OPA: calcite contents, aqueous carbonate concentrations and calculated inorganic ^{14}C sorption values for porewater types from the Jura Ost (JO) siting region

	OPA porewater types JO			
	Reference	High pCO_2	Low pCO_2	High salinity
Isotopic exchangeable carbonate	2.7×10^{-2} mol/kg			
$H^{14}CO_3^-/^{14}CO_3^{2-}$ [mol/kg_{H2O}]	3.24×10^{-3}	5.24×10^{-3}	1.60×10^{-3}	5.31×10^{-3}
R_d for 100 % calcite [m^3/kg]	8.33×10^{-3}	5.15×10^{-3}	1.69×10^{-2}	5.08×10^{-3}
Calcite content [wt.%]	R_d value [m^3/kg]			
11	9.17×10^{-4}	5.67×10^{-4}	1.86×10^{-3}	5.59×10^{-4}
3.1	2.58×10^{-4}	1.60×10^{-4}	5.23×10^{-4}	1.58×10^{-4}
40.2	3.35×10^{-3}	2.07×10^{-3}	6.78×10^{-3}	2.04×10^{-3}

6.4.1.2 Sorption onto cementitious materials

It is currently uncertain whether carboxylates are the only oxygenated carbon compounds released during the corrosion of activated metals. Note that Guillemot et al. (2021b, 2022) could only assign ~ 50% of the $TO^{14}C$ to ^{14}C-bearing carboxylates (Section 5.1.3). It is conceivable that ^{14}C-bearing alcohols or aldehydes contribute to the remaining ~ 50% $TO^{14}C$ fraction, which has not yet been characterised at the species level. In addition, current modelling of the porewater of the cementitious near-field indicates a high Cl^- content, which could enhance sorption competition with the organics due to the non-specific interaction of the organic molecules (e.g., by hydrogen bonding, van der Waals forces) with the oxidic surface sites of cement phases (Tits & Wieland 2023). Thus, a cautious approach is taken by assigning a reference $R_d = 0$ m^3/kg for the retention of ^{14}C-bearing carbon compounds in the cementitious near-field, while the upper bound has been assigned based on the study of Wieland et al. (2016) (Tab. 6-1).

The sorption values for inorganic ^{14}C in the near- and far-fields were estimated based on the assumption that isotopic exchange between $^{14}CO_3^{2-}$ and CO_3^{2-} on calcite is the predominant retention mechanism (Section 6.2; Wieland 2014, Tits & Wieland 2023). Strong sorption of $^{14}CO_3^{2-}$ is expected in the cementitious near-field as a result of the relatively large amount of calcite in HCP and the low CO_3^{2-} concentration in cement porewater (Tits & Wieland 2023).

6.4.2 Gaseous ^{14}C

6.4.2.1 Sorption onto clay minerals

Jacops and co-workers studied the diffusion of dissolved gas molecules of different sizes (He, Ne, Ar, CH_4, Xe and C_2H_6) in fully saturated clay materials (e.g., Boom Clay, OPA, bentonite, Callovo-Oxfordian-Clay) (Jacops et al. 2013, 2017a,b). The authors report a variation in the effective diffusion coefficient with the size of the diffusing molecules for non-reactive gases, while they assumed no sorption or retardation of the gaseous molecules (e.g., CH_4, C_2H_6). Note that measurements of the diffusion of CH_4 and C_2H_6 in OPA failed (Jacops et al. 2017b).

Vinsot et al. (2017) determined the retention properties of CH_4, C_2H_6 and C_3H_8 by OPA in gas circulation experiments carried out at the Mont Terri Rock Laboratory. Modelling of the diffusional transport of the gases through OPA allowed the following sorption values to be derived: $CH_4 = 2\times10^{-5}$ m^3/kg, $C_2H_6 = 2.8\times10^{-4}$ m^3/kg, $C_3H_8 = 8.8\times10^{-4}$ m^3/kg. These values were found to correlate linearly with the n-octanol-water partition coefficient (K_{ow}) of the alkanes. This finding suggests that the organic matter present in the OPA controls the adsorption of the alkanes. Van Loon & Chen (2021) recently determined $R_d = 2\times10^{-5}$ m^3/kg for CH_4 sorption on OPA under fully saturated conditions, assuming that CH_4 sorption is controlled by interaction with OM of the OPA (1 wt.% OM content) and that the distribution ratio between CH_4 sorbed by OM and dissolved in solution can be quantified in terms of the octanol-water partitioning. This value is set as an upper bound for the sorption of gaseous ^{14}C-bearing species (Tab. 6-1). It should be noted that the assumed carbon content agrees quite well with the previously reported carbon content of 0.6 and 0.8 wt.% for different OPA samples (Mazurek et al. 2008).

Organic carbon contents ranging from 0.2 to 0.4 wt.% have been determined for bentonite (Karnland et al. 2006; Kumpulainen & Kiviranta 2010; Müller-Vonmoos & Kahr 1983). Information on the chemical form of either the organic carbon or the organic matter present in bentonite is limited (Jenni et al. 2019). Due to the low content of organic matter in bentonite and the limited information on its chemical nature, no sorption of gaseous ^{14}C is assumed in bentonite (Tab. 6-1).

6.4.2.2 Sorption onto cementitious materials

The content of natural organic matter in cements is negligible due to the very high temperature reached during clinker production (up to 1,450 °C). Small organic molecules are usually added as grinding aids; these include glycols (e.g., ethylene glycol), alkanolamines (e.g., triethanolamine) and phenol-type compounds. However, these organic compounds are not expected to act as sorbents for gaseous HCs. Therefore, the retention properties of the HCs cannot be assessed on the basis of the n-octanol-water partitioning, in contrast to retention by clay rocks. In addition, retention by the hydrated cement phases is considered negligible. It is therefore assumed that no sorption of gaseous ^{14}C on cementitious materials takes place (Tab. 6-1).

6.5 Summary of chapter

^{14}C will be present in the near-field and host rock of a deep geological repository in inorganic form (carbonate), organic form (small C1-C5 molecules such as aliphatic carboxylates, alcohols, aldehydes) and in gaseous form (HCs, mainly CH_4).

For the base case, the retention of the organic form is considered negligible on bentonite (HLW near-field; $R_d = 0$ m^3/kg), cementitious materials (L/ILW near-field; $R_d = 0$ m^3/kg) and the OPA host rock ($R_d = 0$ m^3/kg) due to the weak interaction between the molecules and the oxidic surfaces sites on the clay minerals and cement phases through electrostatic attraction, hydrogen bonding,

or van der Waals forces. In addition, the high Cl^- concentrations of the porewaters may strongly reduce the uptake of small organic molecules by these materials due to sorption competition.

The retention of inorganic ^{14}C occurs primarily by precipitation of calcite in the near-field. Sorption of inorganic ^{14}C is considered in terms of an isotopic exchange process between $^{14}CO_3^{2-}$ and CO_3^{2-} on calcite. The sorption values depend on the calcite content of the near-field backfill or the host rock, respectively, and the CO_3^{2-} concentration of the corresponding equilibrium porewaters. Therefore, reference sorption values vary from weak ($R_d = 7.35\times10^{-5}$ m^3/kg for bentonite) to moderate ($R_d = 1.41\times10^{-3}$ m^3/kg and 9.17×10^{-4} m^3/kg for OPA) to strong ($R_d = 1.5$ m^3/kg for cement-type backfill).

No or very weak retention also applies to the gaseous species. Sorption onto bentonite, OPA and cementitious materials is assumed to be negligible for the reference case ($R_d = 0$ m^3/kg). For the upper bound, very weak retention is attributed to CH_4 sorption on OPA under fully saturated conditions ($R_d = 2\times10^{-5}$ m^3/kg), assuming that the sorption process is due to interaction with organic matter of the OPA.

7 Fate of ^{14}C in a deep geological repository

The following summary focuses on the most important processes that influence the fate of ^{14}C-carrying carbon compounds in the near-field over the period under consideration for the combined deep geological repository with HLW/SF and L/ILW. It draws on the more detailed descriptions of the geochemical evolution of the near-field briefly given in Section 2.3 and fully in Curti et al. (2023), Kosakowski et al. (2023) and Nagra (2024i, in prep.). The evolution of the near-field is driven by the interaction of the various components of the EBS with one another, with the waste and with the host rock over time. These interactions alter the mineralogy, porosity and physico-chemical characteristics of the involved barrier materials. The presence of water (i.e., in the waste matrix and after saturation of the near-field) plays a key role.

7.1 Speciation and release of ^{14}C compounds in the L/ILW near-field

Design and layout were briefly discussed in Section 2.3.1 and in detail in Nagra (2021b). The L/ILW waste forms are embedded in a cementitious matrix or, in a few cases, in bitumen, polystyrene or a borosilicate glass matrix (Nagra 2023). They are characterised by low radio-toxicity compared to HLW/SF, however, the total volume of L/ILW is significantly larger than that of HLW/SF. The variability and heterogeneity in the physicochemical properties of L/ILW are also significantly greater than in the case of HLW/SF (Kosakowski et al. 2023; Curti et al. 2023). L/ILW contains various waste materials with very different reactivities, such as organics, as well as metals.

The development of the chemical conditions in the deep geological repository for L/ILW is determined by the degradation of the waste materials (organics, metals) and the aggregates used to fabricate the cementitious materials, as well as the interaction of the degradation products with the cement paste (Section 2.3.1). The degradation reactions, which include the abiotic/biotic degradation of organic substances, the corrosion of metals and the dissolution of aggregates, only take place if sufficient water is available in the near-field as an aqueous phase or in the form of moisture (Kosakowski et al. 2014, 2023). The sources and processes of gas generation in the HLW and L/ILW repositories are comparable in most respects (Nagra 2024e, in prep.). Gas production by metal corrosion and, in the case of the L/ILW repository, the degradation of organic substances will significantly hinder resaturation of the near-field and therefore delay its geochemical evolution. In the current safety scenarios, no period of complete containment for L/ILW is assumed (Nagra 2024h, in prep.). After repository closure, the internal components of the L/ILW drums are exposed to porewater entrapped in the saturated near-field. From then on, several processes will control ^{14}C release with time.

The ^{14}C inventory and its chemical forms in the metallic and non-metallic L/ILW were discussed in detail in Sections 2.3, 3.1. and 3.2. A brief summary of the relevant information is presented in Tab. 7-1, Tab. 7-2 and Fig. 7-1. In the case of stainless steel, the relevant parameters, such as the instantaneously and slowly released ^{14}C fraction and the chemical forms of ^{14}C released, are assigned on the basis of the results from the corrosion experiments with activated stainless steel (Tab. 5-3). It should be noted that for the Zircaloy inventories and their associated proportions of ^{14}C accommodated by the oxide layer, the values are estimated based on similarity with ^{14}C release from activated stainless steel.

In contact with water, ^{14}C in water-soluble form is expected to be immediately released from the oxide (or corrosion) layers of activated Zircaloy and steel. To some extent, this may already arise during the packaging of the waste material. From activated steel, an IRF of 0.01% of the total ^{14}C inventory is assumed based on experimental data (Section 5.1.5), while in the case of activated Zircaloy, the same IRF is set for consistency. There is evidence to suggest that most of the ^{14}C IRF is in dissolved form as organic or inorganic ^{14}C, while the proportion of gaseous carbon

compounds released instantaneously is considered comparatively small. A simplifying assumption is made that the ^{14}C IRF from activated metals consists of 50% organic and 50% inorganic aqueous carbon. In the long term, however, ^{14}C is mainly released in gaseous form in accordance with the corrosion rate of the respective metal (Tab. 7-1; Tab. 7-2).

From spent IERs, filter cartridges and contaminated (unspecified) MIR waste, it is assumed that the entire inventory of ^{14}C is instantaneously released it is adsorbed on the surface of these materials. Based on few experimental data, the proportions of organic and inorganic ^{14}C instantaneously released from spent IERs was defined to be predominantly in the form of dissolved inorganic (BWR: 90%; PWR: 70%) and only a small portion is in the dissolved organic form (BWR: 10%; PWR: 30%) (Tab. 7-1; Tab. 7-2). However, the proportions of organic and inorganic ^{14}C in filter cartridges and contaminated MIR wastes are only estimates. Equal proportions of 50% dissolved organic ^{14}C and 50% dissolved inorganic ^{14}C instantaneously released are assumed (Tab. 7-1; Tab. 7-2), with the organic form consisting of ^{14}C-bearing small organic molecules that may further degrade, producing equal amounts of $^{14}CH_4$ and $^{14}CO_2$ (see Section 5.4).

The chemical form of ^{14}C released from $BaCO_3$ in reprocessing waste and MIR waste is assumed to be purely inorganic as $^{14}CO_3^{2-}$ (Tab. 7-1; Tab. 7-2). This further applies to the speciation of ^{14}C in activated concrete. As $^{14}CO_3^{2-}$ is strongly retained by both materials, especially in $BaCO_3$ due to its low solubility, no significant release of ^{14}C is expected from either material (Tab. 7-1; Tab. 7-2).

In activated graphite, most of the ^{14}C present in activated graphite is expected to be retained in the bulk material (RWM 2016; Toulhoat et al. 2018). A very small fraction of ^{14}C is released instantaneously in solution, in equal proportions of organic and inorganic ^{14}C (Tab. 7-1; Tab. 7-2). The residual majority of the ^{14}C will be released very slowly, predominantly in the dissolved inorganic form (99%), with only small amounts of gaseous species (1%) released.

Tab. 7-1: Characteristics of L/ILW waste forms

Chemical form of waste	**^{14}C-containing materials**	**^{14}C chemical form (carbon species)**
Metallic	Zircaloy	Bulk: elemental $^{14}C(0)$ and carbide ($^{14}C^{4-}$)
		Oxide: organic ("CH_2O") and inorganic (CO_3^{2-})
	Stainless steel	Bulk: elemental $^{14}C(0)$ and carbide ($^{14}C^{4-}$)
		Oxide: organic ("CH_2O") and inorganic (CO_3^{2-})
	Carbon steel	Bulk: elemental $^{14}C(0)$ and carbide ($^{14}C^{4-}$)
		Oxide: organic ("CH_2O") and inorganic (CO_3^{2-})
Organic	Spent IERs Filter cartridges	BWR: inorganic (CO_3^{2-}) and organic ("CH_2O") PWR: inorganic (CO_3^{2-}) and organic ("CH_2O")
Organic / Inorganic / metallic	Contaminated MIR waste*	Inorganic (CO_3^{2-}) and organic ("CH_2O")
Inorganic	$Ba^{14}CO_3$ $BaCO_3$ crud Activated concrete	Inorganic (CO_3^{2-})
Inorganic	Graphite	Inorganic (CO_3^{2-}) and organic ("CH_2O")

Assessment based on experimental studies (metallic waste forms) and expert judgement (non-metallic waste forms).

* Estimated contributions based on Nagra (2023).

Tab. 7-2: Assessment of ^{14}C release from L/ILW

Waste form	Inventory (^{14}C-I)	Release rate	^{14}C form* (corrosion products)
Zircaloy	0.0001 × ^{14}C-$I_{Zircaloy}$	Instant release	50% organic ("CH_2O") 50% inorganic (CO_3^{2-})
	0.9999 × ^{14}C-$I_{Zircaloy}$	Congruent release with corrosion**	100% gaseous (CH_4)
Stainless steel	0.0001 × ^{14}C-I_{St}	Instant release	50% organic ("CH_2O") 50% inorganic (CO_3^{2-})
	0.9999 × ^{14}C-I_{St}	Congruent release with corrosion**	100% gaseous (CH_4)
Carbon steel	0.0001 × ^{14}C-I_{Cs}	Instant release	50% organic ("CH_2O") 50% inorganic (CO_3^{2-})
	0.9999 × ^{14}C-I_{Cs}	Congruent release with corrosion**	100% gaseous (CH_4)
Spent IERs Filter cartridges	n.a.	Instant release	90% inorganic (CO_3^{2-}) 10% organic ("CH_2O")
Contaminated waste	n.a.	Instant release	50% inorganic (CO_3^{2-}) 50% organic ("CH_2O")
$Ba^{14}CO_3$ and $BaCO_3$ crud Activated concrete	n.a.	No release	100% inorganic (CO_3^{2-})
Graphite***	~ 0.95× ^{14}C-I_G	No release	
	0.0002× ^{14}C-I_G	Instant release	50% inorganic (CO_3^{2-}) 50% organic ("CH_2O")
	0.05× ^{14}C-I_G	Congruent release with matrix dissolution**	99% inorganic (CO_3^{2-}) 1% gaseous (CH_4, CO)

* The chemical forms can tentatively be represented by the following carbon species: inorganic: HCO_3^-/CO_3^{2-}, organic: "CH_2O", gaseous: CH_4. "CH_2O" corresponds to an average composition of organic matter and is considered here as a surrogate for organic molecules if no detailed information on the species formed is available. Sorption values for the retention of the different chemical forms by cementitious materials are listed in Tab. 6-1.

** Corrosion rates are reported by Diomidis et al. (2023). Rates of matrix dissolution are given in Nagra (2024f).

*** Parameters taken from Toulhoat et al. (2018).

n.a.: not applicable.

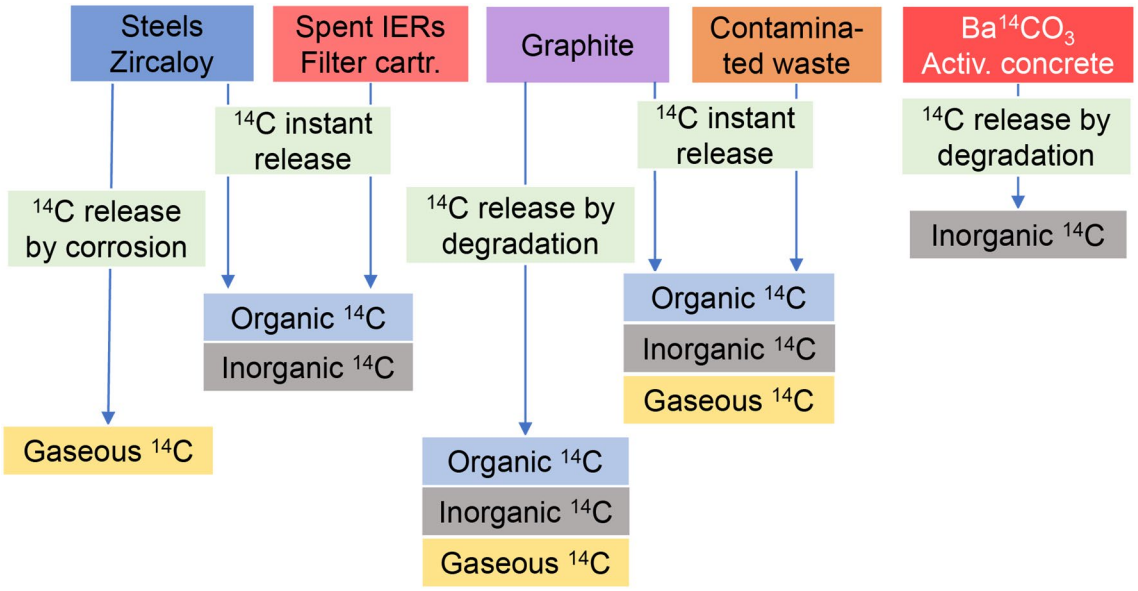

Fig. 7-1: Overview of the chemical forms of ^{14}C released from L/ILW

7.2 Fate of ^{14}C-compounds in the L/ILW near-field

^{14}C-bearing organic carbon compounds

^{14}C in the organic form (small molecules with < 5 carbon atoms) is expected to disperse through the water pathway. The retention of organic ^{14}C is very weak in the cementitious near-field. There is no evidence that abiotic degradation of water-soluble small ^{14}C-bearing molecules, excluding HCOOH, occurs over time. This is due to the lack of a catalytic effect that allows C-C bond cleavage under repository-relevant conditions (Guillemot et al. 2023). In contrast, the conversion of ^{14}C-formate (organic) to $^{14}CO_3^{2-}$ (inorganic) is possible, which probably affects only a small part of the organic ^{14}C inventory. Microbial degradation of the small organic molecules is limited in cementitious environments with pH > 11, unless niches in the near-field provide more favourable living conditions (i.e., sufficient space, availability of water and pH < 11). They may exist locally in some waste containers and possibly in the backfilled operational tunnels and the excavation-damaged zone (Guillemot et al. 2023). Under these conditions, organic materials can be degraded by microorganisms to produce CO_2 and CH_4. It is considered unlikely that microbial activity will significantly influence the generation rate of ^{14}C-bearing gases in a cement-based near-field (NDA 2016).

^{14}C-bearing carbonate

Inorganic ^{14}C ($^{14}CO_3^{2-}$ or $H^{14}CO_3^-$) is strongly retained in the cementitious near-field of a deep geological repository for L/ILW by interaction with cementitious materials and calcite (Tab. 6-1; Section 6.2). Therefore, ^{14}C in the inorganic form will decay with time and not contribute to dose release. Remobilisation of inorganic ^{14}C by autotrophic microorganisms, leading to the formation of $^{14}CH_4$, is considered unlikely due to the low solubility of carbonates at high pH and the expected limited microbial activity under L/ILW repository conditions, except in niches with favourable living conditions (in terms of pH, space and water).

^{14}C-bearing gaseous carbon compounds

Production, consumption and transport of gaseous compounds in a deep geological repository for L/ILW have been discussed in detail elsewhere (Nagra 2024e, in prep.). Gaseous ^{14}C, mainly as $^{14}CH_4$, is subject to the same coupled processes that control the behaviour of bulk gas in the L/ILW near-field and host rock. As with organic ^{14}C, the microbial utilisation of gaseous ^{14}C-bearing carbon compounds can only take place in microbially favourable, local environments where there is sufficient space and water with pH < 11. As with the water-soluble oxygenated carbon compounds, microbial activity is unlikely to contribute to the production of ^{14}C-bearing gases (NDA 2016). The retention of gaseous ^{14}C species, mainly $^{14}CH_4$, due to sorption processes in the cementitious near-field is considered negligible (Tab. 6-1).

7.3 Speciation and release of ^{14}C-compounds in the HLW near-field

The HLW repository will contain two main waste forms, namely SF (activated fuel rods filled with UO_2/MOX pellets) and vitrified HLW from reprocessing of SF (Nagra 2023). The ^{14}C-speciation and release rate from these waste forms are listed in Tab. 7-3 and Tab. 7-4, respectively, and illustrated in Fig. 7-2.

The overall geochemical evolution of the HLW near-field is described in detail in Section 2.3.2. In this sub-section, only the specific aspects related to the fate of ^{14}C are addressed. In the current concept, the HLW/SF canisters are expected to maintain their integrity for at least 10,000 years (Nagra 2024d, in prep.). Therefore, it can be assumed that the release of ^{14}C from the waste forms (HLW, SF) starts at the earliest after the first 10,000 years of storage, i.e., after about two half-lives of ^{14}C ($t_{1/2}$ of ^{14}C = 5,700 years).

Canister breaching will expose the waste forms, Zircaloy and the internal components of the canister to porewater. From then on, several processes will control ^{14}C release. The radionuclide release model considers two processes with different release rates for ^{14}C (and other activation products) (Johnson 2014; Johnson et al. 2023): a) rapid release from Zircaloy and other metal parts of the fuel assemblies, as well as from the SF; b) slow release resulting from the uniform corrosion of Zircaloy and steels, as well as from the dissolution of the SF (Tab. 7-4).

The IRF is composed of the following fractions: a) ^{14}C in the Zircaloy oxide film and the oxide layers of metal parts of the fuel assemblies; b) ^{14}C released from the gap at the fuel-cladding interface and from U(Pu)O_2 grain boundaries (Johnson 2014; Johnson et al. 2023). Only very limited experimental information about the release behaviour is available (Curti 2021b; Johnson 2014). CANDU fuel data reported by Stroes-Gascoyne et al. (1994) form the basis for the estimated IRF of ^{14}C used for safety assessments (Johnson 2014; Johnson et al. 2004, 2005; Johnson et al. 2023). The measured ^{14}C inventories in leaching tests were found to be lower than the estimated ^{14}C inventories by a factor of 11.5 ± 3.9, indicating that activation calculations overestimate ^{14}C inventories, probably due to overly conservative estimates of the N content. Measured IRFs for ^{14}C ranged from 0.06 to 5.04% of the total ^{14}C inventories (average of 2.7 ± 1.6%). In leaching tests on other LWR SF reported by Wilson & Shaw (1987) and Wilson (1990a,b), IRF values ranging between 0.05 and 3.5% of the estimated ^{14}C inventories were reported. Based on these studies, an average IRF of 3% for ^{14}C has been defined (Johnson et al. 2023) and is applied to all components of SF, i.e., the UO_2 matrix, Zircaloy cladding and metallic (steel alloy) parts of the fuel assemblies (Tab. 7-4).

The chemical form of the instantaneously released ^{14}C from SF is still uncertain. Based on available experimental evidence, it is assumed that most of the ^{14}C released immediately from SF (UO_2 matrix, Zircaloy cladding, steel parts) is accommodated in the respective oxide layers, both in the organic and inorganic chemical forms of carbon (Sections 5.1.4, 5.2.3 and 5.3.3). The release of gaseous ^{14}C-bearing carbon compounds is likely to be very low at this stage. The release of organic and inorganic ^{14}C species in solution requires direct contact of the surfaces of the SF

components with water. A cautious approach is taken by assuming the presence of both chemical forms, i.e., 50% organic and 50% inorganic, although thermodynamic calculations suggest that the concentration of organic carbon compounds (e.g., aliphatic carboxylates) could be significantly lower than that of carbonate (Section 4.1.2). Furthermore, equal distribution of the chemical forms of ^{14}C can be assumed (50% organic, 50% inorganic) for the IRF (Tab. 7-3; Tab. 7-4).

The remaining ^{14}C inventory of the SF and the assembly parts (Zircaloy, steel) will be slowly released over time by the dissolution of SF and uniform metal corrosion (Tab. 7-4). ^{14}C is expected to be released in gaseous form, congruently with metal corrosion or SF dissolution, respectively. The dissolution of SF and metal corrosion will take place under anoxic, strongly reducing conditions, even if radiolysis occurs at the metal-water interfaces, as the presence of H_2 neutralises radiolytic oxidants (Section 5.2.4). Very low UO_2 (and PuO_2) solubility under reducing conditions will lead to slow SF dissolution (Bradbury et al. 2014; Johnson et al. 2023). Hence, very slow congruent release of ^{14}C would occur from the fuel pellets via this process (Section 5.3.2). One may speculate that gaseous ^{14}C could be enriched in gas nano-bubbles formed by the accumulation of fission gas and helium from alpha decay. These bubbles tend to migrate (diffuse) to grain boundaries during reactor operation and "outgas" in the gap, thus contributing to the IRF of ^{14}C. However, many nano-bubbles will remain trapped inside the grains, being immobile at low temperatures. A concern was that in the deep geological repository, the internal He pressure caused by alpha decay would lead to the rupture of the bubbles with time, releasing gas to the gap, and increasing the IRFs of volatile nuclides far above the value of 3% recently defined in Johnson et al. (2023). Ferry et al. (2008), however, excluded that the critical pressure needed for the bubble rupture would be achieved. Thus, the rate of ^{14}C release during SF dissolution is expected to be largely dependent on the spatial distribution of the He-nano-bubbles within the grains as observed in present-day fuel pellets. The distribution is probably not uniform due to the tendency of gas to migrate to the periphery.

In the long-term, the ^{14}C release from SF is assumed to be in the gaseous form (i.e., $^{14}CH_4$) and occur in accordance with the dissolution rate of the SF (Johnson et al. 2023) (Tab. 7-3; Tab. 7-4). Note that gaseous ^{14}C is also released as a result of the corrosion of the activated Zircaloy and stainless steel parts of SF (Tab. 7-2; Tab. 7-4). The corrosion rates of these materials under the circumneutral pH conditions of an HLW repository have been reported by Diomidis et al. (2023).

In the case of vitrified HLW, ^{14}C release is assumed to be dissolved inorganic ^{14}C, in accordance with the long-term dissolution rates defined by Curti (2023) (Tab. 7-3; Tab. 7-4).

Tab. 7-3: Characteristics of HLW/SF waste forms

Chemical form of waste	^{14}C-containing materials	^{14}C chemical form (carbon species)
Metallic	SF	UO_2 matrix: elemental ($^{14}C(0)$ and carbide ($^{14}C^{4-}$))
		Fuel oxide layer: organic ("CH_2O") and inorganic (CO_3^{2-})
Metallic	Zircaloy cladding*	Zircaloy bulk: elemental $^{14}C(0)$ and carbide ($^{14}C^{4-}$)
		Zircaloy oxide layer: organic ("CH_2O") and inorganic (CO_3^{2-})
Inorganic	Vitrified HLW**	Inorganic (CO_3^{2-})

* The amount of metallic parts (activated steel) is considered to be small and thus not listed separately. The chemical form is expected to be identical to that of Zircaloy.

** see Mysen & Richet (2019).

Tab. 7-4: Assessment of ^{14}C release from HLW/SF

Waste form	Inventory (^{14}C-I)	Release rate*	^{14}C form** (corrosion products)
SF	$0.03 \times {}^{14}C\text{-}I_{SF}$	IRF	50% organic ("CH_2O") 50% inorganic (CO_3^{2-})
	$0.97 \times {}^{14}C\text{-}I_{SF}$	Congruent release with SF dissolution	100% gaseous (CH_4)
Activated Zircaloy and stainless steel***	$0.0001 \times {}^{14}C\text{-}I_{Zircaloy}$	IRF	50% organic ("CH_2O") 50% inorganic (CO_3^{2-})
	$0.9999 \times {}^{14}C\text{-}I_{Zircaloy}$	Congruent release with corrosion	100% gaseous (CH_4)
Vitrified HLW	$^{14}C\text{-}I_{HLW}$	Congruent release with glass dissolution	100% inorganic (CO_3^{2-})

* See discussions in Sections 5.1.2., 5.2.2 and 5.3.2 and Johnson et al. (2023) for SF dissolution, and Diomidis et al. (2023) for Zircaloy and stainless steel corrosion; for the two reference glasses SON68 (reprocessing by Areva, France) and Magnox waste (MW) (reprocessing by BNFL, UK) see Curti (2023).

** The chemical forms can tentatively be represented by the following carbon species: inorganic: HCO_3^-/CO_3^{2-}, organic: "CH_2O", gaseous: CH_4. "CH_2O" corresponds to an average composition of organic matter and is considered as a surrogate for organic molecules if no detailed information on the species formed is available. Sorption values for the retention of the different chemical forms in the bentonite backfill and OPA host rock are listed in Tab. 6-1.

*** The proportions of the inventories released as IRF and by corrosion are set in agreement with those in L/ILW (Tab. 7-2).

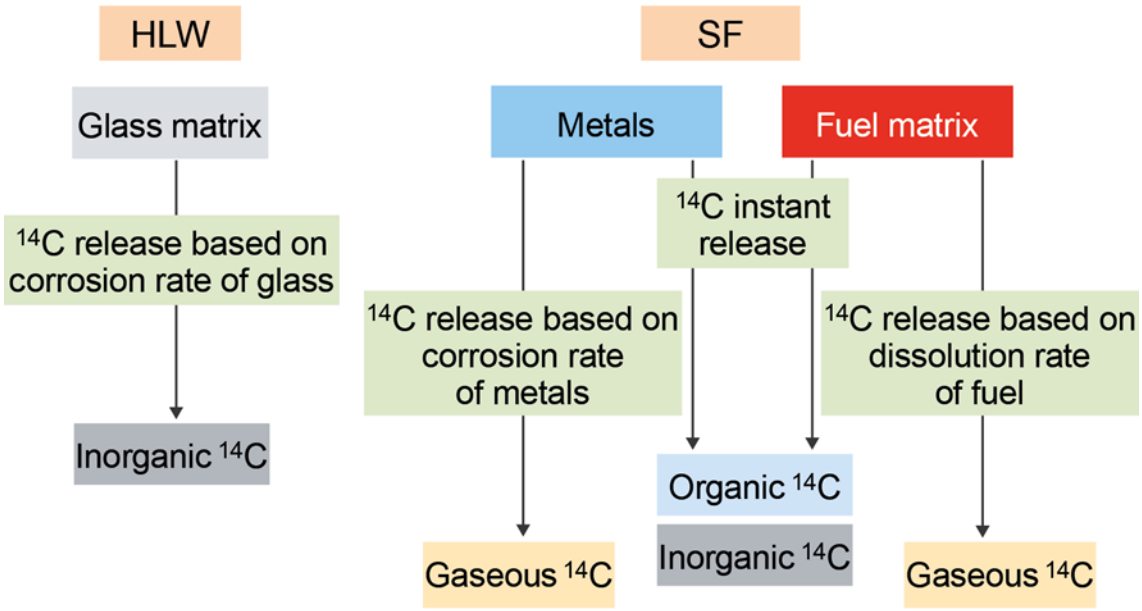

Fig. 7-2: Overview of the chemical forms of ^{14}C released from HLW

7.4 Fate of ^{14}C-compounds in the HLW near-field

^{14}C-bearing organic carbon compounds

Organic ^{14}C is expected to be released in the form of small molecules (with < 5 carbon atoms), which migrate via the water pathway. The retention of organic ^{14}C is very weak in the bentonite backfill. As for alkaline conditions, there is no evidence that abiotic degradation of the small ^{14}C-bearing molecules could occur, the potential exception being ^{14}C-formate, which could convert into $^{14}CO_3^{2-}$ (Guillemot et al. 2023 and reference therein). However, ^{14}C-formate is likely only a small fraction of the organic ^{14}C inventory. Degradation of the small ^{14}C-bearing organic molecules by microbial metabolism can occur where sufficient space and water activity are available.

^{14}C-bearing carbonate

^{14}C-bearing carbonate is released by the dissolution of vitrified HLW. Inorganic ^{14}C is expected to contribute to both the ^{14}C IRF of fuel pellets and activated metals. Inorganic ^{14}C, as HCO_3^- and CO_3^{2-} species, is retained by interaction with the carbonate fraction of the bentonite backfill and is therefore expected to decay over time in this environment (Tab. 6-1). Remobilisation of inorganic ^{14}C by autotrophic microorganisms (Section 4.2.2.2), leading to a significant contribution to the formation of $^{14}CH_4$, could be a relevant process. This depends on the respective inventory and solubility of carbonates under HLW repository conditions and on the provision that microbial life is possible (in terms of space and water availability).

^{14}C-bearing gaseous carbon compounds

Production, consumption and transport of gaseous compounds in a deep geological repository for HLW/SF have been discussed in detail elsewhere (Nagra 2024e, in prep.). Gaseous ^{14}C, mainly as $^{14}CH_4$, is subject to the same coupled processes that control the behaviour of bulk gas in the near-field and host rock of a deep geological repository (Leupin et al. 2016b). As with organic

^{14}C, microbial utilisation of gaseous ^{14}C-bearing carbon compounds can occur in the near-field if sufficient space and water activity are available. The transport of gaseous ^{14}C in the near-field is barely influenced by sorption processes (Tab. 6-1).

7.5 Fate of ^{14}C-bearing carbon compounds in the host rock

Small ^{14}C-bearing molecules are expected to migrate from the EBS of the HLW and L/ILW repositories into the host rock. These are:

- ^{14}C-bearing dissolved oxygenated carbon compounds typically with less than 5 carbon atoms, especially carboxylates and possibly alcohols and aldehydes in smaller proportions. For example, carboxylates are produced by the corrosion of activated metals, but can also be released in smaller proportions from spent IERs and filter cartridges (Sections 5.5.3 and 5.6).
- ^{14}C-bearing gaseous carbon compounds (mostly HCs), in particular $^{14}CH_4$, mainly produced during the anoxic corrosion of metals and possibly also during biotic degradation of the carbon compounds released from the surface of contaminated waste.

Possible reaction and migration pathways of ^{14}C in the organic form were discussed by Van Loon (2019) (Fig. 7-3). The author assigned ^{14}C in the inorganic form to a slow carbon cycle and ^{14}C in the organic form to a fast carbon cycle. The conversion of organic ^{14}C into inorganic ^{14}C by microbial activity during migration through the EBS and in the host rock shifts ^{14}C from the fast to the slow carbon cycle, leading to ^{14}C decay in the host rock. Van Loon (2019) suggested that the decay of ^{14}C, which limits its contribution to dose release, could occur in the repository environment as a result of the following processes: i) conversion of the ^{14}C-carrying organic molecules to $^{14}CO_2$ followed by its incorporation in calcite, thereby feeding ^{14}C into the slow C-cycle and its associated decay in the host rock; ii) irreversible uptake by minerals of the host rock leading to complete decay of ^{14}C in the formation; and iii) strong, reversible retention by the host rock leading to delayed migration that allows ^{14}C to decay in the host rock.

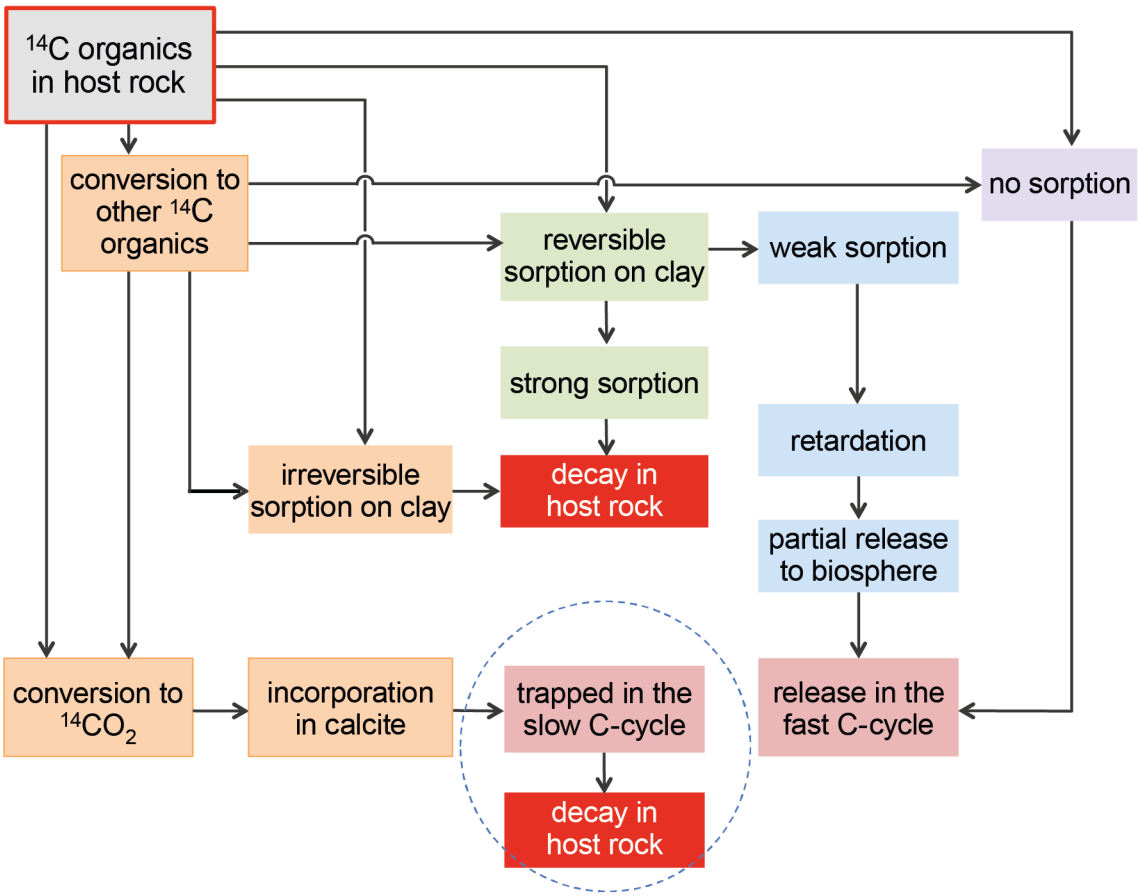

Fig. 7-3: Potential reaction and migration pathways of ^{14}C in the organic chemical form in the repository environment

From Van Loon (2019)

The question arises whether the conversion of organic ^{14}C to $^{14}CO_2$ takes place in the host rock, which enables the retention of $^{14}CO_2$ through an isotopic exchange between ^{14}C- and ^{12}C-carbonate in the carbonates of the host rock, because the retention of inorganic ^{14}C by the host rock is strong (Tab. 6-1). Microbial activity is thought to be the only way to convert carbon compounds in the organic form into carbonate, e.g., by sulphate-reducing microorganisms. Oxidation of small, oxygenated carbon compounds by sulphate-reducing microorganisms is the most likely reaction pathway for the conversion of the organics into the inorganic form. Sulphate is abundant in the porewater of the OPA and is an important electron acceptor in anaerobic respiration. However, unequivocal evidence for microbial oxidation of CH_4 under the conditions in the OPA host rock is still lacking (Leupin et al. 2017 and references therein), although the anaerobic oxidation of CH_4 by microbes is possible in principle (Alperin & Hoehler 2009). For a further discussion of the metabolic potential of microorganism in OPA and the microbial activities leading to the conversion of carbon compounds and gases in deep geological repository environments, the reader is referred to Guillemot et al. 2023 and Nagra, 2024e. The same conceptual considerations apply to gaseous organic carbon compounds.

In general, OPA is not considered to be a favourable environment for microbial life for several reasons (Leupin et al. 2017; Guillemot et al. 2023):

- the low porosity is likely to limit microbial growth and mobility,
- the very low amount of free water available for metabolism,
- lack of easily accessible and easily degradable energy sources.

The latter constraint would be overridden in a deep geological repository environment due to the diffusion of organic and gaseous carbon compounds from the EBS into the host rock. Further, it is conceivable that these constraints are less pronounced at the interface between the EBS and the host rock (i.e., the EDZ) where disturbed zones (e.g., fractures) may exist that allow spatial expansion and water accumulation. For example, microbial activity was observed in a borehole in OPA when sufficient water and space as well as the necessary nutrients were available. Under these conditions, a variety of microorganisms were detected (Bagnoud 2015; Leupin et al. 2017; Leupin et al. 2016a).

8 Summary and conclusions

^{14}C is a radionuclide considered for post-closure safety assessments due to its rather long half-life (5,700 years), its presence in both liquid and gas phases, and the low sorption of dissolved and gaseous ^{14}C-organic compounds in the near-field and the geosphere. The chemical form of the ^{14}C-bearing carbon species dictates the routes of ^{14}C migration in the engineered barrier system of a deep geological repository and the surrounding host rock and therefore determines the long-term contribution of ^{14}C to the potential dose release from a deep geological repository. Furthermore, ^{14}C could be subject to substantial accumulation in the biosphere, given the use of carbon by all life forms.

This report provides an appraisal of ^{14}C sources, generation, reactions and interactions, and transport in the context of a Swiss deep geological repository for both HLW and L/ILW, based on the current state of knowledge available in the literature.

In L/ILW, ^{14}C is present in different waste forms. The main inventory is associated with activated metals (i.e., steel, Zircaloy), in which ^{14}C originates from the activation of ^{14}N impurities present in the metal matrix. A non-negligeable proportion of ^{14}C is also associated with contaminated materials (including metals, inorganic and organic substances). Smaller ^{14}C inventories can be attributed to spent IERs, graphite, activated concrete and ^{14}C-bearing $BaCO_3$ from both reprocessing and MIR waste. In HLW, ^{14}C in SF assemblies originates from the activation of ^{14}N impurities in metallic fuel assembly components (steel, Zircaloy) and the SF, while the activation of ^{17}O, which is contained in UO_2 and mixed oxide fuel, is another source of ^{14}C. Vitrified HLW is expected to contain ^{14}C mostly in dissolved inorganic form, provided that ^{14}C was not previously released during reprocessing.

The types of ^{14}C-bearing carbon compounds that could be present under repository conditions were assessed on the basis of thermodynamic modelling of the C-H-O system under the relevant geochemical conditions and with a view to the degradation processes of the reactive ^{14}C-containing waste materials that lead to the release of ^{14}C-bearing carbon compounds. The thermodynamic modelling (at equilibrium) shows the predominance of small carbon compounds (< 5 carbon atoms) under the expected reducing conditions of the L/ILW and HLW repositories, such as carbonate (HCO_3^-, CO_3^{2-}), aliphatic monocarboxylates (e.g., formate, acetate) and alcohols (e.g., methanol, ethanol), as well as small HCs like CH_4 and C_2H_6. However, complete thermodynamic equilibrium is rarely attained in the C-H-O system, at least at moderate temperatures, and therefore the predicted speciation depends on kinetics and assumptions about the metastability of the system.

Information on the carbon species formed during metal corrosion is available from experimental studies with activated and non-activated metals. Experimental studies with non-activated materials (Zircaloy, steel) confirm the formation of mainly small carbon compounds during the immersion of metals in solution. These carbon compounds have different redox states, i.e., they are present in the reduced (HCs) and oxygenated forms (carboxylates, alcohols). The corrosion of metals generates volatile HCs, especially CH_4, in accordance with an F-T-type process due to the reaction of carbides present in the metal. However, due to the oxic conditions during the service life of the materials, oxygen-containing carbon compounds, such as monocarboxylates and carbonate, are also released in solution from the oxide layer of the metals. Thus, it is expected that both ^{14}C-bearing reduced and oxygenated carbon species are present in metallic iron/steel-water systems. This conclusion is drawn on the basis of corrosion experiments with non-activated iron and further supported by the results from experimental studies with activated steel. Of the oxygenated carbon compounds, only formate is likely to undergo abiotic degradation under repository conditions, leading to the formation of carbonates through a decarboxylation process. However, the larger carboxylates with two or more carbon atoms (e.g., acetate) are unlikely to be

decomposed by abiotic degradation at ambient temperature and pressure due to the high activation energy of C-C bond cleavage. In contrast, microbially mediated degradation of oxygenated carbon compounds can occur locally in favourable niches in the near-field (pH < 11, availability of space and water).

New experimental studies on the corrosion of activated materials, especially activated stainless steel, confirm previous observations on the nature of the carbon species formed during the corrosion of metals under alkaline conditions. In particular, the results support the release of ^{14}C-bearing carbon compounds in two steps, namely the immediate release of dissolved ^{14}C-bearing oxygenated carbon compounds (^{14}C-carboxylates, ^{14}C-carbonate) in the initial phase of the corrosion process upon contact of the materials with water (defined as IRF in safety assessments) and the slow, continuous release of ^{14}C-bearing gas phase species, especially CH_4, in the further course of the corrosion process. The ^{14}C IRF corresponds to the ^{14}C-bearing carbon compounds present in the oxide layer and were formed when the metals were exposed to oxic conditions. The fraction of ^{14}C released rapidly is expected to be less than 0.01% of the total ^{14}C inventory of activated stainless steel. The slow release of ^{14}C in the long term occurs according to the corrosion rate of activated stainless steel (defined as congruent release fraction in safety assessments). Given the similar material history (e.g., exposure to radiation), material properties (e.g., reducing conditions at solid-water interface despite radiolysis) and exposure of the waste to the same geochemical conditions in a deep geological repository, the processes leading to the release of ^{14}C-bearing carbon compounds are assumed to be similar for the activated metals (stainless steel, Zircaloy) and SF. In the long term, gaseous ^{14}C species, mainly $^{14}CH_4$, will be congruently released in a deep geological repository according to the corrosion rate of the activated metals and the dissolution rate of SF.

In contrast to activated metallic waste forms, experimental information on the ^{14}C speciation in non-metallic wastes is limited, such as in the case of spent IERs and graphite, or even non-existent, such as in the case of contaminated materials and activated concrete. In these cases where information is completely lacking (e.g., contaminated waste, activated concrete), the ^{14}C speciation was assigned based on expert judgement. Rapid release of ^{14}C is expected from spent IERs and contaminated materials (e.g., filter cartridges, MIR waste), releasing dissolved ^{14}C as LMW organic carbon compounds, which might further be degraded into CO_2 and CH_4, and dissolved inorganic carbon compounds. Only a small fraction of ^{14}C is expected to be released from graphite, mainly as organic and inorganic ^{14}C. Activated concrete and ^{14}C-containing $BaCO_3$ in vitrified reprocessing waste and MIR waste are assumed to release mainly dissolved inorganic ^{14}C, which is retained and further decays in these waste forms due to the low solubility of $BaCO_3$ and $CaCO_3$ in the cementitious near-field of the L/ILW repository.

In an HLW repository, activated metals (Zircaloy, steel), SF and vitrified waste are the only sources of ^{14}C. In case of the activated metals and SF, only a very small fraction of the ^{14}C inventory is expected to be released instantaneously, i.e., on first contact with groundwater, either as dissolved organic or inorganic ^{14}C species. On the other hand, most of the inventory will be released by slow reactions of the bulk materials, such as corrosion of the activated metals or dissolution of the SF, as organic gaseous ^{14}C compounds (especially $^{14}CH_4$). In the case of vitrified waste, ^{14}C is assumed to be mainly released in dissolved inorganic form as ^{14}C-carrying carbonates, being slowly released by glass corrosion.

With the knowledge that is now available on the representative carbon species in the three forms of ^{14}C (i.e., ^{14}C-carbonates in the case of inorganic ^{14}C; ^{14}C-carboxylates in the case of organic ^{14}C; $^{14}CH_4$ in the case of gaseous ^{14}C), retention and reactivity of ^{14}C in the near-fields of the deep geological repositories for L/ILW and HLW/SF, as well as the host rock, have been assessed. The retention of organic ^{14}C in the near-fields of both repositories is very weak due to the weak interaction forces between dissolved oxygenated carbon compounds (aliphatic monocarboxylates, alcohols, aldehydes) and the oxidic sites on the surfaces of cement phases and clay minerals. This

is also true for the gaseous ^{14}C (mainly $^{14}CH_4$). In contrast, the retention of inorganic ^{14}C (^{14}C-carbonates) is much greater due to an isotopic exchange between $^{14}CO_3^{2-}$ and CO_3^{2-} on carbonates (e.g., calcite) and the limited solubility of carbonates. The extent of retention depends on the carbonate content of the near-field backfills (cementitious materials, bentonite) and the CO_3^{2-} concentrations of the corresponding near-field porewaters. This also applies to the retention of ^{14}C-inorganics by the OPA host rock. On the other hand, the retention of gaseous ^{14}C-organics in OPA is very low. For ^{14}C-containing oxygenated carbon compounds, this is due to the weak interaction with the clay minerals of the host rock. For gaseous ^{14}C-organics, it can be assumed that any retention occurs through interaction with the organic matter of the OPA.

This review of available experimental results and scientific literature allows an overarching analysis of the behaviour of ^{14}C in the near-field and host rock of a deep geological repository to be presented. The proportions of water-soluble ^{14}C-organics, ^{14}C-inorganics and gaseous ^{14}C-organics released from the various waste types could also be estimated. Collectively, these assessments of ^{14}C speciation, release from the waste and transport in the near field of a deep geological repository for both L/ILW and HLW will be used as the scientific basis for post-closure safety assessments within the framework of the general licence application.

9 References

Adamson, M.G. (1971): Thermal diffusion of oxygen in hyperstoichiometric urania with very low carbon content. Journal of Nuclear Materials 38, 213-216.

Adamson, R. B. & Rudling, P. (2013): Properties of zirconium alloys and their applications in light water reactors (LWRs), in: Murty, K.L. (Ed.), Materials' ageing and degradation in light water reactors: Mechanisms and management. Woodhead Publishing, Oxford, United Kindgom, 151-245.

Ahn, T.M. (1994): Long-term C-14 source term for a high-level waste repository. Waste Management 14/5, 393-408.

Alder, J.C. & McGinnes, D.F. (1993): Model radioactive waste inventory for Swiss waste disposal projects - Vol 1 main report. Nagra Technical Report NTB 93-21, Nagra, Wettingen, Switzerland.

Alperin, M.J. & Hoehler, T.M. (2009): Anaerobic methane oxidation by archaea/sulfate-reducing bacteria aggregates: 1. Thermodynamic and physical constraints. American Journal of Science 309, 869-957.

Amend, J.P. & Helgeson, H.C. (1997): Group additivity equations of state for calculating the standard molal thermodynamic properties of aqueous organic species at elevated temperatures and pressures. Geochimica et Cosmochimica Acta 61, 11-46.

Amend, J.P., LaRowe, D.E., McCollom, T.M. & Shock, E.L. (2013): The energetics of organic synthesis inside and outside the cell. Philosophical Transactions B 368, 20120255.

Anderson, R.B. (1984): The Fischer-Tropsch synthesis. Academic Press, Orlando, FL, USA.

Ataman, E., Andersson, M.P., Ceccato, M., Bovet, N. & Stipp, S.L.S. (2016): Functional group adsorption on calcite: I. Oxygen containing and nonpolar organic molecules. Journal of Physical Chemistry C 120, 16586-16596.

Baeyens, B., Thoenen, T., Bradbury, M.H. & Marques Fernandes, M. (2014): Sorption data bases for argillaceous rocks and bentonite for the provisional safety analyses for SGT-E2. Nagra Technical Report NTB 12-04, Nagra, Wettingen, Switzerland.

Bagnoud, A. (2015): Microbial metabolism in the deep subsurface; case study of Opalinus Clay. Ecole Polytechnique Federal Lausanne (EPFL), Lausanne, Switzerland.

Bart, G. & Bertsch, J. (2005): Zirconium alloys for fuel element structures. Chimia 59, 938-943.

Baston, G.M.N., Marshall, T.A., Otlet, R.L., Walker, A.J., Mathier, I.D. & Williams, S.J. (2012): Rate and speciation of volatile carbon-14 and tritium releases from irradiated graphite, Mineralogical Magazine 76(8), 3293-3302, 2012.

Bell, J.L.S., Palmer, D.A., Barnes, H.L. & Drummond, S.E. (1994): Thermal decomposition of acetate. 3. Catalysis by mineral surfaces. Geochimica et Cosmochimica Acta 58, 4155-4177.

Bennett, J.A., Parlett, C.M.A., Isaacs, M.A., Durndell, L.J., Olivi, L., Lee, A.F. & Wilson, K. (2017): Acetic acid ketonization over Fe_3O_4/SiO_2 for pyrolysis bio-oil upgrading. ChemCatChem 9, 1648-1654.

Bhadeshia, H.K.D.H. & Honeycombe, R.W.K. (2017): Steel: microstructure and properties. Elsevier, Amsterdam, the Netherlands.

Blumenthal, W.B. (1958): The chemical behaviour of zirconium. Van Nostrand, Princeton NJ, USA.

Bovet, N., Yang, M., Javadi, M.S. & Stipp, S.L.S. (2015): Interaction of alcohols with the calcite surface. Physical Chemistry Chemical Physics 17, 3490-3496.

Boylan, A.A., Stewart, D.I., Graham, J.T., Trivedi, D. & Burke, I.T. (2017): Mechanisms of inorganic carbon-14 attenuation in contaminated groundwater: Effect of solution pH on isotopic exchange and carbonate precipitation reactions. Applied Geochemistry 85, 137-147.

Bracke, G. & Müller, W. (2008): Contribution to a more realistic approach in assessing the release of C-14 from low-level radioactive waste repositories. Journal of Contaminant Hydrology 102, 210-216.

Bradbury, M.H. & Baeyens, B. (2009): Experimental and modelling studies on the pH buffering of MX-80 bentonite porewater. Applied Geochemistry 24, 419-425.

Bradbury, M.H., Berner, U., Curti, E., Hummel, W., Kosakowski, G. & Thoenen, T. (2014): The long term geochemical evolution of the nearfield of the HLW repository. Nagra Technical Report NTB 12-01, Nagra, Wettingen, Switzerland.

Bradley, M. J. & Ferris, L. M. (1962): Hydrolysis of uranium carbides between 25 and 100°. I. Uranium monocarbide. Inorganic Chemistry 1, 683−687.

Bradley, M.J., Goode, J.H., Ferris, L.M, Flanary, J. R. & Ullmann, J.M. (1964). Hydrolysis of neutron irradiated uranium monocarbid. Inorganic Chemistry 3, 454.

Bradley, M.J., Goode J.H., Ferris L.M, Flanary J. R. & Ullmann J.M. (1965): Reaction of reactor irradiated uranium monocarbide with water and with aqueous solutions of NaOH, HCl and H_2SO_4, Nucl. Sci & Eng. 31, 159-164.

Bradley Sears, M., Pattengill, M. D. & Ferris, L. M. (1968): Reactions of uranium carbides with aqueous sodium hydroxide solutions. Journal of Inorganic Nuclear Chemistry, 30, 2111−2116.

Brady, P.V. & Kozak, M.W. (1995): Geochemical engineering of low-level radioactive waste in cementitious environment. Waste Management 15, 293-301.

Bragg-Sitton, S. (2012): Light water reactor sustainability program - advanced LWR nuclear fuel cladding system development: Technical program plan. Idaho National Laboratory Report INL/MIS-12-25696, Idaho National Laboratory, Idaho Falls, USA.

Brinkman, G.A. (1987): Reactions of radioactive recoil carbon atoms with inorganic compounds. Applied Radiation and Isotopes 38, 415-429.

Broecker, W.S. (2014): Radiocarbon, in: Turekian, K.K., Holland, H.D. (Eds.), Treatise on Geochemistry. Elsevier Science, Oxford, United Kingdom, pp. 257-271.

Broczkowski, M.E., Noël, J.J. & Shoesmith, D.W. (2005): The inhibiting effects of hydrogen on the corrosion of uranium dioxide under nuclear waste disposal conditions. Journal Nuclear. Materials 346, 16-23.

Broczkowski, M.E., Noël, J.J. & Shoesmith, D.W. (2007): The influence of dissolved hydrogen on the surface composition of doped uranium dioxide under aqueous corrosion conditions. Journal of Electroanalytical Chemistry 602, 8-16.

Broomfield, J.P. (2003): Corrosion of steel in concrete: Understanding, investigation and repair, 2n ed. Taylor & Francis, London, United Kingdom.

Bucur, C., Rizzato, C., Shcherbina, N. & Reiller, P.E. (2017): Final report on gaseous release of C-14 from BWR and CANDU spent ion exchange resins (D4.7), CAST Deliverable D4.7, European Union, Brussels, Belgium.

Bucur, C., Florea, I., Reiller, P.E. & Dumitrescu, D. (2018): C-14 content in CANDU spent ion exchange resins and its release under alkaline conditions. Radiocarbon 60, 1797-1808.

Budi, A., Stipp, S.L.S. & Andersson, M.P. (2018): The effect of solvation and temperature on the adsorption of small organic molecules on calcite. Physical Chemistry Chemical Physics 20, 7140-7147.

Bush, R.P., Smith, G.M. & White, I.F. (1984): Carbon-14 waste management, EUR 8749, Commission of the European Communities, Brussels, Belgium.

Caes, S., Druyts, F. & Thomas, P. (2018): Release and speciation of carbon from Zircaloy-4 in anaerobic and highly alkaline conditions: Comparison of simple immersion and potentiostatic corrosion tests. Radiocarbon 60, 1787-1796.

Capouet M., Boulanger, D., Vandoorne, T., Gaggiano, R., Norris, S., Williams, S., Schumacher, S., Rübel, A., Nummi, O., Poskas, P., Narkuniene, A., Grigaliuniene, D., Vokál, A., Mibus, J., Rosca-Bocancea, E., Hart, zJ., Ferrucci, B., Levizzari, R., Luce, A., Diaconu, D., Cuñado Peralta, M., Owada, H., Kienzler, B., Wieland, E., Van Loon L.R. & Walker, R. (2017): Knowledge Supporting Safety Assessments of ^{14}C, EU CAST Project Report (D6.2), European Union, Brussels, Belgium.

Chalmers, G.R.L. & Bustin, R.M. (2007): The organic matter distribution and methane capacity of the lower Cretaceous strata of northeastern British Columbia, Canada. International Journal Coal Geology 70, 223-239.

Chalmers, G.R.L. & Bustin, R.M. (2008): Lower Cretaceous gas shales in northeastern British Columbia, Part I: geological controls on methane sorption capacity. Bulletin of Canadian Petroleum Geology 56, 1-21.

Charyulu, M. M., Karekar, C. V., Rao, V. K. & Natarajan, P. R. (1991): Studies on the dissolution of carbide fuels. Journal of Radioanalytical and Nuclear Chemistry 148, 339−347.

Chen, J., Xu, J., Wang, S.S., Sun, Z.Y., Li, Z., Jia, W.L. & Peng, P.A. (2021): Dissolution of different reservoir rocks by organic acids in laboratory simulations: Implications for the effect of alteration on deep reservoirs. Geofluids 2021, article ID 6689490, 1-16.

Chen, Y., Glaus, M.A., Van Loon, L.R. & Mäder, U. (2018a): Transport behaviour of low molecular weight organic compounds in multi-mineral clay systems. A comparison between measured and predicted values. Applied Clay Science 165, 247-256.

Chen, Y., Glaus, M.A., Van Loon, L.R. & Mäder, U. (2018b): Transport of low molecular weight organic compounds in compacted illite and kaolinite. Chemosphere 198, 226-237.

Cloet, V., Schwyn, B. & Wieland, E. (2014): Geochemische Nahfeld-Daten für die provisorische Sicherheitsanalyse in SGT Etappe 2. Nagra Arbeitsbericht NAB 14-52, Nagra, Wettingen, Switzerland.

Compton, R.G. & Brown, C.A. (1995): The inhibition of calcite dissolution precipitation - 1,2-dicarboxylic acids. Journal of Colloid and Interface Science 170, 586-590.

Cotton, F.A.& Wilkinson, G. (1980): Advanced inorganic chemistry. Wiley-Interscience, New York, USA.

Cowan, C.E., Zachara, J.M. & Resch, C.T. (1990): Solution ion effects on the surface exchange of selenite on calcite. Geochimica et Cosmochimica Acta 54, 2223-2234.

Cox, J.D., Wagman, D.D. & Medvedev, V.A. (1989): CODATA key values for thermodynamics, Hemisphere Publ. Corp., New York, USA.

Curti, E. (1997): Coprecipitation of radionuclides: basic concepts, literature review and first applications. Nagra Technical Report NTB 97-08, Nagra, Wettingen, Switzerland.

Curti, E. (2021a): Bentonite pore waters (BPW) for the sectoral plan, phase SGT-3: Model development, testing and final calculations. Nagra Work Report NAB 22-43.

Curti, E. (2021b): Research on LWR spent fuel alteration and radionuclide release: literature review 2000 - 2020. Unpublished. PSI internal documentation, Paul Scherrer Institut, Villigen PSI, Switzerland.

Curti, E. (2023): Aqueous corrosion of vitrified nuclear waste: Current process understanding, literature review and recommended rates. Nagra Work Report NAB 23-09, Nagra, Wettingen, Switzerland.

Curti, E., Thoenen, T., Kosakowski, G., Miron, G.D., Baeyens, B., Van Loon, L.R. & Leupin, O.X. (2023): The chemical near-field evolution within the HLW/SF repository (update of NTB 12-01). Nagra Technical Report NTB 23-02. Nagra, Wettingen, Switzerland.

Curti, E. & Kulik, D.A. (2020): Oxygen potential calculations for conventional and Cr-doped UO2 fuels based on solid solution thermodynamics. Journal of Nuclear Materials 534, 152140.

Cvetković, B., Rothardt, J., Buttler, A., Kunz, D., Schlotterbeck, G. & Wieland, E. (2018a): Formation of low-molecular-weight organic compounds during anoxic corrosion of zero-valent iron. Environmental Engineering Science 35, 447-461.

Cvetković, B., Salazar, G., Kunz, D., Szidat, S. & Wieland, E. (2018b): Analysis of C-14-bearing compounds released by the corrosion of irradiated steel using accelerator mass spectrometry. Analyst 143, 3059-3067.

Cvetković, B.Z., Salazar, G., Kunz, D., Tits, J., Szidat, S. & Wieland, E. (2018c): Quantification of dissolved organic C-14-containing compounds by accelerator mass spectrometry in a corrosion experiment with irradiated steel. Radiocarbon 60, 1711-1727.

Dagnelie, R.V.H., Descostes, M., Pointeau, I., Klein, J., Grenut, B., Radwan, J., Lebeau, D., Georgin, D. & Giffaut, E. (2014): Sorption and diffusion of organic acids through clayrock: Comparison with inorganic anions. Journal of Hydrology 511, 619-627.

Dagnelie, R.V.H., Rasamimanana, S., Blin, V., Radwan, J., Thory, E., Robinet, J.C. & Lefèvre, G. (2018): Diffusion of organic anions in clay-rich media: Retardation and effect of anion exclusion. Chemosphere 213, 472-480.

Dario, M., Molera, M. & Allard, B. (2004): Effect of organic ligands on the sorption of europium on TiO_2 and cement at high pH. SKB Technical Report TR-04-04, Swedish Nuclear Fuel and Waste Management Co, Stockholm, Sweden.

Daub, K., Zhang, X., Noel, J.J. & Wren, J.C. (2010): Effects of gamma-radiation versus H_2O_2 on carbon steel corrosion. Electrochimica Acta 55, 2767-2776.

Daub, K., Zhang, X., Noel, J.J. & Wren, J.C. (2011): Gamma radiation-induced carbon steel corrosion. ECS Transactions 33, 15-24.

Davis, J.A., Fuller, C.C. & Cook, A.D. (1987): A model for trace-metal sorption processes at the calcite surface - adsorption of Cd^{2+} and subsequent solid-solution formation. Geochimica et Cosmochimica Acta 51, 1477-1490.

Davis, J.R. (1991): Metals Handbook Vol 1: Properties and selection: Irons, steels, and high-performance alloys. American Society of Metals, Materials Park OH, USA.

De Deugd, R.M. (2004): Fischer-Tropsch synthesis revisited: Efficiency and selectivity benefits from imposing temporal and/or spatial structure in the reactor. Technical University of Delft, Delft, the Netherlands, p. 159.

De Visser-Týnová, E., Stijkel, M.P., Swanton, S., Otlet, B. & Walker, J. (2018a): C-14 release and speciation from irradiated stainless steel under alkaline reducing conditions (D2.8). CAST Deliverable D2.8, issue 2, European Union, Brussels, Belgium.

De Visser-Týnová, E., Swanton, S.W., Williams, S.J., Stijkel, M.P., Walker, A.J. & Otlet, R.L. (2018b): C-14 release from irradiated stainless steel. Radiocarbon 60, 1671-1681.

Deng, B.L., Campbell, T.J. & Burris, D.R. (1997): Hydrocarbon formation in metallic iron/water systems. Environmental Science & Technology 31, 1185-1190.

Dey, R., Sarkar, T., Subramanian, C., Anand, S., Singh, K.D. & Kulkarni, M.S. (2020): Temporal evolution of activation products in a zircaloy-4 guide tube and the estimation of its external gamma dose rate for decommissioning activities. Journal of Radiological Protection 40, 197-214.

Diomidis, N. (2014): Scientific basis for the production of gas due to corrosion in a deep geological repository. Nagra Work Report NAB 14-21, Nagra, Wettingen, Switzerland.

Diomidis, N., King, F. & Guillemot, T. (2023): Definition of the reference corrosion rates for performance assessmens in the framework of the general license application. Nagra Work Report NAB 23-22, in prep Nagra, Wettingen, Switzerland.

Dobberschütz, S., Nielsen, M.R., Sand, K.K., Civioc, R., Bovet, N., Stipp, S.L.S. & Andersson, M.P. (2018): The mechanisms of crystal growth inhibition by organic and inorganic inhibitors. Nature Communications 9, 1578.

Drummond, S.E. & Palmer, D.A. (1986): Thermal decarboxylation of acetate. 2. Boundary conditions for the role of acetate in the primary migration of natural gas and the transportation of metals in hydrothermal systems. Geochimica et Cosmochimica Acta 50, 825-833.

Druyts, F., Caes, S. & Thomas, P. (2018): Carbon-14 release and speciation from carbon steel in highly alkaline conditions. Radiocarbon 60, 1683-1690.

Dry, M.E. (1981): The Fischer-Tropsch synthesis, in: Anderson, J.R., Boudart, M. (Eds.), Catalysis science and technology. Springer, Weinheim, Germany, pp. 159-255.

Dubinin, M.M. (1975): Physical adsorption of gases and vapors in micropores. Progress in Surface and Membrane Science Vol. 9, 1-70.

Dubinin, M.M. (1980): Water-vapor adsorption and the microporous structures of carbonaceous adsorbents. Carbon 18, 355-364.

Ekeroth, E. & Jonsson, M. (2003): Oxidation of UO2 by radiolytic oxidants. Journal of Nuclear Materials 322, 242-248.

Ekeroth, E., Roth, O. & Jonsson, M. (2006): The relative impact of radiolysis products in radiation induced oxidative dissolution of UO2. Journal of Nuclear Materials 355, 38-46.

Ekeroth, E., Cui, D., Low, J., Granfors, M., Zwicky, H.-U., Spahiu, K. & Zetterström Evins, L. (2012): Instant release fractions from corrosion studies with high burnup LWR fuel. Material Research Society Symposium Proceedings 1475, 125-130.

Engelhardt, G.R., Kursten, B. & Macdonald, D.D. (2020): Corrosion of carbon steel in physically constrained locations in high-level nuclear waste isolation systems. Corrosion Science 177, 108974.

European Committee for Standardization (2005): Stainless steel - Part 3: Technical delivery conditions for semi-finished products, bars, rods, wire, sections and bright products of corrosion resisting steels for general pruposes, EN 10088-3:1995.

Fan, K.K., Li, Y.J., Elsworth, D., Dong, M.Z., Yin, C.B., Li, Y.C. & Chen, Z.L. (2018): Three stages of methane adsorption capacity affected by moisture content. Fuel 231, 352-360.

Feron, D. (2012): Nuclear corrosion science and engineering. Woodhead Publishing, Cambridge, United Kingdom.

Ferrari, H.N. (1963): Nitrogen release from UO_2 pellets at elevated temperatures. Nuclear Science and Engineering 17, 503-512.

Ferry, C., Piron, J.-P., Poulesquen, A. & Poinssot, C. (2008): Radionuclides release from the spent fuel under disposal conditions: Re-evaluation of the instant release fraction. Material Research Society Symposium Proceedings 1107, 447-454.

Fischer, F. & Tropsch, H. (1923): Ueber die Herstellung synthetischer Ölgemische (Synthol) durch Aufbau aus Kohlenoxyd und Wasserstoff. Brennstoff-Chemie 4, 276-285.

Flory, P.J. (1936): Molecular size distribution in linear condensation polymers. Journal of the American Chemical Society 58, 1877-1885.

Fraker, A.C. (1989): Corrosion of Zircaloy spent fuel cladding in a repository, NIST Report 89-4114. National Institute of Standards and Technology, Washington, USA.

Fredd, C.N. & Fogler, H.S. (1998): The kinetics of calcite dissolution in acetic acid solutions. Chemical Engineering Science 53, 3863-3874.

Friedel, R.A. & Anderson, R.B. (1950): Composition of synthetic liquid fuels. 1. Product distribution and analysis of C-5 - C-8 paraffin isomers from cobalt catalyst. Journal of the American Chemical Society 72, 2307-2307.

Gadikota, G., Dazas, B., Rother, G., Cheshire, M.C. & Bourg, I.C. (2017): Hydrophobic solvation of gases (CO_2, CH_4, H_2, noble gases) in clay interlayer nanopores. Journal of Physical Chemistry C 121, 26539-26550.

Garcia, D., Henocq, P., Riba, O., López-Garcia, M., Madé, B. & Robinet, J.C. (2020): Adsorption behaviour of isosaccharinic acid onto cementitious materials. Applied Geochemistry 118, 104625.

Garzarolli, F., Stehle, H. & Steinberg, E. (1996): Behavior and properties of Zircaloys in power reactors: A short review of pertinent aspects in LWR fuel, in: Bradley, E.R., Sabol, G.P. (Eds.), Zirconium in the nuclear industry: Eleventh international symposium, ASTM STP 1295. American Society for Testing and Materials, USA, pp. 12-32.

Gasparik, M., Bertier, P., Gensterblum, Y., Ghanizadeh, A., Krooss, B.M. & Littke, R. (2014): Geological controls on the methane storage capacity in organic-rich shales. International Journal of Coal Geology 123, 34-51.

Gasparik, M., Ghanizadeh, A., Bertier, P., Gensterblum, Y., Bouw, S. & Krooss, B.M. (2012): High-pressure methane sorption isotherms of black shales from the Netherlands. Energy and Fuels 26, 4995-5004.

Gauld, I.C., Hermann, O.W. & Westfall, R.M. (2009): ORIGEN scale system module to calculate fuel depletion, actinide transmutation, fission product buildup and decay, and associated radiation terms, ORNL/TM 2005/39, version 6, Vol. II, Sect. F7. In: Rearden, B.T., Jesse, M.A.. Eds., SCALE Code System, ORNL/TM-2005/39, Version 6.2.3, Oak Ridge national Laboratory, Oak Ridge, Tennessee (2018). Available from Radiation Safety Information Computational Center as CCC-834.

Giroud, N., Tomonaga, Y., Wersin, P., Briggs, S., King, F., Vogt, T., Diomidis, N. (2018): On the fate of oxygen in a spent fuel emplacement drift in Opalinus Clay. Applied Geochemistry 97, 270-278.

Glaus, M.A. & Van Loon, L.R. (2008): Degradation of cellulose under alkaline conditions: New insights from a 12 years degradation study. Environmental Science & Technology 42, 2906-2911.

Glaus, M.A., Laube, A., Stallone, S. & Van Loon, L.R. (1998): Importance of the alkaline degradation of cellulose in performance assessment of a cementitious radioactive waste repository. Material Research Society Symposium Proceedings 506, 977-978.

Glaus, M.A., van Loon, L.R., Achatz, S., Chodura, A. & Fischer, K. (1999): Degradation of cellulosic materials under the alkaline conditions of a cementitious repository for low and intermediate level radioactive waste. Part I: Identification of degradation products. Analytica Chimica Acta 398, 111-122.

Gras, J.-M. (2014): State of the art of 14C in Zircaloy and Zr alloys - ^{14}C release from zirconium alloy hulls (D3.1). CAST Deliverable D3.1, European Union, Brussels, Belgium.

Grasemann, M. & Laurenczy, G. (2012): Formic acid as a hydrogen source - recent developments and future trends. Energy & Environmental Science 5, 8171-8181.

Grauer, R. (1988): The corrosion behaviour of carbon steel in Portland cement. Nagra Technical Report NTB 88-02E, Nagra, Wettingen, Switzerland.

Griess, J.C. Jr. (1974): The hydrolysis of lanthanide and actinide carbides: a survey of the recent literature, Report ORNL-TM-4489, Oak Ridge National Laboratory, USA.

Guillemot, T., Cvetković, B.Z., Kunz, D. & Wieland, E. (2020a): Processes leading to reduced and oxidised carbon compounds during corrosion of zero-valent iron in alkaline anoxic conditions. Chemosphere 250. 126230.

Guillemot, T., Salazar, G., Cvetković, B.Z., Kunz, D., Szidat, S. & Wieland, E. (2020b): Determination of ultra-low concentrations of gaseous C-14-bearing hydrocarbons produced during corrosion of irradiated steel using accelerator mass spectrometry. Analyst 145, 7870-7883.

Guillemot, T., Cvetković, B.Z., Kunz, D., Salazar, G., Rauber, M., Szidat, S. & Wieland, E. (2021a): Development of analytical methods for the detection of 14C-bearing carbon compounds at ultra-low concentrations. Nagra Work Report NAB 21-03, Nagra, Wettingen, Switzerland.

Guillemot, T., Kunz, D., Salazar, G., Rauber, M., Szidat, S. & Wieland, E. (2021b): Long-term monitoring of dissolved and gaseous 14C-bearing carbon compounds during alkaline anoxic corrosion of irradiated steel. Nagra Work Report NAB 21-26, Nagra, Wettingen, Switzerland.

Guillemot, T., Salazar, G., Rauber, M., Kunz, D., Szidat, S. & Wieland, E. (2022): Carbon-14 release during corrosion of irradiated steel studied by accelerator mass spectrometry. Science of the Total Environment 817, 152596.

Guillemot, T., Wieland, E., Warthmann, R. & Mosberger, L. (2023): Degradation of organic materials in a L/ILW repository. Nagra Work Report NAB 23-11, Nagra, Wettingen, Switzerland.

Guo, N., Disdier, Z., Thory, E., Robinet, J.C. & Dagnelie, R.V.H. (2021): Mobility of organic compounds in a soft clay-rich rock (Tegulines clay, France). Chemosphere 275. 130048.

Guo, X.L., Gin, S., Liu, H.S., Ngo, D., Luo, J.W., Kim, S.H., Mohanty, C., Vienna, J.D., Ryan, J.V. & Frankel, G.S. (2020): Near-field corrosion interactions between glass and corrosion resistant alloys. Npj Materials Degradation 4, 1-15

Hakim, S.S., Olsson, M.H.M., Sorensen, H.O., Bovet, N., Bohr, J., Feidenhans'l, R. & Stipp, S.L.S. (2017): Interactions of the calcite {10.4} surface with organic compounds: Structure and behaviour at mineral - organic interfaces. Scientific Reports 7, 7592.

Hallbeck, L. (2010): Principal organic materials in a repository for spent nuclear fuel. SKB Technical Report TR-10-19, Swedish Nuclear Fuel and Waste Management Co, Stockholm, Sweden.

Hardy, L.O. & Gillham, R.W. (1996): Formation of hydrocarbons from the reduction of aqueous CO_2 by zero-valent iron. Environmental Science & Technology 30, 57-65.

He, X.H., Ahn, T. & Gwo, J.P. (2017): Carbon steel corrosion in simulated anoxic concrete pore water for nuclear waste disposal application. Corrosion 73, 1381-1393.

Heikola, T. (2014): Leaching of ^{14}C in repository conditions, VTT Technology Report 157, VTT, Finland.

Heikola, T. & Ollila, K. (2018): Release and speciation of carbon from stainless steel under mildly and highly alkaline, reducing conditions (D2.9). CAST Deliverable D2.9, European Union, Brussels, Belgium.

Helgeson, H.C., Owens, C.E., Knox, A.M. & Richard, L. (1998): Calculation of the standard molal thermodynamic properties of crystalline, liquid, and gas organic molecules at high temperatures and pressures. Geochimica et Cosmochimica Acta 62, 985-1081.

Henrici-Olivé, G. & Olivé, S. (1976): Fischer-Tropsch synthesis - molecular-weight distribution of primary products and reaction-mechanism. Angewandte Chemie-International Edition in English 15, 136-141.

Herm, M., de Visser-Týnová, E., Heikola, T., Ollila, K., Gonzalez-Robles, E., Böttle, M., Müller, N., Bohnert, E., Dagan, R., Caruso, S., Kienzler, B. & Metz, V. (2017a): Final report on C-14 release from steels under low pH and acidic conditions (D2.16). CAST Deliverable D2.16, European Union, Brussels, Belgium.

Herm, M., Gonzalez-Robles, E., Böttle, M., Müller, N., Bohnert, E., Dagan, R., Caruso, S., Kienzler, B. & Metz, V. (2017b): Report on ^{14}C release speciation from stainless steel under acidic conditions (D2.11). CAST Deliverable D2.11, European Union, Brussels, Belgium.

Herm, M., Sakuragi, T., Gonzalez-Robles, E., Böttle, M., Müller, N., Bohnert, E., Dagan, R., Caruso, S., Kienzler, B. & Metz, V. (2017c): Final report on ^{14}C release and speciation from Zircaloy (D3.15). CAST Deliverable D3.15, European Union, Brussels, Belgium.

Herm, M., Dagan, R., Gonzalez-Robles, E., Müller, N. & Metz, V. (2018): Comparison of calculated and measured radionuclide inventory of a Zircaloy-4 cladding tube plenum section. MRS Advances 3, 1031-1037.

Hesböl, R., Puigdomenech, I. & Evans, S. (1990): Source terms, isolation and radiological consequences of carbon-14 waste in the Swedish SFR repository. SKB Technical Report 90-02, Swedish Nuclear Fuel and Waste Management Co, Stockholm, Sweden.

Hoch, A.R., Rochelle, C.A., Humphreys, P.N., Lloyd, J.R., Heath, T.G. & Thatcher, K.E. (2016): Carbon-14 project phase 2 - formation of a gas phase and its migration, AMEC/200047/007, issue 1, Harwell, Didcot, United Kingdom.

Hu, Y.N., Devegowda, D., Striolo, A., Phan, A.T.V., Ho, T.A., Civan, F. & Sigal, R. (2015): Microscopic dynamics of water and hydrocarbon in shale-kerogen pores of potentially mixed wettability. SPE Journal 20, 112-124.

Hummel, W. & Thoenen, T. (2023): The PSI chemical thermodynamic data base 2020. Nagra Technical Report NTB 21-03, Nagra, Wettingen, Switzerland.

Hummel, W., Anderegg, G., Puigdomènech, I., Rao, L. & Tochiyama, O. (2005): Chemical thermodynamics of compounds and complexes of U, Np, Pu, Am, Tc, Zr, Ni and Se with selected organic ligands, Chemical Thermodynamcis Vol. 9, Nuclear Energy Agency, Paris, France.

Ishidera, T., Xia, X.B., Idemitsu, K. & Kikuchi, Y. (2008): Corrosion products from carbon steel formed in compacted bentonite under reducing conditions. Journal of Nuclear Science and Technology 45, 763-772.

Ishikawa, T., Kondo, Y., Yasukawa, A. & Kandori, K. (1998): Formation of magnetite in the presence of ferric oxyhydroxides. Corrosion Science 40, 1239-1251.

Jacops, E., Volckaert, G., Maes, N., Weetjens, E. & Govaerts, J. (2013): Determination of gas diffusion coefficients in saturated porous media: He and CH_4 diffusion in Boom Clay. Applied Clay Science 83-84, 217-223.

Jacops, E., Aertsens, M., Maes, N., Bruggeman, C., Krooss, B.M., Amann-Hildenbrand, A., Swennen, R. & Littke, R. (2017a): Interplay of molecular size and pore network geometry on the diffusion of dissolved gases and HTO in Boom Clay. Applied Geochemistry 76, 182-195.

Jacops, E., Aertsens, M., Maes, N., Bruggeman, C., Swennen, R., Krooss, B., Amann-Hildenbrand, A. & Littke, R. (2017b): The dependency of diffusion coefficients and geometric factor on the size of the diffusing molecule: Observations for different clay-based materials. Geofluids, 8652560.

Jelinek, J. & Neufeld, P. (1982): Kinetics of hydrogen formation from mild-steel in water under anaserobic conditions. Corrosion 38, 98-104.

Jenni, A., Wersin, P., Thoenen, T., Baeyens, B., Ferrari, A., Gimmi, T., Mäder, U., Marschall, P., Hummel, W. & Leupin, O. (2019): Bentonite backfill performance in a high-level waste repository: a geochemical perspective. Nagra Technical Report NTB 19-03, Nagra, Wettingen, Switzerland.

Ji, L.M., Zhang, T.W., Milliken, K.L., Qu, J.L. & Zhang, X.L. (2012): Experimental investigation of main controls to methane adsorption in clay-rich rocks. Applied Geochemistry 27, 2533-2545.

Johnson, L. (2014): A model for radionuclide release from spent UO_2 and MOX fuel. Nagra Work Report NAB 13-37, Nagra, Wettingen, Switzerland.

Johnson, L.H. & McGinnes, D.F. (2002): Partitioning of radionuclides in Swiss power reactor fuels. Nagra Technical Report NTB 02-07, Nagra, Wettingen, Switzerland.

Johnson, L. & King, F. (2008): The effect of the evolution of environmental conditions on the corrosion evolutionary path in a repository for spent fuel and high-level waste in Opalinus Clay. Journal of Nuclear Materials 379, 9-15.

Johnson, L. & Schwyn, B. (2008): Proceedings of a Nagra/RWMC workshop on the release and transport of C-14 in repository environments. Nagra Work Report NAB 08-22, Nagra, Wettingen, Switzerland.

Johnson, L., Poinssot, C., Ferry, C. & Lovera, P. (2004): Estimates of the instant release fraction for UO_2 and MOX fuel at t = 0. Nagra Technical Report NTB 04-08, Nagra, Wettingen, Switzerland.

Johnson, L., Ferry, C., Poinssot, C. & Lovera, P. (2005): Spent fuel radionuclide source-term model for assessing spent fuel performance in geological disposal. Part I: Assessment of the instant release fraction. Journal of Nuclear Materials 346, 56-65.

Johnson, L., Günther-Leopold, I., Waldis, J.K., Linder, H.P., Low, J., Cui, D., Ekeroth, E., Spahiu, K. & Evins, L.Z. (2012): Rapid aqueous release of fission products from high burn-up LWR fuel: Experimental results and correlations with fission gas release. Journal of Nuclear Materials 420, 54-62.

Johnson, L., Curti, E. & Spahiu, K. (2023), A radionuclide release model for spent UO_2 and MOX fuel for safety assessment with application to waste to be disposed of in a deep geological reportory in Switzerland, Nagra Work Report NAB 23-10, Nagra, Wettingen, Switzerland.

Jonsson, M., Nielsen, F., Roth, O., Ekeroth, E., Nilsson, S. & Hossain, M.M. (2007): Radiation induced spent nuclear fuel dissolution under deep repository conditions. Environmental Science & Technology 41, 7087-7093.

Kaminsky, M.P., Winograd, N., Geoffroy, G.L. & Vannice, M.A. (1986): Direct SIMS observation of methylidine, methylene, and methyl intermediates on a Ni(111) methanation catalyst. Journal of the American Chemical Society 108, 1315-1316.

Kaneko, S., Tanabe, H., Sasoh, M., Takahashi, R., Shibano, T. & Tateyama, S. (2003): A study on the chemical forms and migration behavior of carbon-14 leached from the simulated hull waste in the underground condition. Materials Research Society Symposium Proceedings 757, 621-626.

Kani, Y., Noshita, K., Kawasaki, T., Nasu, Y., Nishimura, T., Sakuragi, T. & Asano, H. (2008): Decomposition of C-14 containing organic molecules released from radioactive waste by gamma-radiolysis under repository conditions. Radiation Physics and Chemistry 77, 434-438.

Karnland, O., Olsson, S. & Nielsson, U. (2006): Mineralogy and sealing properties of various bentonites and smectite-rich clay materials. SKB Technical Report TR-06-30, Swedish Nuclear Fuel and Waste Management Co, Stockholm, Sweden.

Kato, O., Tanabe, H., Sakuragi, T., Nishimura, T. & Tateishi, T. (2014): Corrosion tests of Zircaloy hull waste to confirm applicability of corrosion model and to evaluate influence factors on corrosion rate under geological disposal conditions. Materials Research Society Symposium Proceedings 1665, 195-202.

KEG (2003): Kernenergiegesetz (KEG), vom 21. März 2003, Stand am 01. Juli 2023. Systematische Sammlung des Bundesrechts SR 732.1, Schweiz.

Kharaka, Y.K., Carothers, W.W. & Rosenbauer, R.J. (1983): Thermal decarboxylation of acetic acid - implications for origin of natural gas. Geochimica et Cosmochimica Acta 47, 397-402.

King, F. (2008): Corrosion of carbon steel under anaerobic conditions in a repository for SF and HLW in Opalinus clay. Nagra Technical Report NTB 08-12, Nagra, Wettingen, Switzerland.

Klewiah, I., Berawala, D.S., Walker, H.C.A., Andersen, P.O. & Nadeau, P.H. (2020): Review of experimental sorption studies of CO2 and CH4 in shales. Journal of Natural Gas Science and Engineering 73.103045.

Knill, C.J. & Kennedy, J.F. (2003): Degradation of cellulose under alkaline conditions. Carbohydrate Polymers 51, 281-300.

Kosakowski, G., Berner, U., Wieland, E., Glaus, M. & Degueldre, C. (2014): Geochemical evolution of the L/ILW near field. Nagra Technical Report NTB 14-11, Nagra, Wettingen, Switzerland.

Kosakowski, G., Huang, Y. & Wieland, E. (2020): Influence of material heterogeneities, process couplings and aggregate reactivity on the geochemical evolution of the L/ILW repository. Nagra Work Report NAB 20-11, Nagra, Wettingen, Switzerland.

Kosakowski, G., Churakov, S., Glaus, M., Guillemot, T., Kulik, D., Ma, B., Martin, L., Miron, G.D. & Prasianakis, N. (2023): Geochemical evolution of the L/ILW near field. Nagra Technical Report NTB 23-03, Nagra, Wettingen, Switzerland.

Kumpulainen, S. & Kiviranta, L. (2010): Mineralogical and chemical characterization of various bentonite and smectite-rich clay materials part a: Comparison and development of mineralogical characterization methods part b: Mineralogical and chemical characterization of clay materials. Posiva Working Report 2010-52. B + Tech Oy, Eurajoki, Finland.

Kulik, D.A., Wagner, T., Dmytrieva, S.V., Kosakowski, G., Hingerl, F.F., Chudnenko, K.V. & Berner, U.R. (2013): GEM-Selektor geochemical modeling package: revised algorithm and GEMS3K numerical kernel for coupled simulation codes. Computational Geoscience 17, 1-24.

Kunz, C. (1985) C-14 discharge at 3 light-water reactors. Health Physics 49, 25-35.

Kurashige, T., Fujisawa, R., Inagaki, Y. & Senoo, M. (1999): Gas generation behavior of Zircaloy-4 under waste disposal conditions. Radioactive Waste Management and Environmental Remediation (ICEM1999), ASME, Nagoya, Japan.

Kursten, B. (2019): Uniform corrosion evaluation of C-steel in cementitious environments relevant to the supercontainer design. SCK·CEN Technical Report ER-094, Mol, Belgium.

Kursten, B., Macdonald, D.D., Smart, N.N. & Gaggiano, R. (2017): Corrosion issues of carbon steel radioactive waste packages exposed to cementitious materials with respect to the Belgian supercontainer concept. Corrosion Engineering, Science and Technology 52, 11-16.

Kursten, B., Smart, N.R., Senior, N.A., Macdonald, D.D., Caes, S., de Souza, V. & Gaggiano, R. (2021): Overview of anaerobic corrosion of carbon steel radioactive waste packages in alkaline media in support of the Belgian supercontainer concept. Materials and Corrosion 72, 32-51.

Larivière, D. & Guérin, N. (2010): Natural radioactivity, in: Atwood, D.A. (Ed.), Radionuclides in the environment. Wiley Interscience, New York, USA, pp. 1-19.

Le Caer, S. (2011): Water radiolysis: Influence of oxide surfaces on H_2 production under ionizing radiation. Water 3, 235-253.

Lefebvre, F. & Lemaignan, C. (1997): Irradiation effects on corrosion of zirconium alloy claddings. Journal of Nuclear Materials 248, 268-274.

Legand, S., Bouyer, C., Dauvois, V., Casanova, F., Lebeau, D. & Lamouroux, C. (2014): Uranium carbide dissolution in nitric acid :Speciation of organic compounds. Journal of Radio-analysis and Nuclear Chemistry 302, 27−39.

Leupin, O.X., Zeyer, J., Cloet, V., Smith, P., Bernier-Latmani, R., Marschall, P., Papafotiou, A., Schwyn, B. & Stroes-Gascoyne, S. (2016a): An assessment of the possible fate of gas generated in a repository for low- and intermediate-level waste. Nagra Technical Report NTB 16-05. Nagra, Wettingen, Switzerland.

Leupin, O.X., Smith, P., Marschall, P., Johnson, L., Savage, D., Cloet, V., Schneider, J.W. & Senger, R. (2016b): High-level waste repository-induced effects. Nagra Technical Report NTB 14-13, Nagra, Wettingen, Switzerland.

Leupin, O.X., Bernier-Latmani, R., Bagnoud, A., Moors, H., Leys, N., Wouters, K. & Stroes-Gascoyne, S. (2017): Fifteen years of microbiological investigation in Opalinus Clay at the Mont Terri rock laboratory (Switzerland). Swiss Journal of Geosciences 110, 343-354.

Leupin, O.X., Smart, N.R., Zhang, Z.D., Stefanoni, M., Angst, U., Papafotiou, A. & Diomidis, N. (2021): Anaerobic corrosion of carbon steel in bentonite: An evolving interface. Corrosion Science 187, 109523.

Li, J., Li, X.F., Wang, X.Z., Li, Y.Y., Wu, K.L., Shi, J.T., Yang, L., Feng, D., Zhang, T. & Yu, P.L. (2016): Water distribution characteristic and effect on methane adsorption capacity in shale clay. International Journal of Coal Geology 159, 135-154.

Liepins, L.Z. & Thomas, K.W. (1988): Survey of C-14 literature relevant to a geologic nuclear waste repository. Radioactive Waste Management and Environmental Restoration 10, 357-380.

Liu, C., Wang, J., Zhang, Z. & Han, E.-H. (2017): Studies on corrosion behaviour of low carbon steel canister with and without γ-irradiation in China's HLW disposal repository. Corrosion Engineering, Science and Technology 52, 136-140.

Loges, B., Boddien, A., Gartner, F., Junge, H. & Beller, M. (2010): Catalytic generation of hydrogen from formic acid and ist derivatives: Useful hydrogen storage materials. Topics in Catalysis 53, 902-914.

Lothenbach, B. & Wieland, E. (2006): A thermodynamic approach to the hydration of sulphate-resisting Portland cement. Waste Management 26, 706-719.

Lu, X.C., Li, F.C. & Watson, A.T. (1995): Adsorption studies of natural gas storage in Devonian shales. Spe Formation Evaluation 10, 109-113.

Macdonald, D.D., Kursten, B. & Engelhardt, G.R. (2013): Corrosion of iron in physically-constrained locations. ECS Transactions 50, 457-468.

Madigan, M., Martinko, J., Bender, K., Buckley, D. & Stahl, D. (2015): Brock biology of microorganisms, 14th ed., Pearson, London, United Kingdom.

Magnusson, A. & Stenström, K. (2005): ^{14}C produced in Swedish nuclear power reactors - measurements on spent ion exchange resins, various process water systems and ejector off-gas, SKB Rapport R-05-78, Swedish Nuclear Fuel and Waste Management Co, Stockholm, Sweden.

Maiella, P.G. & Brill, T.B. (1998): Spectroscopy of hydrothermal reactions. Evidence of wall effects in decarboxylation kinetics of 1.00 m HCO_2X (X = H, Na) at 280-330 degrees C and 275 bar. Journal of Physical Chemistry A 102, 5886-5891.

Marimbeau, P. & Esbelin, E. (2008): N and C-14 content of spent fuel, in: Johnson, L., Schwyn, B. (Eds.), Nagra/RWMC workshop on the release and transport of C-14 in repository environments. Nagra Work Report NAB 08-22, Nagra, Wettingen, Switzerland, pp. 41-49.

Martin, J.E. (1986): C-14 in low-level radioactive waste from two nuclear power plants. Health Physics 50, 57-64.

Maslennikov, A., Genin, X., Vermeleun, J. & Moisy, P. (2009): UC oxidation with HNO_2 in aqueous solutions of HNO_3 and $HClO_4$. Radiochim. Acta, 97, 571−580.

Matsumoto, J. & Banba, T. (1999): Sorption beahvior of organic carbon-14 onto cementitious materials 7th International conference on Radioactive Waste Management and Environmental Remediation (ICEM1999), ASME, Nagoya, Japan.

Matsumoto, J., Banba, T. & Muraoka, S. (1995): Adsorption of carbon-14 on mortar. Material Research Society Symposium Proceedings 353, 1029-1035.

Mazurek, M., Gautschi, A., Marschall, P., Vigneron, G., Lebon, P. & Delay, J. (2008): Transferability of geoscientific information from various sources (study sites, underground rock laboratories, natural analogues) to support safety cases for radioactive waste repositories in argillaceous formations. Physics and Chemistry of the Earth 33, S95-S105.

McCollom, T.M. (2016): Abiotic methane formation during experimental serpentinization of olivine. Proceedings of the National Academy of Sciences of the United States of America 113, 13965-13970.

McCollom, T.M. & Seewald, J.S. (2003a): Experimental constraints on the hydrothermal reactivity of organic acids and acid anions: I. Formic acid and formate. Geochimica et Cosmochimica Acta 67, 3625-3644.

McCollom, T.M. & Seewald, J.S. (2003b): Experimental study of the hydrothermal reactivity of organic acids and acid anions: II. Acetic acid, acetate, and valeric acid. Geochimica et Cosmochimica Acta 67, 3645-3664.

McCollom, T.M. & Seewald, J.S. (2007): Abiotic synthesis of organic compounds in deep-sea hydrothermal environments. Chemical Reviews 107, 382-401.

Merkel, A., Fink, R. & Littke, R. (2015): The role of pre-adsorbed water on methane sorption capacity of Bossier and Haynesville shales. International Journal of Coal Geology 147, 1-8.

Mibus, J., Diomidis, N., Wieland, E. & Swanton, S.W. (2018): Release and speciation of C-14 during the corrosion of activated steel in deep geological repositories for the disposal of radioactive waste. Radiocarbon 60, 1657-1670.

Mincher, B.J. & Mezyk, S.P. (2009): Radiation chemical effects on radiochemistry: A review of examples important to nuclear power. Radiochimica Acta 97, 519-534.

Mitchell, B.S. (2004): An introduction to materials engineering and science for chemical and materials engineers. Wiley Interscience, Holboken NJ, USA.

MNCP team (2003): MCNP; A general Monte Carlo n particle transport code, version 5, LA-UR-03-1987 (2003, revised 2008). Los Alamos National Lab, Los Alamos NM, USA.

Moeller, D.W., Ryan, M.T., Cherry, R.N. & Sun, L.S.C. (2006): Significance of C-14 and Ra-228 in terms of the proposed Yucca Mountain high-level radioactive waste repository. Health Physics 91, 238-248.

Müller-Vonmoos, M. & Kahr, G. (1983): Mineralogische Untersuchungen von Wyoming Bentonit MX-80 und Montigel. Nagra Technical Report NTB 83-12, Nagra, Wettingen, Switzerland.

Mysen B. & Richet P. (2019): Silicate glasses and melts (Section 16.3), 2nd ed. Elsevier, Amsterdam, the Netherlands.

Nagra (2002): Project Opalinus Clay: Safety report. Demonstration of disposal feasibility for spent fuel, vitrified high-level waste and long-lived intermediate-level waste (Entsorgungs-nachweis). Nagra Technical Report NTB 02-05, Nagra, Wettingen, Switzerland.

Nagra (2005): Spent fuel evolution under disposal conditions. Synthesis of results from the EU spent fuel stability (SFS) project. Nagra Technical Report NTB 04-09, Nagra, Wettingen, Switzerland.

Nagra (2008a): Effects of post-disposal gas generation in a repository for low- and intermediate-level waste sited in the Opalinus Clay of Northern Switzerland. Nagra Technical Report NTB 08-07, Nagra, Wettingen, Switzerland.

Nagra (2008b): Modellhaftes Inventar für radioaktive Materialien. Nagra Technical Report NTB 08-06, Nagra, Wettingen, Switzerland.

Nagra (2021a): Entsorgungsprogramm 2021 der Entsorgungspflichtigen. Nagra Technical Report NTB 21-01, Nagra, Wettingen, Switzerland.

Nagra (2021b): The Nagra Research, Development and Demonstration (RD&D) plan for the disposal of radioactive waste in Switzerland. Nagra Technical Report NTB 21-02, Nagra, Wettingen, Switzerland.

Nagra (2023): Modellhaftes Inventar für radioaktive Materialien - MIRAM 22. Nagra Technischer Bericht NTB 22-05, Nagra, Wettingen, Switzerland.

Nagra (2024a, in prep.): Rahmenbewilligungsgesuch Geologisches Tiefenlager für radioaktive Abfälle der Schweiz: Argumentenbericht. Nagra Technischer Bericht NTB 24-01, Nagra, Wettingen, Switzerland.

Nagra (2024b, in prep.): Safety concept and requirements. Nagra Work Report NAB 24-18, Nagra Wettingen, Switzerland.

Nagra (2024c, in prep.): Consequence analysis report. Nagra Technical Report NTB 24-18, Nagra Wettingen, Switzerland.

Nagra (2024d, in prep.): Design and performance assessment of SF/HLW disposal canisters. Nagra Technical Report NTB 24-20, Nagra Wettingen, Switzerland.

Nagra (2024e, in prep.): Gas synthesis report. Nagra Technical Report NTB 24-23, Nagra Wettingen, Switzerland.

Nagra (2024f, in prep.): Treatment of ^{14}C in the post-closure safety assessments. Nagra Work Report NAB 24-07, Nagra, Wettingen, Switzerland.

Nagra (2024g, in prep.): Geological characterisation of the siting regions Jura Ost, Nördlich Lägern and Zürich Nordost. Nagra Work Report NAB 24-10, Nagra Wettingen, Switzerland.

Nagra (2024h, in prep.): Safety scenario report. Nagra Technical Report NTB 24-21, Nagra, Wettingen, Switzerland.

Nagra (2024i, in prep.): Phenomenological description of the evolution of a combined geological repository for radioactive waste at Nördlich Lägern in Opalinus Clay. Nagra Work Report NAB 24-20, Nagra Wettigen, Switzerland.

NDA (2012): Carbon-14 Project - Phase 1 Report, NDA report NDA/RWMD/092. Nuclear Decommissioning Authority, Harwell, Didcot, United Kingdom.

NDA (2016): Carbon-14 Project Phase 2 - Formation of a gas phase and its migration. AMEC/200047/007, issue 1, Nuclear Decommissioning Authority, Harwell, Didcot, United Kingdom.

Necib, S., Ambard, A., Bucur, C., Caes, S., Cochin, F., Fulger, M., Gras, J.M., Herm, M., Kasprzak, L., Legand, S., Metz, V., Perrin, S., Sakuragi, T. & Suzuki-Muresan, T. (2018a): Final report on 14C behaviour in Zr fuel clad wastes under disposal conditions (D3.20). CAST Deliverable D3.20, European Union, Brussels, Belgium.

Necib, S., Bucur, C., Caes, S., Cochin, F., Cvetković, B., Fulger, M., Gras, J., Herm, M., Kasprzak, L., Legand, S., Metz, V., Perrin, S., Sakuragi, T. & Suzuki-Muresan, T. (2018b): Overview of C-14 release from irradiated zircaloys in geological disposal conditions. Radiocarbon 60, 1757-1771.

Necib, S., Linard, Y., Crusset, D., Michau, N., Daumas, S., Burger, E., Romaine, A. & Schlegel, M. (2016): Corrosion at the carbon steel-clay borehole water and gas interfaces at 85 degrees C under anoxic and transient acidic conditions. Corrosion Science 111, 242-258.

Necib, S., Schlegel, M., Bataillon, C., Daumas, S., Diomidis, N., Keech, P. & Crusset, D. (2019): Long-term corrosion behaviour of carbon steel and stainless steel in Opalinus clay: influence of stepwise temperature increase. Corrosion Engineering, Science and Technology 54, 516-528.

Neeb, K-H. (1997): The radiochemistry of nuclear power plants with light water teactors, Walter de Gruyter, Berlin-New York.

Neeft, E.A.C. (2018): C-14 exposure from disposal of radioactive waste compared to C-14 exposure from cosmogenic origin. Radiocarbon 60, 1911-1923.

Ngo, V.V., Clement, A., Michau, N. & Fritz, B. (2015): Kinetic modeling of interactions between iron, clay and water: Comparison with data from batch experiments. Applied Geochemistry 53, 13-26.

Nilsson, S. & Jonsson, M. (2008): On the catalytic effect of Pd(s) on the reduction of UO_2^+ with H_2 in aqueous solution. Journal of Nuclear Materials 374, 290-292.

Ning, J., Zheng, Y.G., Young, D., Brown, B. & Nesic, S. (2014): Thermodynamic study of hydrogen sulfide corrosion of mild steel. Corrosion 70, 375-389.

Noshita, K. (2008): Fundamental study of C-14 chemical form under irradiated condition, in: Johnson, L., Schwyn, B. (Eds.), Proceedings of a Nagra/RWMC workshop on the release and transport of C-14 in repository environments. Nagra Work Report NAB 08-22, Nagra, Wettingen, Switzerland, pp. 65 - 70.

Nydal, R. & Lovseth, K. (1965): Distribution of radiocarbon from nuclear tests. Nature 206, 1029-1031.

Oberg, E., Jones, F.D., Horton, H.L. & Ryffel, H.H. (2012): Machinery's handbook. Industrial Press Inc., 29th Ed., New York, USA.

Ordomsky, V.V., Legras, B., Cheng, K., Paul, S. & Khodakov, A.Y. (2015): The role of carbon atoms of supported iron carbides in Fischer-Tropsch synthesis. Catalysis Science & Technology 5, 1433-1437.

Palmer, D.A. & Drummond, S.E. (1986): Thermal decarboxylation of acetate .1. The kinetics and mechanism of reaction in aqueous-solution. Geochimica et Cosmochimica Acta 50, 813-823.

Pastina, B., Isabey, J. & Hickel, B. (1999): The influence of water chemistry on the radiolysis of the primary coolant water in pressurized water reactors. Journal of Nuclear Materials 264, 309-318.

Pastina, B. & LaVerne, J.A. (2001): Effect of molecular hydrogen on hydrogen peroxide in water radiolysis. Jounal of Physical Chemistry A 105, 9316-9322.

Pavasars, I., Hagberg, J., Boren, H. & Allard, B. (2003): Alkaline degradation of cellulose: Mechanisms and kinetics. Journal of Polymers and the Environment 11, 39-47.

Plank, J. & Bassioni, G. (2007): Adsorption of carboxylate anions on a $CaCO_3$ surface. Zeitschrift für Naturforschung 62, 1277-1284.

Plyasunov, A.V. & Shock, E.L. (2000a): Standard state Gibbs energies of hydration of hydrocarbons at elevated temperatures as evaluated from experimental phase equilibria studies. Geochimica et Cosmochimica Acta 64, 2811-2833.

Plyasunov, A.V. & Shock, E.L. (2000b): Thermodynamic functions of hydration of hydrocarbons at 298.15 K and 0.1 MPa. Geochimica et Cosmochimica Acta 64, 439-468.

Plyasunova, N.V., Plyasunov, A.V. & Shock, E.L. (2004): Database of thermodynamic properties for aqueous organic compounds. International Journal of Thermophysics 25, 351-360.

Poinssot, C., Ferry, C., Lovera, P., Jegou, C. & Gras, J.M. (2005): Spent fuel radionuclide source term model for assessing spent fuel performance in geological disposal. Part II: Matrix alteration model and global performance. Journal of Nuclear Materials 346, 66-77.

Pointeau, I., Coreau, N. & Reiller, P. (2003): Etude experimentale et modélisation de la rétention de 14CO32- par les matériaux constituant le béton dans le cadre des études de faisabilité d'un stockage de déchets graphites. Andra Report FRP 18CEA 03-001. Andra, Paris, France.

Pointeau, I., Hainos, D., Coreau, N. & Reiller, P. (2006): Effect of organics on selenite uptake by cementitious materials. Waste Management 26, 733-740.

Pointeau, I., Coreau, N. & Reiller, P.E. (2008): Uptake of anionic radionuclides onto degraded cement pastes and competing effect of organic ligands. Radiochimica Acta 96, 367-374.

Ramos, M.E., Cappelli, C., Rozalen, M., Fiore, S. & Huertas, F.J. (2011): Effect of lactate, glycine, and citrate on the kinetics of montmorillonite dissolution. American Mineralogist 96, 768-780.

Ramos, M.E. & Huertas, F.J. (2014): Adsorption of lactate and citrate on montmorillonite in aqueous solutions. Applied Clay Science 90, 27-34.

Rao, Q. & Leng, Y.S. (2014): Methane aqueous fluids in montmorillonite clay interlayer under near-surface geological conditions: A grand canonical Monte Carlo and molecular dynamics simulation study. Journal of Physical Chemistry B 118, 10956-10965.

Rasamimanana, S., Lefevre, G. & Dagnelie, R.V.H. (2017): Adsorption of polar organic molecules on sediments: Case-study on Callovian-Oxfordian claystone. Chemosphere 181, 296-303.

Rearden, B.T., Jesse, M.A.. Eds., SCALE Code System, ORNL/TM-2005/39, Version 6.2.3, Oak Ridge national Laboratory, Oak Ridge, Tennessee (2018). Available from Radiation Safety Information Computational Center as CCC-834.

Reiller, P.E. (2018): Final synthesis report of spent ion-exchange resins ^{14}C source term and leaching (D4.9). CAST Deliverable D4.9, European Union, Brussels, Belgium.

Rizzato, C., Rizzo, A., Heisbourg, G., Večernik, P., Bucur, C., Comte, J., Lebeau, D. & Reiller, P.E. (2015): State of the art review on sample choice, analytical techniques and current knowledge of release from spent ion-exchange resins (D4.1). CAST Deliverable D4.1, European Union, Brussels, Belgium.

Rizzo, A., Bucur, C., Comte, J., Källström, K., Rizzato, C., Večernik, P. & Reiller, P.E. (2017): Final report on the estimation of the source term and speciation of ^{14}C in spent ion-exchange resins (D 4.5). CAST Deliverable D4.5, European Union, Brussels, Belgium.

Rodriguez, M., Gascon, J.L., Magro, E., Pina, G., Lara, E. & Sevilla, L. (2018): C-14 release from steels under aerobic conditions. Radiocarbon 60, 1729-1741.

Röllin, S., Spahiu, K. & Eklund, U.B. (2001): Determination of dissolution rates of spent fuel in carbonate solutions under different redox conditions with a flow-through experiment. Journal of Nuclear Materials 297, 231−243.

Ross, D.J.K. & Bustin, R.M. (2008): Characterizing the shale gas resource potential of Devonian-Mississippian strata in the Western Canada sedimentary basin: Application of an integrated formation evaluation. AAPG Bulletin 92, 87-125.

Ross, D.J.K. & Bustin, R.M. (2009): The importance of shale composition and pore structure upon gas storage potential of shale gas reservoirs. Marine and Petroleum Geology 26, 916-927.

RWM (2016): Geological Disposal. Carbon-14 project phase 2: Overview report. (NDA/RWM/137). RWM.

Sakuragi, T. (2017a): Final report on Zr alloys corrosion studies at RWMC (3.19). CAST Deliverable D3.19, European Union, Brussels, Belgium.

Sakuragi, T. (2017b): Report on corrosion behaviour of stainless steel (D2.12). CAST Deliverable D2.12, European Union, Brussels, Belgium.

Sakuragi, T., Miyakawa, H., Nishimura, T. & Tateishi, T. (2012): Corrosion rates of Zircaloy-4 by hydrogen measurement under high pH, low oxygen and low temperature conditions. Material Research Society Symposium Proceedings 1475, 311-316.

Sakuragi, T., Tanabe, H., Hirose, E., Sakashita, A. & Nishimura, T. (2013): Estimation of carbon-14 inventory in hull and end-piece wastes from Japanese commercial reprocessing operation. 15th International conference on Environmental Remediation and Radioactive Waste Mangement (ICEM2013), ASME, Brussels, Belgium.

Sakuragi, T., Yamashita, Y., Akagi, M. & Takahashi, R. (2016a): Carbon-14 distribution in irradiated fuel cladding and released carbon-14 after aqueous immersion of 6.5 years. Procedia Chemistry 21, 341-348.

Sakuragi, T., Yoshida, S., Kato, O. & Tateishi, T. (2016b): Study of stainless steel corrosion by hydrogen measurement under deoxygenated, low-temperature and basic repository conditions. Progress in Nuclear Energy 87, 26-31.

Sakuragi, T., Yoshida, S., Kinugasa, J., Kato, O. & Tateishi, T. (2016c): Corrosion kinetics of stainless steel by hydrogen measurement under deep geological repository conditions. WM2016 Conference, March 6-10, Phoenix, USA.

Sasoh, M. (2008a): The study for the chemical forms of C-14 released from activated metals, in: Johnson, L., Schwyn, B. (Eds.), Proceedings of a Nagra/RWMC workshop on the release and transport of C-14 in repository environments. Nagra Work Report NAB 08-22, Nagra, Wettingen, Switzerland, pp. 19 - 22.

Sasoh, M. (2008b): Study on chemical behaviour of organic C-14 under alkaline conditions, in: Johnson, L., Schwyn, B. (Eds.), Proceedings of a Nagra/RWMC workshop on the release and transport of C-14 in repository environments. Nagra Work Report NAB 08-22, Nagra, Wettingen, Switzerland, pp. 79 - 82.

Schikorr, G. (1933): Über Eisen(II)-hydroxyd und ein ferromagnetisches Eisen(III)-hydroxyd. Zeitschrift für Anorganische und Allgemeine Chemie 212, 33-39.

Schlegel, M., Necib, S., Daumas, S., Labat, M., Blanc, C., Foy, E. & Linard, Y. (2018): Corrosion at the carbon steel-clay borehole water interface under anoxic alkaline and fluctuating temperature conditions. Corrosion Science 136, 70-90.

Schlegel, M.L., Bataillon, C., Benhamida, K., Blanc, C., Menut, D. & Lacour, J.L. (2008): Metal corrosion and argillite transformation at the water-saturated, high-temperature iron-clay interface: A microscopic-scale study. Applied Geochemistry 23, 2619-2633.

Schulte, M.D. & Shock, E.L. (1993): Aldehydes in hydrothermal solution - standard partial molal thermodynamic properties and relative stabilities at high temperatures and pressures. Geochimica et Cosmochimica Acta 57, 3835-3846.

Schumann, D., Stowasser, T., Volmert, B., Guenther-Leopold, I., Linder, H. & Wieland, E. (2014): Determination of the C-14 content in activated steel components from a neutron spallation source and a nuclear power plant. Analytical Chemistry 86, 5448-5454.

Sedriks, A.J. (1996): Corrosion of stainless steels. John Wiley, New York, USA.

Seewald, J.S., Zolotov, M.Y. & McCollom, T. (2006): Experimental investigation of single carbon compounds under hydrothermal conditions. Geochimica et Cosmochimica Acta 70, 446-460.

Seifert, H.-P. & Ritter, S. (2005): The role of water chemistry for environmentally assisted cracking in low-alloy reactor pressure vessel and piping steels under boiling water reactor condition. Chimia 59, 944-949.

Senior, N.A., Newman, R., Wang, S. & Diomidis, N. (2017): Understanding and quantifying the anoxic corrosion of carbon steel in a Swiss L/ILW repository environment. Corrosion Engineering, Science and Technology 52, 78-83.

Senior, N.A., Martino, T., Diomidis, N., Gaggiano, R., Binns, J. & Keech, P. (2020): The measurement of ultra low uniform corrosion rates. Corrosion Science 176, 108913.

Senior, N.A., Martino, T., Gaggiano, R. & Diomidis, N. (2023a): Experimental factors and their impact on understanding corrosion in anoxic environments. Materials and Corrosion (in press).

Senior, N.A., Martino, T., Diomidis, N. & Gaggiano, R. (2023b): The anoxic corrosion of mild steel in a cementitious repository environment. Materials and Corrosion (in press).

Shock, E.L. (1988): Organic acid metastability in sedimentary basins. Geology 16, 886-890.

Shock, E.L. (1995): Organic acids in hydrothermal solutions - standard molal thermodynamic properties of carboxylic acids and estimates of dissociation constants at thigh temperatures and pressures. American Journal of Science 295, 496-580.

Shock, E.L. & Helgeson, H.C. (1990): Calculation of the thermodynamic and transport properties of aqueous species at high pressures and temperatures - standard partial molal properties of organic species. Geochimica et Cosmochimica Acta 54, 915-945.

Shoesmith, D.W. (2008): The role of dissolved hydrogen on the corrosion/dissolution of spent nuclear fuel. NWMO TR-2008-19, Nuclear Waste Management Organization, Toronto, Canada.

Shoesmith, D.W. & Zagidulin, D. (2011): The corrosion of zirconium under deep geologic repository conditions. Journal of Nuclear Materials 418, 292-306.

Smart, N.R. (2002): A survey of steel corrosion data for use in the GAMMON computer program. SERCO/ERRA-0484,. Serco, Harwell, Didcot, United Kingdom.

Smart, N.R. (2009): Corrosion behavior of carbon steel radioactive waste packages: A summary review of Swedish and U.K. research. Corrosion 65, 195-212.

Smart, N.R., Blackwood, D.J. & Werme, L.O. (2001): The anaerobic corrosion of carbon steel and cast iron in artificial groundwaters. SKB Technical Report TR-01-22, Swedish Nuclear Fuel and Waste Management Co, Stockholm, Sweden.

Smart, N.R., Blackwood, D.J. & Werme, L. (2002): Anaerobic corrosion of carbon steel and cast iron in artificial groundwaters: Part 1 - Electrochemical aspects. Corrosion 58, 547-559.

Smart, N.R., Blackwood, D.J., Marsh, G.P., Naish, C.C., O'Brien, T.M., Rance, A.P. & Thomas, M.I. (2004): The anaerobic corrosion of carbon and stainless steel in simulated cementitious repository environments: A summary review of Nirex Research. AEA Technology, Harwell, Didcot, United Kingdom.

Smart, N.R., Rance, A.P. & Werme, L.O. (2008): The effect of radiation on the anaerobic corrosion of steel. Journal of Nuclear Materials 379, 97-104.

Smart, N.R., Rance, A.P., Fennell, P.A.H. & Kursten, B. (2014): Effect of sulphur species on anaerobic corrosion of carbon steel in alkaline media. Corrosion Engineering Science and Technology 49, 473-479.

Smart, N.R., Rance, A.P., Reddy, B. & Diomidis, N. (2016): Anoxic corrosion of carbon steel in bentonite in relation to the Swiss deep geological repository concept. NACE International - Corrosion 2016 Proceedings, Vancouver, Canada, pp. 2389-2400.

Smart, N.R., Rance, A.P., Nixon, D.J., Fennell, P.A.H., Reddy, B. & Kursten, B. (2017): Summary of studies on the anaerobic corrosion of carbon steel in alkaline media in support of the Belgian supercontainer concept. Corrosion Engineering, Science and Technology 52, 217-226.

Smart, N.R., Rance, A.P., Fennell, P.A.H., Gaggiano, R. & Padovani, C. (2021): Further studies on the anaerobic corrosion of carbon steel in alkaline media in support of the Belgian supercontainer concept. Materials and Corrosion-Werkstoffe Und Korrosion 72, 75-93.

Soma, Y. & Soma, M. (1989): Chemical reactions of organic-compounds on clay surfaces. Environmental Health Perspectives 83, 205-214.

Spahiu, K. (2021): Spent fuel as a waste form. State of the knowledge report (SoK), EURAD, Spent Nuclear Fuel Domain 3.1.1.

Spahiu, K., Cui, D.Q. & Lundstrom, M. (2004): The fate of radiolytic oxidants during spent fuel leaching in the presence of dissolved near field hydrogen. Radiochimica Acta 92, 625-629.

Spinks, J.W.T. & Woods, R.J. (1990): An introduction to radiation chemistry, 3rd ed., John Wiley and Sons, New York, USA.

Stenström, K. & Magnusson, A. (2008): Methods for measuring ^{14}C on spent ion exchange resins - a review, in: Johnson, L., Schwyn, B. (Eds.), Nagra/RWMC workshop on the release and transport of C-14 in repository environments. Nagra Work Report NAB 08-22, pp. 23-40, Nagra, Wettingen, Switzerland.

Stroes-Gascoyne, S., Tait, J.C., Porth, R.J., McConnell, J.L. & Lincoln, W.J. (1994): Release of ^{14}C from the gap and grain-boundary regions of used CANDU fuels to aqueous solutions. Waste Management 14, 385-392.

Stroes-Gascoyne, S. (2011): Microbiological characteristics of compacted bentonite for a dry density of 1450 kg/m^3: A literature review. Nagra Work Report NAB 11-05, Nagra, Wettingen, Switzerland.

Suess, E. (1973): Interaction of organic compounds with calcium-carbonate .2. Organo-carbonate association in recent sediments. Geochimica et Cosmochimica Acta 37, 2435-2447.

Swanton, S.W., Baston, G.M.N. & Smart, N.S. (2015): Rates of steel corrosion and carbon-14 release from irradiated steel - state of the art review (D2.1). CAST Deliverable D 2.1, European Union, Brussels, Belgium.

Swanton, S.W., de Visser-Týnová, E., Stijkel, M., Otlet, R.L. & Walker, A.J. (2022): Measurement of carbon-14 release from irradiated stainless steel under high-pH, anoxic conditions. RWM Report 206134/01 Issue 2 Rev 1, Radioactive Waste Management Limited, Didcot, United Kingdom.

Takahashi, R., Sasoh, M., Yamashita, Y., Tanabe, H. & Sakuragi, T. (2014): Improvement of inventory and leaching rate measurements of C-14 in hull waste, and separation of organic compounds for chemical species identification. Materials Research Society Symposium Proceedings 1665, 139-148.

Tamaura, Y., Ito, K. & Katsura, T. (1983): Transformation of g-FeO(OH) to Fe_3O_4 by absorption of iron(II) ion on γ-FeO(OH). Journal of the Chemical Society Dalton Transactions 189-194.

Tanabe, H., Nishimura, T., Kaneko, M., Sakuragi, T., Nasu, Y. & Asano, H. (2007): Characterization of hull waste in underground condition. Mobile Fission and Activation Products in Nuclear Waste Disposal. Workshop Proceedings La Baule, France, OECD/NEA, 207-220.

Tanabe, H., Sakuragi, T., Miyakawa, H. & Takahashi, R. (2014): Long-term corrosion of Zircaloy hull waste under geological disposal conditions: Corrosion correlations, factors influencing corrosion, corrosion test data, and preliminary evaluation. Materials Research Society Symposium Proceedings 1665, 203-214.

Thorstenson, D.C. (1970): Equilibrium distribution of small organic molecules in natural waters. Geochimica et Cosmochimica Acta 34, 745-770.

Tits, J., Miron, D.G., Guillemot, T., Kunz, D., Laube, A. & Wieland, E. (2019): Experimental investigations on the stability of formate and acetate under cementitious near-field conditions. Unpublished. PSI internal documentation, Paul Scherrer Institut, Villigen PSI, Switzerland.

Tits, J. & Wieland, E. (2023): Radionuclide retention in the cementitious near field of a repository for L/ILW: Composition of reference pore waters and cement pastes and development of the cement sorption data base for use in the RBG. Nagra Technical Report NTB 23-07, Nagra, Wettingen, Switzerland.

Toijer, E. & Jonsson, M. (2019): H_2O_2 and gamma-radiation induced corrosion of 304L stainless steel in aqueous systems. Radiation Physics and Chemistry 159, 159-165.

Toste, A.P., Polach, K.J. & White, T.W. (1994): Degradation of citric-acid in a simulated, mixed nuclear waste - radiolytic versus chemical forces. Waste Management 14, 27-34.

Toth, L.E. (1971): Transition metal carbides and nitrides. Academic Press, New York and London.

Toulhoat, N., Moncoffre, N., Narkunas, E., Poskas, P., Bucur, C., Ichim, C., Petit, L., Schumacher, S., Catherin, S., Capone, M., Shcherbina, N., Bukaemskiy, A., Rodríguez Alcalá, M., Magro, E., Márquez, E.M., Piña, G., Fachinger, J., Fugaru, V., Norris, S. & Zlobenko, B. (2018): Final report on results from Work Package 5: Carbon-14 in irradiated graphite. CAST deliverable D5.19, European Union, Brussels, Belgium.

Trummer, M. & Jonsson, M. (2010): Resolving the H_2 effect on radiation induced dissolution of UO2-based spent nuclear fuel. Journal of Nuclear Materials 396, 163-169.

Trummer, M., Nilsson, S. & Jonsson, M. (2008) On the effects of fission product noble metal inclusions on the kinetics of radiation induced dissolution of spent nuclear fuel. Journal of Nuclear Materials 378, 55-59.

Trummer, M., Roth, O. & Jonsson, M. (2009): H_2 inhibition of radiation induced dissolution of spent nuclear fuel. Journal of Nuclear Materials 383, 226-230.

UNSCEAR (2008): Sources and effects of ionizing radiation. United Nations, New York, USA.

Uyama, M., Saito, H. & Iioka, T. (2020): Heating impact on corrosion mechanism of carbon steel surrounded by bentonite. International Conference on Nuclear Engineering. ASME, Virtual, ICONE2020-16765.

Van der Laan, G.P. & Beenackers, A.A.C.M. (1999): Kinetics and selectivity of the Fischer-Tropsch synthesis: A literature review. Catalysis Reviews 41, 255-318.

Van Loon, L.R. (2019): Can organic ^{14}C be trapped in the near field or in the far field? Unpublished. PSI internal documentation, Paul Scherrer Institut, Villigen PSI.

Van Loon, L.R. & Glaus, M.A. (1998): Experimental and theoretical studies on alkaline degradation of cellulose and its impact on the sorption of radionuclides. PSI Report 98-07, Paul Scherrer Institut, Villigen, Switzerland, and Nagra Technical Report NTB 97-04, Nagra, Wettingen, Switzerland.

Van Loon, L.R. & Mibus, J. (2015): A modified version of Archie's law to estimate effective diffusion coefficients of radionuclides in argillaceous rocks and its application in safety analysis studies. Applied Geochemistry 59, 85-94.

Van Loon, L.R. & Chen, Y. (2021): Sorption of methane (CH_4) on Opalinus Clay. Unpublished. PSI internal documentation, Paul Scherrer Institut, Villigen PSI, Switzerland.

Van Loon, L.R., Glaus, M.A., Stallone, S. & Laube, A. (1997): Sorption of isosaccharinic acid, a cellulose degradation product on cement. Environmental Science & Technology 31, 1243-1245.

Vance, J.L., Cline, J.E. & Robertson, D.E. (1995): Characterization of carbon-14 generated by the nuclear power industry. Epri Report TR-105715, Electric Power Research Institute, Palo Alto, CA, USA.

Van Konynenburg, R.A. (1994): Behavior of C-14 in waste packages for spent fuel in a tuff repository. Waste Management 14, 363-383.

Van Konynenburg, R.A., Smith, C.F., Culham, H.W. & Smith, H.D. (1987): Carbon-14 in waste packages for spent fuel in a tuff repository, Report UCRL-94708, Lawrence Livermore National Laboratory, Livermore, CA, USA.

Večernik, P., Bucur, C., Comte, J., Legand, S., Rizzato, C., Shcherbina, N. & Reiller, P. (2018): Final report on leaching and desorption experiments of 14C from spent ion exchange resins (D4.6). CAST Deliverable D4.6, European Union, Brussels, Belgium.

Vinsot, A., Appelo, C.A.J., Lundy, M., Wechner, S., Cailteau-Fischbach, C., de Donato, P., Pironon, J., Lettry, Y., Lerouge, C. & De Cannière, P. (2017): Natural gas extraction and artificial gas injection experiments in Opalinus Clay, Mont Terri rock laboratory (Switzerland). Swiss Journal of Geosciences 110, 375-390.

Volmert, B. & Pantelias, M. (2013): Nuclear power plant activation analysis for the Swiss decommissioning study 2011. Proceedings of Jahrestagung Kerntechnik, Berlin.

Wada, R., Nishimura, T., Fujiwara, K., Tanabe, M. & Mihara, M. (1999): Experimental study on hydrogen gas generation rate from corrosion of zircaloy and stainless steel under anaerobic alkaline conditions. Radioactive Waste Management and Environmental Remediation (ICEM1999). ASME, Nagoya, Japan.

Wang, S. & Iglesia, E. (2017): Experimental and theoretical assessment of the mechanism and site requirements for ketonization of carboxylic acids on oxides. Journal of Catalysis 345, 183-206.

Wang, X.C.& Lee, C. (1993): Adsorption and desorption of aliphatic-amines, amino-acids and acetate by clay-minerals and marine-sediments. Marine Chemistry 44, 1-23.

Wareing, A., Abrahamsen, L., Banford, A., Metcalfe, M. & Van Lensa, W. (2013): Final Publishable CARBOWASTE Report. CARBOWASTE deliverable D-0.3.12, European Union, Brussels, Belgium.

Was, G. (2012): Irradiation assisted corrosion and stress corrosion cracking (IAC/IASCC) in nuclear reactor systems and components, in: Feron, D. (Ed.), Nuclear corrosion science and engineering. Woodhead Publishing, Cambridge, United Kingdom.

Wersin, P., Johnson, L.H., Schwyn, B., Berner, U. & Curti, E. (2003): Redox conditions in the near field of a repository for SF/HLW and ILW in Opalinus clay. Nagra Technical Report NTB 02-13, Nagra, Wettingen, Switzerland.

Wieland, E. (2014): Sorption data base for the cementitious near field of L/ILW and ILW repositories for provisional safety analysis for SGT-E2. Nagra Technical Report NTB 14-08, Nagra, Wettingen, Switzerland.

Wieland, E. & Hummel, W. (2015): Formation and stability of C-14-containing organic compounds in alkaline iron-water systems: preliminary assessment based on a literature survey and thermodynamic modelling. Mineralogical Magazine 79, 1275-1286.

Wieland, E. & Kosakowski, G. (2020): Review of the compositions of hydrated cement and cement-type pore water at different stages of the cement degradation. Nagra Work Report NAB 20-12, Nagra, Wettingen, Switzerland.

Wieland, E., Jakob, A., Tits, J., Lothenbach, B. & Kunz, D. (2016): Sorption and diffusion studies with low molecular weight organic compounds in cementitious systems. Applied Geochemistry 67, 101-117.

Wieland, E., Cvetković, B.Z., Kunz, D., Salazar, G. & Szidat, S. (2017): Identification and formation of carbon-14 containing organic compounds during anoxic corrosion of activated steel in alkaline conditions. 16th International High-Level Radioactive Waste Management Conference (IHLRWM 2017), Charlotte NC, USA.

Wieland, E., Cvetković, B., Kunz, D., Salazar, G. & Szidat, S. (2018): Carbon-14 speciation during anoxic corrosion of activated steel in a repository environment. Atw-International Journal for Nuclear Power 63, 34-39.

Wilson, C. N. (1990a): Results from NNWSI series 2 bare fuel dissolution tests. Report PNL-7169, Pacific Northwest Laboratories, Richland WA, USA.

Wilson, C. N. (1990b): Results from Nevada Nuclear Waste Storage Investigation (NNWSI) series 3 spent fuel dissolution tests. Report PNL-7170, Pacific Northwest Laboratories, Richland WA, USA.

Wilson, C. N. & Shaw, H. F. (1987): Experimental study of the dissolution of spent fuel at 85°C in natural groundwater. Materials Research Society Symposium Proceedings 84,123-130.

Yamaguchi, T., Tanuma, S., Yatsutomi, I., Nakayama, T., Tanabe, H., Katsurai, K., Kawamura, W., Maeda, K., Kitao, H. & Saigusa, M. (1999): A study on chemical forms and migration behaviour of radionuclides in hull wastes. Radioactive Waste Management and Environmental Remediation (ICEM1999), ASME, Nagoya, Japan.

Yamashita, Y., Tanabe, H., Sakuragi, T., Takahashi, R. & Sasoh, M. (2014): C-14 release behavior and chemical species from irradiated hull waste under geological disposal conditions. Materials Research Society Symposium Proceedings 1665, 187-194.

Yim, M.-S. & Caron, F. (2006): Life cycle and management of carbon-14 from nuclear power generation. Progress in Nuclear Energy 48, 2-36.

Zhang, T.W., Ellis, G.S., Ruppel, S.C., Milliken, K. & Yang, R.S. (2012): Effect of organic-matter type and thermal maturity on methane adsorption in shale-gas systems. Organic Geochemistry 47, 120-131.

10 Acknowledgement

The authors would like to thank Steve Swanton (Jacobs Clean Energy Limited) for a careful review of the report and helpful suggestions for improvements. The authors would also like to express their gratitude to Kastriot Spahiu (Kaspa Consult AB) for important advice and crucial information on the release of carbon-14 from spent fuel, particularly including the preparation of a paragraph on the reaction of uranium carbides with water that was instrumental to improving the present report. If the relevant comments are not correctly reproduced in the report, this is the sole responsibility of the authors. Bart Baeyens (Paul Scherrer Institute) is warmly thanked for his assistance in calculating the sorption coefficients based on the geodata sets.

App. A Designation of stainless steel

Tab. A-1: Designations of stainless steel grades

European Norm Material Number	European Norm Short Name	ASTM/AISI Designation	UNS Number
1.4016	X6Cr17	430	S43000
1.4509	X2CrTiNb18	441	S44100
1.4510	X3CrTi17	439	
1.4512	X2CrTi12 (alt X6 CrTi 12)	409	S40900
1.4526	X6CrMoNb17-1	436	S43600
1.4310	X10CrNi18-8 (alt X12 CrNi17 7)	301	S30100
1.4318	X2CrNiN18-7	301LN	
1.4307	X2CrNi18-9	304L	S30403
1.4306	X2CrNi19-11	304L	S30403
1.4311	X2CrNiN18-10	304LN	S30453
1.4301	X5CrNi18-10	304	S30400
1.4948	X6CrNi18-11	304H	S30409
1.4303	X4CrNi18-12 (alt X5 CrNi18 12)	305	S30500
1.4541	X6CrNiTi18-10	321	S32100
1.4878	X10CrNiTi18-10 (alt X12 CrNiTi18 9)	321H	S32109
1.4404	X2CrNiMo17-12-2	316L	S31603
1.4401	X5CrNiMo17-12-2	316	S31600

European Norm Material Number	European Norm Short Name	ASTM/AISI Designation	UNS Number
1.4406	X2CrNiMoN17-11-2	316LN	S31653
1.4432	X2CrNiMo17-12-3	316L	S31603
1.4435	X2CrNiMo18-14-3	316L	S31603
1.4436	X3CrNiMo17-13-3	316	S31600
1.4571	X6CrNiMoTi17-12-2	316Ti	S31635
1.4429	X2CrNiMoN17-13-3	316LN	S31653
1.4438	X2CrNiMo18-15-4	317L	S31703
1.4539	X1NiCrMoCu25-20-5	904L	N08904
1.4547	X1CrNiMoCuN20-18-7	F 44	S31254
1.4462	X2CrNiMoN22-5-3	F 51	S31803

Tab. A-2: Carbon and nitrogen contents (wt.%) of stainless steels used in nuclear applications
From Swanton et al. (2015)

Stainless steels				
AISI	**Short name**	**DIN EN**	**% C**	**% N**
304	X5CrNi18-10	1.4301	≤ 0.08	≤ 0.1
304L	X2CrNi19-11	1.4306	≤ 0.03	≤ 0.1
304L	X2CrNi18-9	1.4307	≤ 0.03	≤ 0.1
309	X15CrNiSi20-12	1.4828	≤ 0.2	n.s.
316	X5CrNiMo17-12-2	1.4401	≤ 0.08	≤ 0.1
316L	X2CrNiMo17-12-2	1.4404	≤ 0.03	≤ 0.1
316L	X2CrNiMo17-12-3	1.4432	≤ 0.03	≤ 0.1
316L	X2CrNiMo18-14-3	1.4435	≤ 0.03	≤ 0.1
316L(N)	X2CrNiMoN17-11-2	1.4406	≤ 0.03	0.1-0.16
316L(N)	X2CrNiMoN17-13-3	1.4429	≤ 0.03	0.1-0.16
321	X6CrNiTi18-10	1.4541	≤ 0.08	n.s.

n.s. not specified

App. B Composition of representative porewaters

The composition of the porewaters in equilibrium with different repository materials was considered: OPA, MX80 bentonite, and CEM I at different stages of cement degradation. The carbon concentrations of the porewaters result from their calculated composition, and no additional carbon source or buffer was considered. Due to changes in the chemical systems, some mineral phases were found to precipitate, which has an additional influence on the speciation. Mineral phases were switched off, and only the aqueous phase was considered, which was the focus of the thermodynamic calculations of the carbon speciation for different scenarios.

Tab. B-1: Composition of highly alkaline cement-type porewaters

From Wieland & Kosakowski 2020

	Stage I	**Stage II**	**Stage III**
pH	13.28	12.90	9.83
Pe	7.36	7.73	10.91
IS (m)	0.268	0.357	0.761
Element	Molality (mol/kg_w)	Molality (mol/kg_w)	Molality (mol/kg_w)
Na	4.18×10^{-2}	0.154	0.141
K	0.233	0.194	0.296
Ca	1.80×10^{-3}	6.38×10^{-3}	0.112
Mg	1.49×10^{-9}	3.84×10^{-9}	1.37×10^{-5}
Sr	7.81×10^{-8}	3.70×10^{-4}	9.70×10^{-4}
Ba	4.94×10^{-8}	1.57×10^{-7}	4.09×10^{-7}
Al	3.20×10^{-5}	1.37×10^{-5}	7.28×10^{-7}
Fe	3.66×10^{-8}	1.59×10^{-8}	3.06×10^{-10}
C(IV)	1.41×10^{-4}	3.58×10^{-5}	8.50×10^{-6}
S(VI)	2.83×10^{-3}	6.25×10^{-4}	1.64×10^{-2}
Cl	2.08×10^{-7}	0.240	0.628
Si	4.81×10^{-5}	3.03×10^{-5}	5.68×10^{-5}
log pCO_2 (bar)	-12.8	-12.8	-12.8

Tab. B-2: Composition of bentonite and OPA porewater

From Tab. 17 in Curti (2021a)

	Bentonite*	**OPA***
pH	7.24	7.10
Eh (V)	-0.173	- 0.167
IS (m)	0.452	0.319
Element	Molalities (mol/kg_w)	Molalities (mol/kg_w)
Na	0.375	0.215
K	1.83×10^{-3}	2.13×10^{-3}
Ca	1.77×10^{-2}	2.03×10^{-2}
Mg	1.02×10^{-2}	1.45×10^{-2}
Sr	1.72×10^{-4}	3.70×10^{-4}
Ba	7.19×10^{-8}	1.57×10^{-7}
Al	2.08×10^{-8}	2.09×10^{-8}
Fe	2.09×10^{-5}	2.56×10^{-5}
Mn	1.84×10^{-5}	8.24×10^{-5}
C(IV)	2.94×10^{-3}	2.21×10^{-3}
S(VI)	7.86×10^{-2}	2.29×10^{-2}
Cl	0.239	0.240
F	1.74×10^{-4}	1.74×10^{-4}
Si	1.70×10^{-4}	1.72×10^{-4}
log pCO_2 (bar)	-2.2	-2.2

Tab. B-3: Thermodynamic database for modelling the C-H-O system at 25 °C and 1 bar

Values in bold are taken from the cited references; all other values are recalculated from these values. Δ_fG^o is the standard molar Gibbs energy of formation of the elements in their reference state, Δ_rG^o is the molar Gibbs energy of the reaction and $\log_{10} K^o$ is the equilibrium constant of the reaction (adapted from Wieland & Hummel 2015).

Species Name	**Species formula**	**Δ_fG^o Kcal mol^{-1}**	**Δ_fG^o kJ mol^{-1}**	**Ref.**	**Reaction**	**Stoichiometry CO_2(aq)**	**Stoichiometry H_2O(l)**	**Δ_rG^o kJ mol^{-1}**	**$\log_{10} K^o$**
Methane	CH_4(aq)	**-8.234**	-34.451	1	$CO_2(aq) + 8H^+ + 8e^- = CH_4(aq) + 2H_2O(l)$	-1	2	-122.761	21.507
Ethane	C_2H_6(aq)	**-3.886**	-16.259	1	$2CO_2(aq) + 14H^+ + 14e^- = C_2H_6(aq) + 4H_2O(l)$	-2	4	-192.879	33.791
Propane	C_3H_8(aq)	**-1.963**	-8.213	1	$3CO_2(aq) + 20H^+ + 20e^- = C_3H_8(aq) + 6H_2O(l)$	-3	6	-273.143	47.852
n-butane	C_4H_{10}(aq)	**0.036**	0.151	1	$4CO_2(aq) + 26H^+ + 26e^- = C_4H_{10}(aq) + 8H_2O(l)$	-4	8	-353.089	61.858
n-pentane	C_5H_{12}(aq)	**2.130**	8.912	1	$5CO_2(aq) + 32H^+ + 32e^- = C_5H_{12}(aq) + 10H_2O(l)$	-5	10	-432.638	75.794
Ethylene	C_2H_4(aq)	**19.450**	81.379	1	$2CO_2(aq) + 12H^+ + 12e^- = C_2H_4(aq) + 4H_2O(l)$	-2	4	-95.241	16.685
l-propene	C_3H_6(aq)	**17.910**	74.935	1	$3CO_2(aq) + 18H^+ + 18e^- = C_3H_6(aq) + 6H_2O(l)$	-3	6	-189.995	33.285
l-butene	C_4H_8(aq)	**20.310**	84.977	1	$4CO_2(aq) + 24H^+ + 24e^- = C_4H_8(aq) + 8H_2O(l)$	-4	8	-268.263	46.997
l-pentene	C_5H_{10}(aq)	**22.470**	94.014	1	$5CO_2(aq) + 30H^+ + 30e^- = C_5H_{10}(aq) + 10H_2O(l)$	-5	10	-347.536	60.885
Ethyne	C_2H_2(aq)	**51.890**	217.108	1	$2CO_2(aq) + 10H^+ + 10e^- = C_2H_2(aq) + 4H_2O(l)$	-2	4	40.488	-7.093
l-propyne	C_3H_4(aq)	**47.880**	200.330	1	$3CO_2(aq) + 16H^+ + 16e^- = C_3H_4(aq) + 6H_2O(l)$	-3	6	-64.600	11.317

Species Name	Species formula	$\Delta_f G^o$ Kcal mol^{-1}	$\Delta_f G^o$ kJ mol^{-1}	Ref.	Reaction	Stoichiometry CO_2(aq)	Stoichiometry H_2O(l)	$\Delta_r G^o$ kJ mol^{-1}	$\log_{10} K^o$
l-butyne	C_4H_6(aq)	**50.030**	209.326	1	$4CO_2(aq) + 22H^+ + 22e^- = C_4H_6(aq) + 8H_2O(l)$	-4	8	-143.914	25.213
l-pentyne	C_5H_8(aq)	**52.160**	218.237	1	$5CO_2(aq) + 28H^+ + 28e^- = C_5H_8(aq) + 10H_2O(l)$	-5	10	-223.313	39.122
Methanol	CH_3OH(aq)	**-42.050**	-175.937	1	$CO_2(aq) + 6H^+ + 6e^- = CH_3OH(aq) + H_2O(l)$	-1	1	-27.107	4.749
Ethanol	C_2H_5OH(aq)	**-43.330**	-181.293	1	$2CO_2(aq) + 12H^+ + 12e^- = C_2H_5OH(aq) + 3H_2O(l)$	-2	3	-120.773	21.158
l-propanol	C_3H_7OH(aq)	**-41.910**	-175.351	1	$3CO_2(aq) + 18H^+ + 18e^- = C_3H_7OH(aq) + 5H_2O(l)$	-3	5	-203.141	35.589
l-butanol	C_4H_9OH(aq)	**-38.840**	-162.507	1	$4CO_2(aq) + 24H^+ + 24e^- = C_4H_9OH(aq) + 7H_2O(l)$	-4	7	-278.607	48.809
l-pentanol	$C_5H_{11}OH$(aq)	**-38.470**	-160.958	1	$5CO_2(aq) + 30H^+ + 30e^- = C_5H_{11}OH(aq) + 9H_2O(l)$	-5	9	-365.368	64.009
Formaldehyde	CH_2O(aq)	**-26.130**	-109.328	2	$CO_2(aq) + 4H^+ + 4e^- = CH_2O(aq) + H_2O(l)$	-1	1	39.502	-6.920
Acetaldehyde	C_2H_4O(aq)	**-33.470**	-140.038	2	$2CO_2(aq) + 10H^+ + 10e^- = C_2H_4O(aq) + 3H_2O(l)$	-2	3	-79.518	13.931
Propanal	C_3H_6O(aq)	**-32.730**	-136.942	2	$3CO_2(aq) + 16H^+ + 16e^- = C_3H_6O(aq) + 5H_2O(l)$	-3	5	-164.732	28.860
Butanal	C_4H_8O(aq)	**-28.720**	-120.164	2	$4CO_2(aq) + 22H^+ + 22e^- = C_4H_8O(aq) + 7H_2O(l)$	-4	7	-236.264	41.392

Species Name	Species formula	$\Delta_f G^o$ Kcal mol^{-1}	$\Delta_f G^o$ kJ mol^{-1}	Ref.	Reaction	Stoichiometry CO_2(aq)	Stoichiometry H_2O(l)	$\Delta_r G^o$ kJ mol^{-1}	$\log_{10} K^o$
Pentanal	$C_5H_{10}O$(aq)	**-27.020**	-113.052	2	$5CO_2(aq) + 28H^+ + 28e^- = C_5H_{10}O(aq) + 9H_2O(l)$	-5	9	-317.462	55.617
Formic acid	HCOOH(aq)	**-88.982**	-372.301	1	$CO_2(aq) + 2H^+ + 2e^- = HCOOH(aq)$	-1	0	13.669	-2.395
Acetic acid	CH_3COOH(aq)	**-94.760**	-396.476	1	$2CO_2(aq) + 8H^+ + 8e^- = CH_3COOH(aq) + 2H_2O(l)$	-2	2	-98.816	17.312
Propanoic acid	C_2H_5COOH(aq)	**-93.430**	-390.911	1	$3CO_2(aq) + 14H^+ + 14e^- = C_2H_5COOH(aq) + 4H_2O(l)$	-3	4	-181.561	31.808
Butanoic acid	C_3H_7COOH(aq)	**-91.190**	-381.539	1	$4CO_2(aq) + 20H^+ + 20e^- = C_3H_7COOH(aq) + 6H_2O(l)$	-4	6	-260.499	45.637
Pentanoic acid	C_4H_9COOH(aq)	**-89.210**	-373.255	1	$5CO_2(aq) + 26H^+ + 26e^- = C_4H_9COOH(aq) + 8H_2O(l)$	-5	8	-340.525	59.657
Formate	$HCOO^-$	**-83.862**	-350.879	1	$CO_2(aq) + H^+ + 2e^- = HCOO^-$	-1	0	35.091	-6.148
Acetate	CH_3COO^-	**-88.270**	-369.322	1	$2CO_2(aq) + 7H^+ + 8e^- = CH_3COO^- + 2H_2O(l)$	-2	2	-71.662	12.555
Propanate	$C_2H_5COO^-$	**-86.770**	-363.046	1	$3CO_2(aq) + 13H^+ + 14e^- = C_2H_5COO^- + 4H_2O(l)$	-3	4	-153.696	26.926
Butanoate	$C_3H_7COO^-$	**-84.610**	-354.008	1	$4CO_2(aq) + 19H^+ + 20e^- = C_3H_7COO^- + 6H_2O(l)$	-4	6	-232.968	40.814
Pentanoate	$C_5H_9COO^-$	**-82.600**	-345.598	1	$5CO_2(aq) + 25H^+ + 26e^- = C_4H_9COO^- + 8H_2O(l)$	-5	8	-312.868	54.812
Oxalic acid	$C_2H_2O_4$(aq)	-170.264	**-712.384**	3	$2CO_2(aq) + 2H^+ + 2e^- = C_2H_2O_4(aq)$	-2	0	59.556	-10.434
Hoxalate	$C_2HO_4^-$	-168.354	**-704.393**	3	$2CO_2(aq) + H^+ + 2e^- = C_2HO_4^-$	-2	0	67.547	-11.834

Species Name	Species formula	$\Delta_f G^o$ Kcal mol^{-1}	$\Delta_f G^o$ kJ mol^{-1}	Ref.	Reaction	Stoichiometry $CO_2(aq)$	Stoichiometry $H_2O(l)$	$\Delta_r G^o$ kJ mol^{-1}	$\log_{10} K^o$
Oxalate	$C_2O_4^{2-}$	-162.556	**-680.134**	3	$2CO_2(aq) + 2e^- = C_2O_4^{2-}$	-2	0	91.806	-16.084
Bicarbonate	HCO_3^-	-140.259	**-586.845**	4	$CO_2(aq) + H_2O(l) = HCO_3^- + H^+$	-1	-1	36.265	-6.353
Carbonate	CO_3^{2-}	-126.171	**-527.900**	4	$CO_2(aq) + H_2O(l) = CO_3^{2-} + 2H^+$	-1	-1	95.210	-16.680

References: 1: Shock & Helgeson (1990), 2: Schulte & Shock (1993), 3: Hummel et al. (2005), 4: Cox et al. (1989)

Tab. B-4: Specific information

Master species	**$\Delta_f G^o$**	**$\Delta_f G^o$**	**Reference**
	cal·mol^{-1}	kJ·mol^{-1}	
CO_2(aq)	-92,249	**-385.970**	Cox et al. (1989)
H_2O(l)	-56,678	**-237.140**	Cox et al. (1989)
H^+		**0.000**	Cox et al. (1989)
e^-		**0.000**	Cox et al. (1989)
R	8.314510	J K^{-1} mol^{-1}	
T	298.15	K	
ln(10)	2.302585		

$R \cdot T \cdot \ln(10)/1000 = 5.708042$ kJ mol^{-1}
$\log_{10} K = -\Delta_r G^o / (R \cdot T \cdot \ln(10)/1000) = -\Delta_r G^o / 5.708042$